AD706643

FTD-HT-23-237-69
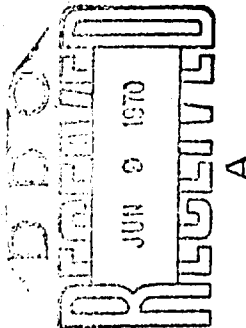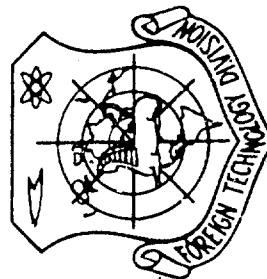
FOREIGN TECHNOLOGY DIVISION

MAGNETOHYDRODYNAMICS IN MARINE ENGINEERING

by

L. G. Vasil'yev and A. I. Khozhainov

NOTICE TO USERS

EDITED TRANSLATION

MAGNETOHYDRODYNAMICS IN MARINE ENGINEERING

By: L. G. Vasil'yev and A. I. Khozhainov

English pages: 220

Source: Magnitnaya Gidrodinamika v Sudovoy Tekhnike, 1967, pp. 1-247.

Translated under: Contract No. F33657-68-D-0866 P002

PREPARED BY:

TRANSLATION DIVISION
FOREIGN TECHNOLOGY DIVISION
WP-AFB, OHIO.

Best Available Copy

TABLE OF CONTENTS

EDITOR'S NOTE

With the exception of certain trigonometric and hyperbolic functions, Soviet mathematical symbols are the same as those encountered in the American literature. For the reader's convenience a list of such exceptions and their American equivalents is given below.

Soviet Usage	American Equivalent
Arch	$\cosh^{-1}$
Arcth	$\coth^{-1}(\text{ctnh}^{-1})$
Arsh	$\sinh^{-1}$
Arth	$\tanh^{-1}$
arccos	$\cos^{-1}$ (arc cos)
arcctg	$\cot^{-1}$ (arc cot)
arcsin	$\sin^{-1}$ (arc sin)
arctg	$\tan^{-1}$ (arc tan)
ch	cosh
cosec	csc
ctg	cot (ctn)
cth	coth (ct nh)
lg	log
rot	curl
sch	sech
sh	sinh
tg	tan
th	tanh

ANNOTATION

This book is devoted to magnetohydrodynamics, a new, rapidly developing branch of science, and to its applications in marine engineering.

The book describes the state of the art in magnetohydrodynamics and the devices operating on this principle. Magnetohydrodynamic effects, produced by interaction between incompressible conducting liquid and a transverse magnetic field are examined. Elements of theory, design and operating characteristics of magnetic flowmeters, electromagnetic pumps, MHD generators, shipboard MHD engines and MHD power units for the transportation industry are presented.

Much attention is devoted to original experimental studies. The book is based on published data of Soviet and foreign scientists, as well as on studies by its authors.

The book is intended for scientific workers and engineers of the shipbuilding industry and related areas. It can also be useful to graduate and undergraduate students of the applicable specialties.

FOREWORD

While magnetohydrodynamics is still a very new science, it has become extremely popular because of the wide possibilities for its prospective engineering applications.

Among such applications are controlled thermonuclear reactions, plasma engines for space ships, direct conversion of thermal into electric energy, transportation, and measurement of flow of conducting liquids. These applications constitute a very incomplete list of problems whose solution is related to development of magnetohydrodynamics.

The magnetohydrodynamics of incompressible fluids, as magnetoplasma dynamics or plasma physics, has by now become a separate branch of science and many of its engineering applications are already used in various branches of industry.

Extensive studies have been conducted during the past several years of the feasibility of using MHD devices and units in the transportation industry, in particular, for seagoing vessels. The results obtained thus far are promising.

Practical solution of this problem requires that the relationships governing magnetohydrodynamics and its possible engineering application in ship propulsion be well understood by a wide range of scientific workers, engineers and designers. So far, these problems have not been generalized in a monograph.

The book by L. G. Vasil'yev and A. I. Khozhainov, which is hereby offered to the reader, is the first of such monographs. Its distinguishing feature is the fact that it examines simultaneously the theoretical and experimental magnetohydrodynamics of viscous incompressible fluids and its engineering applications. The book presents MHD equations and examines MHD phenomena occurring in a flow of conducting fluid, phenomena which follow from the solution of several well known problems of classical hydrodynamics.

The present authors describe elements of theory, design and operating characteristics of MHD measuring devices, electromagnetic pumps, MHD engines and power units employing MHD generators. Because of the relative complexity of the theory of MHD phenomena and devices, which are based on a simultaneous employment of a system of hydrodynamic and electrodynamic equations, and striving to produce a monograph accessible to a wide range of specialists, the present authors have paid particular attention to the physics of the phenomena and to the operating principles of MHD devices.

The extensive list of references appended to the book will enable a more extensive familiarization with individual aspects of the MHD problem.

The book will be useful to a wide range of specialists who are interested in the use of MHD relationships in shipbuilding and marine engineering. It can also be recommended as a textbook for students of the applicable specialties.

Professor A. N. Patrashev
Honored Scientist of the RSFSR
Doctor of Technical Sciences

AUTHOR'S FOREWORD

This book attempts to present the main achievements of theoretical and experimental magnetohydrodynamics of incompressible conductive fluids as applied to flow in channels and past bodies, as well as to familiarize the reader with the theory and design of MHD devices pertaining to future marine power plants. The wide range of the topic and the space limitations inherent in a book resulted in certain difficulties in writing it. The authors will be grateful to the readers for all the critical remarks and requests.

The authors wish to express their profound appreciation to Professor R. S. Petukhov and Candidate of Technical Sciences G. V. Genin for their comments on the book's general outline, as well as to Candidate of Technical Sciences L. M. Korsunskiy, Doctor of Technical Sciences N. M. Okhremenko and Candidate of Physical-Mathematical Sciences A. G. Ryabinin, who have critically reviewed individual chapters.

Particular thanks are due to the overall reviewer of this book, the Corresponding Member of the Ukrainian Academy of Sciences Professor I. L. Povkh, for his recommendations and for supplying data which aided in improving the book.

<div align="right">L. G. Vasil'yev and A. I. Khozhainov</div>

INTRODUCTION

Magnetohydrodynamics is a new scientific discipline which has been rapidly developing during the past 10-15 years. It deals with the motion of conducting liquids and gases in the presence of electromagnetic fields. This motion is accompanied by the so-called magnetohydrodynamic effects, which in turn can be used for acting upon the conducting media.

Initially, the primary concern of magnetohydrodynamics was the study of cosmic phenomena. Because of its high temperature, stellar matter and the interstellar gas constitute a highly ionized plasma, i.e., a good conductor of electricity. The presence of large magnetic fields in the outer space does under these conditions produce strong magnetohydrodynamic effects.

Recently, the high interest in MHD (magnetohydrodynamics) has become due to the newly-apparent possibilities of MHD under conditions prevailing on earth. Thus, MHD phenomena are involved in the control of thermonuclear reactions, where a high-temperature plasma interacts with a magnetic field. In this case the magnetic field is used for heating the plasma to the temperature of the onset of the reaction (several tens of millions of degrees), and for maintaining it in a stable state. Solution of this problem will provide mankind with a virtually inexhaustible energy source.

Of tremendous interest is also the problem of direct conversion of heat to electricity, the solution of which is expected to come about from the application of magneto-gasdynamic phenomena. MHD generators, just as ordinary electrical machines, embody the principle of electromagnetic induction during motion of low-temperature electrically conducting plasma ($T°C \simeq 2000$-3000) through a transverse magnetic field, but have appreciable advantages over the common electrical machines, in that they can deliver high power at higher efficiencies. In the future they could be used as the primary power sources for interplanetary, air, overwater and underwater propulsion systems.

There also are many other interesting applications of interaction of a plasma with a magnetic field for purposes of solving important engineering problems. These include atmospheric reentry of intercontinental ballistic missiles, development of plasma jet engines, and so forth.

Recently, that area of MHD which is concerned with the interaction of plasma with a magnetic field has acquired the frequently used name of magnetoplasmadynamics.

Various engineering applications of magnetoplasmadynamics have been widely discussed in Soviet and foreign publications. Many international symposia, conferences and meetings of various societies were devoted to these problems.

Along with the extremely important problems of magnetoplasmadynamics, the research and development of MHD devices employing conducting liquids (liquid metals, electrolytes, sea water) has also become very important. Individual units employing this phenomenon are already in practical use. These devices are most advantageous in nuclear power engineering.

Conversion of nuclear into thermal energy in an atomic reactor, with removal of the generated heat by a carrier fluid [coolant] and its transfer in a heat exchanger to a third fluid is now the basic mode of operation of nuclear power installations. Among the most important coolants are liquid metals, which permit the use of efficient, low-pressure circulation systems. Such circulation loops could also employ MHD devices (electromagnetic pumps, low-power MHD generators, magnetic flowmeters, etc.).

The advantages of the various MHD devices over their corresponding mechanical and electromechanical equivalents are the absence of rotating parts, complete airtightness, noiseless operation, compactness, as well as simplicity of design and of operation. These advantages become particularly valuable when MHD devices are contemplated for use in future marine nuclear power plants in conjunction with liquid metal coolants.

Since sea water is a conducting medium, ships could also use MHD propulsion and many special measuring devices (electromagnetic logs, sea current velocity meters, etc.).

Various engineering applications of magnetoplasmadynamics have been widely discussed in Soviet and foreign publications. Many international symposia, conferences and meetings of various societies were devoted to these problems.

Along with the extremely important problems of magnetoplasmadynamics, the research and development of MHD devices employing conducting liquids (liquid metals, electrolytes, sea water) has also become very important. Individual units employing this phenomenon are already in practical use. These devices are most advantageous in nuclear power engineering.

Conversion of nuclear into thermal energy in an atomic reactor, with removal of the generated heat by a carrier fluid [coolant] and its transfer in a heat exchanger to a third fluid is now the basic mode of operation of nuclear power installations. Among the most important coolants are liquid metals, which permit the use of efficient, low-pressure circulation systems. Such circulation loops could also employ MHD devices (electromagnetic pumps, low-power MHD generators, magnetic flowmeters, etc.).

The advantages of the various MHD devices over their corresponding mechanical and electromechanical equivalents are the absence of rotating parts, complete airtightness, noiseless operation, compactness, as well as simplicity of design and of operation. These advantages become particularly valuable when MHD devices are contemplated for use in future marine nuclear power plants in conjunction with liquid metal coolants.

Since sea water is a conducting medium, ships could also use MHD propulsion and many special measuring devices (electromagnetic logs, sea current velocity meters, etc.).

CHAPTER 1

THE DEVELOPMENT AND CURRENT STATE OF MAGNETOHYDRODYNAMICS

The creation of magnetohydrodynamics of conducting liquids as an independent branch of science must be related to the publication, in 1937, of a theoretical paper of J. Hartmann [1] and of experimental results of J. Hartmann and F. Lazarus, although isolated empirical facts were known much earlier. It should be noted that the first patents for MHD devices were issued even before 1937.

In substance, during the first several years MHD as a science developed independently of the development and patenting of devices operating on the MHD principle. The latter were developed in the context of existing electromagnetic devices, without considering the MHD effects. Recently, however, these devices are being developed and studied with utilization of achievements in MHD.

Given this historical development, it is best to review the development and state of MHD and of its engineering application separately.

1. Magnetohydrodynamics

Major Theoretical Results

In his theoretical study [1] J. Hartmann was the first to present the theory of laminar flow of an incompressible conducting liquid in a long flat channel in the presence of a transverse magnetic field perpendicular to the larger side of the channel. He also deserves the credit of discovering a dimensionless ratio describing the effect of the magnetic field on the flow of the conducting liquid. This ratio is now called the Hartmann number.

Hartmann found that a transverse magnetic field has an appreciable effect on the laminar flow of the conducting fluid in a flat (i.e. rectangular) channel, flattening the velocity distribution in the flow core and increasing its gradient at the wall. This produced a higher friction factor in the flow. Hartmann's solution is presented in a number of books [2-5]. Subsequently, all the possible versions of this problem were examined [6-9].

The transverse dimensions of real MHD channels are limited. But the ratio of dimensions of the sides in a rectangular channel can be arbitrary. This made it necessary to analyze the problem of laminar flow of a conducting liquid in an MHD channel in a broader context [10-12].

Certain special problems involving laminar flows of conducting liquids in long, rectangular MHD channels with an arbitrary ratio of sides were studied by D. Shercliff [13], Ya. S. Uflyand [14] and G. A. Grinberg [15, 16].

Shercliff and Uflyand analyzed the idealized problem, assuming that all the walls of the channel are ideal insulators and ideal conductors, respectively. These studies determined the effect of the side walls on the local and overall flow variables. In addition, it was found that at large Hartmann numbers, the properties of boundary layers on channel walls perpendicular and parallel to the magnetic field are different. Similar problems were also examined in [17, 18]. Analysis of these solutions at the limit are presented in [19, 20].

The laminar flow of a conducting liquid in MHD channels containing electrodes (a case approaching reality) was analyzed by G. A. Grinberg [15, 16]. However, it is quite difficult to use the results obtained by him in engineering applications. The attempts to improve Grinberg's solution so far did not succeed [21]. The approximate solution for this problem should also be rechecked [22].

The effect of the side walls on the variables of laminar flow of a conducting liquid in flat MHD channels of finite width was taken approximately into account in [23]. A method for calculating the friction factor in a flow of conducting fluid through a rectangular MHD channel with an arbitrary ratio of sides and lateral electrodes is presented in [24].

The problem of laminar flow of a conducting liquid in round MHD channels with differing wall conductivities was analyzed in its exact and approximate statements in [25-31]. It was found that at high Hartmann numbers the flow is not axisymmetric, and that the friction factor always increases with the magnetic field, being higher than in ordinary fluid flow.

Laminar MHD flow in more complex channels (elliptical cross section, diverging duct, etc.) is analyzed in [32-34].

All the aforementioned theoretical studies pertain to infinitely long channels. The length of real MHD channels is finite, so that it becomes important to study the simultaneous effect of the channel walls and of the magnetic field on the reshaping of the inlet velocity distribution. As in normal fluid flow, it is still impossible to solve such problems exactly.

Most of the studies of flow development published so far pertain to flow in flat channels. For a flat (i.e., rectangular) channel with dielectric walls situated in a transverse magnetic field, this problem was solved by four methods: the linearization method [35], the method of overall relationships [36], Schlichting's method [37], and numerical integration of the boundary layer equations over the entire flow [38]. The results, which agree quantitatively fairly well, showed that the magnetic field decreases appreciably the length of the inlet-effect section (by comparison with the equivalent length in common fluid flow channels).

Among other problems of laminar MHD flow, those concerning the flow of a conducting liquid past solids in the presence of a transverse magnetic field are also of interest.

One of the first such problems was that of flow over a plate [39]. After that, solutions were found for the flow of conducting liquids around bodies of various shapes (wedge, sphere, cylinder, etc.) [40-42]. These solutions showed that the transverse magnetic field exerts an appreciable effect on the flow resistance of these bodies and on the nature of the laminar flow around them.

The magnetic field affects the flow stability by reshaping the velocity distribution in the liquid and suppressing turbulent pulsations. This was first noted by Hartmann and Lazarus in experiments with mercury, and prompted subsequent theoretical analysis of the phenomenon.

Theoretical studies on the stability of MHD flow in flat channels at various orientations of the magnetic field and at various values of flow variables were done by D. Stuart [43], R. Lock [44] and Ye. P. Velikhov [45]. In [46], Lock's results were generalized to include moderate magnetic Reynolds numbers. The problem of stability of flow of conducting liquid over a plate in the presence of a transverse magnetic field was solved by V. N. Arkhipov [47].

The above studies showed that the magnetic field stabilizes the laminar MHD flow by increasing the critical value of the Reynolds number. The stabilizing effect of the transverse magnetic field is much stronger than that of a longitudinal field.

Subsequently, the stabilizing effect of a transverse magnetic field on Couette flow was also investigated [48, 49]. In this case, there is a deformation of the velocity profile, accompanied by the formation of an inflection point, so that the stabilizing effect of the magnetic field is much smaller.

One of the most complex applied MHD problems is the effect of the magnetic field on the turbulent flow of a conducting liquid. Attempts to elucidate the mechanism of MHD turbulence were made by D. Batchelor [50] and S. Chandrasekhar [51] via extension of the statistical theory of turbulence to MHD flow. Unfortunately, at its present level, this application of the theory is even less developed than its application to common fluid flow, so that it cannot be used for solving engineering problems.

A semiempirical theory of turbulent flow of conducting liquid in a flat channel in the presence of a transverse magnetic field was first developed by L. Harris [52] who, using MHD equations, dimensional analysis and some experimental data, showed that in this case the velocity distribution over the channel cross section can be represented by a known logarithmic relationship, supplemented by a function of the magnetic field. Harris has also obtained an expression for the friction factor.

A general expression for the velocity distribution in turbulent flow of a conducting liquid in a flat channel of finite width and in the presence of a transverse magnetic field was obtained in [53]. This paper also gave a semiempirical relationship for the friction factor. A simpler model of turbulent MHD channel flow was considered in [54].

A phenomenological attempt to analyze the transition zone between laminar and turbulent liquid flow in MHD channels is given in [55]. However, the basic assumptions of that study contradict physical concepts and run counter to experimental results.

References [56-59] examine the effect of a longitudinal magnetic field on the turbulent flow of conducting liquids in channels. They show that a magnetic field superposed on a turbulent flow decreases the pulsation energy. When the magnetic field is

longitudinal, this decreases flow resistance. Unlike the longitudinal, the transverse magnetic field flattens the velocity profile, increasing the velocity gradient at the walls, which should increase the friction factor. The overall effect depends on the specific flow variables.

A study of the effect of a transverse magnetic field on the turbulent flow of conducting liquid over a plate is considered in [60]. A similar problem for a longitudinal magnetic field was examined in [61]. The results are in agreement with data of similar studies for channel flows.

In addition to the above major theoretical studies of flow of conducting liquid in channels and about bodies in a constant magnetic field, many exact and approximate solutions for various complex problems, such as those of flows of conducting liquids in MHD channels with permeable boundaries [62], of the effect of magnetic field on heat transfer [63-65], unsteady flow in magnetic fields [66-67], etc., appeared in the past few years. These studies are reviewed by S.A. Regirer [78].

Dimensional and similitude analyses of MHD flows of conducting liquids were developed by I.M. Kirko [79] and I.L. Povkh [80], respectively.

A special class of problems of practical importance is related to flows of conducting liquids in variable magnetic fields. Exact solutions for these problems have not yet been found even for the case of laminar flow: all the available approximate solutions involve the use of linearized equations employing time-averaged flow variables, neglecting important nonlinear effects [78].

The major theoretical results examined above show that the effect of a constant magnetic field on the flow of viscous incompressible conducting fluids in channels and past bodies is already fairly well known. These results can be used in practical design of various MHD devices. However, many of these results must be experimentally verified. Experimental studies at the present stage of development are of decisive importance.

Experimental Studies

The number of experimental studies devoted to the flow of viscous, incompressible conducting fluid in a magnetic field is relatively small. It is usually assumed that the first of these is that of Hartmann and Lazarus [81], even though isolated experimental results were published prior to theirs [82].

Hartmann and Lazarus [81] studied the flow of mercury in rectangular and round channels of small diameter, with a constant transverse magnetic field applied to the flow. They measured the pressure drop in the "active" part of the channel and the average mercury velocity. The results thus obtained supported Hartmann's theoretical assumption [1] that the friction factor in a laminar channel flow increases upon application of a transverse magnetic field. These experiments also demonstrated the stabilizing effect of the magnetic field, which has lead the authors to the conclusion that turbulent pulsations are damped by that field.

These experiments, done in channels of small cross section, involved primarily low Hartmann and Reynolds numbers.

In 1953 W. Murgatroyd published results obtained in experimental studies of the flow of mercury in a rectangular channel with a side ratio of 1:15 in the presence of a transverse magnetic field [83]. The transverse dimensions of this channel were much greater than of those used by Hartmann and Lazarus, so that the range of Reynolds and Hartmann numbers was also much greater.

Murgatroyd confirmed Hartmann's theory for laminar MHD flow in rectangular channels at large Hartmann numbers, and suggested an empirical formula for the critical Reynolds number, characterizing the transition from laminar to turbulent flow. In turbulent MHD mercury flow he observed. depending on the specific flow parameters, either an increase or decrease of friction factor over its value in common fluid flow.

Effects which agreed qualitatively with those described above were observed by B. Lehnert in 1952 in his study of flow of mercury between two coaxial cylinders under a transverse magnetic field [84].

The Hartmann and Lazarus experiments in round channels were continued by D. Shercliff (1956) at high Hartmann numbers [85]. Other qualitative studies on MHD flows in round channels were performed by Grausse and Poirier [86].

In 1959 Globe reported on the effect of longitudinal magnetic flux on the mercury flow in a round tube [87]. He found that at any given Reynolds number in turbulent flow there is a monotonic decrease of friction factor with increasing magnetic field density. This clearly illustrates the effect of damping of turbulent pulsations by a magnetic field.

From 1960 on, the number of published experimental studies on the effect of magnetic field on the flow of conducting liquids started to increase.

Of considerable interest is a series of experiments performed in the Institute of Physics of the Latvian SSR under the leadership of I. M. Kirko. These experiments solved some major problems of applied MHD, i.e., of flow of liquid metals in channels and flow past bodies in the presence of a transverse magnetic field [88-99]. Many interesting experiments were done with electrolytes [100]. The effect of the transverse magnetic field on the friction factor in the flow of liquid metal was studied primarily in flat channels [95, 96, 98]. These studies supplemented previously available experimental data. In addition, O. A. Liyelausis and G. G. Branover used their own experimental data to refine Murgatroyd's empirical formula for the critical Reynolds number at low Hartmann numbers [90, 95].

Murgatroyd's experimental data were somewhat extended toward higher Reynolds numbers by E. C. Bronillette and P. S. Lykoudis [101].

All the above studies dealt with an overall parameter (friction factor) of magnetohydrodynamic channel flows. However there is also undoubted interest in experimental study of local flow variables, in order to observe directly the effect of electromagnetic forces on the flow structure.

The first velocity distributions in channel flow of liquid metals were measured at the Physics Institute of the Latvian Academy of Sciences [97, 98]. The first experiments were done on an open ring channel (a circular trough) but centrifugal forces interfered with clear determination of the effect of the transverse magnetic field on the deformation of the velocity profile. A second series of experiments was performed with mercury flowing in a straight channel with a free surface (open channel). The velocity profile

flattening with increasing Hartmann number became clearly evident, but because the experimental channels were small, the results of these studies are primarily qualitative.

Along with study of MHD channel flows, experiments were performed on flow of conducting liquids past solids in the presence of magnetic and external electric fields. These problems are of great practical interest, because they afford an approach to boundary-layer control, control of local resistances by magnetic fields, etc.

Among studies on these topics one must note the Grausse and Cachon [102] experiments on the effect of magnetic and electric fields on the flow of an electrolyte past a cylinder. These authors produced superb photographs which illustrate changes in the boundary layer as a function of the electric current flowing through the electrolyte. Experimental results of similar nature were also published in [100].

These studies show that the field of electromagnetic ponderomotive forces produced by interaction between directly applied (by conduction) electric fields and superposed magnetic fields can be used for controlling the boundary layer in the flow of a weakly-conducting liquid past bodies. This is a relatively promising approach for reducing drag of bodies in sea water. Some data on this reduction were obtained by I. L. Kuznetsov [103].

A series of experimental studies was devoted to the effect of a transverse magnetic field on the flow of liquid metal past bodies [93, 99, 104, 105]. In this case the boundary layer is controlled by the field of ponderomotive electromagnetic forces produced by the interaction of currents induced in the fluid with an applied magnetic field. Results with mercury flowing past a plate, a cylinder, or a sphere show that a transverse magnetic field increases the drag of these bodies, and that the degree of this increase depends appreciably on the conductivity of these bodies. In the case of blunt bodies, the magnetic field shifts the point of boundary layer separation downstream.

Experiments of the effect of surface roughness on the friction factor for mercury flow in channels [96, 98] show that, as in common fluid flow, roughness has an appreciable effect on the flow.

Recent studies show more careful preparation of experiments, encompass a greater range of flow variables, use other liquid metals, etc.

In 1963 N. M. Turchin published experimental data on the effect of a transverse magnetic field on pressure drop in the flow of a Na-K alloy in round steel and copper pipes at high Hartmann numbers [106]. The conductivity of walls in this case produced an electromagnetic pressure drop in addition to the fluid-flow drop. These two types of drop were not separated. Similar studies with a Na-K alloy were performed in square stainless steel channels in 1964 [107].

In 1965 D. S. Kovner and Ye. Yu. Krasil'nikov studied the effect of a longitudinal magnetic field on the flow of liquid gallium in a round pipe [108]. They have used larger Reynolds and Hartmann numbers than Globe (see above). Similar studies for mercury were performed by L. G. Genin and V. G. Zhilin [109].

A. I. Khozhainov studied the effect of a transverse magnetic field on the friction factor for mercury flow in rectangular channels (side ratio of 1:2.5) and in round pipes [110, 111]. These experiments were performed over a wide range of flow variables and small Reynolds number increments.

In 1965 P. S. Lykoudis, in his report to the Moscow International Symposium on the Properties and Utilization of Low-Temperature Plasma [112], presented data on mercury flow in an MHD channel (side ratio of 1:5) at high Hartmann numbers. In addition to data on the overall flow variable, i.e., the friction factor, the report gave experimental velocity distributions in the plane parallel to the magnetic field.

Interesting studies of the effect of a transverse magnetic field on the turbulence of electrolyte flow were performed by investigators at the Donetsk Research Institute of Ferrous Metals under the leadership of I. L. Povkh [113]. Using an induction anemometer, they measured the intensity distribution of longitudinal and transverse turbulence in 30% sulfuric acid flowing through a magnetic field; these measurements directly verified the damping of turbulent velocity pulsations by the field.

In conclusion, we should note studies on the effect of the transverse magnetic field on the unsteady flow of liquid metal in channels, which showed that, all other conditions being equal, the magnetic field effect reduces to decrease the transition flow mode.

The experimental studies mentioned have verified many theoretical results. However, they do not suffice for constructing semiempirical theories of turbulent MHD flows. This is true most of all of measurements of local flow variables.

2. Magnetohydrodynamic Devices

The idea of measuring the velocity of a fluid flowing through a magnetic field by means of the emf induced in it is due to M. Faraday [116]. Subsequently, this idea was used in the design of various meters.

In 1917 a device based on the electromagnetic induction phenomenon, was patented for measuring the speed of ships [117]. However, electromagnetic logs have come into use only during the past few years.

After M. Dolivo-Dobrovol'skiy has invented the three-phase system and asynchronous motors, L. Chubb in 1915 suggested the use of traveling and rotating magnetic fields for moving liquid metal and, in his patent application [118] in particular, has given a description of a volute-type induction pump.

The first real dc electromagnetic pump was designed by J. Hartmann in 1918, and was used for pumping mercury in an experimental loop.

In 1927, P. Ye. Tryapitsin patented an electromagnetic induction pump [119] in which he utilized the interaction of currents induced in a liquid metal with the magnetic field. A similar patent was issued in 1931 to A. Einstein and L. Szillard [120].

The first designs of magnetic flowmeters also started to appear at that time. In 1930 E. J. Williams described a constant magnetic field magnetic flowmeter for liquids and demonstrated its operation on aqueous copper sulfate, as well as mercury [121]. In 1934 magnetic flowmeters came into use for measuring blood circulation rates; this preceded by approximately 15 years the industrial use of such instruments.

During the next few years, there were many suggestions for the use of electromagnetic pumps and magnetic flowmeters in various industries [122, 123]. However,

the greatest development of MHD devices was contemporaneous with the birth of the nuclear power industry. During these years the technology of electromagnetic liquid metal transport and the study of its flow made great strides.

First reports on the use of electromagnetic pumps and magnetic flowmeters in experimental atomic power plants employing liquid metal coolants appeared in the beginning of the fifties [124-128].

In the U.S., the design and development of electromagnetic pumps for liquid metals was concentrated in three laboratories (Argonne National Laboratory. Oak Ridge National Laboratory and the National Laboratory), which later cooperated with many private firms. In England production of electromagnetic pumps was started by four companies (English Electric, British Thomson-Houston, Palatine Tool and Engineering Co., and Campbell and Isherwood).

Experimental working characteristics of the first electromagnetic pumps for liquid metals are presented in [127].

The following firms had under development magnetic flowmeters for media with a variety of conductivities: Alto (Holland), SNECMA (France), Eckart (West Germany), Foxboro (USA), Foxboro-Wauxhall (England), etc.

In the USSR, much R & D work on electromagnetic pumps was done by the Institute of Physics of the Latvian Academy of Sciences, by the IPL of the Ukrainian SSR Academy of Sciences, and by the Tallin, Leningrad and Donets Polytechnic Institutes. The first Soviet-made flowmeters were developed by the Institute of Automation and Remote Control of the Academy of Sciences of the USSR for experimental purposes [129, 130]. The first industrial models were produced by the Heat Instruments Research Institute [131-133]: their large-scale production was subsequently undertaken by the instrument-making industry.

The USSR experience of operating magnetic flowmeters in liquid metal loops was reported to the 2nd International Conference on Peaceful Uses of Atomic Energy in Geneva in 1958 [134, 135].

At the same time MHD meters for measuring ocean-current velocities were developed [136-138].

The theory of magnetic flowmeters and of electromagnetic pumps has developed rapidly during the fifties. While the first theoretical studies dealt only with electrical engineering problems, subsequently the theoretical problems were solved with consideration on the MHD effects.

The theory of magnetic flowmeters was developed by A. Kolin, D. Shercliff, L.M. Korsunskiy, and others [139-154].

The theory of electromagnetic pumps was developed abroad by A.H. Barnes, L.R. Blake, D.A. Watt and others [155-161], and in the USSR by A.I. Vol'dek [162-167], I.M. Kirko [168, 169], I.A. Tyutin [170-172], N.M. Ohremenko [173-177], Yu.A. Birzvalk [178-181], Ya.Ya. Livelpeter [182-184], Kh.I. Yanes [185-187] and others [188-196].

Many studies on experimental electromagnetic pumps appeared at that time [197-208].

Development of the theory of MHD devices, together with the accumulated experience in running them in experimental setups produced better design techniques, as well as improvements in engineering and operating characteristics. This in turn promoted the use of MHD devices by various industries, and in particular, in marine engineering.

In 1958 the American nuclear submarine Nautilus, on the first passage over the North Pole during the voyage from the Pacific to the Atlantic Oceans, successfully measured the vessel's speed by means of an electromagnetic log [147]. The second American nuclear submarine Seawolf used a powerful electromagnetic pump for pumping the liquid metal coolant [147].

There are many suggestions for meters for incompressible conducting fluids [147] and for composite devices which employ electromagnetic pumps and magnetic flowmeters. In particular, a magnetic flowmeter is used for measuring the density and temperature of liquids [147]. Miniature electromagnetic pumps are used in pressure measuring devices [87] and in new types of relays [209, 210].

There is great promise for MHD bearings of high load-bearing capacity [211, 212].

The operating principles and designs of various MHD devices, as well as their experimental characteristics are described in [213-217].

In the beginning of the sixties, consideration was given to the use of liquid metals in MHD conversion of thermal into electric energy. The use of liquid metal as the working fluid in MHD generators (instead of plasma) makes it possible to reduce the upper temperatures of the cycle and to develop a more compact power plant, which is particularly important for transport units employing nuclear reactors.

The basic part of such a unit employing an MHD generator is the converter which transforms the heat from the reactor into the kinetic energy of the liquid metal. This can be done, in theory, by using a two-phase nozzle with the flow of two different metals, one which is in the liquid and the other in the vapor phase. This scheme was described by D. Elliot in 1961 [218].

The above work by Elliot provided the impetus in developing liquid metal units for transport power plants. This is shown by a large number of publications dealing with studies of liquid metal MHD generators proper [219-223], as well as with possible schemes of liquid metal power units [224-240].

Lately, special attention is devoted to the design of marine MHD engines, since they have a number of advantages over the presently used marine screws; these include direct use of the ship's electrical power for propulsion, reducing the vibrations level and the hydrodynamic noise, using the energy of extremely high-power MHD generators for obtaining high propulsion velocities, etc.

The first engines, using ordinary magnetic systems, were found to be inefficient for high-speed submarine propulsion [241]. Later other suggestions appeared on the design of MHD marine engines [242-244], of which the version of a marine MHD power plant employing superconducting magnets was found to be most interesting [244]. The high efficiency of this device at high submarine speeds makes it possible to regard this engine as promising, although its practical realization requires the solution of many complex scientific and engineering problems.

CHAPTER 2

MAGNETOHYDRODYNAMIC EFFECTS

When a conducting fluid flows through a transverse magnetic field, the electromagnetic induction produces electromotive forces and currents in this fluid: the density vector of these currents j_{ind}, is perpendicular to the velocity v and the magnetic flux density vector B (Fig. 1).

The interaction between the currents in the fluid and the applied magnetic field results in appearance in the flow of electromagnetic ponderomotive forces f_{ind} which affect the flow structure. This effect is in general characterized by changes in the local and overall laminar and turbulent flow variables, as well as in the flow stability.

When a potential difference is externally applied to a conducting fluid at rest, and a transverse magnetic field is imposed on it, the liquid is set into motion by the conductive electromagnetic ponderomotive forces f_c. In addition, a field of electromagnetic forces f_{ind} is induced in the flow, and these forces, as in the first case, affect the flow structure.

By varying the electromagnetic field distribution, one can affect the entire liquid or its individual layers.

We shall say that the effect of the electromagnetic field on the flow of a conducting fluid is an MHD effect of the first kind.

Under certain conditions, a conducting fluid can affect the externally applied electric and magnetic fields. This phenomenon characterizes the fluid's reaction, which is similar to the reaction of the armature in electric machines.

If weakly conducting fluids flow through a transverse magnetic field, the induced ponderomotive forces may be so low as to leave the flow structure virtually nonaffected; however, the nonuniform distribution of local flow variables will result in a nonuniform distribution of the induced emf and currents in the flow. We shall say that this is an MHD effect of the second kind.

Obviously, MHD effects of the first kind are always accompanied by effects of the second kind. The extent to which these effects manifest themselves depends on the characteristic criteria, which can be found from the equations of magnetohydrodynamics.

1. Characteristic Criteria of Magnetohydrodynamic Flows and Physical Properties of Conducting Fluids

Magnetohydrodynamic processes are described by a system of simultaneous equations of hydro- and electrodynamics. Here the hydrodynamic (fluid flow) equations take into account the force of interaction between the electric current and the magnetic field (f) while the equations of electrodynamics make use of the local velocity of the conducting fluid.

The Navier-Stokes and continuity equations for viscous, incompressible conducting fluid are respectively written as

Fig. 1. An element of a conducting fluid moving through a magnetic field.

KEY: 1) c. 2) ind.

$$\varrho \left[\frac{\partial v}{\partial t} + (v\nabla)v \right] = -\nabla p + \eta \Delta v + [J \times B]; \tag{2.1}$$

$$\operatorname{div} v = 0, \tag{2.2}$$

where p is the pressure in the fluid.

The interaction of electric charges with the electric and magnetic field is usually neglected as are the magnetostatic forces, since these are small as compared with the force $f = [j \times B]$.

The basic equations of electrodynamics for slow moving (as compared with the speed of light) isotropic media are

$$J = \frac{1}{\mu} \operatorname{rot} B; \tag{2.3}$$

$$\operatorname{curl} \quad \operatorname{rot} E = -\frac{\partial B}{\partial t}; \tag{2.4}$$

$$\operatorname{div} B = 0; \tag{2.5}$$

$$J = \sigma [E + [v \times B]], \tag{2.6}$$

where E is the vector of the electric field strength.

Since the fluids which one encounters in magnetohydrodynamics have relatively high electrical conductivities, displacement and convection currents can be neglected.
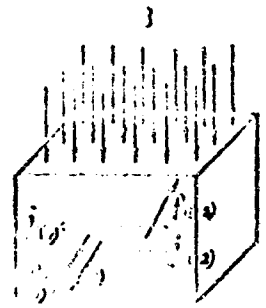
11

Equation (2.1) is regarded as the first basic equation of magnetohydrodynamics. From Eqs. (2.3), (2.4) and (2.6) we get a second basic equation, which is frequently called the induction equation:

$$\frac{\partial B}{\partial t} = \text{curl}\ [v \times B] + \frac{1}{\mu\sigma}\Delta B. \tag{2.7}$$

The physical variables of the fluids, i.e., ρ (density), η (viscosity) and σ (electrical conductivity) are treated as independent of the electric and magnetic field strengths. The fluid is regarded as nonmagnetic and the magnetic permeability μ is assumed equal to the permeability of vacuum ($\mu \simeq 1.257 \cdot 10^{-6}$ henry/m).

The effect of an electromagnetic field on the hydrodynamic system is also manifested by dissipation of Joule heat. In this case the energy equation, which is a part of the system of hydrodynamic equations, is supplemented by a term for the heat released per unit time.

For incompressible conducting fluids operating over a relatively moderate temperature range, over which the temperature-dependent variations in the physical variables of the fluid can be neglected, the energy equation is written as

$$c\rho\left(\frac{\partial T}{\partial t} + v\nabla T\right) = \text{div}\,(\varkappa\nabla T) + \frac{j^2}{\sigma} + W_{fr}, \tag{2.8}$$

where $\frac{j^2}{\sigma}$ is the power used up as Joule heat; c_p and $\varkappa$ are the specific heat and thermal conductivity of the fluid, and $W_{fr} = \frac{1}{2}\eta \sum_{i,k}\left(\frac{\partial v_i}{\partial x_k} + \frac{\partial v_k}{\partial x_i}\right)^2$ is a term expressing the work done by frictional forces.

In solving problems of flow of incompressible fluids in electromagnetic fields we employ the equation system (2.1)-(2.7) without the energy equation.

The assumption about incompressibility of liquids is valid provided that they move at velocities much below the speed of sound.

Table 1 presents data on the propagation of sound in liquid metals, electrolytes and sea water [245, 246]. It should be noted that the speed of sound in sea water initially drops off slightly with depth and in particular, is 1460 m/sec at a depth of 1200 m [246], wherefrom it starts increasing.

The speed of sound in a conducting fluid flowing through a strong magnetic field which is perpendicular to the direction of sound waves increases somewhat, and is a function of the conductivity of the fluid [247].

No effect of the electric field on the speed of sound in various fluids was discovered [248]. The effect discovered by Nolle [249] was found to be due to Joule heating [245].

The data of Table 1 show that in all practical cases liquids can be treated as incompressible.

Table 1. Speed of Sound in Conducting Fluids

Fluid	T. °C	a, m/sec
Bismuth	271	1635
Gallium	29.5	2740
Potassium	64	1820
Sodium	98	2395
Tin	232	2270
Mercury	50	1440
Rubidium	39	1260
Lead	327	1635
Cesium	28.5	967
Hydrochloric acid	15.5	1520
Sodium chloride (c = 20%)	15	1650
Sea water	15	1520

To analyze the MHD equations and to find the features accompanying the manifestation of MHD effects, these equations must be reduced to dimensionless form.

We introduce the following dimensionless quantities

$$\bar{v} = \frac{v}{v_0}; \quad \bar{l} = \frac{l v_0}{R_0}; \quad \bar{p} = \frac{p}{\rho v_0^2};$$

$$\bar{B} = \frac{B}{B_0}; \quad \bar{E} = \frac{E}{v_0 B_0};$$

$$\bar{j} = \frac{j}{\sigma v_0 B_0}; \quad \bar{T} = \frac{T}{T_0}; \quad \bar{\nabla} = \nabla R_0,$$

where v_0, R_0, B_0 and T_0 are the characteristic velocity, linear dimension, magnetic flux density, and temperature.

When these quantities are substituted into Eqs. (2.1)–(2.8), we obtain the dimensionless magnetohydrodynamic equations

$$\frac{\partial \bar{v}}{\partial t} + (\bar{v} \bar{\nabla}) \bar{v} = -\bar{\nabla} \bar{p} + \frac{1}{Re} \Lambda \bar{v} + \frac{M^2}{Re} \{[\bar{v} \times \bar{B}] \times \bar{B}\} + \frac{M^2}{Re} [\bar{E} \times \bar{B}]; \qquad (2.9)$$

$$\frac{\partial \bar{B}}{\partial t} = \frac{1}{R_m} \Delta \bar{B} + \text{curl} \ (\bar{v} \times \bar{B}); \qquad (2.10)$$

$$\bar{j} = \frac{1}{R_m} \text{curl} \ \bar{H}; \qquad (2.11)$$

$$\text{curl} \ \bar{E} = -\frac{\partial \bar{B}}{\partial t}; \qquad (2.12)$$

$$\bar{j} = \{\bar{E} + [\bar{v} \times \bar{B}]\}; \qquad (2.13)$$

$$\overline{\text{div}} \, \bar{v} = 0; \qquad (2.14)$$

$$\operatorname{div} \vec{B} = 0; \qquad (2.15)$$

$$\left(\frac{\partial T}{\partial t} + \vec{v}\nabla T \right) = \frac{1}{Re \, Pr} \Delta T + \frac{M^2 Re_m}{\theta} j^2 + \frac{Re}{\theta} W_{v}. \qquad (2.16)$$

Here $Re = \frac{\rho R_0 v_0}{\eta}$ is the fluid-flow Reynolds number; $R_m = \mu \sigma R_0 v_0$ is the magnetic Reynolds number; $M = R_0 B_0 \sqrt{\frac{\sigma}{\eta}}$ is the Hartmann number; $Pr = \frac{\eta c_p}{\varkappa}$ is the Prandtl number; $\theta = \frac{R_0^2 v_0^2 c_p T_0}{\eta^2}$ is a dimensionless temperature term.

Analysis of dimensionless MHD equations shows that MHD flows are described by three dimensionless ratios: Re, Re_m and M.

As is known, the hydrodynamic (fluid flow) Reynolds number is the ratio of the convective inertia forces to the viscosity forces. The magnetic Reynolds number describes the drag of magnetic lines of force on the conducting fluid moving in the magnetic field. If, by analogy with kinematic viscosity ν, we introduce the so-called magnetic viscosity $\nu_m = 1/\mu\sigma$, then the magnetic Reynolds number takes on the form similar to that of hydrodynamic Reynolds number.

On the cosmic scale, the magnetic Reynolds number may reach very high values and the drag effect of magnetic lines of forces on the moving medium shows up quite strongly. For MHD flows of weakly conducting fluids (electrolytes, sea water) R_m is always much less than unity, i.e., there is no coupling between the magnetic field and the conducting fluid. In high velocity liquid metal flows, the magnetic Reynolds number can be greater than 1.

The force produced by interaction between induced currents and the applied magnetic field and acting on a unit volume of the conducting fluid is of the order of $\sigma v_0 B_0^2$, while the force due to ordinary viscosity is of the order of $\eta \frac{v_0}{R_0^2}$. The ratio of these forces is expressed by the Hartmann number.

When M < 1, the magnetic field has virtually no effect on the motion of the conducting fluid, which will be approximately the same as in common fluid flow, with the exception that emf's will be induced in the fluid and currents will flow through it. This phenomenon is used for measuring the velocity of fluids with low conductivity, in particular, of sea water.

For liquid metals, we always have M ≫ 1. Here, the magnetic field exerts an appreciable effect on the flow. However, the extent of this effect is also governed by the Reynolds number, and hence the flow of liquid metals in a magnetic field is analyzed in terms of dimensionless groups.

As follows from Eq. (2.9), the measure of effect of the magnetic field on the flow of a conducting fluid is the ratio M^2/Re, which is the ratio of ponderomotive forces to quantity B_0^2/R_0. Sometimes the ratio M^2/Re is called the Stuart number.

14

When $M \gg 1$, but $M^2/Re \ll 1$, the electromagnetic forces are small as compared to inertia forces and the fluid behaves as in the absence of a magnetic field. The magnetic field has a particularly strong effect on the flow when $M \gg 1$ and $M^2/Re \geq 1$.

I. M. Kirko [168-169], using the quantity $\bar{E} = E/E_0$ as the dimensionless electric field strength, obtained as the last term of Eq. (2.9) the dimensionless group MN/Re^2, where $N = \dfrac{F_0 c R_0^2 \sigma^{1/2}}{\eta^{1/2}}$ is a dimensionless ratio, characterizing the electric field strength. This ratio is convenient in analyzing the flow of conducting fluids in ducts of electromagnetic pumps and in certain other cases, when the electric field is externally applied.

By comparison with liquid metals, electrolytes exhibit lower (4-5 orders of magnitude) conductivity.

Due to smallness of M and of M^2/Re, the effect of electromagnetic ponderomotive forces, produced by interaction of the induced currents with the applied magnetic field, can usually be neglected in electrolytes. However, the term reflecting the force produced by externally supplied currents may be appreciable. Hence at small linear dimensions, MHD effects of the first kind are observed in electrolytes only in the case of externally supplied currents.

If, upon substitution of number N into the system of equations for Prandtl's boundary layer, we rewrite the dimensionless equation (2.9) we obtain for the axial velocity component [169]

$$\frac{\partial \bar{v}_z}{\partial t} + \bar{v}_z \frac{\partial \bar{v}_z}{\partial z} + \bar{v}_x \frac{\partial \bar{v}_z}{\partial x} \dots = -\frac{\partial \bar{p}}{\partial z} + \frac{1}{Re}\frac{\partial^2 \bar{v}_z}{\partial x^2} - \frac{M^2}{Re}(\bar{v}_z \bar{B}^2) + \frac{NM}{Re^2}(\bar{E}\bar{B}). \qquad (2.17)$$

Term $\dfrac{\partial^2 \bar{v}_z}{\partial x^2}$ is of the order of $1/\delta^2$, where δ is the boundary layer thickness. When $M = 0$ and $N = 0$,

$$\frac{1}{Re}\frac{\partial^2 \bar{v}_z}{\partial x^2} \approx \frac{1}{Re}\frac{1}{\delta^2} \sim 1, \text{ т. e. } \delta \sim \frac{1}{\sqrt{Re}}.$$

The value and sign of the third term in the right-hand side of Eq. (2.17) depends on the directions of the electric and magnetic fields in the boundary layer.

In flow of liquid metal in a transverse magnetic field and in the absence of an external electric field, M^2/Re can be greater than unity. This means that the boundary layer forms primarily due to the effect of electromagnetic ponderomotive forces induced in the fluid. In our case the current density in the boundary layer will be of the order of $\sigma B_0 U$, since it is produced by a potential difference $\sim B_0 U$. Hence the electromagnetic force acting in the boundary layer (per unit area of the wall surface) is of the order of $\sigma B_0^2 U \delta$, while the viscous friction force is of the order of $\eta U/\delta$. These forces should be of the same order, i.e.,

$$\sigma B_0^2 U \delta \approx \frac{\eta U}{\delta}.$$

whence

$$\delta \approx \frac{1}{B_0}\left(\frac{\eta}{\sigma}\right)^{1/2} \sim \frac{1}{M}; \quad \frac{1}{Re}\cdot\frac{1}{\delta^2} \sim \frac{M^2}{Re}.$$

The ratio M^2/Re is negligibly small in electrolytes. However, the ratio NM/Re^2 may be appreciable, and hence the effect of conductive electromagnetic forces on the boundary layer will be evident.

When the direction of the vector product $[E \times \cdot]$ coincides with that of axis Oz, the fourth term in the right-hand side of Eq. (2.17) will describe the formation of the boundary layer, and its thickness will be defined by the ratio

$$\frac{1}{Re}\cdot\frac{\partial^2 v_r}{\partial x^2} \sim \frac{NM}{Re^2}, \quad \text{т. е. } \delta \sim \sqrt{\frac{Re}{NM}}.$$

The variation in the temperature of a volumetric fluid element is governed by existing convection, thermal conductivity, as well as the Joule heat and dissipation of energy of viscous friction, i.e., by the corresponding terms of Eq. (2.16). It follows from this equation that when $M \gg 1$ one can neglect the temperature variations produced by viscous dissipation because it is much smaller than the Joule heat. In the case of liquid metals, the effect of Joule heat can be controlling if the condition

$$\frac{M^2 Re}{\theta} \geqslant \frac{1}{Re\,Pr}.$$

is satisfied.

Thus, the dimensionless ratios Re, R_m, M, N, Pr and θ and some of their combinations allow one to estimate the influence of MHD effects of the first kind, as well as of the Joule heat, on heat transfer.

Obviously, in order to calculate the dimensionless ratios and groups it is necessary to know the physical characteristics of the conducting fluids, the parameters of the applied magnetic and electric fields, as well as the flow conditions.

Data characterizing physical properties of certain liquid metals and alloys are given in Appendix 1 [170]. Figures 2 and 3 show the conductivities of liquid metals as a function of temperature. Changes in physical properties of electrolytes as a function of concentration and temperature are shown in Figs. 4-8 and in Appendices 2 and 3 [250].

Sea water which has properties close to those of electrolytes, is an aqueous solution of various salts whose concentration fluctuates over a certain range depending on the given sea or on the ocean region. Studies show that even if the total amount of salts changes within wide limits, the relative quantity of ions remains the same in all the seas and in all the ocean regions [246].

Figure 9 shows the conductivity of sea water as a function of the salt concentration at different temperatures [246]. The salt composition in sea water and its viscosity are tabulated in Appendices 4 and 5.

Analysis of the salt composition shows that the physical properties of sea water
are determined primarily by its sodium chloride content. It is usually assumed that a
3-3.5 percent aqueous NaCl solution has properties corresponding to those of sea water.
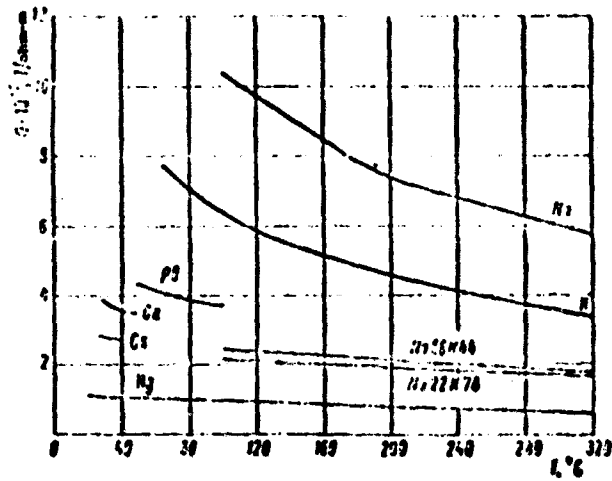

Fig. 2. Conductivity of liquid metals as a func-
tion of temperature in the range $20 \leq T \leq 320°C$.
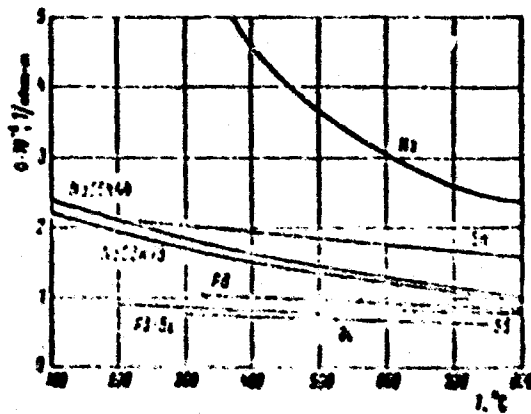

Fig. 3. Conductivity of liquid metals as
a function of temperature in the range
$100 \leq T \leq 800°C$.
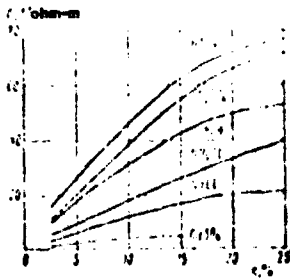
Fig. 4. Conductivity of electrolytes as a function of concentration at $T = 18°C$.
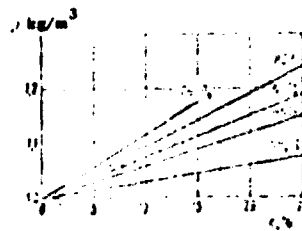
Fig. 5. Density of electrolytes as a function of concentration at $T = 18°C$.
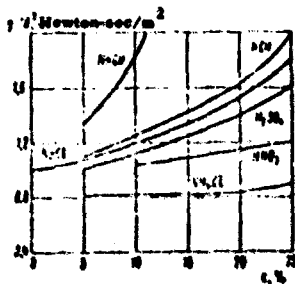
Fig. 6. Dynamic viscosity of electrolytes as a function of concentration.

For NH_4Cl at 30°C; for H_2SO_4 at 25°C; for other electrolytes at 20°C.
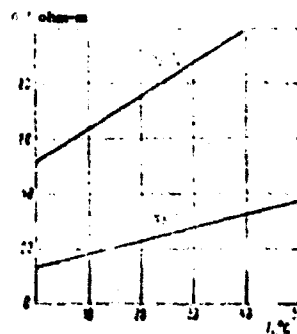
Fig. 7. Conductivities of 30% H_2SO_4 and of saturated aqueous NaCl solutions as a function of temperature.

Fig. 8. Dynamic viscosities of a 20% electrolyte solution as a function of temperature.

Figure 10 shows changes in the sea water characteristics as a function of temperature (c ≈ 3.5%).

The temperature of sea water depends on a number of factors (region, time of year, depth). Figure 12 shows the seasonal variation of temperature with depth in the Atlantic Ocean. The measurements were made in a region to the northeast of the Bahama Islands [251].
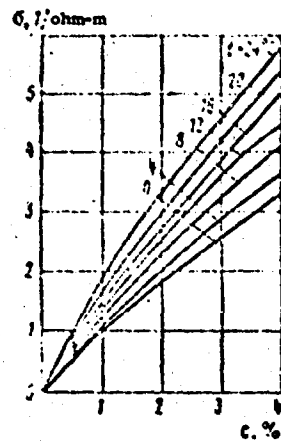
Fig. 9. Conductivity of sea water as a function of salt concentration at different temperatures.
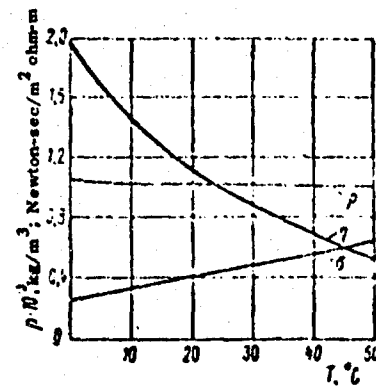
Fig. 10. The physical variables of sea water as a function of temperature.
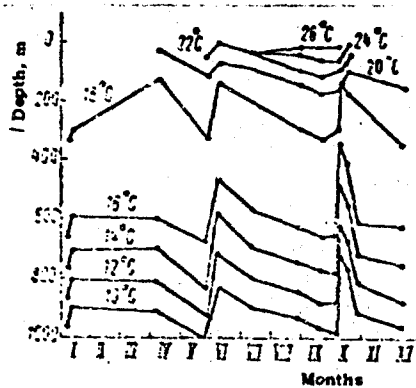
Fig. 11. Annual isotherms of water in the Atlantic Ocean.
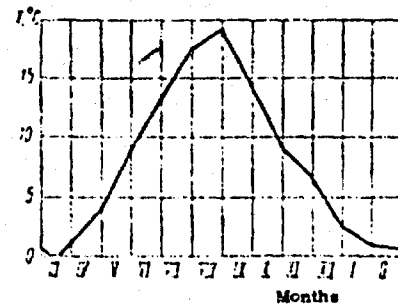
Fig. 12. Annual change in the temperature of surface waters in the Black Sea.

Table 2. Numerical values of dimensionless ratios for certain conducting fluids

| Критерий η	Bi	Na	Na50K50	Pb—Bi	Hg	HNO₃ (c=25%)	NaCl (c=20%)	Морская вода [3]
	при T=300°C					при T=20°C		
$Re = \dfrac{\rho_0 c_0 \Omega}{\eta}$	6.5·10⁴	2.55·10⁴	2.3·10⁴	6·10⁴	8.75·10⁴	9.6·10³	7.52·10³	9.23·10³
$Rm = \mu\sigma R_0 v_0$	2.55·10⁻²	7.55·10⁻²	2.32·10⁻²	1.07·10⁻²	1.33·10⁻²	9.67·10⁻⁷	2.5·10⁻⁷	0.5·10⁻⁷
$M = R_0 B_0 \sqrt{\dfrac{\sigma}{\eta}}$	211	1320	765	222	252	2.54	1.15	0.6
$Pr = \dfrac{\eta c_p}{\chi}$	1.32·10⁻²	0.58·10⁻²	1.176·10⁻²	2.3·10⁻²	2.4·10⁻²	7.23	9.6	7.25
$\theta = \dfrac{\rho_0^2 c_p^2 T_0}{\eta^2}$	6.2·10¹²	3.57·10¹²	9.12·10¹²	5.27·10¹²	10.6·10¹²	2.65·10¹²	2.08·10¹²	3.37·10¹²
$\dfrac{M^2}{Re}$	0.703	63	22	0.823	0.781	0.672·10⁻³	0.176·10⁻³	0.388·10⁻¹
$\dfrac{M^2 Re}{\theta}$	4.8·10⁻⁴	0.52·10⁻²	0.5·10⁻⁴	5.61·10⁻⁴	5.66·10⁻⁴	3.0·10⁻⁹	4.73·10⁻⁹	10⁻⁹
$\dfrac{1}{Re\,Pr}$	1.1·10⁻³	6.59·10⁻³	3.01·10⁻³	0.723·10⁻³	0.476·10⁻³	0.133·10⁻¹	0.133·10⁻¹	0.148·10⁻¹

Жидкая среда [2]

KEY: 1) Dimensionless ratio; 2) liquid medium; 3) sea water; 4) at.

Figure 12 shows the annual change in the temperature of surface waters in the Black Sea.

The above data suffice, when flow variables and electromagnetic field characteristics are known, to determine the dimensionless MHD ratios and to estimate the extent of influence of MHD effects.

Table 2 presents numerical values of dimensionless ratios and groups for various conducting fluids. The calculations were made for the following values of characteristic quantities:

$$x_0 = 0.01 \text{ m}; \quad B_0 = 1 \text{ tesla } (10^4 \text{ c}); \quad v_0 = 1 \text{ m/sec}$$
$$T_0 = 10^3 \text{ C}.$$

2. Laminar Magnetohydrodynamic Channel Flow

For steady flow of conducting fluids in straight cylindrical channels, the magnetohydrodynamic equations become appreciably simplified.
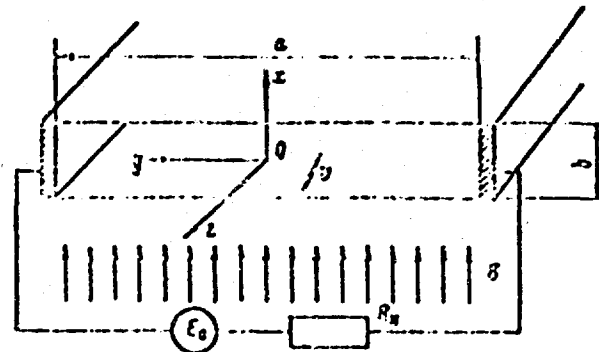
Fig. 13. Schematic of a magnetohydrodynamic channel.

Let us examine steady-state flow of a conducting fluid in a rectangular channel, two walls of which, $x = \pm b/2$, are nonconducting magnet poles, while the two others, $y = \pm a/2$, are well conducting electrodes, closed through an external circuit containing an emf source and a load resistance R_L (Fig. 13).

Using Eqs. (2.2) and (2.5), the first term in the right-hand side of Eq. (2.7) can be represented in the form

$$\text{curl } [v \times B] = (B\nabla) v - (v\nabla) B. \tag{2.18}$$

We shall regard the channel as sufficiently long. In this case we may set $\partial \mathcal{B}/\partial z = 0$, whence

$$(\cdot \nabla) \mathcal{B} = 0, \tag{2.19}$$

which reduces Eq. (2.7) to the form

$$\Delta \mathcal{B} + \ldots (\cdot \nabla) v = 0. \tag{2.20}$$

The last term in Eq. (2.1) can be transformed to

$$[J \times \mathcal{B}] = \frac{1}{\mu} \; \text{curl} \; \mathcal{B} \times \mathcal{B}] = \frac{1}{\mu} \left[(\mathcal{B} \nabla) \mathcal{B} - \frac{1}{2} \nabla |\mathcal{B}|^2 \right]. \tag{2.21}$$

Using Eq. (2.21), the momentum equation is reduced to the form

$$\eta \Delta v + \frac{1}{\mu} (\mathcal{B} \nabla) \mathcal{B} = \nabla p. \tag{2.22}$$

Projections of Eqs. (2.20) and (2.22) onto the channel axis are written as

$$\frac{\partial^2 v_z}{\partial x^2} + \frac{\partial^2 v_z}{\partial y^2} + \frac{1}{\mu \eta} B_0 \frac{\partial B_z}{\partial x} - \frac{1}{\eta} \frac{\partial p}{\partial z} = 0; \tag{2.23}$$

$$\frac{\partial^2 B_z}{\partial x^2} + \frac{\partial^2 B_z}{\partial y^2} + \mu \sigma B_0 \frac{\partial v_z}{\partial x} = 0. \tag{2.24}$$

For nonconducting and ideally conducting channel walls, the boundary conditions for the magnetic field have, correspondingly, the forms

$$\left. \frac{\partial B_z}{\partial s} \right|_s = 0; \tag{2.25}$$

$$\left. \frac{\partial B_z}{\partial n} \right|_s = 0, \tag{2.26}$$

where s and n are the channel's contour and the normal to this contour. These conditions are supplemented by the obvious condition for velocity

$$\left. v_z \right|_s = 0. \tag{2.27}$$

We note that the boundary conditions for the magnetic field follow directly from equations of electrodynamics.

For laminar flow of a conducting fluid, the system of equations (2.23) and (2.24) with boundary conditions (2.25)-(2.27) makes it possible to solve a wide range of problems pertaining to the velocity distribution and to the distribution of electric current density in long MHD channels when the electric field in the flow is nonuniform. When this is done, it becomes possible to separate losses due to viscous friction, including the effect of the magnetic field on such losses.

The simplest problem is that of flow of conducting fluid in flat channels (a ≫ b). It gives a quantitative estimate of the MHD effects on the local and overall flow variables.

In accordance with the assumption of a $\gg$ b, the partial derivatives in Eqs.(2.23)-(2.24) can be replaced by total differentials

$$\frac{d^2 v_z}{dx^2} + \frac{B_0}{\mu\eta}\frac{dB_z}{dx} - \frac{1}{\eta}\frac{dp}{dz} = 0;$$
(2.28)

$$\frac{d^2 B_z}{dx^2} + \mu\sigma B_0\frac{dv_z}{dx} = 0.$$
(2.29)

As a rule, when solving this system of equations one limits itself to the condition [1-5]

$$v_z\big|_{x = \pm\frac{b}{2}} = B_z\big|_{x = \pm\frac{b}{2}} = 0.$$

We shall solve this problem in its most general form. In particular, we assume that the conductivity of channel walls $x = \pm$ b/2 is arbitrary, and that $B_z\big|_{x = \pm\frac{b}{2}} = 0$ s is generally not satisfied.

Integrating Eq. (2.29), we get

$$\frac{dB_z}{dx} + \mu\sigma B_0 v_z + C = 0.$$
(2.30)

By substituting the above expression, Eqs. (2.28)-(2.29) are reduced to a single equation for velocity

$$\frac{d^2 v_z}{dx^2} - \frac{M^2}{b^2}v_z + Q = 0.$$
(2.31)

In Eq. (2.31), the boundary conditions for the magnetic field determine only the constant Q; from this follows the interesting conclusion that the manner in which the velocity of a conducting fluid in flat channels changes does not depend on the conductivity of the walls.

The solution of Eq. (2.31) is given by the function

$$v_z = C_1\,\text{ch}\,\frac{M}{b}x + C_2\,\text{sh}\,\frac{M}{b}x + Q\frac{b^2}{M^2}.$$
(2.32)

The integration constants are determined from the condition of zero velocity at the channel walls

$$C_2 = 0; \quad C_1 = -\frac{Qb^2}{M^2\,\text{ch}\,0.5M}.$$
(2.33)

Using Eq. (2.33), the solution takes the form

$$v_z = \frac{Qb^2}{M^2}\left[1 - \frac{\text{ch}\,\frac{Mx}{b}}{\text{ch}\,0.5M}\right]$$
(2.34)

23

The above expression is conveniently represented in the dimensionless form

$$\frac{v_z}{v_m} = \frac{\operatorname{ch}0.5M - \operatorname{ch}M\frac{x}{b}}{\operatorname{ch}0.5M - 1} \qquad (2.35)$$

$$\frac{v_z}{v_0} = \frac{\left(\operatorname{ch}0.5M - \operatorname{ch}M\frac{x}{b}\right)0.5M}{\operatorname{ch}0.5M(0.5M - \operatorname{th}0.5M)}, \qquad (2.36)$$

where v_m and v_0 are, respectively, the maximum and average flow velocities.

Figure 14 shows velocity distributions constructed from Eqs. (2.35) and (2.36), respectively. The same figures show (by dashed lines) the velocity distribution corresponding to the case when there is no magnetic field. It follows from these graphs that at a constant average velocity, the contribution of the transverse magnetic field reduces to flattening the distribution and increasing the velocity gradient at the channel walls. This last fact increases the viscous friction losses, which is one of the demonstrations of MHD effects.

A more complete examination of these effects requires returning to Eq. (2.34) and clarifying the effect of the magnetic field boundary conditions on the value of Q. For simplicity of analysis, we shall consider flow in the electric-power generation mode ($E_0 = 0$).

Condition $\left.\frac{dB_z}{dy}\right|_{x = \pm\frac{b}{2}} = 0$ points to the fact that along the nonconducting channel

wall $B_z = \text{const}$. The selection of $B_z|_s = 0$ reduces to the requirement that the total current through the channel cross section be zero. This last condition follows directly from integrating Eqs. (2.3) and (2.6) within the limits $\pm 0.5b$. This condition corresponds to the limiting case of operation of an MHD generator, when its electrodes are connected via an infinite load resistance ($R_\ell = \infty$, no-load mode). Here

$$C = -\mu_0 B_0 v_0; \qquad Q = \frac{P}{\eta\ell} \cdot \frac{0.5M}{\operatorname{th}0.5M}, \qquad (2.37)$$

where ℓ is the channel length.

Substituting Eqs. (2.37) into Eq. (2.34), we get

$$v_z = \frac{P b^2}{2\eta\ell M}\left[\frac{\operatorname{ch}0.5M - \operatorname{ch}M\frac{x}{b}}{\operatorname{th}0.5M}\right]. \qquad (2.38)$$

In this case the direct decelerating effect of the magnetic field is absent, i.e., the sum of electromagnetic forces decelerating the fluid is zero.

Figure 15 shows dimensionless velocity distributions ($v\eta\ell/pb^2$) constructed from Eq. (2.38) for different values of $M = \text{const.}$, showing the effect of viscous losses. It is easy to see that in this case the magnetic field effect reduces to slowing down the flow. We note that the velocity gradient at the walls for different $M = \text{const.}$ remains unchanged due to the assumed constant pressure.

24
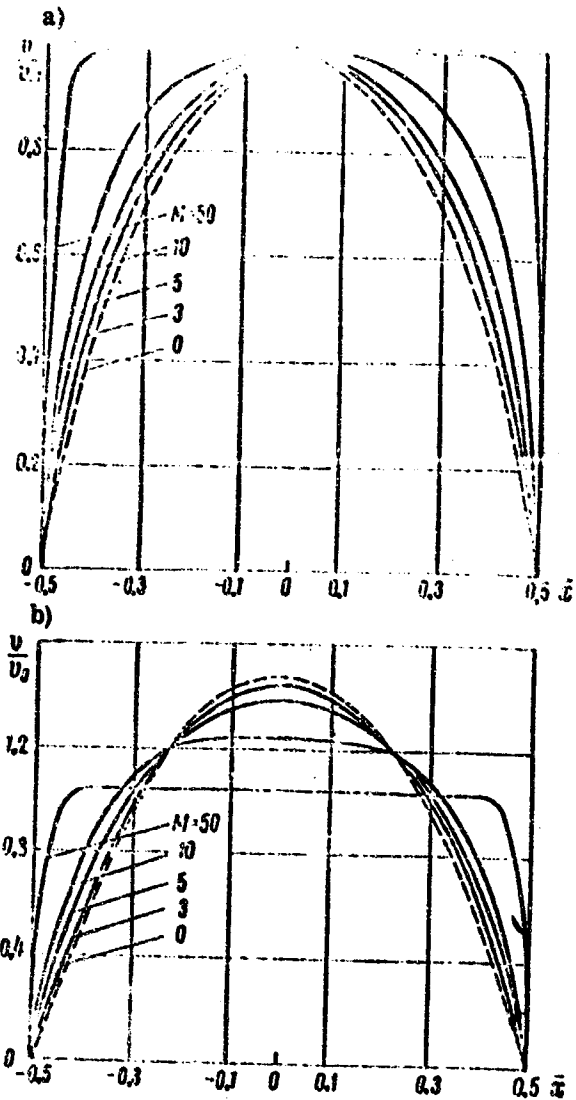
Fig. 14. Velocity distribution in a conducting fluid flowing in a flat MHD channel.

As follows from Eqs. (2.3) and (2.6), condition $\frac{dB_z}{dx}\Big|_{x=\pm 0.5b} = 0$, is equivalent to the condition $E_y = 0$; this corresponds to the flow of a conducting fluid in a flat channel with insulating walls perpendicular to the applied magnetic field, and short-circuited lateral electrodes ($E_0 = R_l = 0$). This case also corresponds to the second limiting mode of operation of an MHD generator (the short-circuit mode). Here

$$C = 0;$$

$$Q = -\frac{1}{\eta}\frac{dp}{dz} = \frac{p}{\eta l}. \tag{2.39}$$

25
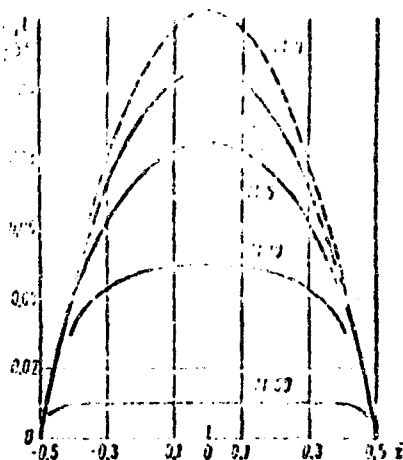
Fig. 15. Velocity distribution in
a conducting liquid flowing in a
flat MHD channel, assuming vis-
cous losses.

Upon substitution of Eq. (2.39), the velocity equation becomes

$$v_s = \frac{pb^3}{\eta l M^2}\left[\frac{ch\,0.5M - ch\,M\frac{x}{b}}{ch\,0.5M}\right]. \tag{2.40}$$

In this case, the value of p is composed of the pressure drop required for over-coming electromagnetic forces acting in the conducting fluid, and the pressure drop due to viscous friction.

Figure 16 shows distributions of $(v\eta l/pb^2)$ constructed from Eq. (2.40) for different values of M = const.; they describe the effect of the total pressure drop.

Comparison of curves shown in Figs. 15 and 16 shows that for a given p, the velocity in the second case drops more sharply with increasing magnetic field strength. This is due to the effect of pressure drop caused by electromagnetic forces.

Flow in a flat channel with horizontal walls of arbitrary conductivity is equivalent to the flow in the duct of an MHD generator with electrodes closed via a finite load resistance. Here the statement of the problem is not unique, since the condition B_z = const. $\neq$ 0 at the insulator walls becomes indeterminate.

It follows from Eqs. (2.3), (2.6) and (2.30) that

$$C = \mu\frac{l}{bl} - \mu\sigma B_s v_s; \quad Q = \left(\frac{p}{\eta l} - \frac{lB_s}{\eta lb}\right)\frac{0.5M}{th\,0.5M}, \tag{2.41}$$

where I is the total current flowing through the conducting fluid in the channel and through the load.

26
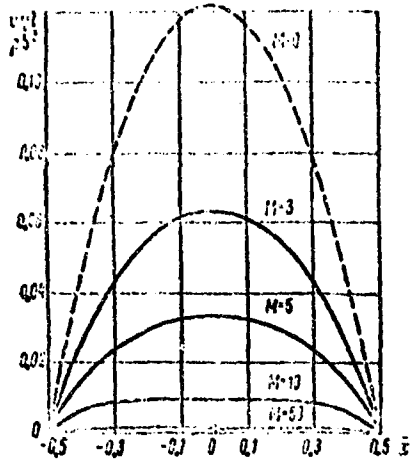
Fig. 16. Velocity distribution in
a conducting fluid flowing in a flat
MHD channel, with consideration
of viscous and electromagnetic
pressure drops.

In accordance with Eq. (2.41), the general flow velocity is

$$v_z = \frac{b^2}{2M}\left(\frac{p}{\eta l} - \frac{IB}{\eta b}\right)\frac{\operatorname{ch}0.5M - \operatorname{ch}M\frac{z}{b}}{\operatorname{ch}0.5M}. \tag{2.42}$$

Integrating this over the channel cross section, we obtain the expressions for the average fluid velocity and for the pressure

$$v_0 = \frac{b^2}{M^2}\left(\frac{IB_0}{\eta b} - \frac{p}{\eta l}\right)\left(1 - \frac{0.5M}{\operatorname{th}0.5M}\right); \tag{2.43}$$

$$p = \frac{IB_0}{b} + \frac{M\operatorname{th}0.5M}{b\operatorname{Re}\left(1 - \frac{\operatorname{th}0.5M}{0.5M}\right)}\cdot\frac{\varrho v_0^2}{2}l. \tag{2.44}$$

In Eq. (2.44) the first term gives the drop for overcoming the electromagnetic forces, while the second describes the drop due to viscous friction.

This problem becomes unique upon stipulation of an additional condition for I, which is determined by the parameters of the external circuit.

With a conducting fluid in the duct of an electromagnetic pump ($E_0 \neq 0$), the pressure gradient in the direction of motion is positive and the second term in Eq. (2.44) will be negative. Here, the first term will correspond to the electromagnetic pressure head developed by the pump, while the overall expression will describe the pump operating head.

27

It should also be noted that since the velocity distribution in a conducting fluid flowing in an MHD channel is independent of the various pertinent boundary conditions for magnetic flux density at the walls perpendicular to the magnetic flux, the effect of the magnetic field on the flow structure can be examined without considering the parameters of the external circuit.

In engineering hydrodynamics it is customary to relate the pressure drop to the average flow velocity by means of a dimensionless friction factor λ. In particular, the pressure drop in a pipe of length l is determined from the well-known formula [252, 253]

$$\Delta p = p_1 - p_2 = \frac{\lambda}{R_0} \frac{\rho v_0^2}{2} l,$$ (2.45)

where $R = 2S/\pi$ is the hydraulic radius, S and ii are, respectively, the pipe cross sectional area and wetted perimeter.

Equation (2.45) is also valid for the flow of conducting fluids in MHD channels. However, in this case Δp includes only the friction head drop which, as was pointed out above, is only a part of the total pressure drop.

In ordinary laminar fluid flow at a specified Re, the friction factor λ_ℓ^0 depends only on the channel geometry; in magnetohydrodynamics, this factor also depends on the Hartmann number under these conditions.

In laminar flow of a conducting fluid in an MHD channel it is convenient to represent the [magnetic] friction factor λ_ℓ^m as [24, 53]

$$\lambda_\ell^m = \frac{K(\gamma, M)}{Re}.$$ (2.46)

The factor $K(\gamma, M)$, which is a function of the channel geometry and of the Hartmann number, can in general be written as

$$K(\gamma, M) = \frac{1}{\left(1 + \frac{2}{\pi}\gamma\right)} \iint_{(\omega)} v \, dS,$$ (2.47)

where $\gamma = \pi b/2a$.

All the quantities are dimensionless in Eq. (2.47), with the velocity referred to its average value.

In the special case of $a \gg b$, the expression for $K(\gamma, M)$ becomes

$$K(\gamma, M) \approx 4M \frac{\mathrm{th}\, 0.5M}{1 - \frac{\mathrm{th}\, 0.5M}{0.5M}}.$$ (2.48)

For $M \gg 1$

$$K(\gamma, M) \approx 4M.$$ (2.49)

28

For $M \to 0$

$$K(\gamma, M) = K(\gamma) = 24.$$ (2.50)

Equation (2.50) is the exact solution for normal fluid flow in a flat channel [252, 253].
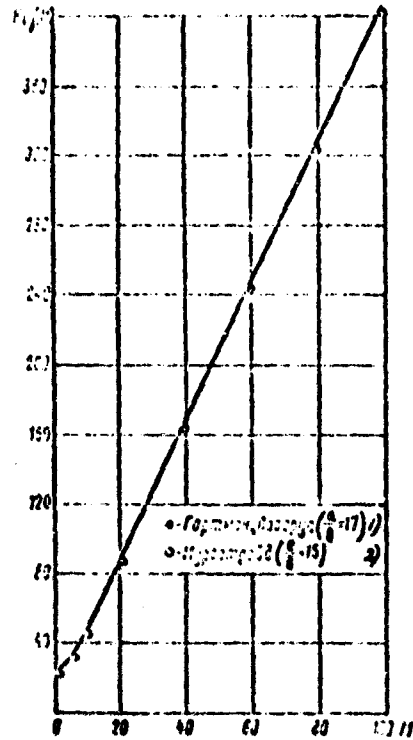
Fig. 17. Curve of $K(\gamma, M)$ as a function of the Hartmann number.

1) Hartmann and Lazarus; 2) Murgatroyd.

Figure 17 shows a curve of $K(\gamma, M)$ as a function of the Hartmann number, constructed from Eq. (2.48). It also shows experimental data obtained by Hartmann and Lazarus [81] and by Murgatroyd [83] for the flow of mercury in MHD channels with side ratios of 1:17 and 1:15. The experimental and theoretical data are in good agreement.

These data show that for a given Reynolds number, the friction factor for flow of conducting fluid in a channel always increases with the Hartmann number M, and can exceed the friction factor measured without a magnetic field by several tens of times.

3. Magnetohydrodynamic Couette Flow

Let us consider the flow of conducting fluid between two parallel flat walls one of which, $x = 0$, is conducting and is at rest, while the other, $x = b$, is an insulator and

moves in its plane with constant velocity U (Fig. 18). A uniform magnetic field is perpendicular to both walls. This problem corresponds to flow of conducting fluid in an annulus between two coaxial infinite cylinders, the distance between which is appreciably smaller than their radii. Here a radial magnetic field is superposed on the motion of the fluid.
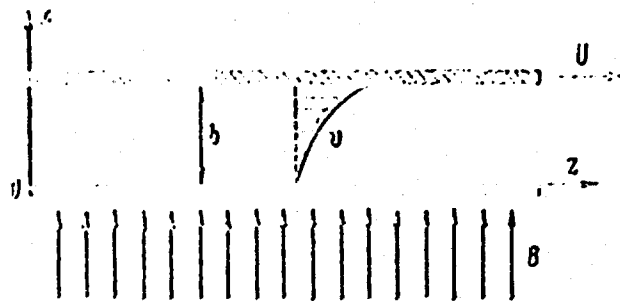
Fig. 18. Magnetohydrodynamic Couette flow.

The Couette flow problem may be treated as an approximation of the boundary layer problem, whereby the stationary wall is treated as a body past which flow takes place and the moving wall as an external flow. Unlike boundary layer problems, the solution to the Couette flow problem may be obtained in finite form and can be used for clarifying various relationships governing the behavior of boundary layers.

In this case, we can set $dp/dz = 0$, $E_y = 0$ and solve the problem by using Eq. (2.31) with the boundary conditions

$$v_z|_{x=0} = 0; \tag{2.51}$$

$$v_z|_{x=b} = U. \tag{2.52}$$

The solution has the form

$$v_z = C_1 \operatorname{ch} \frac{M}{b} x + C_2 \operatorname{sh} \frac{M}{b} x + Q \frac{b^2}{M^2}. \tag{2.53}$$

In accordance with the boundary conditions and the condition that $\left.\frac{dv_z}{dx}\right|_{x=0} = 0$ Eq. (2.53) is transformed to the form

$$v_z = U \frac{\operatorname{sh} \frac{M}{b} x}{\operatorname{sh} M}. \tag{2.54}$$

When $M \to 0$, Eq. (2.54) becomes the solution for Couette flow in common fluid flow [252]

$$v_z = U \frac{x}{b}. \tag{2.55}$$
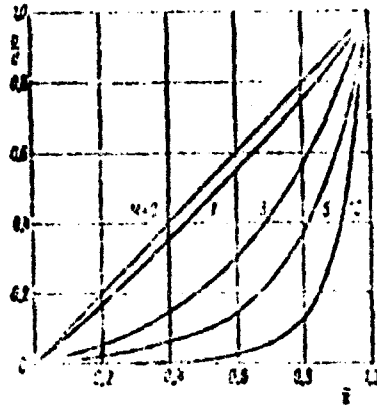
Fig. 19. Velocity distribution in two-dimensional Couette flow in the presence of transverse magnetic field.

Figure 19 shows velocity distributions constructed from Eq. (2.54) for various values of M = const. It can be seen from these curves that increasing M reduces the frictional stress $\left(\tau = \eta \frac{\partial v_z}{\partial x}\right)$ at the lower wall. At the upper wall, conversely, the frictional stress increases.

Using the solution obtained above, one can determine the temperature distribution in Couette flow [4]. Neglecting the variations of dissipative factors, we can write the energy equation (2.8) as

$$\varkappa \frac{d^2 T}{dx^2} + \frac{1}{\sigma} \cdot j_s^2 + \eta \left(\frac{dv_z}{dx}\right)^2 = 0. \tag{2.56}$$

Since according to Eqs. (2.3) and (2.30)

$$j_y = -\frac{1}{\mu} \cdot \frac{\partial B_z}{\partial x} = \sigma B_0 v_z$$

Eq. (2.56) reduces to

$$\frac{\varkappa}{\eta} \cdot \frac{d^2 T}{dx^2} + \frac{M^2}{b^2} \cdot v_z^2 + \left(\frac{dv_z}{dx}\right)^2 = 0. \tag{2.57}$$

Since the velocity distribution is given by Eq. (2.54), we find

$$\frac{\varkappa}{\eta} \cdot \frac{d^2 T}{dx^2} = -\frac{M^2 U^2}{b^2 \operatorname{sh}^2 M} \left(\operatorname{sh}^2 \frac{M}{b} x + \operatorname{ch}^2 \frac{M}{b} x\right) \cdots = -\frac{M^2 U^2}{b^2 \operatorname{sh}^2 M} \operatorname{ch} 2 \frac{M}{b} x. \tag{2.58}$$

31

The solution of Eq. (2.58) has the form

$$\frac{x}{\eta} T = \frac{U^2}{1.5 \eta M} \, \text{ch} \, 2\frac{M}{\delta} x + C_1 x + C_2 \tag{2.59}$$

If the wall is thermally insulating, then $dT/dx = 0$ and $C_1 = 0$. The constant of integration C_2 can be found by setting $x = b$:

$$C_2 = \frac{x}{\eta} T_\infty + \frac{U^2}{1.5 \eta M} \, \text{ch} \, 2M,$$

where T_∞ is the temperature of the moving wall. Consequently,

$$\frac{x}{\eta} T = \frac{x}{\eta} T_\infty + \frac{U^2}{1.5 \eta M} \left(\text{ch} \, 2M - \text{ch} \, 2\frac{M}{\delta} x \right). \tag{2.60}$$

The temperature of the lower wall at $M \gg 1$ is

$$T|_{x=0} = T_\infty + \frac{U^2 \eta}{2\kappa}. \tag{2.61}$$

It follows from the above expression that, given our assumptions, the wall temperature does not depend on the applied magnetic field.

If the temperature of the stationary wall $T|_{x=0}$ has been specified, then the heat flux to the wall is

$$q|_{x=0} = \frac{x}{\eta} \cdot \frac{T_\infty - T|_{x=0}}{b} + \frac{U^2}{2b} \tag{2.62}$$

and also does not depend on the applied magnetic field.

Studies of Couette flow make it possible to predict a number of effects produced by a transverse magnetic field, and inherent in a boundary layer. In particular, it follows from these studies that the effect of a transverse magnetic field due to a body past which flow takes place should result in reduction of viscous friction losses and in an increase in the thickness of the boundary layer. As seen from Eq. (2.62), the heat transfer should deteriorate when the boundary layer thickness is increased.

4. Laminar Flow of a Conducting Fluid over a Plate in the Presence of a Transverse Magnetic Field

Let us consider the flow in a laminar boundary layer, created on the surface of a plate fixed in a flowing conducting fluid in the presence of a magnetic field which is stationary relative to the plate.

We assume that the plate is flat. The z axis is parallel to the wall, and the x axis is perpendicular to it (Fig. 20). The magnetic Reynolds number is assumed to be small, so that the induced magnetic field may be neglected as compared to the applied field $B = B_0$.

In this case one can assume that the velocity has two components, v_z and v_x, while the electric current and the electric flux density have components only along the y axis. At low conductivity of the fluid and small magnetic Reynolds numbers [R_m], the ponderomotive force component in the z direction can, in the first approximation, be represented in the form [5]

$$f_z = -\sigma v_z B_0^2. \tag{2.63}$$

The other components of the ponderomotive force can be neglected.
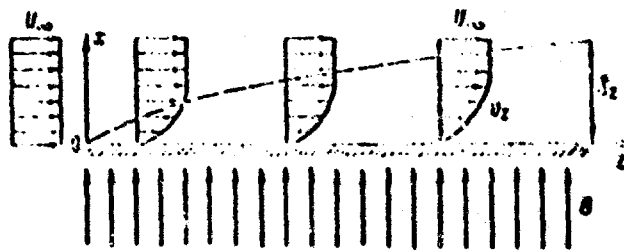
Fig. 30. Laminar magnetohydrodynamic boundary layer on a flat plate.

Under the above conditions, the momentum and continuity equations can be written as

$$\frac{\partial v_z}{\partial t} + v_z \frac{\partial v_z}{\partial z} + v_x \frac{\partial v_z}{\partial x} = -\frac{1}{\rho}\frac{\partial p}{\partial z} + \nu \frac{\partial^2 v_z}{\partial x^2} - \frac{\sigma}{\rho} B_0^2 v_z; \tag{2.64}$$

$$\frac{\partial v_z}{\partial z} + \frac{\partial v_x}{\partial x} = 0. \tag{2.65}$$

The boundary conditions for Eqs. (2.64) and (2.65) are

$$v_z = v_x = 0 \text{ for } x = 0; \quad v_z = U(z, t) \text{ for } x \to \infty. \tag{2.66}$$

Equations (2.64) and (2.65) differ from Prandtl boundary layer equations [252] only by the presence of an additional term in Eq. (2.64).

The potential flow $U(z, t)$ should be treated as a known function. In addition, one must specify the flow in the boundary layer for the conditions of the problem at $t = 0$ for the entire range of z and x under consideration.

For steady flow, Eqs. (2.64) and (2.65) simplify to

$$v_z \frac{\partial v_z}{\partial z} + v_x \frac{\partial v_z}{\partial x} = -\frac{1}{\rho}\frac{\partial p}{\partial z} + \nu \frac{\partial^2 v_z}{\partial x^2} - \frac{\sigma}{\rho} B_0^2 v_z; \tag{2.67}$$

$$\frac{\partial v_z}{\partial z} + \frac{\partial v_x}{\partial x} = 0. \tag{2.68}$$

To simplify analysis, we consider the flow over the plate in the absence of a pressure gradient. The equation of motion (2.67) is then rewritten as

$$v_z \frac{\partial v_z}{\partial z} + v_x \frac{\partial v_z}{\partial x} = \nu \frac{\partial^2 v_z}{\partial x^2} - m_1 v_z. \tag{2.69}$$

The boundary conditions are written as

$$
\left.
\begin{aligned}
v_z = v_x = 0 \qquad & \text{for } x = 0; \\
\frac{\partial v_z}{\partial x} = 0; \quad \frac{\partial v_z}{\partial z} = -m_1 \text{ for } x = \infty.
\end{aligned}
\right\} \tag{2.70}
$$

To integrate Eq. (2.69) with boundary conditions (2.70) we can introduce the stream function $\psi(z, x)$, which satisfies the continuity equation, i.e., as in fluid flow, we can set

$$v_z = \frac{\partial \psi}{\partial x}; \quad v_x = -\frac{\partial \psi}{\partial z}. \tag{2.71}$$

We first introduce the new variables suggested by Blasius

$$z = z; \quad \eta = x \sqrt{\frac{U}{\nu z}}. \tag{2.72}$$

The stream function can be as

$$\psi = \sqrt{U \nu z}\,[f_0 + (mz)f_1 + (mz)f_2 + (mz)^2 f_3 + (mz)^3 f_4 + \cdots]. \tag{2.73}$$

where f_0, f_1 and f_2 are functions only of η and $m = m_1/U$.

The velocity components and their derivatives are determined from the expressions

$$v_z = \frac{\partial \psi}{\partial x} = \frac{\partial \psi}{\partial \eta}\cdot\frac{\partial \eta}{\partial x} = \frac{\partial \psi}{\partial \eta}\cdot\eta_x$$

$$v_x = \frac{\partial \psi}{\partial z} = \frac{\partial \psi}{\partial \eta}\cdot\frac{\partial \eta}{\partial z} = \frac{\partial \psi}{\partial \eta}\cdot\eta_z$$

whence

$$
\left.
\begin{aligned}
v_z &= U\,[f_0' + mz f_2' + (mz)f_4' + \cdots]; \\
v_x &= \frac{1}{2}\sqrt{\frac{U\nu}{z}}\,[f_0 + mz f_2 + (mz)^2 f_4 + \cdots] = \\
&\quad \frac{1}{2}\sqrt{\frac{U\nu}{z}}\,[f_0 - 3mz f_2 + 5(mz)^2 f_4 + \cdots].
\end{aligned}
\right\} \tag{2.74}
$$

$$\frac{\partial v_x}{\partial z} = \frac{U}{v_z}\left[f_0' + mzf_2' + (mz)^2 f_4' + \cdots\right]$$
$$+ \frac{U}{2z}\left[\eta_0 f_0' + \eta(mz)^2 f_4' + \cdots\right];$$
$$\frac{\partial v_z}{\partial z} = U\left[-\frac{U}{v_z}[f_0 + mzf_2 + (mz)^2 f_4 + \cdots];\right.$$
$$\frac{\partial^2 v_z}{\partial x^2} = \frac{U}{v_z}[f_0'' + mzf_2'' + (mz)^2 f_4'' + \cdots].$$

(2.75)

Substituting Eqs. (2.74) and (2.75) into Eq. (2.69) and equating the coefficients of the same powers of parameter mz, where

$$mz = \frac{-\sigma v}{g U} = \frac{M_z^2}{Re_z},$$

we will get a system of ordinary differential equations determining function f_n

$$2f_0'' = f f_0'' \tag{2.76}$$

$$2f_2'' = 2f_0'f_2' - ff_2'' - f_2f_0'' - f_0' \tag{2.77}$$

$$2f_4'' = 4f_0'f_4' + 2f_2'^2 - ff_4'' - f_2f_2'' - f_4f_0'' - 2f_2' \tag{2.78}$$

etc.

The boundary conditions for Eqs. (2.76)-(2.78) are

$$\left.\begin{array}{lll} f_0 = f_2 = f_4 = \cdots = 0 & \text{for } \eta = 0; \\ f_0' = f_2' = f_4' = \cdots = 0 & \text{for } \eta = 0; \\ f_0' = 1; \ f_2' = -1; \ f_4' = \cdots = 0 & \text{for } \eta = \infty. \end{array}\right\}$$

Equation (2.76) is the Blasius equation, whose solution is known; functions f_0, f_0' and f_0'' have been tabulated by L. Howard [252].

Equations (2.77) and (2.78) are ordinary linear differential equations for f_2, f_4, etc., and can be integrated numerically.

Figure 21 shows the calculated velocity distributions for different values of mz. The solid lines are for the cases in which the series terms with mz to the second and higher powers have been neglected, while the dashed lines were obtained with the squared terms retained.

The above data show that the transverse magnetic field affects the velocity distribution in the boundary layer when mz > 0.1; a transverse magnetic field which is stationary relative to the plate reduces the velocity gradient at the wall.

For this case, we have the following expressions for the friction factor and the displacement thickness

$$\tag{2.79}$$

$$\delta \quad \int\left(1 \quad \right)\,dc \quad \tag{}$$

$$\dashv \;[1.73 \; \; 0.5!mz \quad \;(\;\;)^2 \;\cdots] \;\Big\}\;\frac{x}{u}\,. \tag{2.80}$$

When m = 0, then Eqs. (2.79) and (2.80) become expressions for the ordinary boundary layer [252].
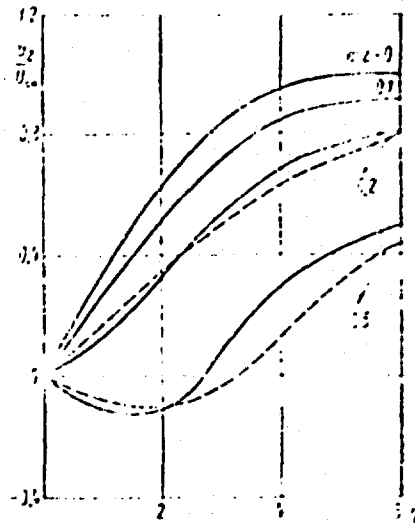
Fig. 21. Velocity distribution in a laminar boundary layer in the presence of a magnetic field stationary relative to the plate.

It follows from the above expressions that in the presence of a transverse magnetic field which is stationary relative to the plate, the surface friction factor decreases with increasing m, while the displacement thickness increases.

The change in friction factor with increasing $\bar{m} = M/\sqrt{Re}$ is shown in Fig. 22.

If the magnetic field moves together with the potential flow relative to a stationary plate, then by virtue of slip of the fluid in the boundary layer relative to the magnetic field and because of changes in the direction of electromagnetic forces, the velocity gradient at the wall will increase with increasing magnetic field intensity; this, in turn, will increase the surface friction factor as compared with the absence of a magnetic field [39]. This fact was confirmed experimentally [93].

36
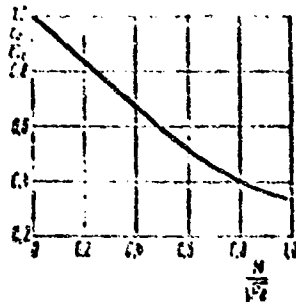
Fig. 22. Friction factor for a plate as a function of $M/\sqrt{Re}$ in the presence of a stationary magnetic field.
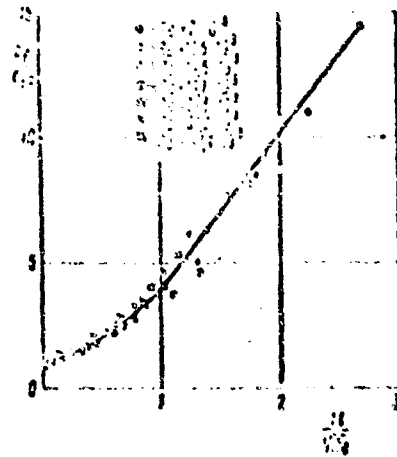
Fig. 23. Friction factor for a plate as a function of $M/\sqrt{Re}$ in the presence of a magnetic field moving with the conducting fluid.

Figure 23 shows an experimentally determined curve of c_f/c_{f_0} as a function of $M/\sqrt{Re}$, obtained for 0.2-0.3 mm thick, 20 x 20 mm, 30 x 30 mm, or 40 x 40 mm dielectric plates placed in a mercury flow.

The above data show that the surface friction factor increases appreciably with an increase in $M/\sqrt{Re}$. In particular, for $M/\sqrt{Re} = 2$ the friction factor increases by an order of magnitude as compared with its value in the absence of a magnetic field.

5. Effect of a Transverse Magnetic Field on the Stability of Flow of a Conducting Fluid

Of primary concern in the study of stability of MHD flows, just as in ordinary hydrodynamics, is the determination of criteria characterizing transition from laminar to turbulent flow.

Theoretical studies of stability are usually based on the method of small perturbations. The basic assumptions underlying the use of this method in the study of stability of plane parallel MHD flows are examined in the book by Pai-Shih-i [5].

Consider the plane parallel flow of a conducting fluid in the z direction in a transverse magnetic field (Fig. 24). In this case we may set

$$v_z = v_z(x); \quad v_y = v_x = 0, \quad p = C_1 z + C_2 + N(x); \\ B_x = B_0; \quad B_z = B_z(x); \quad B_y = 0, \tag{2.81}$$

where C_1, C_2 and B_0 are constants, while v_z, B_z and N are functions of x only.

37

Let us assume the small perturbations are applied to an initially steady flow of the conducting fluid. The velocity, pressure and magnetic flux density components for perturbed flow can be represented in the form

$$
\begin{aligned}
v_z &= v_z(x) + v'_z; \quad v_x = v'_x; \quad v_y = v'_y; \\
\rho &= C_1 z + C_3 + N(x) + \rho'; \\
B_z &= B_z(x) + b'_z; \quad B_x = B_x + b'_x; \quad B_y = b'_y
\end{aligned}
\right\}
\tag{2.82}
$$

where $v'_x,\ v'_y,\ v'_z,\ \rho',\ b'_x,\ b'_y,\ b'_z$ are the magnitudes of the perturbations. It is assumed that these quantities are very small as compared with the corresponding values characterizing the main flow.
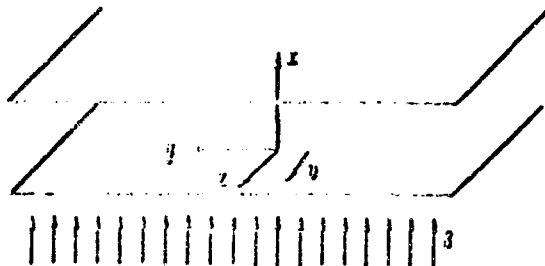
Fig. 24. Schematic of the flow of a conducting fluid between two parallel plates in a transverse magnetic field.

Substituting Eq. (2.82) into Eqs. (2.1), (2.2), (2.5) and (2.7), and making use of Eq. (2.3), we get the following expressions for the perturbations:

$$
\frac{\partial v'_z}{\partial t} + v_z \frac{\partial v'_z}{\partial z} + v'_x \frac{\partial v_z}{\partial x} = -\frac{1}{\rho}\frac{\partial p'}{\partial z} + \frac{1}{\rho\mu}\times
$$

$$
\times\left(B_z \frac{\partial b'_z}{\partial z} + B_x \frac{\partial b'_z}{\partial x} + b'_x \frac{\partial B_z}{\partial x}\right) +
$$

$$
+\ \nu\Delta v'_z - \frac{1}{\mu}\frac{\partial}{\partial z}(B_z b'_z + B_x b'_x);
\tag{2.83}
$$

$$
\frac{\partial v'_x}{\partial t} + v_z \frac{\partial v'_x}{\partial z} = -\frac{1}{\rho}\frac{\partial p'}{\partial x} + \nu\Delta v'_x +
$$

$$
+\ \frac{1}{\rho\mu}\left(B_z \frac{\partial b'_x}{\partial z} + B_x \frac{\partial b'_x}{\partial x}\right) - \frac{1}{\rho\mu}\frac{\partial}{\partial x}(B_z b'_z + B_x b'_x);
\tag{2.84}
$$

$$
\frac{\partial v'_y}{\partial t} + v_z \frac{\partial v'_y}{\partial z} = -\frac{1}{\rho}\frac{\partial p'}{\partial y} + \nu\Delta v'_y + \frac{1}{\rho\mu}\left(B_z \frac{\partial b'_y}{\partial z} + B_0 \frac{\partial b'_y}{\partial x}\right) - \frac{1}{\rho\mu}\frac{\partial}{\partial y}(B_z b'_z + B_x b'_x);
\tag{2.85}
$$

38

$$\frac{\partial b_z'}{\partial t} + v_z \frac{\partial b_z'}{\partial z} + v_z' \frac{\partial B_z}{\partial x} - B_z \frac{\partial v_z'}{\partial z} - B_0 \frac{\partial v_z'}{\partial x} - v_z' \frac{\partial v_z}{\partial x} = \frac{1}{\mu \sigma} \Delta b_z'; \tag{2.86}$$

$$\frac{\partial b_x'}{\partial t} + v_z \frac{\partial b_x'}{\partial z} - B_z \frac{\partial v_x'}{\partial z} - B_0 \frac{\partial v_x'}{\partial x} = \frac{1}{\mu \sigma} \Delta b_x'; \tag{2.87}$$

$$\frac{\partial b_y'}{\partial t} + v_z \frac{\partial b_y'}{\partial z} - B_z \frac{\partial v_y'}{\partial z} - B_0 \frac{\partial v_y'}{\partial x} = \frac{1}{\mu \sigma} \Delta b_y'; \tag{2.88}$$

$$\frac{\partial v_x'}{\partial x} + \frac{\partial v_y'}{\partial y} + \frac{\partial v_z'}{\partial z} = 0; \tag{2.89}$$

$$\frac{\partial b_x'}{\partial x} + \frac{\partial b_y'}{\partial y} + \frac{\partial b_z'}{\partial z} = 0, \tag{2.90}$$

where

$$\Delta = \frac{\partial^2}{\partial x^2} + \frac{\partial^2}{\partial y^2} + \frac{\partial^2}{\partial z^2}.$$

Equations (2.83)–(2.86) do not include terms containing squares of perturbations, since these are second-order infinitesimals.

The perturbations are specified in the form

$$\left. \begin{array}{l} v' = \varphi(x) \exp i(\alpha z + \alpha_1 y - \beta t); \\ b' = \psi(x) \exp i(\alpha z + \alpha_1 y - \beta t). \end{array} \right\} \tag{2.91}$$

In the above expressions α and α_1 are positive real numbers, which are called the wave numbers of the perturbations, while β is a complex eigenvalue

$$\beta = \beta_r + i\beta_i,$$

where β_r is the cyclic frequency of fluctuations, while β_1 is an increment factor whose sign governs the behavior of the fluctuations. If $\beta_1 < 0$, then the fluctuations are damped and the laminar flow is stable. If, however, $\beta_1 > 0$, then the fluctuations increase and the laminar flow is unstable.

Frequently use is also made of the parameter

$$c = \frac{\beta}{\alpha} = c_r + ic_i,$$

where c_r is the rate of propagation of the waves, while c_i is, as before, an increment factor, the sign of which determines whether the perturbations are damped or increasing. The amplitude φ of the perturbing motion is assumed to be a function of x only, since the main flow also depends on x.

39

Upon substitution of Eqs. (2.91) into Eqs. (2.82)-(2.90) and appropriate transformations, the latter are reduced to the form [5]

$$DD_1\varphi_x - i\,\frac{\alpha}{v}\,v_z D_1\varphi_x + i\,\frac{\alpha}{v}\,\varphi_x v_z'' = \frac{\partial\alpha}{v\mu}\,\psi_z B_z'' - \frac{1}{\varrho v\mu}(\ldots); \tag{2.92}$$

$$(D_2 - i\varepsilon\mu\omega v_z)\,\psi_x = \ldots\,(\ldots). \tag{2.93}$$

where

$$D = \frac{d^2}{dy^2} - \alpha^2 - \alpha_1^2;$$

$$D_1 = \frac{d^2}{dy^2} + \frac{i\beta}{v} - \alpha^2 - \alpha_1^2;$$

$$D_2 = \frac{d^2}{dy^2} + i\beta\mu\omega - \alpha^2 - \alpha_1^2.$$

Equations (2.92) and (2.93) are the basic equations of the magnetohydrodynamic stability theory for plane parallel flows.

If there is no magnetic field, then Eq. (2.93) becomes an identity, while Eq. (2.92) becomes the ordinary equation of stability of a laminar plane parallel flow with three-dimensional perturbations.

Studies by G. B. Squire [252] showed that in order to determine the critical Reynolds number, that is, the lower boundary of stability, it is sufficient to examine two-dimensional perturbations.

When $v_y' = b_y'$ and $\alpha_1 = 0$, Eqs. (2.92) and (2.93) take the form

$$DD_1\varphi_x - i\,\frac{\alpha}{v}\,v_z D_1\varphi_x + i\,\frac{\alpha}{v}\,\varphi_x v_z'' = i\,\frac{\alpha}{\mu v}\,\psi_z B_z'' - \frac{1}{\varrho v\mu}(\ldots); \tag{2.94}$$

$$(D_2 - i\varepsilon\mu\omega v_z)\,\psi_x = \ldots\,(\ldots). \tag{2.95}$$

In the study of stability of MHD flows the eigenvalues of Eqs. (2.94) and (2.95) must be found at the appropriate boundary conditions.

Theoretical studies of the stability of flow of a conducting fluid in a flat channel in the presence of a transverse magnetic field and $R_m \ll 1$ were done by Lock [44].

In the case of $R_m \ll 1$, the induced magnetic field $B_z(x)$ can be neglected compared with the applied field B_0. Then Eq. (2.95) reduces to the form

$$\frac{1}{\mu\sigma}(\psi_x'' - \alpha^2\psi_x) = - B_0\varphi_x'. \tag{2.96}$$

after which Eq. (2.94) becomes

$$(\ldots)(\psi_x'' - \alpha^2\psi_x) = \ldots - i\,\frac{\alpha B_0^2}{\varrho v}\,\varphi_x''$$
$$\qquad\qquad - i\,\frac{v}{\alpha}(\varphi_x^{IV} - 2\alpha^2\varphi_x'' + \alpha^4\varphi_x). \tag{2.97}$$

40

Introducing dimensionless variables, we get

$$(\bar{v}_x - \bar{c})(\bar{\varphi}_x^{''} - \bar{\alpha}^2 \varphi_x) - \bar{v}_x^{''} \varphi_x +$$
$$+ \frac{i}{\alpha \text{Re}} (\varphi_x^{IV} - 2\bar{\alpha}^2 \bar{\varphi}_x^{''} + \bar{\alpha}^4 \varphi_x) = \frac{iM^2}{\alpha \text{Re}} \bar{\varphi}_x^{''}.$$

$$(2.98)$$

The above expression differs from the Orr-Sommerfeld equation by the presence of the right-hand side. The boundary conditions for it are

$$\bar{\varphi}_x = \bar{\varphi}_x^{'} = 0 \quad \text{for} \quad \bar{x} = \pm 0.5. \qquad (2.99)$$

A solution of Eq. (2.98) with the above boundary conditions was constructed by Lock using Lin's method for the cases of low and high Hartmann numbers.

In order to specify the velocity distribution of unperturbed flow at low Hartmann numbers, Lock used Hartmann's solution. At high Hartmann numbers an exponential velocity distribution was specified; this is justified by the presence, in this case, of a flow core, where the velocity is constant.

The neutral stability curves obtained by Lock for low M are shown in Fig. 25. Examining them we see that the transverse magnetic field has a strong stabilizing effect on the flow of conducting fluids. Physically this is attributed to changes in the fluid's velocity distribution and suppression of turbulent pulsations by the magnetic field.

The neutral stability curve shown by a dashed line was calculated by Lin and corresponds to the case of fluid flow in the absence of a magnetic field.

Lock also established that the stabilizing effect of the magnetic field is, in this case, due primarily to changes in the velocity distribution over the channel cross section. For high M, he obtained the following expression for the critical Reynolds number

$$\text{Re}_{cr}^m = kM, \qquad (2.100)$$

where k = 50,000.

Theoretical studies on the stability of flow of a conducting fluid in the boundary layer at a thin plate in the presence of a transverse magnetic field were done by V. N. Arkhipov [47]. Neglecting all the velocity components of the boundary layer except the longitudinal, he solved this problem by means of Eq. (2.98) with the boundary conditions

$$\left. \begin{array}{l} \varphi_x = \varphi_x^{'} = 0 \quad \text{for} \quad x = 0; \\ \varphi_x = \varphi_x^{'} = 0 \quad \text{for} \quad x \to \infty. \end{array} \right\} \qquad (2.101)$$

Arkhipov specified the velocity distribution in the boundary layer by means of a relationship obtained previously in [39].

The problem was solved by the Galerkin method, using a system of "approximating" functions which satisfy boundary conditions.

41

Taking as the characteristic dimension the thickness of the displacement layer $\delta^* = 1.73 \sqrt{\frac{\nu x}{U}}$, Arkhipov obtained neutral stability curves in the second approximation (Fig. 26). Examining these curves we see that in this case, as in channel flow of a conducting fluid, the effect of a transverse magnetic field reduces to increasing the flow stability.

Subsequent experimental studies by Murgatroyd [83] showed that, at $M \gg 1$, Eq. (2.100) correctly expresses the qualitative relationship between Re^m_{cr} and the Hartmann number, but gives larger quantitative deviations. In particular, he has obtained the expression

$$\mathrm{Re}^m_{cr} \approx 225\, M. \tag{2.102}$$
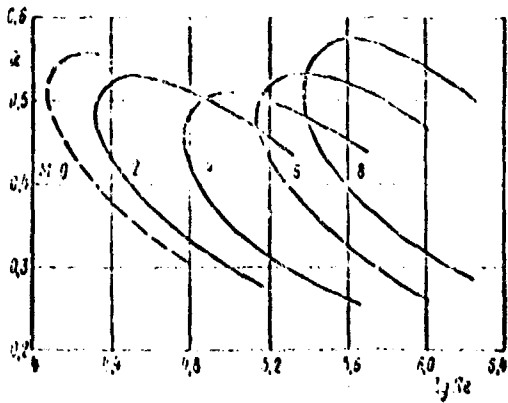
Fig. 25. Neutral stability curves for the flow of a conducting fluid in a flat channel in the presence of a transverse magnetic field.
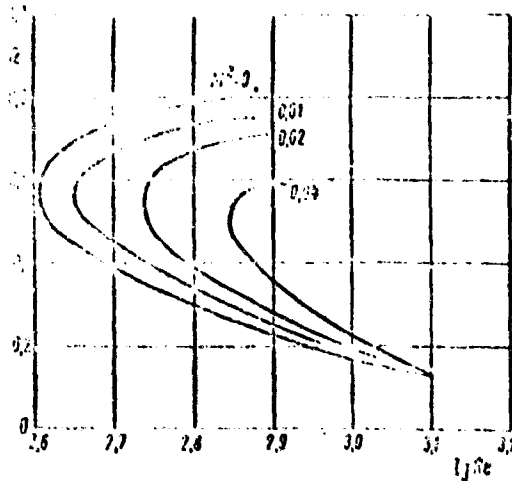
Fig. 26. Neutral stability curves for laminar flow of a conducting fluid over a plate in the presence of a transverse magnetic field.

It follows from Lock's theoretical formula, as well as from Murgatroyd's experimental relationship, that the friction factor corresponding to Re_{cr} is a constant quantity.

It was established by analysis of a large volume of experimental data [53] that the magnitude of the friction factor characterizing the onset of the first turbulence is independent of the shape of the channel cross section and of the applied magnetic field, and may be taken as

$$\lambda = \lambda_{cr} = 0.3177 = \mathrm{const}. \tag{2.103}$$

The validity of Eq. (2.103) is confirmed by available experimental data (Fig. 27).

42
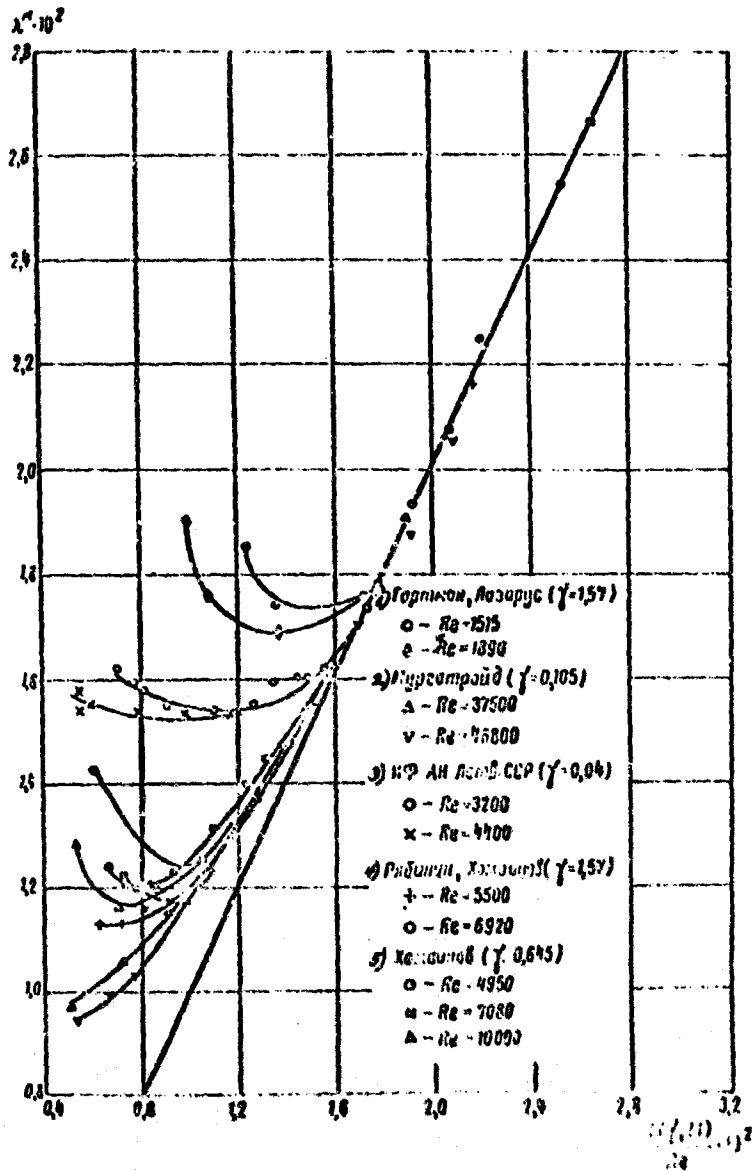
Fig. 27. Comparison of experimentally obtained friction factor in MHD channel flows with the exact solution.

1) Hartmann and Lazarus; 2) Murgatroyd; 3) Physics Institute of the Latvian Academy of Sciences; 4) Ryabinin and Khoshainov; 5) Khoshainov.

In accordance with Eqs. (2. 46) and (2. 103) the stability criterion can be represented as

$$Re_{cr}^{m} = \frac{\lambda(\gamma, M)}{0.0177} . \tag{2.104}$$

In accordance with Eq. (2.49), for flat channels with $M \gg 1$ Eq. (2.104) becomes identical with Murgatroyd's empirical formula.

6. Turbulent Magnetohydrodynamic Channel Flow

One of the most complex problems of applied magnetohydrodynamics is the study of the effect of transverse magnetic fields on the turbulent channel flow of conducting fluids.

The most extensively used methods in the study of turbulent channel flows in engineering hydrodynamics are semiempirical, based on experimental determination of a number of characteristic parameters. These methods are also used in applied magnetohydrodynamics.
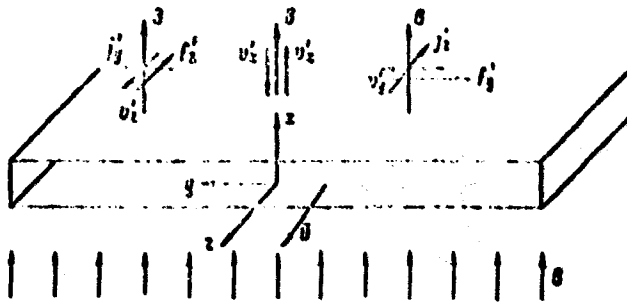
Fig. 28. Schematic of turbulent flow of a conducting fluid in a flat MHD channel.

Let us now examine the turbulent flow of a conducting fluid in a flat MHD channel (Fig. 28).

Studies of the structure of turbulent MHD flows in flat channels using the semi-empirical approach were performed by L. Harris [52]. However, before we examine his results, it is proper to consider the overall flow parameter, i.e., the friction factor.

Analysis of equations of turbulent MHD channel flow [53] written in dimensionless form shows that the friction factor, describing pressure drop in a channel and produced by viscous friction and turbulent mixing, can be represented as a sum of two components

$$\lambda_{fr}^m = \lambda_l^m + \lambda_{t.p.}^m. \qquad (2.105)$$

where λ_l^m is the friction factor of laminar MHD flow, $\lambda_{t.p.}^m$ is a component produced by magnetohydrodynamic pulsations. The expression for λ_l^m was obtained in Sec. 2. We shall now analyze the second component of the friction factor.

It is expedient to represent $\lambda_{t.p.}^m$ in the form [53]

$$\lambda_{t.p.}^m = \lambda_{t.p.}^0 + \varphi\left(Re, \frac{M^2}{Re}\right),$$
(2.106)

where $\lambda_{t.p.}^0$ is the friction factor component of common fluid flow due to pulsations.

It is obvious that when $M \to 0$

$$\varphi\left(Re, \frac{M^2}{Re}\right) \to 0.$$

The magnetic field exerts a stabilizing effect on the channel flow of conducting fluids. Hence, when $Re = $ const., a rise in the Hartmann number should change the flow mode from turbulent to laminar. Consequently, when $Re = $ const. and $M \to \infty$

$$\lambda_{t.p.}^m = \left[\lambda_{t.p.}^0 + \varphi\left(Re, \frac{M^2}{Re}\right)\right] \to 0;$$
$$\varphi\left(Re, \frac{M^2}{Re}\right) \to -\lambda_{t.p.}^0.$$
(2.107)

We represent φ as

$$\varphi\left(Re, \frac{M^2}{Re}\right) = -\lambda_{t.p.}^0 \Psi\left(Re, \frac{M^2}{Re}\right).$$

Then for $Re = $ const. and $M \to \infty$ we can write, in accordance with Eq. (2.107), that

$$\Psi\left(Re, \frac{M^2}{Re}\right) \to 1.$$
(2.108)

To examine the structure of function Ψ for small M^2/Re, we expand it in a series in terms of this parameter in the neighborhood of $M^2/Re = 0$:

$$\Psi\left(Re, \frac{M^2}{Re}\right) = \Psi(Re, 0) + \frac{M^2}{Re}\Psi'(Re, 0) + \cdots,$$

after which Eq. (2.106) reduces to the form

$$\lambda_{t.p.}^m = \lambda_{t.p.}^0 - \lambda_{t.p.}^0\left[\Psi(Re, 0) + \frac{M^2}{Re}\sum_{n=1}^{\infty}\frac{\Psi^{(n)}(Re, 0)}{n!}\left(\frac{M^2}{Re}\right)^{n-1}\right].$$

It is easy to show that $\Psi(Re, 0) = 0$. Consequently, when $M^2/Re \to 0$, function Ψ goes to zero as M^2/Re.

In general, when M^2/Re goes from 0 to ∞, we can write

$$0 < \Psi\left(Re, \frac{M^2}{Re}\right) < 1.$$
(2.109)

45

The expression for $\lambda_{t.p.}^m$ has the form

$$\lambda_{t.p.}^m = \lambda_{t.p.}^0 \left[1 - \psi\left(Re, \frac{M^2}{Re}\right)\right]. \tag{2.110}$$

Thus the expression for the friction factor for turbulent MHD flow of a conducting fluid in a flat channel can be written as

$$\lambda_t^m = \frac{N(\gamma, M)}{Re} + \lambda_{t.p.}^0 \left[1 - \psi\left(Re, \frac{M^2}{Re}\right)\right]. \tag{2.111}$$

For flat channels, function $\lambda_{t.p.}^0$ is given by

$$\lambda_{t.p.}^0 = \lambda_t^0 - \frac{24}{Re}. \tag{2.112}$$

Experimental studies show that in fully developed liquid pipe flow, λ_t^0 is virtually independent of the pipe cross sectional shape and is satisfactorily described by the Blasius law up to Re $\sim 10^5$ [254]

$$\lambda_t^0 = \frac{0.133}{Re^{0.25}}. \tag{2.113}$$

When Re $> 10^5$, λ_t^0 can be determined from Prandtl's general law [252, 253].

To construct function ψ it suffices to know experimental values of λ_t^m at different Re and M. Then, according to Eq. (2.111), function ψ is given by

$$\psi\left(Re, \frac{M^2}{Re}\right) = 1 - \frac{\lambda_t^m}{\lambda_{t.p.}^0}. \tag{2.114}$$

Figure 29 shows curves of ψ (Re, M^2/Re) constructed from experimental data of [83]. A family of these curves is described by

$$\Psi\left(Re, \frac{M^2}{Re}\right) = \frac{M^2}{Re} \cdot \frac{1 + \alpha \frac{M^2}{Re}}{\beta_0 + \beta_1 \frac{M^2}{Re} + \alpha \left(\frac{M^2}{Re}\right)^2} \tag{2.115}$$

which satisfies the limiting conditions (2.109).

Factors α, β_0 and β_1, which for a flat channel are functions of Re only, are defined by the expressions

$$\alpha(Re) = \frac{10^4}{\ldots}$$
$$\beta_0(Re) = \ldots$$
$$\beta_1(Re) = \ldots$$
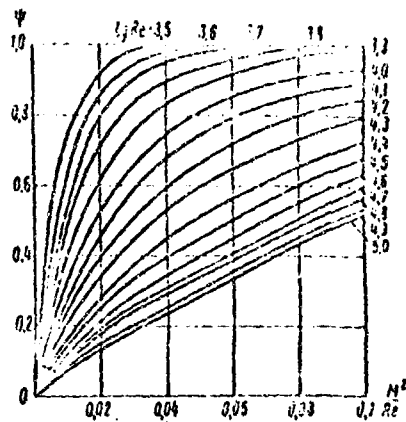
Fig. 29. The normalized function Ψ vs. parameter M^2/Re.

When $M \sim 1$ and $Re \sim 10^3$, the expressions for the friction factor become more complicated

$$\lambda_t^m = \frac{K(\gamma, M)}{Re} + \delta(Re - 1355)\left[\frac{0.133}{Re^{0.25}} - \right.$$

$$\left. - \frac{2.16 \cdot 10^{-2}}{1 + 0.912 \cdot 10^{-3}(Re - 1355)}\right] \cdot \left[1 - \Psi\left(Re, \frac{M^2}{Re}\right)\right], \qquad (2.116)$$

where $\delta(Re - 1355)$ is a unit function

$$\delta = \begin{cases} 0 & \text{for } Re < 1355; \\ 1 & \text{for } Re \geqslant 1355. \end{cases}$$

We note that Eq. (2.116) is valid for turbulent and laminar flows of conducting fluids with and without a magnetic field.

Figure 30 shows the curve of $\lambda_t^m = f(Re, M)$ constructed from Eq. (2.116) for different values of $M = const$. It also shows the values of λ_t^m obtained by analysis of experimental data of Hartmann and Lazarus [81] and Murgatroyd [83]. They are in satisfactory agreement with theoretical data.

Figure 31 shows curves of $\lambda_t^m = f(Re, M)$ obtained by A. I. Khozhainov in a rectangular channel with ratio of sides 1:2.5, as well as data of L. Schiller [255] and J. Nikuradse [256] for water flowing in a similar channel with $M = 0$.

Note that to compare the experimental data of Fig. 31 with theoretical results, a correction term must be introduced in Eq. (2.116) to account for the effect of the side walls [110].

47
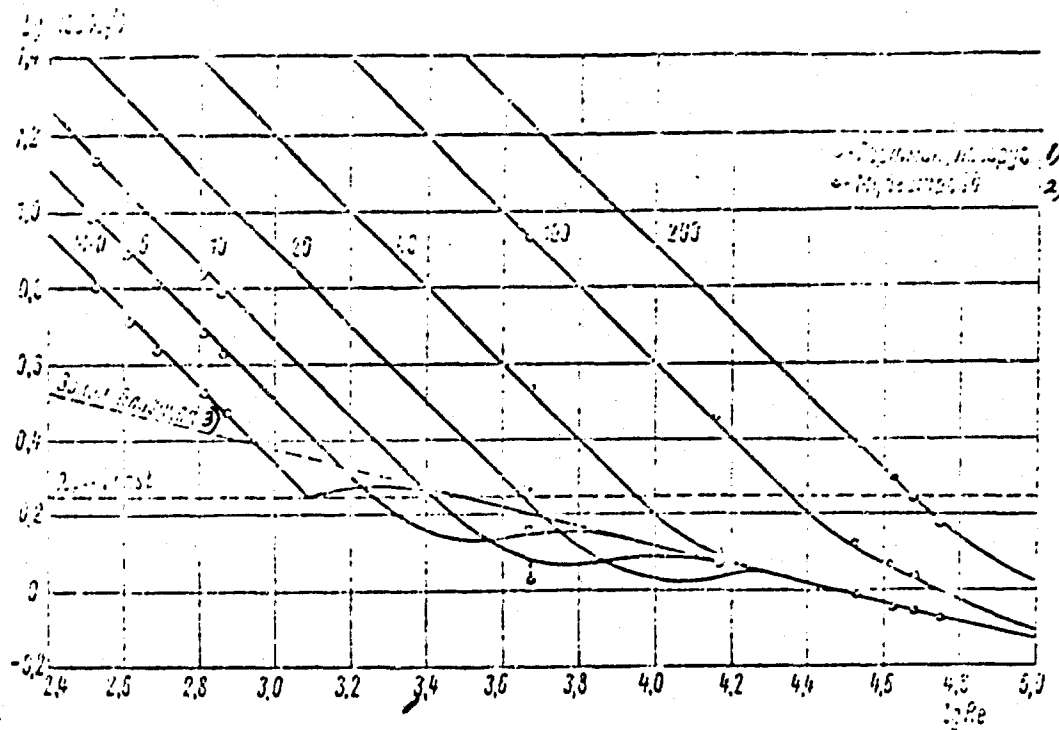
Fig. 30. Friction factor curves for the flow of a conducting fluid in a flat MHD channel.

KEY: 1) Hartmann and Lazarus; 2) Murgatroyd; 3) Blasius law.

It is seen from Figs. 30 and 31 that some experimental data on λ_t^m in turbulent flow of mercury at low M lie appreciably below the curve described by the Blasius law. Conversely, for large M the experimental values of λ_t^m lie above this curve. This is a regular phenomenon and is easily explained from the physical point of view.

Thus, the effect of a transverse magnetic field on turbulent channel flow of a conducting fluid involves changing the velocity distribution over the channel cross section and suppression of turbulent pulsations. At low M, the shape of the velocity distribution is close to that of ordinary hydrodynamics, i.e., the magnetic field does not appreciably increase the velocity gradient at the walls, but suppresses turbulent pulsations. Hence for a given Re one observes a smaller friction factor than in equivalent common fluid flow.

At high M the effect involving the increase in the velocity gradient at the walls dominates over the turbulent pulsation suppression. Hence in this case in a given range of Re the friction factor is greater than λ_t^0.

When M = const., all the $\lambda_t^m = f$ (Re, M) curves tend asymptotically to the curve corresponding to the Blasius (Prandtl) law of higher Re.

48

From the engineering point of view, the region of turbulent MHD channel flow can be divided into two zones, in the first of which (corresponding to low M) the magnetic field reduces the friction factor as compared to its value in ordinary hydrodynamics, and in the second (corresponding to high M) it increases this factor.
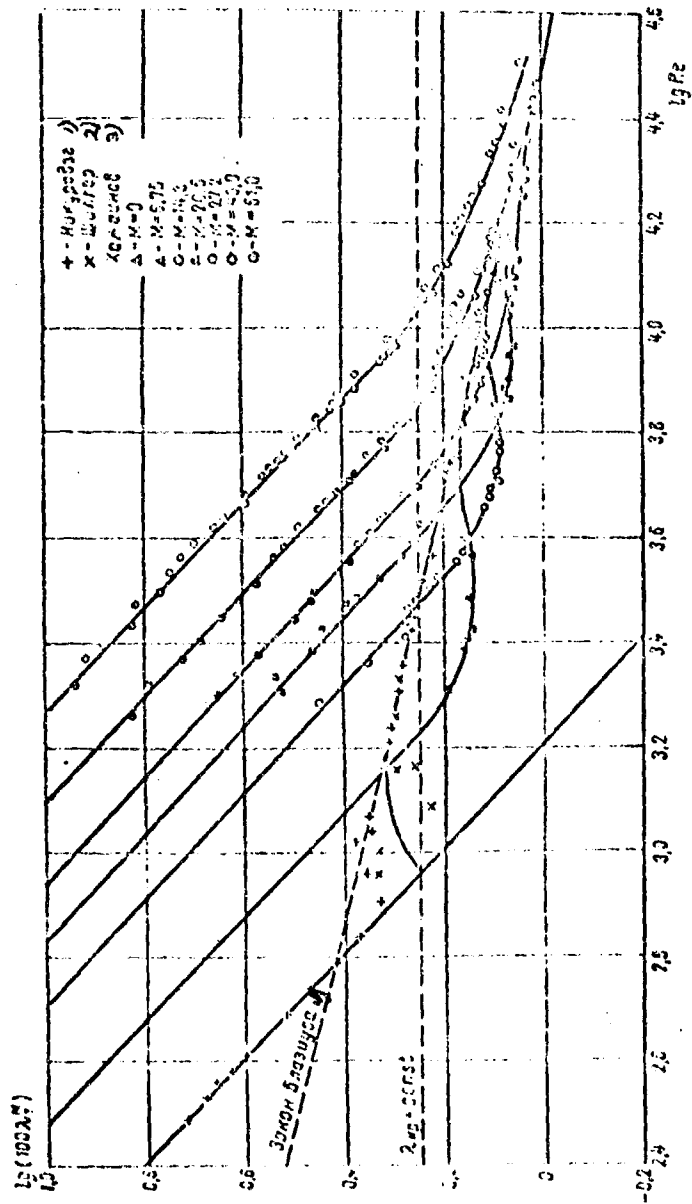
Fig. 31. Friction factor curves for the flow of conducting fluid in an MHD channel with a ratio of sides of 1:2.5.

KEY: 1) Nikuradse; 2) Schiller; 3) Khozhainov; 4) Blasius law.

It follows from the above analysis that it is not generally permissible to calculate λ_t^m from ordinary hydrodynamic formulas.

L. Harris [52] has analyzed the turbulent flow of a conducting fluid in a flat channel, following the method developed by K. Millikan for turbulent flows without a magnetic field.

Using the π-theorem from the theory of similitude, Harris obtained the following functional relationship for the velocity distribution in turbulent flow of conducting fluids in flat channels:

$$\frac{\tilde{v}}{v^*} = f(Re^*, M, x^*), \tag{2.117}$$

where

$$Re^* = \frac{v_*}{4}/\lambda_t^m ; \quad x^* = 1 - \frac{y_c}{b} ; \quad \tilde{v} = \tilde{v}/\lambda_2 .$$

In Eq. (2.117) the tilde denotes averaging with respect to time.

Assuming that the velocity distribution near the wall is independent of the channel size, Eq. (2.117) can be reduced to the form

$$\frac{\tilde{v}}{v^*} = X(Re^*, x^*, Mx^*). \tag{2.118}$$

Considering the fact that the effect of a transverse magnetic field on velocity distribution reduces to flattening the distribution in the core flow, it can be assumed that the local structure of the core will not depend on viscosity. Then the following relationship can be used as the MHD analogy of the velocity distortion:

$$\frac{\tilde{U} - \tilde{v}}{v^*} = \Omega\left(\frac{M^2}{Re^*}, x^*\right). \tag{2.119}$$

where $\tilde{U}$ is the average velocity in the center of the channel.

From the condition that Eqs. (2.118) and (2.119) must yield identical results in a certain region of values of x^*, we get

$$\frac{\tilde{v}}{v^*} = X(Re^*, x^*, Mx^*) = \Phi(Re^*, M) - \Omega\left(\frac{M^2}{Re^*}, x^*\right), \tag{2.120}$$

where $\Phi(Re^*, M) = \dfrac{\tilde{U}}{v^*}$.

Differentiating Eq. (2.120) with respect to x^*, Re^* and M, we get

$$\frac{\partial(\cdots)}{\partial x^*} = Re^* \frac{\partial X}{\partial(Re^* x^*)} + M \frac{\partial X}{\partial(Mx^*)} = \cdots ; \tag{2.121}$$

50

$$\frac{\partial(\tilde{\omega}/\tilde{\omega})}{\partial \text{Re}^*} = x^* \frac{\partial X}{\partial(\text{Re}^*x^*)} \sqrt{\text{Re}^*} + \left(\frac{M}{\text{Re}^*}\right)^2 \cdots \qquad (2.122)$$

$$\frac{\partial(\tilde{\omega}/\tilde{\omega})}{\partial M} = x^* \frac{\partial X}{\partial(Mx^*)} \frac{\partial \Omega}{\partial M} - 2 \frac{M}{\text{Re}^*} \cdots \qquad (2.123)$$

whence

$$\text{Re}^* \frac{\partial D}{\partial \text{Re}^*} + M \frac{\partial D}{\partial M} = - x^* \frac{\partial \Omega}{\partial x^*} + \cdots \qquad (2.124)$$

Since the left-hand side of Eq. (2.124) depends only on Re* and M*, while the right-hand side depends only on x* and M^2/Re^*, both these sides should be functions of M^2/Re^* only. This equation thus reduces to the two relationships

$$\text{Re}^* \frac{\partial D}{\partial \text{Re}^*} + M \frac{\partial D}{\partial M} = g_1\left(\frac{M^2}{\text{Re}^*}\right); \qquad (2.125)$$

$$- x^* \frac{\partial \Omega}{\partial x^*} + \frac{M^2}{\text{Re}^*} \frac{\partial \Omega}{\partial(M^2/\text{Re}^*)} = g_1\left(\frac{M^2}{\text{Re}^*}\right). \qquad (2.126)$$

where g_1 is some arbitrary function.

Eliminating Ω, we find from Eqs. (2.122)-(2.124)

$$2\text{Re}^*x^* \frac{\partial X}{\partial(\text{Re}^*x^*)} + Mx^* \frac{\partial X}{\partial(Mx^*)} = 2\text{Re}^* \frac{\partial D}{\partial \text{Re}^*} + M \frac{\partial D}{\partial M}. \qquad (2.127)$$

Since the left-hand side of the above expression depends only on Re* x*, while its right-hand side is a function of only Re* and M, both these parts should be functions only of M/Re*, whence

$$2\text{Re}^*x^* \frac{\partial X}{\partial(\text{Re}^*x^*)} + Mx^* \frac{\partial X}{\partial(Mx^*)} = g_2\left(\frac{M}{\text{Re}^*}\right); \qquad (2.128)$$

$$2\text{Re}^* \frac{\partial D}{\partial \text{Re}^*} + M \frac{\partial D}{\partial M} = g_2\left(\frac{M}{\text{Re}^*}\right), \qquad (2.129)$$

where g_2 is a second arbitrary function.

Equations (2.125) and (2.129) make it possible to express function Φ in terms of g_1 and g_2. The solution for Φ has the form

$$\Phi(\text{Re}^*, M) = G_1\left(\frac{M^2}{\text{Re}^*}\right) + G_2\left(\frac{M}{\text{Re}^*}\right). \qquad (2.130)$$

where

$$G_1 = \int \frac{g_1(z)}{z} dz; \quad G_2 = -\int \frac{g_2(z)}{z} dz. \qquad (2.131)$$

51

Best Available Copy

The general solutions for Eqs. (2.126) and (2.128) are written as

$$\Omega\left(\tfrac{M^2}{Re^4},x^2\right) \quad G_1\left(\tfrac{M^2x^2}{Re^4}\right) + G_2\left(\tfrac{M^2}{Re^4}\right); \tag{2.132}$$

$$X(Re^4x^2,M^2) \quad G_1\left(\tfrac{M^2x^2}{Re^4}\right) + G_2\left(\tfrac{M^2}{Re^4}\right). \tag{2.133}$$

It follows from the conditions

$$\Omega\left(\tfrac{M^2}{Re^4},1\right) \quad 0$$

that

$$G_1(z) \quad G_2(z).$$

From Eq. (2.120) we get

$$G_1(z) \quad G_2(z).$$

Consequently, functions Φ, Ω and X can all be expressed in terms of G_1 and G_2

$$\Phi(Re^4,M) \quad G_1\left(\tfrac{M^2}{Re^4}\right) + G_2\left(\tfrac{M}{Re^4}\right); \tag{2.134}$$

$$\Omega\left(\tfrac{M^2}{Re^4},x^2\right) \quad G_1\left(\tfrac{M^2x^2}{Re^4}\right) + G_2\left(\tfrac{M^2}{Re^4}\right); \tag{2.135}$$

$$X(Re^4x^2,M^2) \quad G_1\left(\tfrac{M^2x^2}{Re^4}\right) + G_2\left(\tfrac{M}{Re^4}\right). \tag{2.136}$$

As in ordinary hydrodynamics, functions G_1 and G_2 can be represented as

$$G_1(z) \quad A\ln z + F_1(z);$$
$$G_2(z) \quad 2A\ln z + C + F_2(z).$$

Then Eqs. (2.134)-(2.136) can be represented in the form

$$\frac{\tilde{U}}{v^*} \quad A\ln Re^4 + C + F_1\left(\tfrac{M^2}{Re^4}\right) + F_2\left(\tfrac{M}{Re^4}\right); \tag{2.137}$$

$$\frac{\tilde{U}-\tilde{v}}{\tilde{v}^*} \quad A\ln x^* - F_1\left(\tfrac{M^2}{Re^4},x^*\right) + F_1\left(\tfrac{M^2}{Re^4}\right); \tag{2.138}$$

$$\frac{\tilde{v}}{v^*} \quad A\ln(Re^4x^*) + C + F_1\left(\tfrac{M^2}{Re^4},x^*\right) + F_2\left(\tfrac{M}{Re^4}\right). \tag{2.139}$$

Constants A and C contained in Eqs. (2.137)-(2.138) can be taken from experimental data obtained without a magnetic field.

52

Since function $F_2(M/Re^*)$ is not contained in the velocity distortion equations and vanishes when $M = 0$, we may set

$$F_2\left(\frac{M}{Re^*}\right) = 0.$$

We find the following expression for the velocity distribution in a turbulent MHD flow:

$$\frac{\tilde{v}}{v^*} = 5.657 \lg(Re^*x^*) + 6.151 + F_1\left(\frac{M^2}{Re^*}x^*\right). \tag{2.140}$$

When $M \to 0$, Eq. (2.140) becomes identical with the logarithmic velocity distribution of common fluid flow.

Considering the fact that, according to Eq. (2.116), the friction factor is known when M and Re are given, it is convenient to express Eq. (2.140) in the form

$$\frac{\tilde{v}}{v^*} = 5.657 \lg\left(\sqrt{\frac{\lambda_t^=}{4}} \, Re\, x^*\right) + 6.151 + F_1\left(\frac{M^2}{Re}x^*\right). \tag{2.141}$$

A graphical presentation of function $F_1(\frac{M^2}{Re}x^*)$ is given in Fig. 32 (curve 1). Curve 2 of this figure describes, on a magnified scale, the variation of this function for the argument range of 0 to 0.05.
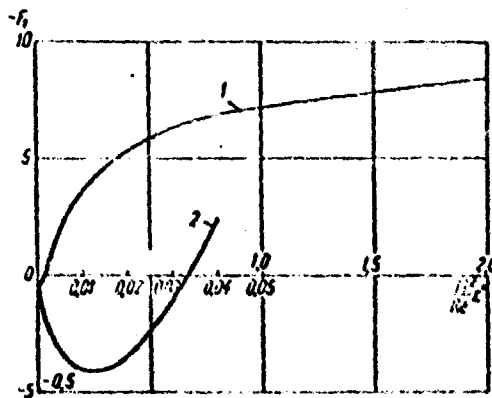
Fig. 32. Curve of function F_t vs. $\frac{M^2}{Re}x^*$.

Figure 33 shows the velocity profiles in a turbulent MHD flow in a flat channel, constructed from Eq. (2.141) for different values of Re at M = 100. For clarity of presentation, the velocity is referred to its maximum value. The velocity distribution shown in Fig. 33 by a dashed line is that of laminar flow.

Figure 34 shows the velocity distributions in a turbulent MHD flow obtained by P.S. Lykoudis [112] for mercury flowing in a channel with a side ratio of 1:5. The measurements were made in the plane perpendicular to large side of the channel and parallel to

53
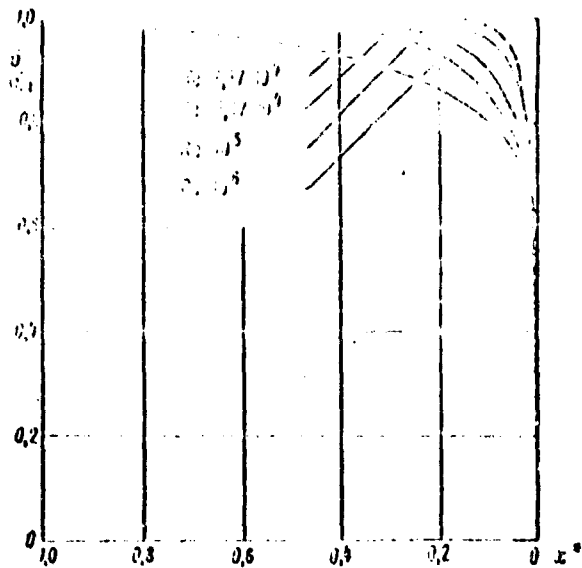
Fig. 33. Velocity distribution in a turbulent flow
of a conducting fluid in a flat MHD channel.

Fig. 34. Experimental ve-
locity distributions in the flow
of mercury in an MHD channel.
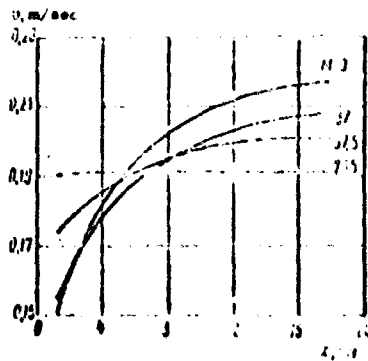
the applied magnetic field, with $Re = 5.05 \cdot 10^4$. The distance from the channel wall, in
mm, is laid off on the abscissa.

The above experimental velocity distributions are in qualitative agreement with
the semiempirical theory developed by L. P. Harris for flow in flat MHD channels.

The distortion of the velocity distribution in turbulent MHD flow with change in the
Hartmann number is due to superposition on the flow of induced ponderomotive forces
and to damping of turbulent velocity pulsations.

The magnetic field interferes with the development of velocity pulsations in planes
perpendicular to the field (Fig. 28). In the plane parallel to the magnetic field, the only
velocity pulsation reduction is that due to correlation phenomena.

54

Figures 35 show measured distributions of root-mean-square pulsations of longitudinal $\sqrt{v_z'^2}$ and transverse $\sqrt{v_y'^2}$ flow velocities, referred to maximum velocity. These data were obtained at the Donets Research Institute of Ferrous Metals under the leadership of I. L. Povkh [113] for flow of 30% aqueous H_2SO_4 in an open trough placed in the gap of an electromagnet ($Re = 50 \cdot 10^3$). It is easy to see that the turbulent intensity of the flow decreases with an increase in M.

Analysis of the above data shows that the magnetic field has an appreciable effect on the flow structure of conducting fluids in channels.
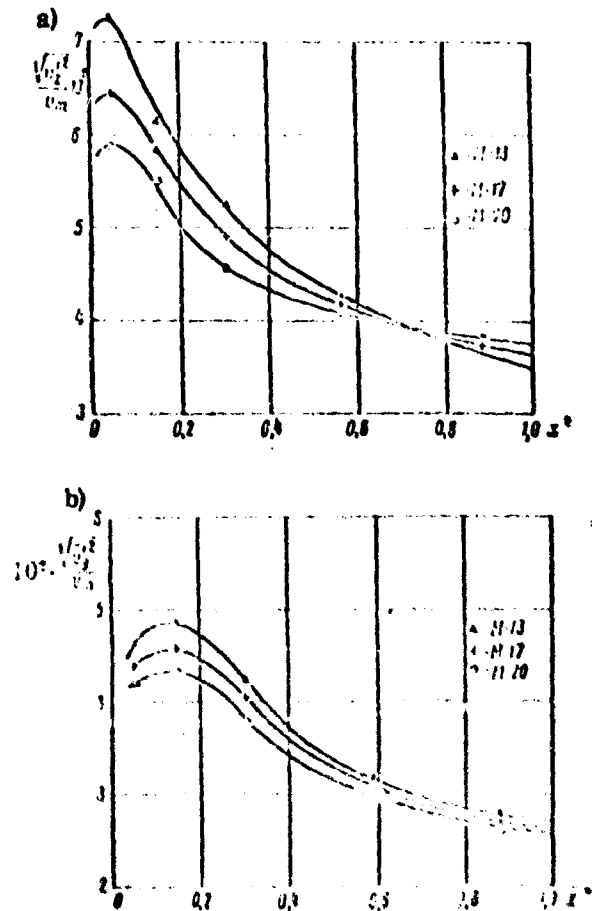
Fig. 35. The distribution of the longitudinal (a) and transverse (b) turbulent intensity in the flow of an electrolyte as a function of magnetic field strength.

7. Effect of Transverse Magnetic Field on the Turbulent Boundary Layer

We now consider the flow of conducting fluid past a flat dielectric plate in the presence of a transverse magnetic field. We assume that the boundary layer on the plate becomes turbulent starting from the leading edge of the plate $(z = 0)$.

As in common fluid flow, the turbulent boundary layer in this case can be computed from the momentum equation which is used to find the relationship between the momentum loss thickness and tangential stresses at the wall. These studies were performed recently by Kruger and Sonju [60].

Using the fact that fully developed MHD channel flows have developed flow cores, Eq. (2.140) can be used for expressing the velocity distribution in the turbulent boundary layer at the plate

$$\frac{\tilde{v}}{v^*} = 5.75 \lg\left(\frac{v^* x}{\nu}\right) + 5.15 + F_1\left(\frac{\sigma B^2}{\varrho v^*}\right), \tag{2.142}$$

where $v^* = \sqrt{\dfrac{\tau_0}{\varrho}}$ (τ_0 is the tangential stress at the wall) and $\nu = \eta/\varrho$.

At the edge of the turbulent boundary layer Eq. (2.142) takes the form

$$\frac{\tilde{U}}{v^*} = 5.75 \lg\left(\frac{v^* \delta}{\nu}\right) + 5.15 + F_1\left(\frac{\sigma B^2 \delta}{\varrho v^*}\right). \tag{2.143}$$

The above expression establishes the relationship between the potential flow velocity U and the boundary layer thickness δ.
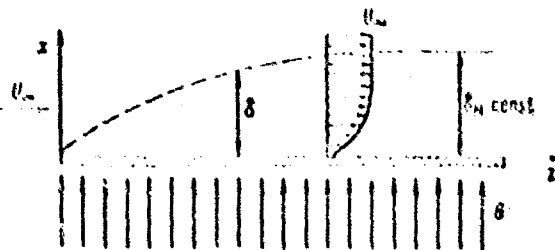
Fig. 36. Turbulent MHD boundary layer at a flat plate.

The integral equation of momentum for the boundary layer can be written as

$$\tau_0 + \delta \frac{dp}{dz} = \int_0^\delta jB\, dx - \frac{d}{dz}\int_0^\delta \varrho v^2\, dx + U \frac{d}{dz}\int_0^\delta \varrho v\, dx. \tag{2.144}$$

56

In the case at hand we can set

$$\frac{dp}{dz} = -j_z B_0 = -\sigma B_0 (E_y + U B_0).$$

(2.145)

Using the above expression and substituting into it the momentum loss thickness θ and the displacement thickness δ^*

$$\theta = \int_0^\delta \frac{\tilde{v}}{U}\left(1 - \frac{\tilde{v}}{U}\right) dx; \quad \delta^* = \int_0^\delta \left(1 - \frac{\tilde{v}}{U}\right) dx,$$

we get the expression

$$U^2 \frac{d}{dz}\theta = \tilde{v}^{*2} - \frac{\sigma B_0^2}{\rho} \delta^* U.$$

(2.146)

In the absence of a magnetic field Eq. (2.146) becomes identical with the momentum equation for a two-dimensional incompressible boundary layer [252, 253].

The system of equations (2.142), (2.143) and (2.146) can be solved numerically. Having done this, Kruger and Sonju found that the transverse magnetic field may have an appreciable effect on all the properties of the turbulent boundary layer.

Figures 37 and 38 show curves of the relative boundary layer thickness $\bar{\delta} = \delta U / \nu$ and the tangential stress at the wall $\bar{\tau} = \bar{v}^{*2}$ as a function of the dimensionless longitudinal coordinate $\bar{z} = zU/\nu$ and of the magnetic field parameter $\bar{B} = \sigma B_0^2 \frac{\nu}{\rho U^2}$.
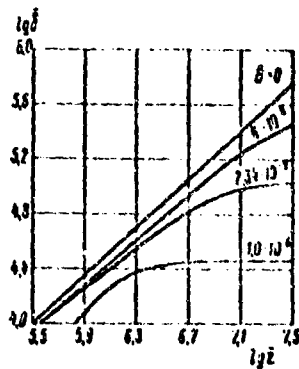
Fig. 37. Thickness of turbulent boundary layer as a function of the longitudinal coordinate for various transverse magnetic field flux densities.
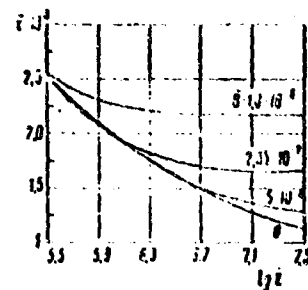
Fig. 38. Tangential stress at the wall of a plate in turbulent flow as a function of the longitudinal coordinate and of the flux density of the transverse magnetic field.

57

Examining the curves we see that, at a given $\bar{z}$, an increase in the field flux density reduces the boundary layer thickness and increases the tangential stress at the wall.

At a given value of $\bar{B}$ and increasing $\bar{z}$, the boundary layer thickness increases to its asymptotic value (in ordinary hydrodynamics the boundary layer thickness increases beyond bounds with increasing $\bar{z}$), while the tangential stress at the wall drops off (but also tends to its asymptotic value).

8. Effect of Transverse Magnetic Field on Unsteady Channel Flow of Conducting Fluids

Let us consider unsteady laminar flow of a conducting fluid in a long rectangular channel in the presence of a uniform magnetic field B_0 perpendicular to the dielectric walls. The channel's lateral walls will be regarded as conducting electrodes closed via load resistance R_ℓ (Fig. 39). It is also assumed that a $\gg$ b, so that the variation of flow variables along the y axis can be neglected by comparison with their changes along the x axis. Under these conditions, Eqs. (2.1)–(2.6) reduce to

$$\rho\,\frac{\partial v_z}{\partial t} = -\frac{\partial p}{\partial z} + \eta\,\frac{\partial^2 v_z}{\partial x^2} - j_y B_0; \tag{2.147}$$

$$\frac{\partial E_y}{\partial x} = -\frac{\partial B_x}{\partial t}; \tag{2.148}$$

$$j_y = -\frac{1}{\mu}\frac{\partial B_x}{\partial x}; \tag{2.149}$$

$$j_y = \sigma(E_y + v_z B_0). \tag{2.150}$$
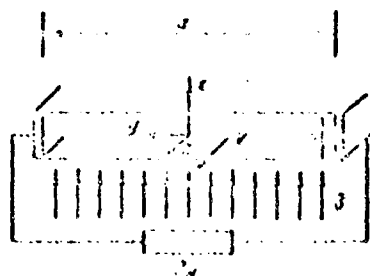
Fig. 39. Schematic diagram of an MHD generator duct.

The general solution of the above equations at arbitrary magnetic Reynolds numbers is, normally, obtained in the form of integrals in the complex plane; it is difficult to evaluate for cases of practical interest [66–72, 74]. However, when $R_m \ll 1$, one can state this problem as an approximation and thus obtain a solution in its final and relatively simple form. We shall now consider the problem for $R_m \ll 1$ and a constant pressure gradient.

58

Integrating Eq. (2. 148) and then dividing through by UB_0 we get

$$1 \sim \frac{E_y}{U B_0} \sim F(t) + R_m \frac{b}{UT},$$

where U and T are the characteristic velocity of the conducting fluid and the characteristic time.

When $R_m \ll 1$ and $b/UT \leqslant 1$, it can be assumed that E_y does not depend on x and is a function of time only. Then Eq. (2. 147), upon substitution of Eq. (2. 150) and use of Ohm's law in the external circuit, reduces to the following integrodifferential equation [76]:

$$\frac{\partial v}{\partial t} = P + v \frac{\partial^2 v}{\partial x^2} + k \frac{M^2 v}{b^2} \cdot \frac{1}{b} \int_{-\frac{b}{2}}^{\frac{b}{2}} v \, dx - \frac{M^2 v}{b^2} v, \qquad (2.151)$$

where

$$P = -\frac{1}{\varrho} \frac{\partial p}{\partial z} = \text{const}; \quad v = v_z(x, 0); \quad k = \frac{R_\ell}{R_\ell + R_{in}};$$

while $R_{in} = \frac{1}{\sigma} \cdot \frac{a}{b\ell}$ is the internal electric resistance of the conducting fluid in a channel of length ℓ.

The boundary conditions for Eq. (2. 151) are:

$$v \Big|_{x = \pm \frac{b}{2}} = 0. \qquad (2.152)$$

The initial conditions shall be specified in the following form: when $t = 0$

$$v(x, 0) = v_0(x) = C_0 \operatorname{ch} \frac{M_0}{2} \left(\frac{\operatorname{ch} \frac{M_0}{b} x}{\operatorname{ch} \frac{M_0}{2}} - 1 \right), \qquad (2.153)$$

where

$$C_0 = \frac{P_0}{\frac{M_0^2 v}{b^2} \operatorname{ch} \frac{M_0}{2} \left[1 + k_0 \left(\frac{2 \operatorname{th} \frac{M_0}{2}}{M_0} - 1 \right) \right]}.$$

Let the magnetic field, the load and pressure gradient change instantaneously at the initial time ($t = 0$); this is physically justified by the short duration of electromagnetic transient processes as compared with the MHD transient processes.

To solve this problem, we represent the flow velocity in the form [76]

$$v = u(x, t) + \int_0^t f(t)\,dt,$$ (2.154)

where f(t) is an arbitrary time function.

Upon substitution of Eq. (2.154), Eq. (2.151) breaks down into two equations

$$\frac{\partial u}{\partial t} = v\frac{\partial^2 u}{\partial x^2} - \frac{H^2 v}{b^2} u;$$ (2.155)

$$f(t) = P + \frac{H^2 v}{b^2} \kappa \frac{1}{b} \int_{-\frac{b}{2}}^{\frac{b}{2}} u\,dx - \frac{H^2 v}{b^2} \int_0^t f(t)\,dt.$$ (2.156)

The boundary and initial conditions for Eq. (2.155) are

$$u\Big|_{x = \pm \frac{b}{2}} = -\int_0^t f(t)\,dt;$$ (2.157)

$$u\Big|_{t=0} = v_0(x).$$ (2.158)

We shall seek the solution of Eq. (2.155) in the form

$$u = F(x) + \sum_{n=1}^{\infty} \Phi_n(t)\,\Psi_n(x).$$ (2.159)

where F(x) corresponds to the asymptotic value of u.

Substituting Eq. (2.159) into Eq. (2.155), we get three ordinary differential equations, the solutions of which are known [257]:

$$F''(x) - \frac{H^2}{b^2} F(x) = 0;$$ (2.160)

$$\Phi_n'(t) + \alpha_n^2 \Phi_n(t) = 0;$$ (2.161)

$$\Psi_n''(x) - \beta_n \Psi_n(x) = 0.$$ (2.162)

The solution for u can be written in the form

$$u = C_1 \operatorname{ch} \frac{H}{b} x + C_2 \operatorname{sh} \frac{H}{b} x + \sum_{n=1}^{\infty} A_n e^{-\alpha_n^2 t} (B_n \operatorname{ch} \beta_n x + D_n \operatorname{sh} \beta_n x).$$ (2.163)

In the above expression, α_n and β_n are related by the equation

$$\alpha_n^2 = \frac{H^2 v}{b^2} - \beta_n v.$$ (2.164)

60

From boundary conditions u and from the fact that the initial velocity distribution is even, we get

$$C_3 = D_\kappa = 0.$$

Upon substitution of Eqs. (2.154) and (2.157), the solution for v takes the form

$$v = C_1 \left(\mathrm{ch}\, \frac{M}{b} x - \mathrm{ch}\, \frac{M}{2} \right) + \sum_{n=1}^{\infty} C_n e^{-\alpha_n^2 t} \left(\mathrm{ch}\, \sqrt{\beta_n} x - \mathrm{ch}\, \sqrt{\beta_n}\, \frac{b}{2} \right). \qquad (2.165)$$

Using Eq. (2.165) we can find the following transcendental equation for the eigenvalues

$$\beta_n = \frac{M^2 k}{b^2} \left(1 - \frac{2\,\mathrm{th}\, \sqrt{\beta_n}\, \frac{b}{2}}{b \sqrt{\beta_n}} \right). \qquad (2.166)$$

Examination of Eq. (2.166) shows that a unique positive real value of β_n exists when $M^2 k > 12$; when $M^2 k < 12$, Eq. (2.166) has an infinite number of negative real roots.

From Eq. (2.165) we also get the integration constant C_1:

$$C_1 = \frac{P}{\frac{M^2 v}{b^2}\, \mathrm{ch}\, \frac{M}{2} \left[1 + k \left(\frac{2\,\mathrm{th}\, \frac{M}{2}}{M} - 1 \right) \right]}. \qquad (2.167)$$

The series coefficients C_n are determined from the initial conditions. Here it is sufficient to use the property of orthogonality of the system of functions $\varphi_n =$

$= \left(\mathrm{ch}\, \sqrt{\beta_n} x - \mathrm{ch}\, \sqrt{\beta_n}\, \frac{b}{2} \right)$ in the range $\pm b/2$. In fact, using Eq. (2.161) and $n \neq m$

$$\int_{-\frac{b}{2}}^{\frac{b}{2}} \left(\mathrm{ch}\, \sqrt{\beta_n} x - \mathrm{ch}\, \sqrt{\beta_n}\, \frac{b}{2} \right) \left(\mathrm{ch}\, \sqrt{\beta_m} x - \mathrm{ch}\, \sqrt{\beta_n}\, \frac{b}{2} \right) dx = 0.$$

Multiplying Eq. (2.153) by φ_n and integrating in the range $\pm b/2$, we get

$$C_n = \frac{C_0 J_1 - C_1 J_2}{J_3}, \qquad (2.168)$$

where

$$J_1 = \mathrm{ch}\, \frac{M_0}{2} \left\{ \frac{\beta_n b^2}{M^2 k} - \frac{2\,\mathrm{th}\, \frac{M_0}{2}}{M_0} + \frac{\beta_n b^2}{M_0^2 - b^2 \beta_n} \left(\frac{2M_0}{b^2 \beta_n}\, \mathrm{th}\, \frac{M_0}{2} + \frac{\beta_n b^2}{M^2 k} - 1 \right) \right\};$$

61

$$I_2 = \operatorname{ch}\frac{M}{2}\left\{\ldots\left[(1-\ldots)\ldots 2\frac{k}{M}\operatorname{th}\frac{M}{2}\right]\right\};$$

$$I_3 = \ldots\frac{b}{2}\ldots\left\{3-\ldots\left(\frac{\beta_n b^2}{M^2 k}-1\right)^2\right\}.$$

Let us consider certain special cases of this solution. Let $v = 0$ at $t = 0$. In this case, C_0 in Eq. (2.168), and the solution denotes acceleration of the fluid from rest to the steady-state value. Here, if $k = 0$, then $\beta_n < 0$, and Eq. (2.165) reduces to the form

$$v = \frac{\ldots}{\ldots v}\left\{\left(1-\frac{\operatorname{ch}\frac{M}{2}x}{\operatorname{ch}\frac{M}{2}}\right) - 4M^2 e^{-\frac{Mvt}{\ldots}}\times\sum_{n=1}^{\infty}\frac{(-1)^{n+1}}{\lambda_n(M^2+\lambda_n^2)}e^{-\frac{\lambda_n^2 vt}{b^2}}\cos\frac{\lambda_n x}{b}\right\}, \quad (2.169)$$

where $\lambda_n = \pi(2n-1)$. We note that Eq. (2.169) is identical with the solution obtained in [67] for this particular case.

When $t \to \infty$, Eq. (2.169) becomes Eq. (2.40) for steady flow. When $M \to 0$, it reduces to the form which holds in ordinary hydrodynamics [258]

$$v = \frac{\ldots}{8v}\left\{\left[1-\left(\frac{2x}{b}\right)^2\right]-32\sum_{n=1}^{\infty}\frac{(-1)^{n+1}}{\lambda_n^3}e^{-\frac{\lambda_n^2 vt}{b^2}}\cos\lambda_n\frac{x}{b}\right\}. \quad (2.170)$$

For zero initial conditions and $k = 1$, Eq. (2.165) coincides with the solution presented in [73]. For zero initial conditions and an arbitrary k, we can integrate Eq. (2.165) over the channel cross section and refer the result thus obtained to the asymptotic value of the average velocity; we then get

$$U = \frac{U}{U_\infty} = 1 - \frac{1}{C_0 M \operatorname{ch}\frac{M}{2}\left(2\operatorname{th}\frac{M}{2}-M\right)}\times\sum_{n=1}^{\infty}C_n(\ldots)e^{-\ldots t}\operatorname{ch}\beta_n\frac{b}{2}. \quad (2.171)$$

This expression can be used for calculating the acceleration times of a conducting fluid in an MHD channel under specified conditions. Similar expressions are obtained for deceleration modes and for transitions from one flow mode to another.

For this case, the viscous friction losses in the channel can be represented as

$$\frac{\eta}{2}\int_{-\frac{b}{2}}^{\frac{b}{2}}\frac{\partial v}{\partial x}dx = \ldots U\eta\frac{K(v, M, t)}{2b^2}. \quad (2.172)$$

62

where

$$K(\gamma, M, t) = \cfrac{4\left[C_1 M \operatorname{sh} \dfrac{M}{2} + \sum_{n=1}^{\infty} C_n b \sqrt{\bar{\beta}_n}\, e^{-a_n^2 t} \operatorname{sh} \sqrt{\bar{\beta}_n}\, \dfrac{b}{2}\right]}{C_1 \operatorname{ch} \dfrac{M}{2}\left(\dfrac{2\operatorname{th}\dfrac{M}{2} - M}{M}\right) - \dfrac{1}{kM^2} \sum_{n=1}^{\infty} C_n b^3 \beta_n e^{-a_n^2 t} \operatorname{ch} \sqrt{\bar{\beta}_n}\, \dfrac{b}{2}}. \tag{2.173}$$

When $t \rightarrow \infty$, Eq. (2.173) becomes identical to the previously cited Eq. (2.48).
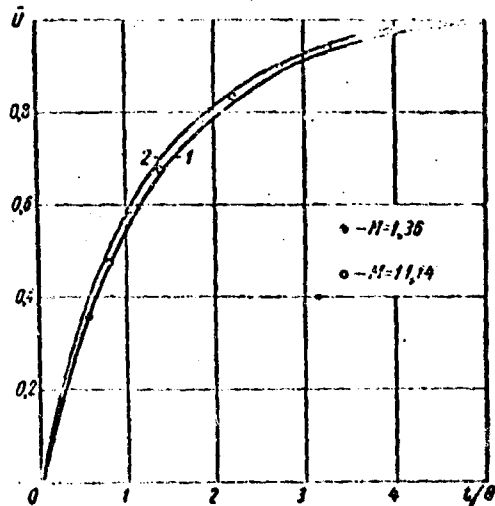
Fig. 40. The relative velocity of a conducting fluid in a flat channel as a function of t/θ.

Figure 40 shows curves of $\bar{U} = \bar{U}(t/\theta)$ constructed from Eq. (2.171). Curve 1 corresponds to the case $M = 0$. Curve 2 is constructed for case $M \gg 1$. Changes in the load ratio are virtually without effect on the curve shape.

The same figure also shows data obtained by analysis of experimental oscillograms presented in [109] and referring to the acceleration of mercury in an MHD channel with a side ratio of 1:10 at $k = 1$.

Here θ is expressed by

$$\theta = \frac{R_0^2}{\nu} \cdot \frac{1}{\frac{K(\gamma, M)}{2} + M^2(1 - k)}.$$

It follows from the above data that theoretical calculations are in satisfactory agreement with the experimental results.

63

The curve for acceleration of the conducting fluid in a flat MHD channel in the coordinate plane ($\overline{U}$, t/θ) holds virtually for all such channels. The acceleration time is approximately 50. This shows that, at a constant pressure gradient, the transverse magnetic field reduces the duration of transient processes.

*   *   *

In this chapter we have analyzed relatively simple magnetohydrodynamic problems as applied to channel flow of conducting fluids and flow past bodies.

The condition $\ell \gg a \gg b$, assumed in examining MHD channel flow, is not always satisfied under real conditions. At a finite ratio of channel walls, the side walls affect the structure and the overall flow variables. In the case $a \approx b$, the flow variables are affected by the conducting electrodes. In addition, in real MHD channels, as a result of finite length of the poles of the magnet, the magnetic field in the edge regions is not uniform in the longitudinal direction.

Solution of the above problems with consideration of finite channel size and of the presence of conducting electrodes is extremely difficult even in the case of laminar flow. Some solutions for conditions close to those encountered in practice are presented in the references.

However, the problems considered by us qualitatively and quantitatively clarify the MHD effects of direct applied interest.

The electromagnetic induction phenomenon in conducting liquids is used in various MHD measuring instruments and devices. Due to the quite high conductivity of these fluids such instruments and devices are relatively simple.

The field of conductive ponderomotive electromagnetic forces conducting liquids is used in electromagnetic pumps and MHD engines. The ability to control boundary layers by means of electric and magnetic fields can be used for reducing vessel drag in sea water.

CHAPTER 3

MAGNETOHYDRODYNAMIC METERS

Magnetohydrodynamic [MHD] meters in use or of prospective use in marine engineering comprise a broad range of instruments. The principal instruments of this clan are magnetic flowmeters and sea-current velocity meters. A special group comprises instruments used for measuring density, temperature [heat], chemical reagents, etc. A separate group is made up of devices for studying the structure of flows of conducting fluids. Each of these groups includes a large number of instruments, which differ from one another by the kind of power used, design execution and measuring principles, frequently determined by the physical properties of the conducting fluids.

Due to the limited scope of this book, we cannot consider all MHD instruments. Hence we shall consider only those which are of greatest practical interest.

1. Operation and General Description of Magnetic Flowmeters

The MHD method of measuring flow velocity is based on the electromagnetic induction phenomenon. As specified by the law of electromagnetic induction, whenever any medium moves relative to a magnetic field, an emf proportional to the flow velocity and independent of the physical properties of the medium is induced in the latter.

When a fluid moves in an MHD channel equipped with electrodes, the emf induced in the flow results in the appearance on electrodes of a potential difference the magnitude of which is indicative of the flow velocity. The conductivity of the fluid governs several effects which determine whether this method is of practical use.

Because of the finite length of the longitudinal magnetic field, the electric currents circulating in the conducting fluid form closed loops at the end zones, and the fluid thus exerts a ponderomotive force on the external magnetic system; the magnitude of this force can also be used for indicating the flow velocity.

A third effect which can be used for designing magnetic flowmeters is the fact that a magnetic field in which a conducting fluid moves is attenuated by the field of the induced currents. The magnitude of this attenuation of the external magnetic field can be used to characterize the flow velocity of the conducting fluid.

Corresponding to the above effects, one distinguishes the following types of mag-
netic flowmeters:

1) conduction type, which measure the potential difference on electrodes, pro-
duced by the emf induced in the flow;
2) ponderomotive [force] type, based on the direct measurement of the force of
interaction between the currents induced in the fluid and the applied magnetic field;
3) induction type, based on measuring the magnetic field of induced currents.

The schematics of these flowmeters are shown in Figs. 41, 42 and 43.
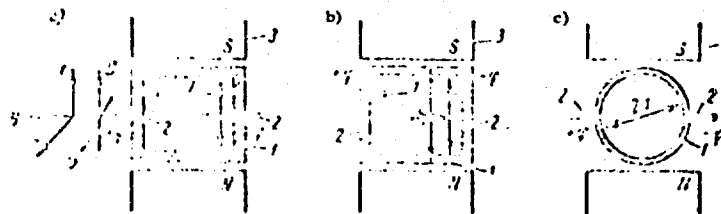
Fig. 41. Conduction-type magnetic flowmeters:

a) With a rectangular duct and point electrodes; b)
with a rectangular duct and continuous electrodes; c)
with a circular duct and point electrodes.

The conduction-type magnetic flowmeter, shown in Fig. 41, consists of rectangu-
lar or circular duct 1 made from nonmagnetic material, with conducting electrodes 2
installed in it. The flowmeter duct is placed in the gap of a permanent magnet 3 or a
DC or AC electromagnet. An instrument measuring the potential difference produced
by the flow of the conducting fluid in the duct is connected across the electrodes.

A rotary force flowmeter is shown in Fig. 42. The instrument uses a magnet
assembly which moves at the same speed as the fluid.
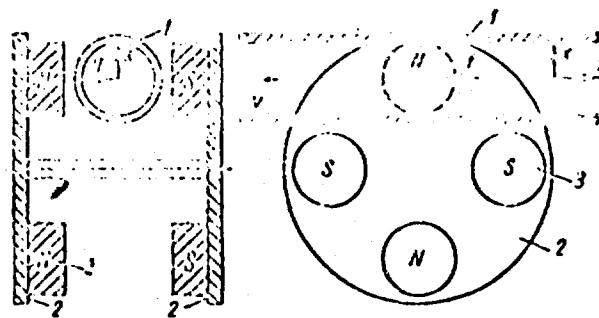
Fig. 42. Schematic of a rotary force [pon-
deromotive] magnetic flowmeter.

The fluid flows through pipe 1 placed between two disks 2 fastened on a common
shaft. Four pairs of permanent magnets 3 are fastened on the disks at points equidistant

66

from the shaft. The electromagnetic forces applied to magnets by the fluid passing through the pipe force the disks to rotate. The velocity or mass flow rate of the fluid is measured on the basis of the angular velocity of this rotation.

The force with which the flow acts on the magnets depends on the conductivity of the fluid, which should be sufficient in order to overcome the friction in the shafts of the instrument. Since the rotational inertia of the instrument is relatively high, it is insensitive to rapid velocity changes, i.e., its dynamic response is quite low.
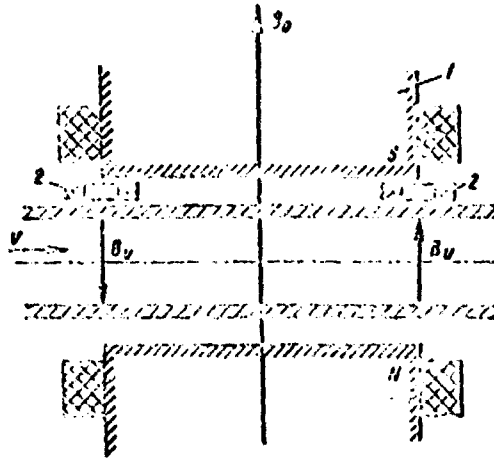
Fig. 43. Schematic of an induction-type magnetic flowmeter.

An induction-type magnetic flowmeter is shown in Fig. 43. In the gap of an AC electromagnet 1, near the pipe, are placed two identical measuring coils 2, connected to a voltmeter. The coils are connected in opposition so that the emfs induced in them by the magnetic field of the main electromagnet cancel each other. The magnetic fields of the currents induced in the conducting fluid have different directions at the instrument's inlet and outlet, so that the emfs produced in the measuring coils by these fields add up.

The most extensively used magnetic flowmeter is the conduction type, although in certain special cases preference is given to induction or force flowmeters.

Magnetic flowmeters have a number of substantial advantages over other flowmeters.

The magnetic flowmeters now produced serially for industrial use are of the 0.5-1 accuracy classes. Magnetic flowmeters of the 0.25 accuracy class are under development [147, 153].

Due to linearity of their characteristics and the use of multi-range meters, magnetic flowmeters have a wide operations range, appreciably exceeding that of other types of flowmeters.

67

Conduction and induction-type magnetic flowmeters have no rotating parts, packing glands, seals, etc., i.e., they are fully sealed. These flowmeters exhibit good dynamic response which makes them useful for measuring unsteady flows.
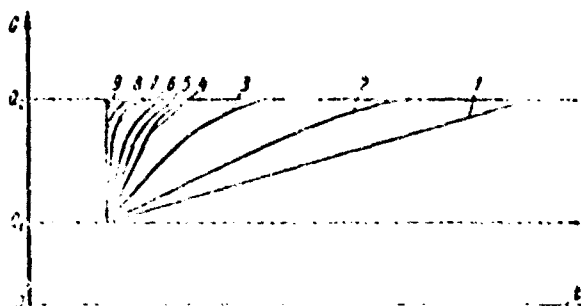
Fig. 44. Response-time curves of various types of flowmeters.

1) Vane; 2) ionization; 3) gyroscopic; 4) flowmeters with Coriolis acceleration; 5) external-flow flowmeters; 6) thermoanemometric; 7) ultrasonic; 8) magnetic flowmeters with AC magnets; 9) magnetic flowmeters with DC or permanent magnets.

Figure 44 shows curves of $G = f(t)Q$, which characterize the response time of flowmeters on sudden change in flowrate from Q_1 to Q_2; these curves show that magnetic flowmeters exhibit high dynamic response.

Because MHD effects in a certain range of M and Re reduce the flow friction factor, magnetic flowmeters for liquid metals can be so designed that they will not introduce additional flow resistance in the circulation loop.

A particularly valuable aspect of magnetic flowmeters is the fact that they can be used with corrosive media and radioactive liquid metals.

Among shortcomings of flowmeters used with liquids with ionic conductivities are their dependence on a number of factors produced by electrochemical processes (in a constant magnetic field) and various interferences (in an alternating magnetic field). However, means are available for combating these interferences.

We shall limit ourselves to discussion of conduction-type flowmeters, which are simple and the most widely used in various branches of technology.

2. Theory of DC Conduction-Type Magnetic Flowmeters

Magnetic Flowmeters with Rectangular Duct and Point Electrodes

Consider the flow of a conducting fluid in the rectangular duct of a conduction-type flowmeter with point electrodes depicted in Fig. 41a. We shall assume that the duct is sufficiently long so that we can neglect edge effects and regard the applied magnetic field as uniform.

Since div $J = 0$, which follows from Eq. (2.3), using Ohm's law in its differential form (2.6) we get the following equation relating the electric potential, flow velocity and applied magnetic field

$$\Delta\varphi = \text{div } [v \times B]. \tag{3.1}$$

Equation (3.1) is the basic equation for magnetic flowmeters and allows, given a velocity distribution and the magnetic flux density, to find the distribution of the electric potential φ.

Expanding div $[v \times B]$, Eq. (3.1) can be rewritten in the form

$$\Delta\varphi = B\,\text{curl } v - v\,\text{curl } B. \tag{3.2}$$

Since it is assumed that the magnetic field is uniform, we can assume in Eq. (3.2) v curl $B = 0$, whereupon it reduces to

$$\frac{\partial^2\varphi}{\partial x^2} + \frac{\partial^2\varphi}{\partial y^2} = B_0 \frac{\partial v(x,\,y)}{\partial y}. \tag{3.3}$$

It is assumed that the walls are insulators. Then the boundary conditions for the electric potential are

$$\frac{\partial\varphi}{\partial x}\Big|_{x=\pm\frac{b}{2}} = \frac{\partial\varphi}{\partial y}\Big|_{y=\pm\frac{a}{2}} = 0. \tag{3.4}$$

Equation (3.3) is the Poisson equation, while the problem itself corresponds to Neumann's second boundary-value problem [259].

The solution of Eq. (3.3) with boundary conditions (3.4) can be sought in the form [111]

$$\varphi = \frac{\varphi_0}{2} + \sum_{n=1}^{\infty} \varphi_n(x)\sin\lambda y, \tag{3.5}$$

where $\lambda = \frac{2(2n-1)\gamma}{b}$; and $\gamma = \frac{\pi b}{2a}$.

Substituting Eq. (3.5) into Eq. (3.3), we get

$$\Delta\varphi = \sum_{n=1}^{\infty} \left(\varphi_n'' - \lambda^2\varphi_n\right)\sin\lambda y = B_0\frac{\partial v(x,\,y)}{\partial y}. \tag{3.6}$$

The flow of the conducting fluid in the duct may be either laminar or turbulent. Since no relationship for the velocity distribution of turbulent flow in rectangular channels with arbitrary ratio of sides is available, we can, following S.A. Regirer [154], specify the velocity distribution as

$$v(x,\,y) = v_0 N_1 N_2 \frac{\text{ch } N_1 - \text{ch } N_1 \frac{2x}{b}}{N_1\text{ch } N_1 - \text{sh } N_1}\cdot\frac{\text{ch } N_2 - \text{ch } N_2 \frac{2y}{a}}{N_2\text{ch } N_2 - \text{sh } N_2}, \tag{3.7}$$

where v_0 is the mean flow velocity. N_1 and N_2 are dimensionless parameters, which characterize the degree of filling of the velocity distribution. When $N_1 \to 0$ and $N_2 \to 0$, a parabolic distribution is obtained from Eq. (3.7), while when $N_1 = N_2 \to \infty$, a uniform (flat) velocity distribution (plug flow) is obtained.

Expanding function (3.7) into a Fourier series with consideration of Eq. (3.6), we get

$$\varphi_n'' - \lambda^2 \varphi_n = V - W \operatorname{ch} N_1 \frac{2x}{b}, \tag{3.8}$$

where

$$W = \frac{4}{a} v_0 b_0 N_1 N_2 \frac{(-1)^{n+1} \operatorname{ch} N_2}{(N_1 \operatorname{ch} N_1 - \operatorname{sh} N_1)(N_2 \operatorname{ch} N_2 - \operatorname{sh} N_2)} \times$$

$$\times \left[1 - \frac{\lambda}{N_2^2 \frac{1}{a^2 \lambda} + \lambda} \right];$$

$$V = W \operatorname{ch} N_1.$$

The general solution of Eq. (3.8) can be written in the form

$$\varphi_n = C_1 \operatorname{sh} \lambda x + C_2 \operatorname{ch} \lambda x - \frac{V}{\lambda^2} - \frac{W}{N_1^2 \frac{4}{b^2} - \lambda^2} \operatorname{ch} N_1 \frac{2x}{b}. \tag{3.9}$$

Here the constants of integration are determined from the condition $\varphi_n' \big|_{x = \pm \frac{b}{2}} = 0$:

$$C_1 = 0; \quad C_2 = \frac{W N_1 \frac{2}{b} \operatorname{sh} N_1}{\left(N_1^2 \frac{4}{b^2} - \lambda^2 \right) \lambda \operatorname{sh} \lambda \frac{b}{2}},$$

after which Eq. (3.5) can be represented in the form

$$\varphi = \frac{v_0}{2} + \sum_{n=1}^{\infty} \left[\frac{W N_1 \frac{2}{b} \operatorname{sh} N_1}{\left(N_1^2 \frac{4}{b^2} - \lambda^2 \right) \lambda \operatorname{sh} \lambda \frac{b}{2}} \operatorname{ch} \lambda x - \right.$$

$$\left. - \frac{V}{\lambda^2} - \frac{W}{N_1^2 \frac{4}{b^2} - \lambda^2} \operatorname{ch} N_1 \frac{2x}{b} \right] \sin \lambda y. \tag{3.10}$$

The potential difference at two point electrodes ($x = 0$, $y = \pm a/2$) is determined by the expression

$$\varphi_1 - \varphi_2 = v_0 b_0 F_1(\gamma, N_1, N_2). \tag{3.11}$$

where

$$\Psi_1(\gamma, N_1, N_2) = \frac{8N_1 N_2 \operatorname{ch} N_2}{a^2(N_1 \operatorname{ch} N_1 - \operatorname{sh} N_1)(N_2 \operatorname{ch} N_2 - \operatorname{sh} N_2)} \times$$

$$\times \sum_{n=1}^{\infty} \left[1 - \frac{\lambda}{N_2^2 \frac{4}{a^2\lambda} + \lambda}\right] \left\{ \frac{N_1 \frac{2}{b} \operatorname{sh} N_1}{\left(N_1^2 \frac{4}{b^2} - \lambda^2\right) \lambda \operatorname{sh} \lambda \frac{b}{2}} - \frac{\operatorname{ch} N_1}{\lambda^2} \cdot \frac{1}{N_1^2 \frac{4}{b^2} - \lambda^2} \right\}.$$

(3.12)

In Eq. (3.11), function $\Psi(\gamma, N_1, N_2)$ characterizes the effect of the velocity field in the plane of the point electrodes on their potential difference.

Examination of Eq. (3.12) shows that for given values of N_1 and N_2 and for a variation in geometric parameter from 0 (flat channel) to 1.57 (square cross section), the effect of the velocity field on the potential difference between point electrodes is particularly strongly manifested in square channels. Here, for $\gamma = 0$, $\Psi = 1$, which shows that the readings of magnetic flowmeters with flat ducts and point electrodes do not depend on the velocity distribution in the conducting fluid.

In the case of $M < 1$, the magnetic field does not appreciably affect the velocity distribution in the fluid, i.e., MHD effects of the first kind may be neglected. In this case, the parameter N will characterize the effect of the Reynolds number on the magnetic flowmeter readings in turbulent flow of the conducting fluid. Here, MHD effects of the second kind take place.

Let us examine these effects in a magnetic flowmeter with a square duct. The velocity distribution in this case can be assumed symmetrical relative to the two coordinate axes, i.e., we can set $N_1 = N_2 = N$. Analysis of Eq. (3.12) shows that for a square duct in which N varies from zero (laminar flow) to infinity, function Ψ_1 varies from 1.12 to 1. The results of calculations for this case are presented in Fig. 45.
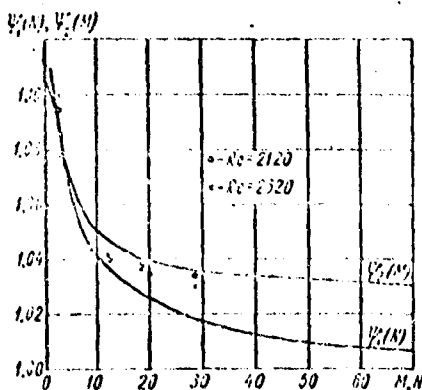
Fig. 45. Curves of Ψ_1 and Ψ_2 as a function of parameter N and Hartmann number for a square duct with point electrodes.

71

It is interesting that when the Boussinesq solution [260] is used for $v(x, y)$, function ψ_1 is equal to 1.105, which shows that Eq. (3.7) satisfactorily describes the symmetric velocity distribution in a square duct.

When $M > 1$, the velocity distribution becomes unsymmetrical relative to the two coordinate axes due to the appearance of MHD effects of the first kind. In this case in Eq. (3.12) for a square duct $N_1 \neq N_2$. Specifying different values of N_1 and N_2, we can clarify the effect of an asymmetric velocity distribution on the potential difference between point electrodes. However, it is better to use for this purpose the exact solution of D.A. Shercliff [13]. Here we get the following expression for the potential difference at point electrodes [111]

$$\Phi_1 - \Phi_2 = \ldots \psi_2(M); \tag{3.13}$$

$$\psi_2(M) = $$

$$\frac{\displaystyle\sum_{n=1} \frac{1}{(2n-1)^4} \left\{ \left(1 - \frac{m_1^2}{\lambda^2}\right) \operatorname{sh}(m_1 \cdot) \frac{b}{2} \left[1 - \frac{m_1}{\lambda} \frac{\operatorname{sh} m_1 \frac{b}{2}}{\operatorname{sh} \lambda \frac{b}{2}}\right]\right\}}{\displaystyle\sum_{n=1} \frac{1}{(2n-1)^4}\left[1 - \frac{K(\operatorname{ch} K - \operatorname{ch} M)}{1.02(2n-1)^2 \operatorname{sh} K}\right]}$$

$$\frac{\displaystyle\sum_{n=1} \frac{1}{(2n-1)^4} \left(1 - \frac{m_1^2}{\lambda^2}\right) \operatorname{sh}(m_1 \cdot) \frac{b}{2} \left[1 - \frac{m_1}{\lambda} \operatorname{sh} \lambda \frac{b}{2}\right]}{\displaystyle\sum_{n=1} \frac{1}{(2n-1)^4}\left[1 - \frac{K(\operatorname{ch} K - \operatorname{ch} M)}{1.02(2n-1)^2 \operatorname{sh} K}\right]} \tag{3.14}$$

where

$$K^2 = M^2 + 9.85(2n-1)^2; \quad M = B_0 \frac{b}{2}\sqrt{\frac{\sigma}{\eta}};$$

$$m_1 = \frac{1}{b}(K + M); \quad m_2 = \frac{1}{b}(K - M).$$

The results obtained using Eq. (3.14) are shown in Fig. 45, which also shows data obtained with laminar mercury flow in a square duct of a magnetic flowmeter with point electrodes. The two sets of data are in satisfactory agreement.

Examining Eq. (3.14), we see that when M goes from zero to infinity, the function ψ_2 changes from 1.105 to 1, and this is what describes the effect of the magnetic field on the potential difference between point electrodes in laminar flow.

In turbulent flow, the velocity distribution as a function of M^2/Re will be intermediate between the velocity distribution for laminar MHD flow and the velocity distribution for ordinary turbulent flow with a given Re. In any case, it can be stated that the value of function ψ will here lie within the above established limits.

72

The dependence of the potential difference at electrodes on a magnetic flowmeter on the velocity distribution can be eliminated by replacing the point electrodes by continuous lateral electrodes, which average the electric field.

Magnetic Flowmeters with Rectangular Ducts and Continuous Electrodes

We shall now consider the problem of flow of a conducting fluid in a rectangular channel, two sides of which, $x = \pm b/2$, have an arbitrary conductivity, while two others, $y = \pm a/2$, are ideally conducting electrodes (Fig. 41b). The magnetic field will, as before, be treated as uniform.

In this case, the system of initial equations is

$$\left.\begin{aligned}
\Delta\varphi &= B_0 \frac{\partial v\,(x,\,y)}{\partial y}; \quad \Delta\varphi_c = 0; \\
y &= \pm \frac{a}{2}; \quad \varphi = \pm\varphi_s; \quad \varphi_c = \pm\varphi_s; \\
x &= 0; \quad \frac{\partial\varphi}{\partial x} = 0; \\
x &= \frac{b}{2}; \quad \frac{\partial\varphi}{\partial y} = \frac{\partial\varphi_c}{\partial y}; \quad \sigma\frac{\partial\varphi}{\partial x} = \sigma_c\frac{\partial\varphi_c}{\partial x}; \\
x &= \frac{b_c}{2}; \quad \frac{\partial\varphi_c}{\partial x} = 0;
\end{aligned}\right\} \tag{3.15}$$

$$\left.\begin{aligned}
j_y &= \sigma\left(-\frac{\partial\varphi}{\partial y} + v_z B_0\right); \quad j_{yc} = \sigma_c\frac{\partial\varphi_c}{\partial y}; \\
j_x &= -\sigma\frac{\partial\varphi}{\partial x}; \quad j_{xc} = -\sigma_c\frac{\partial\varphi_c}{\partial x},
\end{aligned}\right\} \tag{3.16}$$

where the subscript "w" applies to horizontal walls, each of which is $(b_w - b)/2$ thick.

The velocity distribution in the duct can be assumed that given by Eq. (3.7).

Integrating the yth component of the current density over the entire duct cross section (including the walls), and using the boundary conditions, we can obtain the following expression for the potential difference at the electrodes of the magnetic flowmeter [154]:

$$\varphi_1 - \varphi_2 = v_0 B_0 a \frac{1}{\left[1 + \frac{\sigma_c}{\sigma}\left(\frac{b_c}{b} - 1\right)\right]} = v_0 B_0 a k_1. \tag{3.17}$$

It follows from Eq. (3.17) that in this case the potential difference at the side walls does not depend on the velocity distribution, but that the flowmeter sensitivity decreases due to conduction of the horizontal walls. When $\sigma_w \gg \sigma$ and with appreciably thick horizontal walls, the flowmeter sensitivity will be very low.

If the top and bottom walls of the flowmeter are thin, so that we may assume $b_w - b \approx 0$, or if they are made from a dielectric material ($\sigma_w = 0$) then

$$\varphi_1 - \varphi_2 = v_0 B_0 a. \tag{3.18}$$

73
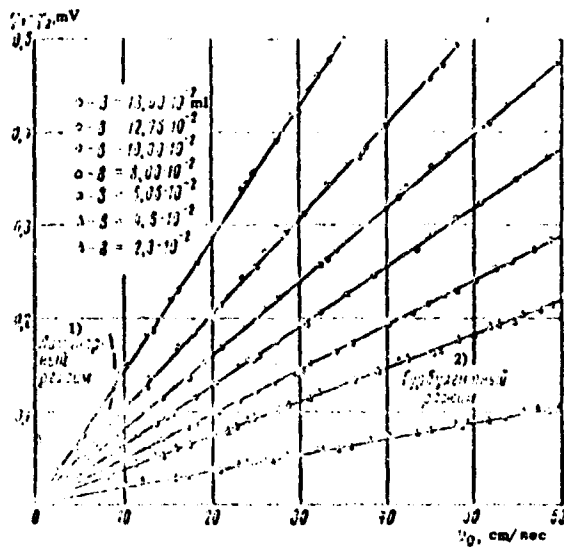
Fig. 46. Experimental characteristics of a
conduction-type DC magnetic flowmeter with a
rectangular duct and continuous lateral (side)
electrodes.

1) Laminar flow, 2) Turbulent flow.

Figure 46 shows experimental data $\psi_1 - \psi_2 = f(v_0)$ for a magnetic flowmeter with
a square duct, whose walls $x = \pm b/2$ are isolating, while the two others $y = \pm a/2$ are
metal electrodes. The data were obtained for mercury and various $B_0 = $ const. The
dashed line on the figure separates data for laminar and turbulent flow. It is easy to
see that the relationships $\psi_1 - \psi_2 = f(v_0)$ for $B_0 = $ const. are linear, which shows
that the readings of this magnetic flowmeter are independent of the velocity distribution.

Magnetic Flowmeters with Circular Ducts and Point Electrodes

Consider the flow of a conducting fluid in a circular duct of a magnetic flowmeter
(Fig. 41c). Assume that the walls are made from insulating material, and that the mag-
netic field is uniform.

The electric potential equation to be solved is, as before,

$$\Delta \psi = B_0 \frac{\partial v(y, x)}{\partial y}. \tag{3.19}$$

The boundary conditions for the electric potential are

$$\frac{\partial \psi}{\partial n}\bigg|_s = 0, \tag{3.20}$$

where n is the normal to contour S.

74

For an arbitrary velocity distribution and boundary conditions (3.20), the solution of Eq. (3.19) is [146]

$$\varphi_1 - \varphi_2 = \text{Im}\left\{\frac{B_0}{\pi}\iint\limits_{(S)} v(\xi, \eta)\left[\frac{1}{\chi - z} + \frac{a^2}{(a^2 - z\chi)\chi}\right]d\xi\,d\eta,\right. \tag{3.21}$$

where Im denotes the imaginary part, while ξ and η are Cartesian coordinates referred to the (x, y) plane:

$$z = x + iy; \quad \chi = \xi + i\eta; \quad \bar{\chi} = \xi - i\eta.$$

Setting $z = \pm ia$ in Eq. (3.21), we get the following expression for the sensitivity of the meter:

$$\gamma = \frac{2}{\pi\varphi_0 i}\cdot\frac{\iint v(x, y) W(x, y)\,dx\,dy}{\iint\limits_{(S)} v(x, y)\,dx\,dy}. \tag{3.22}$$

The function $W(x, y)$ reflects the weighted contribution of flow in various points of the cross section to the potential difference at the point electrodes, and has the form

$$W(x, y) = \frac{a^4 + a^2(x^2 - y^2)}{a^4 + 2a^2(x^2 - y^2) + (x^2 + y^2)^2}. \tag{3.23}$$

Figure 47 shows the contours of $W = \text{const}$. The smallest value of W in the duct is 0.5. Near electrodes $\pm\varphi$ the value of W increases without bounds.
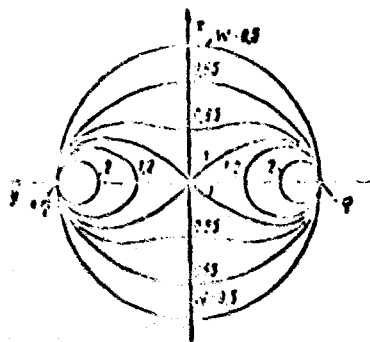
Fig. 47. Isolines of weighted function W.

Previous studies of Kolin [140] showed that for an axisymmetrical velocity distribution in the duct of this flowmeter, the potential difference at the point electrodes does not depend on the flow conditions.

75

P. Gold, considering this problem for laminar flow of the conducting fluid and arbitrary M, established [150] that when M > 1, a velocity distribution asymmetrical relative to the axis has an appreciable effect on the readings of the magnetic flowmeter. In particular, when the Hartmann number increases from very low values, when the flow may be regarded as axisymmetrical, to infinity, the sensitivity of this flowmeter drops from 1 to 0.925 (Fig. 48).
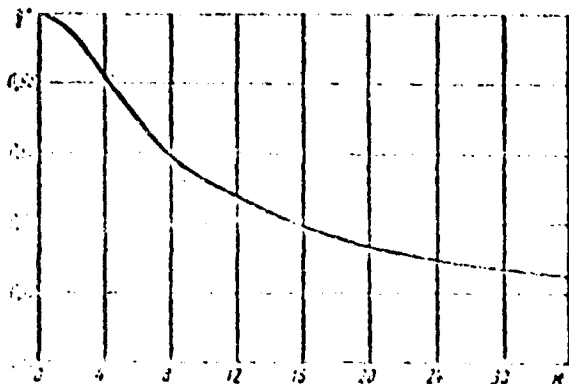
Fig. 48. Factor ψ as a function of the Hartmann number for a circular duct with point electrodes.

Figure 49 shows experimental data for a magnetic flowmeter with a circular channel 12.7 mm in diameter, isolating walls and side-mounted point electrodes. The data were obtained by Shercliff for mercury [30]. The dashed lines in the figure are for the case of $\psi = 1$ (axisymmetric flow).
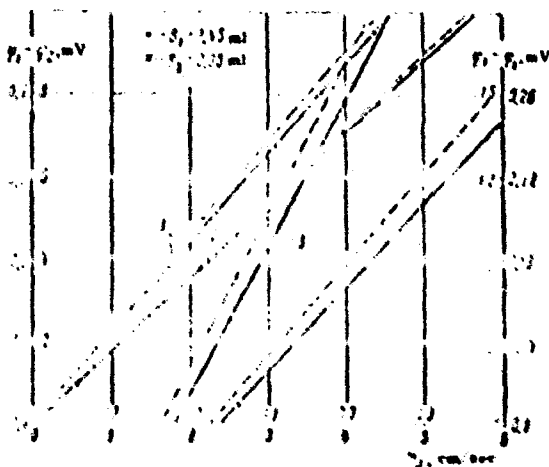
Fig. 49. Experimental characteristics of a conduction-type DC magnetic flowmeter with a circular channel and point electrodes.

Curves 1 and 2 are for inside scales; curves 3 and 4 are for outside scales; here curves 1 and 3 correspond to the left scales, while curves 2 and 4 are for the right scales.

It follows from these data that the characteristics of this type of flowmeter depend on the flow conditions in the liquid metal and are nonlinear.

Shercliff, in analyzing Eq. (3.22), showed [146] that under certain conditions the sensitivity of a magnetic flowmeter with a circular duct and point electrodes may be appreciably below 0.925. He has also established the effect of conducting channel walls.

Because of the shunting effect of the conducting duct walls, the flowmeter sensitivity drops. The correction factor for the shunting effect in axisymmetrical flow is [147]

$$k_1 = \frac{2 \cdot \frac{d}{D}}{1 + \frac{d^2}{D^2} + \frac{\sigma_c}{\sigma}\left(1 - \frac{d^2}{D^2}\right)},$$ (3.24)

where d and D are the inside and outside diameters of the flowmeter duct.

Influence of Longitudinal Edge Effects on the Sensitivity of Magnetic Flowmeters

Readings of magnetic flowmeters can be appreciably affected by end effects due to the finite length of the meter. Theoretically, these effects can be established only upon assuming inviscid flow of conducting fluid in the flowmeter duct.

Let us examine the inviscid flow of a conducting fluid in a flat vertical channel $(b \to \infty)$ with electrodes of length l connected via the load resistance R_l. Let the duct walls (up- and downstream of the electrodes) be isolating, and let the vector of the external magnetic field depend only on the z coordinate.

When $R_m \ll 1$, the induced magnetic field can be neglected, and the induced current density distribution and the electric potential distribution can be found from the equations

$$\operatorname{div} j = 0;$$ (3.25)

$$j = \sigma\left[-\nabla\varphi + [v \times B]\right].$$ (3.26)

Here, vector B is assumed given.

From Eqs. (3.25) and (3.26) we get

$$\Delta\varphi = 0; \quad j_z = -\sigma\frac{\partial\varphi}{\partial z}; \quad j_y = \sigma\left[-\frac{\partial\varphi}{\partial y} + vB(z)\right].$$ (3.27)

Since $B(z) \to 0$ when $z \to \infty$

$$j_z(\pm\infty, y) = 0; \quad j_y(\pm\infty, y) = 0.$$ (3.28)

The boundary conditions can be written as follows:
at the electrodes

$$\varphi\left(z, \pm\frac{a}{2}\right) = \pm\varphi \text{ for } -\frac{l}{2} < z < \frac{l}{2};$$ (3.29)

77

at the insulators

$$\frac{\partial \varphi}{\partial y} = B(z) \quad \text{for} \quad \frac{l}{2} < |z| < \ldots, \, y = \frac{t}{2} \tag{3.30}$$

The electrode potential is obtained from Ohm's law for the external circuit

$$\varphi_e = R_e \int_{-\frac{l}{2}}^{\frac{l}{2}} j_y \left(z, \frac{b}{2} \right) dz. \tag{3.31}$$

Since function $\varphi(z, y)$ satisfies the Laplace equation, we can introduce the analytic function

$$f(z) = \frac{\partial \varphi}{\partial x} + i \frac{\partial \varphi}{\partial y} = u(z, y) + iw(z, y);$$
$$u(z, y) = \frac{\partial \varphi}{\partial x}; \quad w(z, y) = \frac{\partial \varphi}{\partial y}. \tag{3.32}$$

Here, we have the following boundary conditions for $f(x)$:
$u = 0$ at the electrodes; $w = -vB(z)$ at the insulators;

$$f(\infty) = 0; \quad -\int_{-\frac{a}{2}}^{\frac{a}{2}} w(0, y)\,dy =$$
$$= R_e \nu \left[\int_{-\frac{l}{2}}^{\frac{l}{2}} u\left(z, \frac{a}{2} \right) dz + v \int_{-\frac{l}{2}}^{\frac{l}{2}} B(z)\, dz \right]. \tag{3.33}$$

Function $B(z)$ is even; hence, because of the symmetry of conditions, we need only consider the right-hand half of the channel.

This boundary-value problem was solved by A. B. Vatazhin [145] by conformal mapping of the half-band

$$z > 0, \quad -\frac{a}{2} < y < \frac{a}{2}$$

onto the upper half plane, using the Keldysh-Sedov formula. Here the following expression was obtained for the electric potential

$$u = v_0 \frac{2B_0}{\pi} \left[a + \frac{2v}{\pi} \cdot \int_0^\infty B(s) S\left(\frac{\pi s}{l} \right) d\left(\frac{\pi s}{l} \right) \right]. \tag{3.34}$$

78

where

$$\alpha^* = \frac{K(k')}{K(k)}; \quad k'^2 + k^2 = 1; \quad k = \frac{1}{\operatorname{ch}\left(\frac{\pi}{2}\frac{l}{a}\right)};$$

$$G = v \int_{-\frac{l}{2}}^{\frac{l}{2}} B(z)\, dz;$$

$$S\left(\frac{2z}{l}\right) = \frac{l}{d}\, \varrho \sqrt{\frac{\varrho^2 - k^2}{\varrho^2 - 1}}\left[\Pi\left(\frac{\pi}{2}, \frac{k^2}{\varrho^2 - 1}, k'\right) - \varrho^{-2}\varrho^{-1}\Pi\left(\frac{\pi}{2}, -\frac{k^2}{\varrho^2}, k\right)\right];$$

$$\varrho = k\,\operatorname{ch}\left(\frac{\pi}{2}\frac{z}{a}\right);$$

$K(k)$ is a total elliptical integral of the first kind; and $\Pi(\pi/2, h, k)$ is a total elliptical integral of the third kind.

Examining the above expressions, we see that when $0.5 \le l/a$, α^* can be expressed as

$$\alpha^* = 0.44 + \frac{l}{a}. \tag{3.35}$$

When the electrode length exceeds that of the duct, function S can be approximated by

$$S\left(\frac{2z}{l}\right) \approx \frac{\pi}{2}\frac{l}{a}e^{-a\left(\frac{2z}{l}-1\right)} \tag{3.36}$$

where $\alpha = 1 + 2\frac{l}{a} + e^{-1.61\frac{l}{a}}$.

Analysis of experimental data shows that the magnetic field distribution beyond the electrode edge can, in general, be expressed as

$$\frac{B}{B_0} = A_1 e^{-\alpha_1\left[\left(\frac{2z}{l}-1\right)\frac{l}{\delta}\right]} = A_2\left\{1 - \operatorname{th}\left[\alpha_2\left(\frac{2z}{l}-1\right)\frac{l}{\delta}\right]\right\}. \tag{3.37}$$

where B_0 is the uniform magnetic flux density in the electrode zone; δ is the gap between magnet poles; A_1, A_2, α_1 and α_2 are coefficients which depend on the design parameters of the magnet.

Upon substitution of Eqs. (3.36) and (3.37), the integral in Eq. (3.34) can be reduced to the form

$$\int_1^{\infty} B\left(\frac{2c}{l}\right) S\left(\frac{2c}{l}\right) d\left(\frac{2c}{l}\right) \approx B_0 \cdot \frac{\pi}{2} \cdot \frac{l}{a} \times$$

$$\times \left\{ \frac{A_1}{\alpha_1 \frac{l}{\delta} + \alpha} - \frac{A_2}{\alpha} + A_2 \int_1^{\infty} e^{-\alpha\left(\frac{2c}{l} - 1\right)} \times \right.$$

$$\left. \times \, \text{th}\left[\alpha_2 \frac{l}{\delta}\left(\frac{2c}{l} - 1\right)\right] d\left(\frac{2c}{l}\right) \right\}. \tag{3.38}$$

In turn, the integral contained in Eq. (3.38) can be expressed by a β-function

$$\int_1^{\infty} e^{-\alpha\left(\frac{2c}{l} - 1\right)} \text{th}\left[\alpha_2 \frac{l}{\delta}\left(\frac{2c}{l} - 1\right)\right] d\left(\frac{2c}{l}\right) =$$

$$= \frac{\delta}{\alpha_2 l}\left[\beta\left(\frac{1}{2}, \frac{\alpha\delta}{\alpha_2 l}\right) - \frac{\alpha\delta}{\alpha_2 l}\right], \tag{3.39}$$

where

$$\beta\left(\frac{1}{2}, \frac{\alpha\delta}{\alpha_2 l}\right) = \sum_{n=0}^{\infty} \frac{(-1)^n}{\left(\frac{1}{2} + \frac{\alpha\delta}{\alpha_2 l}\right) + n}. \tag{3.40}$$

When the characteristic parameter lies within the limits

$$0.5 < \frac{1}{2} \frac{\alpha\delta}{\alpha_2 l} < 10$$

The above series is approximated, with high accuracy, by the formula

$$\sum_{n=0}^{\infty} \frac{(-1)^n}{\left(\frac{1}{2} + \frac{\alpha\delta}{\alpha_2 l}\right) + n} \approx \frac{0.69}{\left(\frac{1}{2} + \frac{\alpha\delta}{\alpha_2 l}\right)^{1.15}}. \tag{3.41}$$

Finally, we have

$$\int_1^{\infty} B\left(\frac{2c}{l}\right) S\left(\frac{2c}{l}\right) d\left(\frac{2c}{l}\right) \approx B_0 \frac{\pi}{2} \frac{l}{a} \times$$

$$\times \left\{ \frac{A_1}{\alpha_1 \frac{l}{\delta} + \alpha} - \frac{A_2}{\alpha} + \frac{A_2 \delta}{\alpha_2 l}\left[\frac{0.69}{\left(\frac{1}{2} + \frac{\alpha\delta}{\alpha_2 l}\right)^{1.15}} - \frac{\alpha l}{\alpha\delta} \right] \right\}. \tag{3.42}$$

and the expression for the electric potential assuming finite dimension of b is reduced
to the form

$$\varphi_1 - \varphi_2 = \frac{B_0 \alpha_2}{\frac{R_1}{R_u} + \frac{a}{l}\left(0.11 + \frac{l}{a}\right)}, \tag{3.43}$$

where

$$k_2 = 1 + \left\{ \frac{\Lambda_1}{\alpha_1 \frac{l}{\delta} + \alpha} - \frac{\Lambda_2}{\alpha} + \frac{\Lambda_2 \delta}{a_s l} \times \right.$$

$$\left. \times \left[\frac{0.69}{\left(\frac{1}{2} \frac{\sigma \delta}{a_s l} \right)^{1.16}} - \frac{a_s l}{a \delta} \right] \right\}. \tag{3.44}$$

When $R_l \to \infty$, Eq. (3.43) takes the form

$$T_1 - T_2 = v B_c a k_2. \tag{3.45}$$

while when $a/l \to \infty$, it becomes the previously derived Eq. (3.18).

Examining Eq. (3.44) we see that when the magnetic field beyond the electrode edges drops off slowly, the edge effects on the magnetic flowmeter readings can be neglected if $l/a \geq 5$.

Figure 50 shows curves of $k_2 = f_2 (l/a)$ for a slowly attenuated magnetic field beyond the electrode edge (curve 1) and for an abruptly changing field (curve 2).
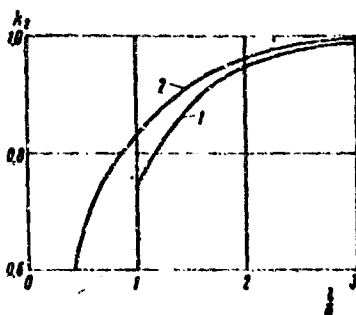
Fig. 50. Curves of k_2 as a function of l/a.

Effect of Temperature on the Sensitivity of Magnetic Flowmeters

Readings of magnetic flowmeters can be affected by changes in the temperature of the conducting fluid. This pertains particularly to magnetic flowmeters for liquid metals, whose temperatures can be quite high.

As follows from Eqs. (3.17) and (3.24), the temperature variations will affect the ratio σ_w/σ; hence the conductivity of the wall material should be matched to the conductivity of the fluid.

Temperature variations may vary somewhat the air gap of the electromagnet and the magnetic flux density.
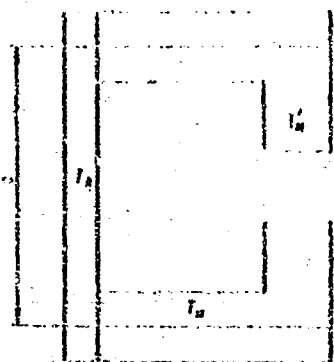
Fig. 51. C-shaped magnet
assembly.

The magnetic field in liquid metal flowmeters is frequently induced by permanent magnets made from Alnico, Magnico and other alloys. In this case the correction factor, taking into account the temperature effect on the readings, can be written as [148]

$$k_3 = \frac{1 - \beta_m(T_m - T_0)}{1 - a_y \frac{\delta}{\delta}(T_m' - T_y) + a_y(T_m - T_0)},\qquad (3.46)$$

where δ is the air gap of the C-shaped magnet (Fig. 51); α_y is the temperature expansion coefficient of the yoke; T_y is the average temperature of the yoke; T_m is the average temperature of one magnet leg, and T_m' is the average temperature of one pole.

If the magnets are not thermally stabilized by being subjected to several heating-cooling cycles, then for the Magnico alloy at temperatures below $T_m = 500\ °C$,

$\beta_m = (2.6-2.8) \cdot 10^{-4}\ °C^{-1}$.

In practice, when the pipe temperature is below 400°C, the magnet is not appreciably heated, and $k_3 \approx 1$.

Generalized Description of Magnetic Flowmeter Readings

In accordance with the above, the potential difference at electrodes of magnetic flowmeters can, in the general case, be represented by

$$\varphi_1 - \varphi_2 = v_0 B_0 a \Psi k_1 k_2 k_3. \qquad (3.47)$$

In expressions for the potential difference, which are given in handbooks and in some other references [148, 153, 261], factor Ψ is taken as unity. However, our previous analysis shows that this is not always the case.

Our previous discussion also makes it possible to present recommendations on the application of various conduction-type flowmeters.

For fluids with ionic conductivity (electrolytes, sea water), one should use magnetic flowmeters with circular ducts and side electrodes. For precise flow measurement of liquid metals, one should use magnetic flowmeters with rectangular ducts and continuous side electrodes. When the magnetic field is produced by air-gap magnets, flowmeters with flat ducts and point electrodes are used to reduce gap resistance.

If the flow of liquid metal is to be measured with an accuracy of several percents, then flowmeters with circular ducts and point electrodes can be used.

In selecting magnetic flowmeters, consideration must also be given to several additional factors due to near-electrode processes.

3. Effect of Near-Electrode Processes on the Readings of Magnetic Flowmeters

Complex electrochemical processes take place at the electrode-fluid interface of conduction-type magnetic flowmeters in flow of liquids with ionic conductivities. The electrostatic forces produce electric charges in the thin liquid layers adjacent to the electrodes; these, together with the electrode surface, form a double electric layer. The electrode surface in this case acts similarly to a charged capacitor.

The appearance of this double layer produces a potential difference between the electrode and the liquid; its magnitude depends on the electrode material, chemical composition of the liquid and other factors, and amounts to 0.5-0.7 V. Usually the electrodes are made from the same material, hence the potential drop between them and the liquid should be opposite in sign and should cancel out. However, due to a certain chemical inhomogeneity of the electrodes, deformation of their surface, as well as oxide films, the potential difference between the electrodes may be as high as a few tens of millivolts and exceed the magnitude of the measured signal. The magnetic flowmeter is thus a kind of galvanic cell, the emf of which depends on the fluid concentration, temperature and pressure, and varies with time.

When the liquid flows past the electrode, this double electric layer is partially detached by the flow, which results in voltage fluctuation in the measuring circuit. As a result of electrolysis, gas is liberated at the electrodes, which also increases the instability of electrode potentials.

The rate of ion neutralization at the electrodes is limited, so that when a current flows, the concentration of ions of opposite signs increases at the electrodes. The latter are polarized, which produces an additional emf between them, weakening the measured signal.

The above processes impose difficulties in the use of the constant magnetic field for measuring the flow of liquids with ionic conductivities.

There are special electrode designs which appreciably reduce the interference of near-electrode electrochemical processes. However, these designs are complex and not too suitable for industrial flowmeters.

In actual practice, one uses flowmeters with an AC magnet for measurements of liquids with ionic conductivities. In these instruments, the instability due to the intrinsic galvanic emf is easily eliminated by high-pass filters [147]. The effect of electrode polarization on flowmeter readings is also reduced.

83

Induction noise, which arises in the instrument circuit when using an AC magnet, can be reduced by special compensating methods [147].

The DC magnetic field is successfully used in conduction flowmeters for liquid metals. These metals exhibit electronic conductivities, so that no difficulties due to near-electrode electrochemical processes are encountered. Alternating magnetic fields can, because of the high conductivities of liquid metals, result in appreciable losses due to eddy currents in the flow.

Flowmeters with a constant magnetic field have the advantage of design simplicity and moderate cost. They do not require an electromagnet with a core made of electric-grade sheet steel or a regulated power supply. At the same time, the so-called contact resistance, which reduces the instrument sensitivity, may arise in DC liquid metal flowmeters under certain conditions. Its effect is particularly felt at low liquid metal temperatures [213]. The contact resistance effect cannot be calculated analytically. This resistance changes with time and depends on the state of the electrode surfaces.
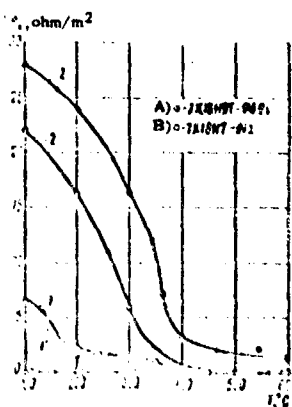
Fig. 52. The contact resistance R_c as a function of temperature.
KEY: A) 1Kh18N9T-PbBi; B) 1Kh18NT-Na.
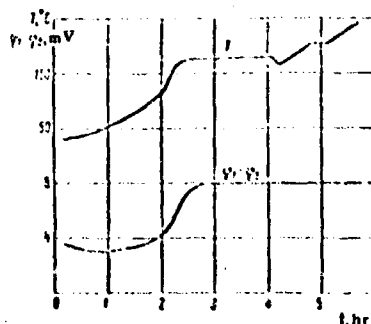
Fig. 53. Time variations in magnetic flowmeter reading upon increase in the liquid metal temperature.

Interesting studies on contact resistance at the electrode-liquid metal interface were done at the Institute of Physics of the Latvian Academy of Sciences [262]. They show that the contact resistance is due to many causes, in particular, the resistance of various oxides and physical adsorption films, which are almost always present. The physical adsorption films in most cases are dielectrics, and may produce an appreciable resistance at ambient temperatures.

The magnitude of contact resistance is also governed by the absence of true contact over the entire electrode surface. It is zero when the surface is wetted, and ranges over very wide limits when it is not. It was also found that contact resistance drops with increase in temperature and in most cases disappears at approximately 400°C.

Figure 52 shows contact resistance at interfaces between stainless steel – liquid sodium, and stainless steel – lead bismuth eutectic mixture. The stainless steels used in these experiments were 1Kh18NT and 1Kh18N9T, respectively. Curves 1 are for clean electrodes, while curves 2 are for oxide-coated electrodes.

Figure 53 shows data on the effect of contact resistance on readings of magnetic flowmeters [134]. It is easy to see that with increasing temperature the sensitivity of magnetic flowmeters (which depends on the contact resistance) increases.

4. Operating Features of AC Flowmeters

As was noted above, conduction-type flowmeters with alternating magnetic field are used with liquids exhibiting ionic conductivities. The AC field produces various kinds of noise. However, the means for combating it are more effective than those used for reducing the detrimental effect of electrochemical processes occurring with a constant magnetic field.

The detrimental effect of near-electrode processes can be eliminated by special filters. The electrode polarization effect is reduced with increasing the field frequency ω, but is still perceptible at 50 cps.

Figure 54 shows the equivalent circuit of a conduction-type flowmeter with an alternating field [153]. In this circuit, the electrode polarization effect is represented by capacitor C_p (several microfarad) in series with the converter. The phase shift produced by electrode polarization can be compensated by a circuit consisting of an intermediate capacitor C and resistance R. The relationship between the potential difference at the electrodes and the emf $\mathscr{E}$, developed in the flow has the form

$$\varphi_1 - \varphi_2 = \frac{\mathscr{E}}{1 + \frac{z}{z_\ell}},$$

(3.48)

where $Z = \cfrac{1}{\frac{1}{R} + j\omega C} + \frac{1}{j\omega C_p}$ is the internal resistance of the meter, while Z_ℓ is the load

resistance.
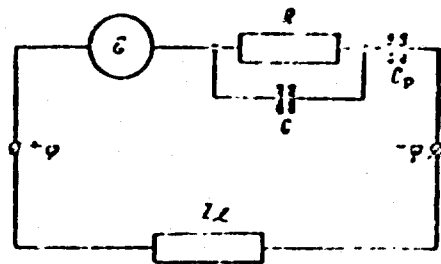
Fig. 54. Equivalent circuit of the AC magnetic flowmeter.

It follows from Eq. (3.48) that in order to obtain high flowmeter sensitivity it is necessary to satisfy the condition

$$Z_\ell \gg Z$$

If Z_ℓ is small, then variations of R, C_p, C and ω will affect the readings. In this case and with liquids of relatively high conductivity, the principal effect on flowmeter readings is that of electrode polarization.

These results were verified experimentally using a flowmeter with $\omega = 60$ cps and $Z_\ell = 0.47$ Megohm in experiments with fibe aqueous solutions (KCL, NaCL, NaOH, HNO_3 and H_2SO_4) of various concentrations. The flowrate and magnetic flux density were held constant throughout the experiments (Q = 0.3 liters/sec, $B_0 = 3.96 \cdot 10^{-2}$ tesla) [153].
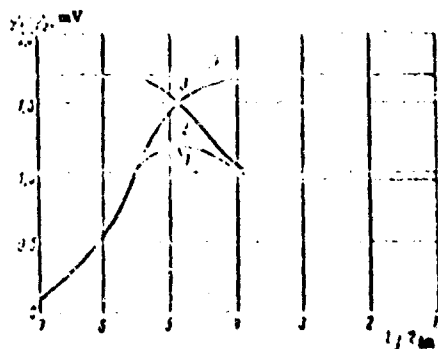
Fig. 55. The measured signal as a function of the internal resistance of the HBO_3 solution.

1) Experimental curve; 2) theoretical curve for $Z_\ell = \infty$ and in the presence of polarization; 3) theoretical curve for $Z_\ell = 0.47$ Megohm and absence of polarization; 4) theoretical curve for $Z_\ell = \infty$ and absence of polarization.

86

Figure 55 shows the experimental results with a HNO_3 solution (curve 1). It is seen that at high concentrations, when R_{in}, the flowmeters internal resistance, was less than 10^4 ohms, the electrode polarization was at maximum. Hence, a further increase in the concentration of the solution and consequently, in its conductivity, was not reflected in the instrument reading. When the concentration was reduced and the internal resistance was raised from 10^4 to 10^5 ohms, an increase in the flowmeter sensitivity was noted, which is attributable to the reduced effect of electrode polarization. Upon further increase in resistance to 10^6 ohms, the instrument readings again dropped off, which is due to the increasing effect of resistance R.

Consequently, changes in concentration and conductivity of electrolyte solutions affect the different components of Z differently.

The capacity C of the converter proper is under ordinary conditions appreciably smaller than C_p, and is important only when the conductivity is very low.

The alternating magnetic fields induces a parasitic emf in the measuring circuit; it is 90° out of phase relative to the measured signal. The magnitude of this emf is determined by the area of the measuring circuit and its alignment relative to the magnetic flux vector. Hence the plane of the measuring circuit, formed by conductors leading from the electrodes, should be parallel to the magnetic force lines. Another method of combating the effect of parasitic emf employs a special winding, connected to the electrode, over the magnetic circuit.

In flowmeters designed by NII Teplopribor [Research Institute for Heat and Power Engineering Measuring Instruments] this method is used in small detectors for duct diameters d = 10, 20 and 25 mm, while the first method is used for ducts with d > 50 mm.

Special compensating systems are used for complete elimination of the effect of parasitic emf.

When the steel of the magnet core approaches saturation, odd harmonics and noise sharply increase [263]. Hence the flux in the magnet core should not exceed a certain limit. According to data of NII Teplopribor [153], this limit is 0.25-0.3 tesla.

It should also be remembered that any change in the power supply of the magnet, when operating over the saturation part of the magnetizing curve, changes the magnetic flux density. Hence a voltage regulator must be placed at the electromagnet input.

5. Design of Magnetic Flowmeters

Proper operation of conduction-type magnetic flowmeters requires that the field in the electromagnet gap be uniform.

Magnet assemblies with flat poles over rectangular or circular flowmeter ducts (see Fig. 41) provide satisfactory field uniformity in the active duct. However, they cannot be used for large circular ducts due to their large size and the appreciable power needed for obtaining the desired flux densities in the gap. In these cases magnet assemblies of special design are used [147, 153].

87
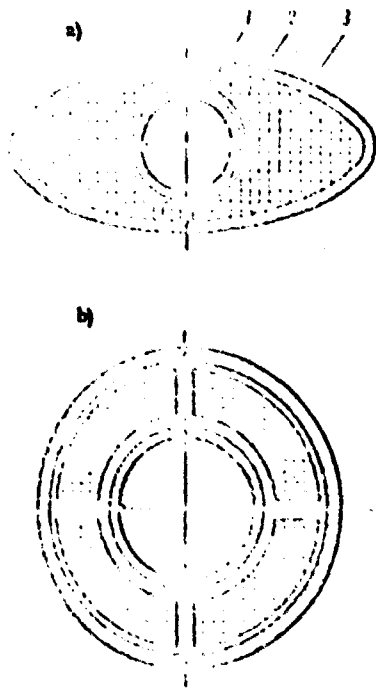
Fig. 56. Magnet assemblies of
flowmeters with distributed wind-
ings.

1) Duct; 2) electromagnet winding;
3) magnetic return circuit.

The magnet assemblies in flowmeters with ducts larger than 25 mm have distrib-
uted windings, similar to the deflecting systems of television tubes. A magnet assembly
with distributed windings is shown in Fig. 56. In this case the magnetic field is pro-
duced by two saddle-shaped windings. The magnetic return circuit shape approaches
the elliptical (Fig. 56a). To provide a uniform magnetic field, its cross sectional shape
is so designed that the magnetomotive force varies along the axis connecting the elec-
trodes in the same manner as the gap. The winding density is maximum at the edges
and decreases toward the middle of the magnet. In magnet assemblies with distributed
windings virtually the entire air gap is utilized.

Design of magnet assemblies with continuous distributed windings for large-size
flowmeter ducts is quite difficult. In this case, the windings are partitioned into several
sections (Fig. 56b).

Magnet assemblies with distributed windings are used in type 3-RI flowmeters
produced in the Soviet Union and in magnetic flowmeters produced by the foreign firms
Alto, Semac, Kent and Eckart.

The magnetic flowmeters produced by Foxboro, Fisher-Porter and Taylor use
magnet assemblies shown schematically in Fig. 57. In these systems the magnetic
field is excited by two lumped saddle-shaped windings and is formed by a magnetic

88

return circuit embracing the windings, without explicit poles. The design of this assembly is simple, but high power is needed for exciting the required magnetic field strength.
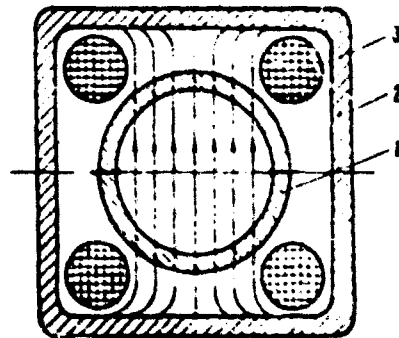
Fig. 57. Magnet assembly of a flowmeter with lumped windings.

1) Duct; 2) magnetic return circuit;
3) electromagnetic winding.

Foxboro flowmeters for 50 mm φ ducts require 200 W for excitation, with 700 W required for 450 mm ducts.

The excitation power for the NII Teplopribor meters is shown in Table 3.

Table 3. Characteristics of Magnet Assemblies of NII Teplo-pribor.

1) Тип расходомера	2) Диаметр сечения, мм	3) Потребляемая мощность, ВА	4) Число витков обмотки	5) Диаметр провода, мм	6) Магнитная индукция, тесла	7) Тип магнитной системы
8) ДРИ-10	10	461	860	1.5	0.171	9) Ш-образный магнитопровод
8) ДРИ-30	30	271	810	1.2	0.0782	
8) ДРИ-25	25	386	960	1.4	0.0819	
8) ДРИ-50R	50	497	860	1.2	0.034	10) Магнитопровод ленточного типа с распределенными обмотками
10) ДРИ-806	80	418	542	1.2	0.0231	

KEY: 1) Flowmeter type; 2) duct diameter, mm; 3) power used, VA; 4) number of windings per coil; 5) diameter of magnetic return, mm; 6) flux density, tesla; 7) magnet assembly type; 8) DRI; 9) E-shaped magnetic return circuit; 10) ribbon-type return circuit with distributed windings.

In flowmeters produced by the KIP [Control and Measuring Instruments = CMI] plant, also with circular ducts, the excitation power increases from 200 VA for d = 25 mm to 400 VA for d = 150 mm and 620 VA for d = 250 mm. The flux density drops then from 0.05 to 0.004 tesla.

An important component of magnetic flowmeters are the electrodes. In circular ducts the electrodes are placed at the ends of the diameter, in the horizontal plane. They are made from stainless steel, platinum and special alloys resistant to corrosive media. The electrodes are inserted through special openings in the duct walls, and airtightness and the required electrical isolation from the duct walls are obtained by means of packing.

Figure 58 shows the construction and mode of attachment of electrodes of Foxboro and NII Teplopribor flowmeters.
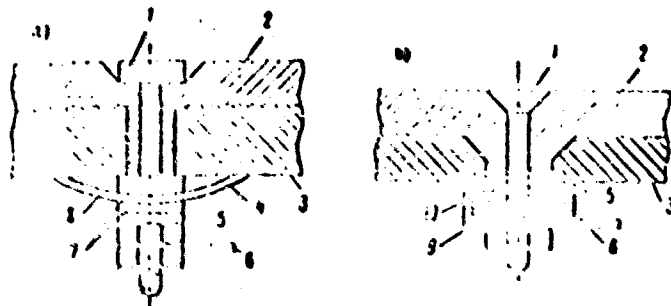
Fig. 58. Electrode construction of magnetic flowmeters.
a) Foxboro; b) NII Teplopribor.

1) Electrode; 2) insulating layer; 3) metal duct wall;
4) force spring; 5) washer; 6) clamp; 7) insulating rings;
8) insulation; 9) spring washer; 10) cup (1Kh18N9T steel).

The signal detectors developed by NII Teplopribor are designed for pressures of $2.35 \cdot 10^6$ Newton/m^2 (24 kilogauss/cm^2) and temperatures of 5–50°C. When heat resistant materials are used for insulating the inner duct surfaces and the electrodes, the temperature can be several hundred degrees. The diameter of the flowmeter is identical to the diameter of the pipe in which the meter is installed.

Tables 4 and 5 present technical data on Altoflux and Fisher-Porter flowmeters [147]. Figure 59 and Table 6 present data on the overall dimensions of two Soviet-made flowmeters.

Magnetic flowmeters with rectangular ducts must be provided by an intricately shaped expanding (or converging) connecting adapter (converting a rectangular to a circular cross section or vice versa) for connection to pipelines.

Magnetic flowmeters with rectangular ducts and continuous side electrodes are developed by the KhGIMIP [Khar'kov State Institute of Measures and Measuring Instruments] [147].

Table 4. Technical data on Altoflux magnetic flowmeters

A) Диаметр канала, мм	B) Верхний предел измеряемого расхода Q, м³/ч	C) Потребляемая мощность, вт	D) Вес, кг	E) Длина, мм
3	0.05	20	18	300
6	0.12	20	18	300
8	0.25	30	18	300
10	0.30	30	20	300
15	0.50	30	20	400
20	0.80	30	20	300
25	1.2	30	20	300
32	3.0	50	25	430
40	5.0	50	30	300
50	8.0	60	32	300
65	10	60	35	550
80	10	60	50	570
100	15	100	50	650
125	25	110	55	750
150	30	130	65	
200	60	170	85	950
250	100	220	120	1100
300	200	300	180	1200
350	250	300	230	1200
400	400	320	290	
450	500	400	300	
500	600	450	410	
550	800	550	460	
600	1000	650	520	
650	1200	650	560	
700	1500	750	630	
750	2000	850	680	
800	2200	1100	750	
900	2500	1300	840	
1000	4000	1650	1100	

KEY: A) Duct diameter, mm; B) maximum flow measured Q, m³/h; C) power used, W; D) weight, kg; E) length, nm.

Fig. 59. Overall dimensions of flowmeter.

Table 5. Technical data on Fisher-Porter electromagnetic flowmeters.

A) Диаметр канала, мм	B) Пределы измерения расхода Q, м³/ч	C) Потребляемая мощность, вт	D) Вес, кг	E) Длина, мм
2,5	0,005—0,18	40	16	200
5,0	0,02—0,7	35	16	200
12,5	0,13—4,4	30	16	200
25,0	0,54—18	50	30	500
37,5	1,2—40	50	30	500
50	2,0—70	50	40	600
80	5,4—180	50	40	600
100	8,5—280	50	80	750
150	19—619	100	140	1050
200	34—1 100	100	140	1050
250	53—1 800	150	320	1500
300	76—2 500	200	400	1500
350	100—3 500	150	440	1800
400	140—4 500	150	480	1800
450	170—5 700	200	640	2100
500	210—7 000	200	800	2100
600	300—10 000	200	1080	2850
750	480—16 000	200	1600	2850
900	690—23 000	200	2400	—
1050	От 930	200	3200	—
1200	» 1 300	200	4000	—
1350	» 1 500	200	4000	—
1500	» 1 900	200	6000	—
1650	» 2 300	200	7200	—
1800	» 2 800	200	8800	—

KEY: A) Duct diameter, mm; B) maximum flow measured Q, m³/h; C) power used, W; D) weight, kg; E) length, mm.

Table 6. Overall dimensions of flowmeters, mm

Tип расходомера [1]	d	L	A	B	D	D₁	Число отверстий на фланце [2]
3-РИ-50 [3]	50	544	262	302	165	125	4
3-РИ-80 [3]	80	660	270	310	200	160	8

KEY: 1) Flowmeter type; 2) number of flange holes, 3) RI.

Table 7. Electromagnetic flow-
meters for liquid metals

Duct diameter, mm [1]	range of flowrates Q, m³/h [2]
16	0-0.1, 0-0.16, 0-0.25; 0-0.4
25	0-0.25, 0-1.9, 0-1.2; 0-6.0
40	0-6.3; 0-10, 0-12.5; 0-16.0; 0-20.0
61	0-32
76	0-100
100	0-100
170	0-250
200	0-1000
300	0-1000, 0-1250
500	0-4000

KEY: 1) Duct diameter, mm;
2) range of flowrates Q, m³/h.

Fig. 60. Photographs of
Soviet DRI electromag-
netic flowmeters.

The NII Teploprlbor organization is developing a series of flowmeters for liquid metals, for operation at 500-600°C. Some data on these are given in Table 7 [133]. Figure 60 shows some Soviet-produced magnetic flowmeters.

6. Measuring Circuits of Electromagnetic Flowmeters

When using magnetic flowmeters with a constant magnetic field for measuring liquid metal flow, the output signal is recorded quite simply. In this case the meters electrodes can be connected directly to a millivoltmeter with a high internal resistance.

When very high reading accuracy is needed, as well as when measuring very low liquid metal flowrates, the flowmeter signal can be displayed by a precision potentiometer, for example, the PPTN-1 laboratory potentiometer.

Signal detection is much more complicated when an AC flowmeter is used for measuring the flows of a liquid with an ionic conductivity. We noted above, that in this case noise due to near-electrode electrochemical processes must be eliminated by filtering the output signal. In addition, special measures must be taken to eliminate noise arising in the measuring circuit.

Thus it became necessary to develop special measuring circuits which provide proper detection of the signal generated at the flowmeter electrodes [147, 153].

Figure 6. shows the measuring circuit of type 3-RI-M magnetic flowmeters, developed by NII Teplopribor. Here the signal from the flowmeter electrodes is fed to a symmetric cathode follower, which has an asymmetric transformer input. The transformer preamplifies the signal.

The cathode follower achieves additional suppression of noise; this is done by feeding a compensating voltage to one of its arms. The compensating voltage is taken from the filament voltage of the power supply unit of the measuring and amplification system; it is adjusted by means of a circuit consisting of potentiometer R_{27} and capacitors C_3 and C_4. The input resistance of each arm of the cathode follower is 10^7 ohms.

The signal flows through a coaxial cable and switch S_1 to the grid of the left triode of tube L_2 which, by means of variable resistor R_6, varies the phase of the signal fed to the grid of the right triode of tube L_2. The output voltage of the amplifier must be shifted by 180° relative to the compensating voltage supplied from the flowmeter.

The right triode of tube L_2 and the two triodes of tube L_3 form an R-C coupled three-stage voltage amplifier. The amplifier output feeds transformer Tr_2; the signal flows from the secondary winding of this transformer to a null balance measuring instrument (EIV, EPID or DSR) with a differential transformer. All the amplifier tubes are 6N2P.

A special feedback scheme is used in the amplifier. The feedback circuit incorporates a saturated-core choke Ch, the control winding of which is fed with DC current provided by transformer Tr_3 via rectifiers D_1 and D_2. The current in the control coil of the choke, and consequently also its inductive reactance, change when the supply current changes. This changes the current in the choke's primary winding, so that the gain remains constant.

The advantage of this arrangement is the ability to use a standard measuring instrument, but it is quite complex. In addition, signal compensation in this arrangement takes place after amplification, so that the accuracy of the instrument is not too high. Flowmeters with this measuring circuit have a class 2.5 precision.

94
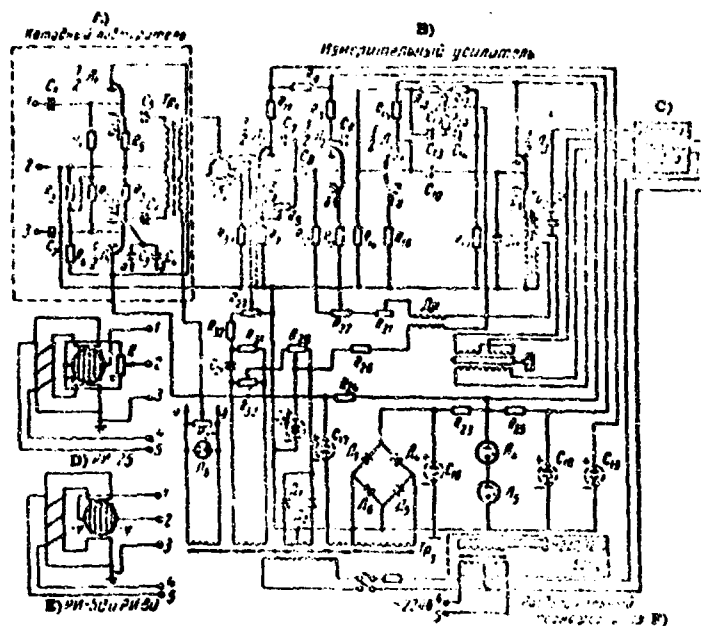
Fig. 61. Schematic diagram of measuring circuit of type 3-RI-M magnetic flowmeters developed by the NII Teplopribor.

KEY: A) Cathode follower; B) measuring amplifier; C) measuring instrument; D) RI-25; E) RI-50 and RI-80; F) tapped power transformer.

Figure 62 shows a circuit for measuring magnetic flowmeter signals developed at the Institute of Automatics and Telemechanics of the USSR Academy of Sciences. This arrangement uses a type EMD-235 electronic bridge as the measuring instrument. The potential difference from the flowmeter electrodes is fed to servomotor 3, where it is compared with the compensating voltage taken from rheostat 6. The measured and the compensating voltages are supplied to the amplifier input 180° out of phase. The rheostat slide is moved by two-phase motor 4, which is connected at the amplifier output. To eliminate the effect of supply-voltage fluctuations, resistor 2 is connected into the electromagnet winding circuit. A phase-shifting circuit 7, for compensating for the phase between the current in the windings and the magnetic flux, is also placed in the electromagnet supply.

The effect of the transformer parasitic emf is eliminated by appropriate positioning of resistor 2 and by selectivity of the two-phase motor with respect to the phase of the measured signal. The motor controls the motion of the pointer of measuring instrument 5. The basic error of this measuring system is ± 1%.

The measuring arrangement developed at the KhGIMIP is shown in Fig. 63. In this arrangement, the potential difference from the electrodes of the magnetic flowmeter 1 is compensated before the input to amplifier 5 by the voltage taken off the slide rheostat 3. To provide phase coincidence between the compared voltages, the slide rheostat is supplied from a section of electromagnet winding through a phase-shifting network 2. This also ensures isolation of the instrument from supply voltage fluctuations.

95
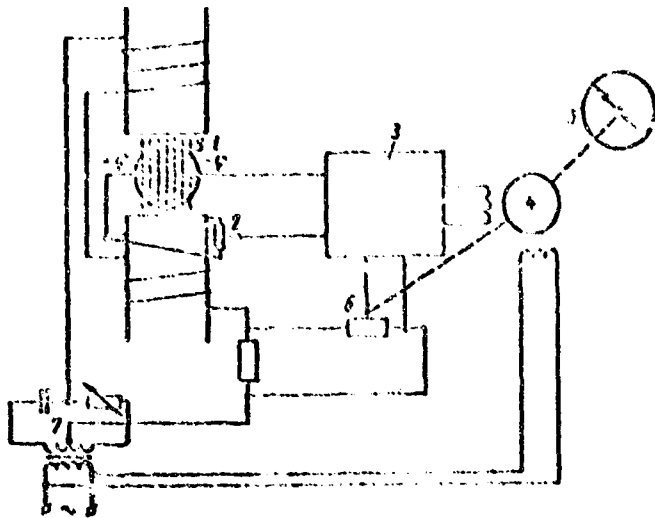
Fig. 62. The measuring circuit for magnetic flowmeters
developed at the Automatics and Telemechanics Institute
of the USSR Academy of Sciences.
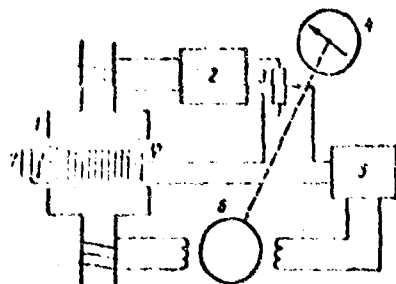
Fig. 63. The magnetic flowmeters
measuring unit developed at the
KhGIMIP.

For coarse compensation of the transformer emf, the output of one of the electrodes
carries a coil 7, which can be rotated about its axis, thus changing the amplitude and polar-
ity of the emf induced in it. In addition, the instrument is provided with a phase selection
element, i.e., two phase capacitor motor 6, whose exciting winding is fed from the second
section of electromagnet winding. The second exciting winding of the motor is connected
to the output of amplifier 5. The motor controls the motion of the rheostat slide and of the
pointer of instrument 4. The measuring error is ±5% of the full scale reading.

Starting with 1960, the CMI Plant started production of magnetic flowmeters with a
measuring circuit shown in Fig. 64. In this circuit the signal, as well as the transformer
emf, are compensated by ferrodynamic converters 7 and 8.

96
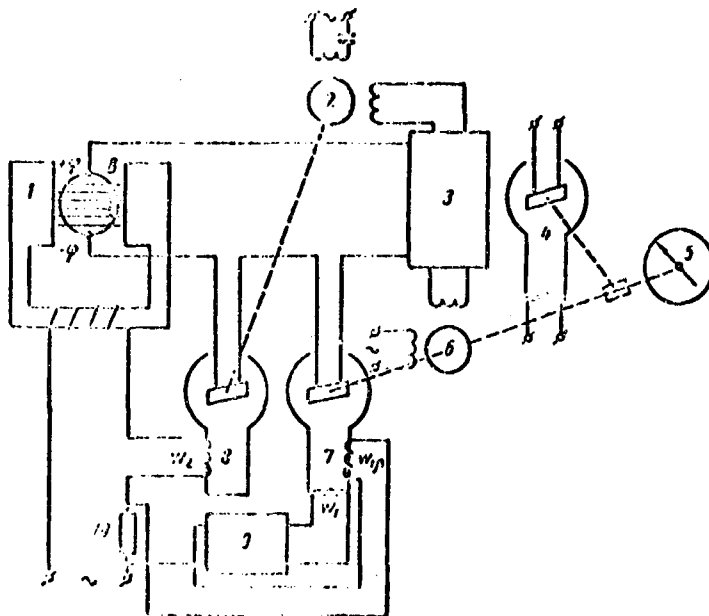
Fig. 64. Measuring system of magnetic flowmeters developed at the CMI Plant.

The exciting winding w_2 of converter 8 is connected in series with the supply of the electromagnet winding 1. Since the power to the winding is much greater than that to the converter, the compensating voltage at the frame of 8 is in phase with the transformer emf. The frame of 8 is rotated by reversible motor 2 until the transformer emf is completely compensated.

The winding w_1 of converter 7 is supplied through amplifier 9 which is fed with the potential difference between resistor 10 and winding w_{16}. The potential from the frame of converter 7 is in phase with the measured signal and is connected in opposition to it.

The reversible motor 6, which responds to the potential difference at the input of amplifier 3, rotates the frame of converter 7 until the measured emf is completely compensated.

Motor 6 also rotates the pointer of indicator 5 and the frame of converter 4 connected to the measuring instrument. The basic measuring error in this case is $\pm(1.5-2.5)\%$.

Figure 65 shows the flowmeter measuring circuit developed by Foxboro-Ioxal[1]. There the potential difference of flowmeter electrodes 1 and the voltage compensating it are fed to difference amplifier 4. A three-winding transformer 3 is connected to the amplifier input. Two of the transformer's windings are connected in series with the flowmeter electrodes. The compensating voltage from the differential transformer 2 is fed

_____
[1] See p.

to the third winding. Upon amplification, the difference (imbalance) signal is detected by phase-sensitive detector 5, and it then is fed to power amplifier 6, which supplies the windings of two solenoids 7; the cores of these solenoids move the ring of the differential transformer and balance the circuit. A counting device 8 is connected mechanically to the differential transformer ring.
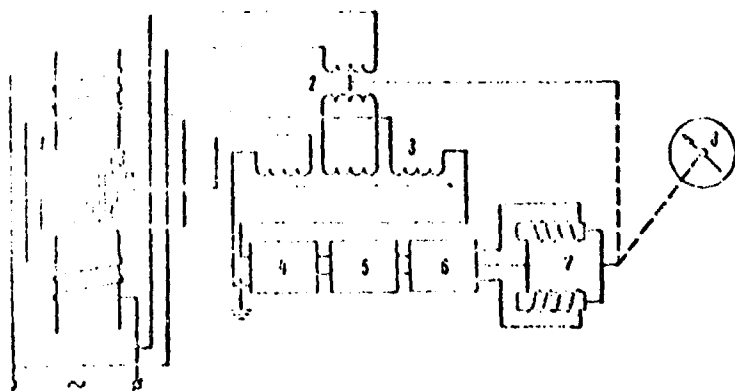
Fig. 65. Schematic diagram of the measuring system of magnetic flowmeters made by the Foxboro-Ioxal Company.

7. The Electromagnetic [Ship's] Log

Higher ship speeds and higher range require improving the accuracy of naval navigation instruments.

Impeller-type and hydraulic logs, which are extensively used by ships for determining their speed and the distance traveled [264] are not sufficiently accurate. Their error is not uniform over the entire range of ship speeds and is difficult to take into account. Their accuracy is ± 0.5 knots.

Magnetohydrodynamic methods make it possible to design a new type of log which is better and gives higher accuracy. A high-accuracy electromagnetic log with a linear characteristic over a wide range of ship speeds is described in [147]. Its velocity transducer is depicted in Fig. 66a.

The transducer consists of electromagnet 2, built into plastic housing 4 protruding from the ship's bottom, and of two electrodes, installed at the surface of this housing. The electromagnet winding is supplied with AC through cable 1.

When the ship is in motion, a directional electric field is created around the log, with the potential difference at the electrodes proportional to the ship's speed. The signal from the electrodes is fed via cable 5 to the measuring systems (Fig. 66b). The log is designed so as to provide isolation of the electromagnet and cables from sea water. The log uses a 60 cps power supply.

The measuring system consists of: signal amplifier 6, velocity indicator 7, velocity transmitter 8, cumulative distance integrator 9, traveled distance transmitter 10, distance servo 11, and counter 12.

98
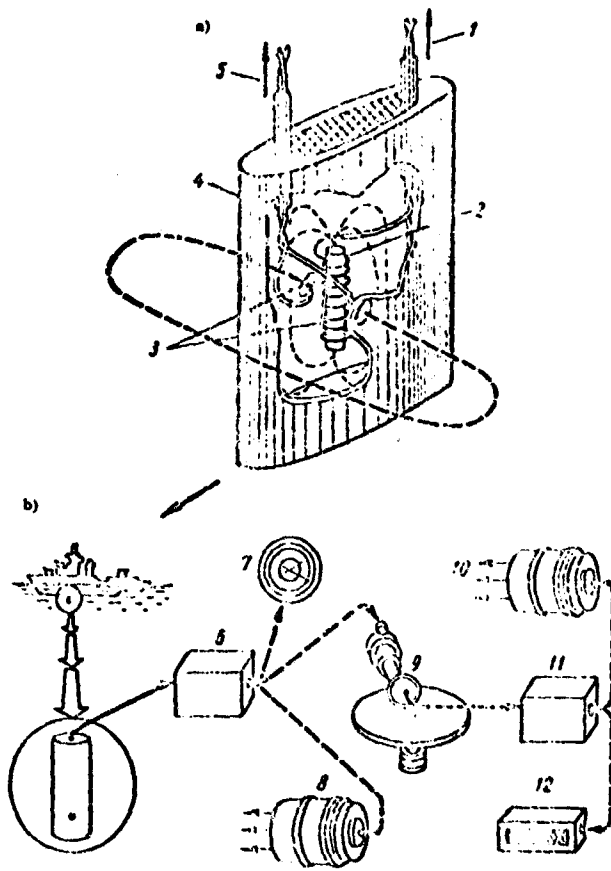
Fig. 66. Schematic diagram of an electromagnetic
log.

The design of this log is simple and the device may be used as part of an automatic control system, with the feedback based on the ship's speed. Its accuracy, over a wide range, is ±0.05 knots.

The electromagnetic log is calibrated over a measured course for each scale range. Here, unlike impeller and hydraulic logs, corrections of its readings are constant and do not depend on the velocity.

Because of the high sensitivity of this log, it responds to the additional motion of the ship due to rolling in swelling seas. This input is eliminated by using a device which changes the instrument's magnetic field synchronously with the ship's roll.

99

8. Electromagnetic Sea Current Measuring Devices
[The Geomagnetic Electrokinetograph] (GEK)

Electromagnetic methods can be used for designing instruments for direct measurement of the flow of sea currents relative to the earth and to measure these from a moving ship, a development which holds great promise in oceanography. These instruments are based on measurement of the potential difference arising at electrodes when sea water moves relative to the vertical component B_x of the earth's magnetic field, whose magnitude at any points can be ascertained from magnetic charts such as the isodynam chart shown in Fig. 67 [246].
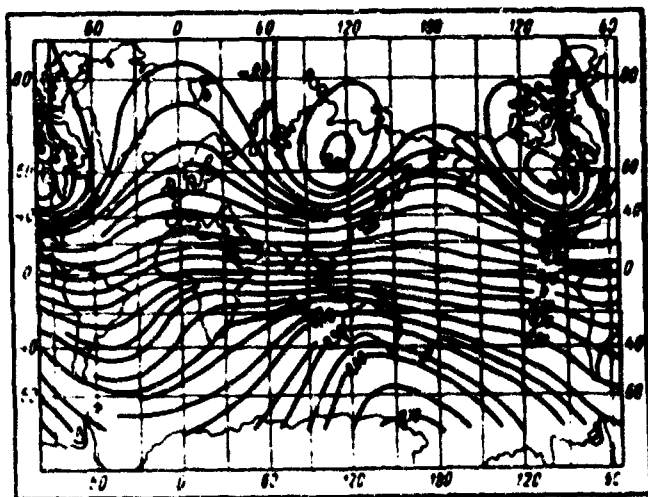
Fig. 67. Chart of isodynams of vertical components of the earth's magnetic field.

Since the vertical component of the earth's magnetic field is of the order of $0.5 \cdot 10^{-4}$ tesla, the distance L between electrodes E_1 and E_2 of the instrument (Fig. 68) must be fairly large to yield a useful signal. With the electrodes 100 m apart, the potential difference between them is of the order of 2.5 millivolts/knot.

With horizontal motion of sea water, as in the case of channel flow of conducting liquids, the sea bottom exerts its effect, which results in a nonuniform distribution of velocity with the depth. This produces a nonuniform distribution of emf in the flow and results in circulation currents; when the bottom is a good conductor, these currents flow in closed paths through the ground's resistance R_g and through the resistance of the stationary water R_{st}, which is analogous to the external load of MHD generators. The resistance R_{mov} of moving water can be identified with the internal resistance of such a generator.

The potential difference at GEK electrodes is determined from a formula similar to (3.43):

$$\varphi_1 - \varphi_2 = B_x L \frac{R_{st}}{R_{mov} + R_{st}} \qquad (3.49)$$

100
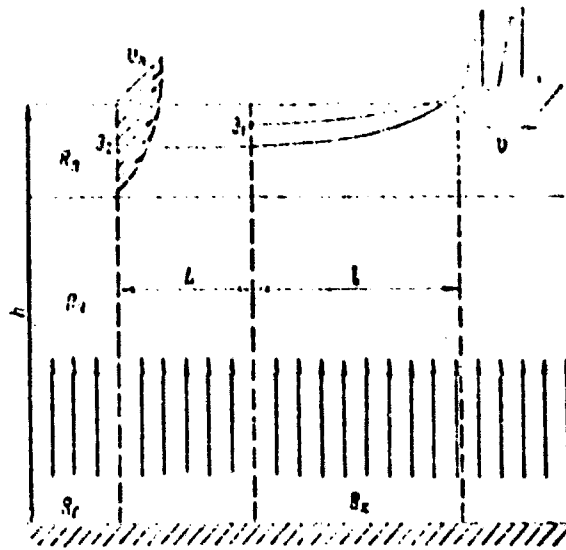
Fig. 68. Schematic of GEK.

where R_{eq} is the equivalent resistance of the ground and of the stationary water. When $R_{eq} \to \infty$

$$\varphi_1 - \varphi_2 = vB_z L. \tag{3.50}$$

Usually the sea current velocities are measured using ship-towed electrodes. The sea current causes the ship to drift from course and it, together with the electrodes, is displaced in a direction perpendicular to the course with velocity v_N. Due to the displacement of the measuring circuit relative to the earth's magnetic field, an emf is induced in it; this emf can be represented in the form

$$(\varphi_1 - \varphi_2)_1 = v_N B_z l; \ (\varphi_1 - \varphi_2)_2 = v_N B_z L.$$

The potential difference at the measuring instrument's input is equal to the algebraic sum of all the components acting in the circuit:

$$\varphi_1 - \varphi_2 = vB_z L \frac{R_{eq}}{R_{mov} + R_{eq}} \tag{3.51}$$

It follows from Eq. (3.51) that the emf induced between the electrodes is

$$\delta \chi = \varphi_1 - \varphi_2 \left(1 + \frac{R_{eq}}{R_{mov}}\right) \ (\varphi_1 - \varphi_2) \tag{3.52}$$

A quantity which is the reciprocal of factor k is the analog of the loading factor in MHD generators. Here, factor k depends on the flow conditions, conductivity of the sea bottom, of the bottom-adjoining water layers, and of the moving water.

101

Values of k for any sea region are determined by statistical processing of a large number of measurements by a GEK and other instruments. Values of k for several sea regions are given in Table 8 [147]. It follows from the table that when measuring sea current velocities in deep waters, the potential velocity at the instrument electrodes differs little from the induced emf. The correction which must be made does not exceed several percents.

Table 8. Values of factor k for several sea regions

1) Глубина моря, м	2) Характер района плавания	k
10—100	3) Материковые отмели	?
~150	4) То же	.1.1
~80	5) Открытое море	~1.01
~30	6) Балтийское море	1.15—1.?

KEY: 1) Water depth, m; 2) description of sailing region; 3) continental shelves; 4) same as above; 5) open seas; 6) Baltic Sea.
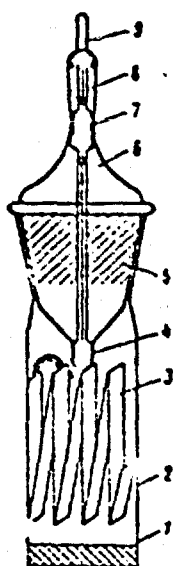
Fig. 69. Design of a nonpolarizing electrode.

The GEK records only one component of the current at any given time. To measure the current's vector, the measurements must be made on two orthogonal courses.

Reliable results using GEK were obtained on the Gulfstream [246].

From the point of view of design, the GEK consists of two nonpolarizing electrodes, connected by cables to a measuring instrument located aboardships. The GEK also includes filters for suppression of wave interferences and a winch for feeding out and taking up the cables with the electrodes. As a rule, the EPP-09 automatic recording potentiometer is used as the regulating instrument.

The most important element of a GEK is the nonpolarizing electrode, (Fig. 69) [265]. A corrugated silver plate 3 is located in the neck of glass bottle 2. A silver wire is soldered to the plate, connecting the latter to bottom 4 of ground-glass stopper 5. Since silver solders poorly to glass, cracks are possible at the solder joint, with consequent leak-in of the sea water. To eliminate this, platinum wire 8, which is soldered into the glass plug at point 7, is welded to the silver wire.

The air cushion in space 6 prevents the sea water seeping in through the solder from reaching the junction of the silver and platinum wires. A copper conductor 9, leading to the external measuring circuit, is connected to the platinum wire.

The plug is tightly sealed into the mouth of bottle 2. To provide for electrical contact with the sea water, a dense, sintered-glass filter 1 is sealed into the bottom of the bottle. The bottle is filled with a chemically-pure 3 % NaCl solution (which is identical to the NaCl content of sea water).

The cable is connected to the electrodes by means of a water-tight plug connection. The electrodes are placed in a special drogue. The intrinsic potential difference of such electrodes when operating at sea amounts to (0.3-0.5) ± 0.05 millivolts.

The Soviet industry is commercially producing the GM-15 sea current measuring device [136]. This instrument includes

102

cables, nonpolarizing silver-chloride electrodes, the PS-01 automatic electronic potentiometer, control and monitoring panel, two hand winches with current pickups and pulleys for paying out and taking in the cables with the electrodes.

The GM-15 is supplied from the 127-220 VAC ship's supply. If the ship's supply is 110-220 VDC, the PO-120-F5 converter is used.

The overall dimensions of the main units are (in mm):

Potentiometer . . . . 330 x 300 x 400

Control and monitoring panel . . . . 480 x 310 x 150

Winch with cable . . . . 400 x 440 x 400

Bracket . . . . 340 x 550 x 900

Case with electrodes . . . . 250 x 150 x 310

The total weight does not exceed 150 kg.

CHAPTER 4

ELECTROMAGNETIC PUMPS

Electromagnetic pumps are a new and rapidly developing type of magnetohydrodynamic devices, used for transporting conducting liquids, primarily liquid metals. Their main advantages are complete sealing, convenient installation, ability of adjusting the flowrate and developed pressure by changing the parameters of the electromagnetic field, simplicity of design and operation.

In terms of their operation, these pumps are similar to electrical machines, but differ from them by their design and utilization of MHD effects. Just as electric motors, electromagnetic pumps are reversible, i.e., under proper conditions they can operate as generators, supplying power. Hence many problems examined below in connection with electromagnetic pumps also pertain to liquid-metal MHD generators. A great deal of attention is paid to the latter, in conjunction with the promise they hold for use in power generation in vehicles.

1. Classification and Principal Designs of Electromagnetic Pumps

In terms of their operating principles, electromagnetic pumps are subdivided into those of conduction and induction type.

Conduction pumps utilize the field of electromagnetic ponderomotive forces, produced by interaction between externally supplied currents in the liquid and the applied magnetic field, to move a conducting liquid.

Motion of a conducting liquid by a field of electromagnetic ponderomotive forces, produced by interaction between currents induced in the fluid and the applied magnetic field, underlies the operation of pumps of the second type.

Conduction pumps are of DC and AC types.

Induction pumps may be flat linear, annular linear and helical. Each type has certain inherent electromagnetic and magnetohydrodynamic properties, governed primarily by various edge effects.

104

A DC electromagnetic conduction pump operates similarly to a DC motor. Such a pump is shown in Fig. 70. The basic element of this pump is a thin-walled rectangular duct 1, made from low-conductivity, nonmagnetic material. Electrodes 2, to which a potential difference from a DC source is supplied, are built into the duct. The magnetic field is produced by electromagnet 3 with an air gap in the magnetic circuit (the core).
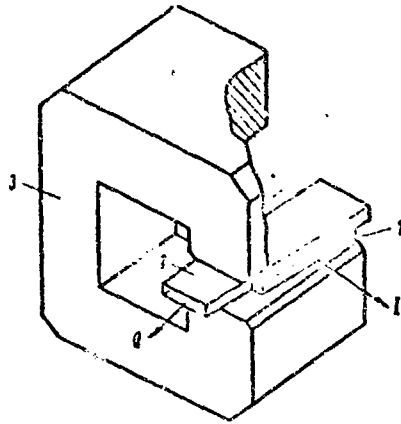
Fig. 70. Diagram of a DC induction-type electromagnetic pump.

The externally supplied potential difference causes current I to flow through the liquid metal, and the interaction between this current and the applied magnetic field produces a pressure difference at the pump inlet and outlet, which sets the fluid into motion.

The magnetic field of the current flowing through the liquid metal may distort the external magnetic field, increasing it at the inlet and decreasing at the outlet. This phenomenon, which is similar to the armature reaction in electric machines, may be called the liquid-metal reaction. It has a negative effect, reducing the pump's efficiency.

The following methods are used for reducing the liquid-metal reaction: 1) a compensating return circuit, situated in the magnet gap and creating a magnetic field equal in magnitude and opposite in direction to the magnetic field induced by currents in the liquid metal; 2) making the duct in the shape of a loop; here, the magnetic field produced by current in one side of the loop is compensated by that produced by the current in the other side of the loop; 3) modifying the magnet pole shape so that the gap between the poles would increase in the direction of motion with simultaneous change in the duct cross section; here, the flow velocity should increase in the direction of motion in a manner providing for constancy of the emf induced in the fluid over the entire active zone.

Because it is difficult to design in practice, the third method is of little use. However, one can use a technique combining the first and the second methods (Fig. 71).

105
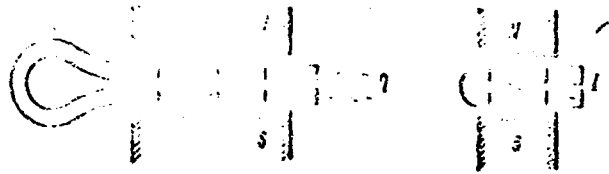
Fig. 71. Compensation of the liquid-metal re-
action.

The exciting winding of the electromagnetic pump may be in series with the elec-
trodes (series connection), or it may be fed independently. Usually liquid-metal pumps
use series-connected windings, since this makes it possible to better utilize the supply
source power. Independent excitation is used in pumps for weakly conducting liquids.

To limit current leakage beyond the region with strong magnetic field, baffles are
sometimes installed in the edge zones of the duct.

An AC conduction-type electromagnetic pump is similar to the DC pump, but its
magnet core is made from electrical-grade sheet steel to reduce eddy current losses,
and the exciting winding is supplied from a single-phase source.

One advantage of an AC conduction pump is the ability to use line current via step-
down transformer, which can utilize as its core the pump's core. Among the disadvan-
tages are the unavoidable vibrations of the thin-walled duct, produced by the pulsations
of the magnetic field in the gap, and appreciable losses to eddy currents in the conduct-
ing fluid (the latter can be reduced by reducing the supply current frequency). A conduc-
tion-type AC electromagnetic pump is shown in Fig. 72.
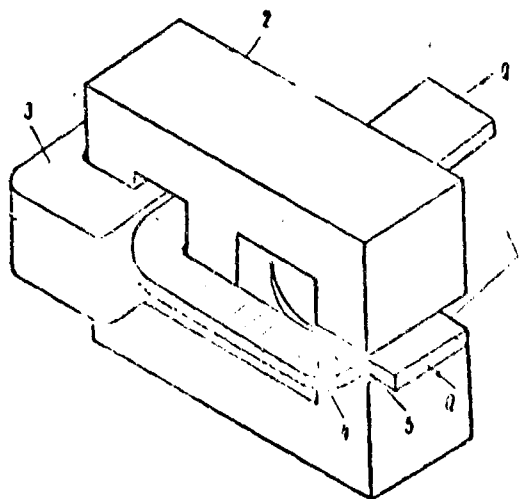
Fig. 72. Diagram of a conduction-type AC
electromagnetic pump.

Pump duct 1 is placed in gap 2 of the magnet core, on which are wound the primary (3) and secondary (4) transformer windings. The secondary winding is closed through pump electrodes 5. The series connection of the secondary winding of the transformer with the pump's electrodes allows, under certain conditions, to obtain phase coincidence of the current and the magnetic flux in the liquid metal [170].

The operating principle of induction pumps is similar to that of asynchronous motors. The helical pump, shown in Fig. 73, is most similar to an asynchronous motor.

The pump consists of magnetic field inductor 1, which is made (just as a stator of an asynchronous motor) from transformer sheet steel, a magnet core 2, also made from sheet steel, two thin-walled cylinders 3, made from nonmagnetic stainless steel and placed between inductor 1 and magnet core 2. The metal ribbon 4, forming a single- or multi-spiral helical channel in which the liquid metal is contained, is wound between the cylinders. The rotating magnetic field produced by the stator interacts with the currents induced in the liquid metal and sets the latter into motion along the helical duct.
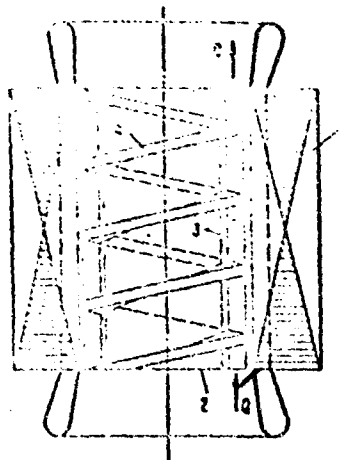
Fig. 73. Schematic diagram
of an AC helical induction pump.

The flat linear induction pump is shown in Fig. 74. Its main elements are magnetic field inductors 1, whose slots contain a three-phase excitation winding 2 which produces a traveling magnetic field. Between the inductors (which form the magnetic system of the pump) is a rectangular duct 4, made from thin-walled, low-conductivity metal. The pump is connected to the piping by means of converging section 3 and diverging section 5.

Flat linear induction pumps with branching ducts have also been designed [170].

107
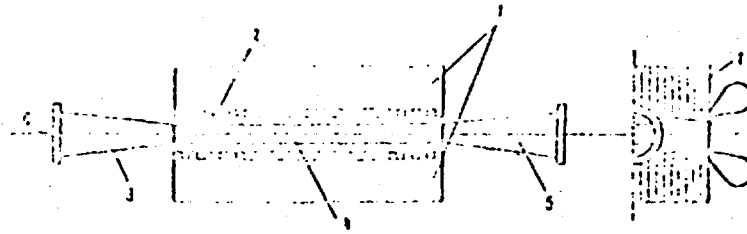
Fig. 74. Schematic of a flat linear induction pump.

Figure 75 shows a schematic of an annular linear induction pump. The pump consists of magnetic field inductor 1, a liquid metal duct formed by two coaxial cylinders 3 and 4, converging piping 6, diverging piping 2 and inner radially-laminated core 5 (the laminae extend along the cylinder's axis). The three-phase winding 7, placed in annular slots of the inductor, produces in the gap an alternating magnetic field traveling along the cylinder axis and setting the liquid metal into motion.
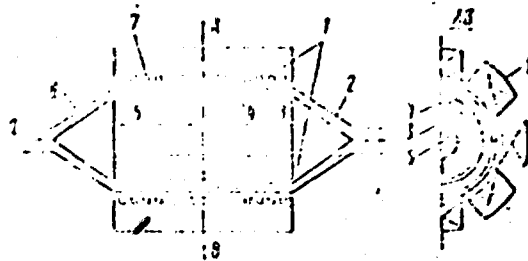
Fig. 75. Schematic diagram of an annular linear induction pump.

Among the disadvantages of annular induction pumps are poorer cooling than in flat pump and low operating efficiency except at high output. Absence of front parts of inductor windings and of transverse edge effects are among its advantages.

Annular induction pumps for liquid metals without ferromagnetic cores have also been designed [216].

Of all the above pumps, the flat linear (FLIP) and annular linear (ALIP) induction pumps are the most extensively used.

2. Theory of DC Conduction-Type Electromagnetic Pumps

The main operating characteristics of electromagnetic pumps are their delivery Q (m^3/hout) and output pressure p (Newtons/m^2). The value of p is smaller than the pressure p_a developed by the pump by the amount of pressure drop in the duct Δp

$$p = p_a - \Delta p. \qquad (4.1)$$

108

For a given liquid metal flow and magnetic field parameters, the Δp should be determined assuming MHD effects of the first kind (see Chap. 2). In particular, for a flat duct (a $\gg$ b) these drops can be determined from Eqs. (2.46) and (2.116).

The main concern of the theory of electromagnetic pumps is determination of the pressure p_a developed by the pump.

As follows from Eq. (2.1), electromagnetic forces acting in a volume of conducting fluid are given by the vector product of the magnetic flux density and the electric current density

$$dF = [J \times B]\, dV. \tag{4.2}$$

To determine p_a, Eq. (4.2) should be integrated over the entire liquid volume V in which the electromagnetic forces act, and the result thus obtained should be divided by the duct's cross sectional area

$$P_a = \frac{1}{S} \iiint_V [J \times B]\, dV. \tag{4.3}$$

The pump will be most efficient when the magnetic flux density and electric current are uniform. In real pump designs, this condition is not entirely satisfied due to the liquid reaction and edge effects. While the liquid-metal reaction can be compensated, the edge effects always remain. Here the edge effects are due to leakage of the current fed and to nonuniform distribution of magnetic flux in the edge zones.

The electromagnetic pump duct is divided into an active zone, where the current and magnetic flux density can be assumed as uniform, and an edge zone, where the distribution of these quantities is not uniform. The electromagnetic pressure of an efficiently designed pump is developed by the active as well as the edge zones. Determination of the two components of the total pressure is the principal task of the theory.
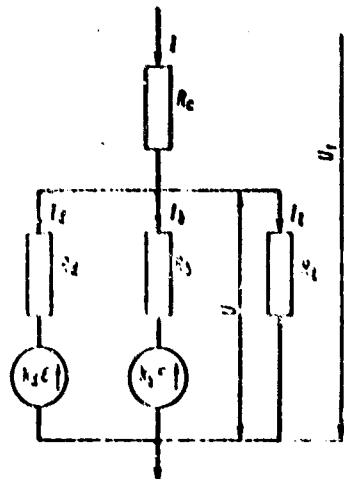
Fig. 76. Equivalent circuit of a DC electromagnetic induction pump.

109

The theory and methods of design of these pumps have been most completely developed by Yu. A. Birzvalk [178-181].

The distribution of electric quantities in an electromagnetic pump duct is usually described in terms of an equivalent circuit, which allows one to divide the electric current in the duct into its components.

Figure 76 shows the equivalent circuit of a DC pump, suggested by Birzvalk. Here, the total current I flowing through the pump duct is a sum of components I_d, I_b and I_v, corresponding to the active zone, bypass zone and the conducting wall of the duct.

The electromotive force $\mathcal{E}$, induced in the conducting liquid moving in a magnetic field is also represented in the form of components $k_d \mathcal{E}$ and $k_b \mathcal{E}$.

The resistance of the liquid and of the duct wall are denoted by R_d, R_b and R_t. It is seen from this equivalent circuit that the electric current components may be represented as

$$I_d = \frac{U - k_d \mathcal{E}}{R_d};$$ (4.4)

$$I_b = \frac{U - k_b \mathcal{E}}{R_b};$$ (4.5)

$$I_t = \frac{U}{R_t}.$$ (4.6)

Using Kirchhoff law for the electric circuit, the operating current becomes

$$I_d = \frac{I - \mathcal{E}\left(\frac{k_d - k_b}{R_b} + \frac{k_d}{R_t}\right)}{1 + \frac{R_d}{R_b} + \frac{R_d}{R_t}}.$$ (4.7)

The resistances R_d and R_b of the liquid and R_t of the duct walls, as well as factor k_d, are expressed in terms of coefficients which depend on the pump design

$$R_d = \frac{1}{\kappa \delta (a_s + a_{sq})};$$ (4.8)

$$R_b = \frac{1}{\kappa \delta a_{sb}};$$ (4.9)

$$R_t = \frac{1}{\kappa_t \delta_t (a_{sk} + 1.11)};$$ (4.10)

$$k_d = 1 + \frac{a_q}{a_{sk} + a_{sq}};$$ (4.11)

$$\alpha_{sk} = \frac{l}{a} - 1.$$

110

where a, b and ℓ are, respectively, the duct width and height, and the length of the electrodes; σ_t and b_t are the duct wall conductivity and thickness.

The values of α_{uq}, α_{ub}, α_q and k_b [181], which can be used for calculating the parameters of the equivalent circuit and for determining the operating current of the pump, developing the electromagnetic pressure, are presented in Tables 9-12. Coordinate z_0, given in the tables, is the amount by which the pole shoe length ℓ_p exceeds the electrode length ℓ

$$z_0 = \frac{l - l_0}{2}.$$

Table 9. Values of coefficients α_{uq}

$\dfrac{a}{2\delta}$	0	$\dfrac{a}{4}$	$\dfrac{a}{2}$	$\dfrac{2a}{4}$	a	$\dfrac{5a}{4}$
1.3	1.1357	1.2651	1.3740	1.1105	1.1273	1.1349
1.2	1.1415	1.2596	1.3760	1.1111	1.1277	1.1351
1.1	1.1533	1.3010	1.3780	1.1123	1.1281	1.1353
1.0	1.1636	1.3066	1.3801	1.1133	1.1285	1.1355
0.9	1.1711	1.3115	1.3823	1.1143	1.1290	1.1357
0.8	1.1853	1.3195	1.3847	1.1151	1.1295	1.1359
0.7	1.1971	1.3240	1.3871	1.1165	1.1300	1.1361
0.6	1.2091	1.3295	1.3896	1.1177	1.1305	1.1361
0.5	1.2220	1.3349	1.3920	1.3187	1.1310	1.1366
0.1	1.2342	1.3497	1.3941	1.1197	1.1311	1.1368

Table 10. Values of coefficients α_{ub}

$\dfrac{a}{2\delta}$	0	$\dfrac{a}{4}$	$\dfrac{a}{2}$	$\dfrac{3a}{4}$	a	$\dfrac{5a}{4}$
1.3	0.3065	0.1459	0.0672	0.0307	0.0130	0.0054
1.2	0.2958	0.1417	0.0663	0.0290	0.0126	0.0052
1.1	0.2875	0.1373	0.0643	0.0269	0.0132	0.0050
1.0	0.2776	0.1327	0.0612	0.0250	0.0128	0.0058
0.9	0.2671	0.1278	0.0589	0.0259	0.0123	0.0055
0.8	0.2569	0.1226	0.0566	0.0259	0.0118	0.0051
0.7	0.2312	0.1171	0.0511	0.0213	0.0113	0.0051
0.6	0.2319	0.1118	0.0517	0.0235	0.0108	0.0019
0.5	0.2193	0.1063	0.0503	0.0225	0.0103	0.0017
0.1	0.2071	0.1016	0.0472	0.0216	0.0103	0.0015

Table 11. Values of coefficients α_q

$\frac{\cdot}{\cdot}$	0	1	2	3	4	5
1.3	0.1...	...	...	...	...	...
1.2	0.1347	...	...	...	...	...
1.1	0.1368	...	...	...	...	...
1.0	-0.1349	...	...	...	...	...
0.9	-0.1329	...	...	...	...	...
0.3	0.1...	...	...	...	...	...
0.7	0.12...	...	...	...	...	...
0.6	0.12...	...	...	...	...	...
0.5	0.12...	...	...	...	...	...
0.1	0.1...	...	...	...	...	...

Table 12. Values of coefficients k_b

$\frac{\cdot}{\cdot}$	0	1	2	3	4	5
1.3	0.1...	...	0.1...	-2.1...	5.8...	13.9...
1.2	0.3...	...	0.17...	-2.13...	5.82...	13.9...
1.1	0.1...	0.2...	0.3...	?.11...	5.68...	13.6
1.0	0.2...	0.2...	...	...	...	13....
0.9	...	0.2...	...	...	5....	13....
0.3	0.3...	...	...	-1....	5....	14....
0.7	0.3...	0.2...	...	1....	5.2...	1?....
0.6	0.5...	0.1...	...	-1....	5.0...	1?....
0.5	0.5...	0.16...	0.5...	1.5...	1.6...	11....
0.1	0.6...	0.12...	0.1...	-1.3...	1.1...	?0....

In accordance with the equivalent circuit, the hydraulic power of the pump is

$$p_a Q = I_a E. \qquad (4.12)$$

To determine $p_a(Q)$, it is convenient to represent the operating current as

$$I_a = \frac{I - \frac{\delta}{R_a} R_0}{1 + R_a}, \qquad (4.13)$$

112

where

$$\bar{R}_D = k_c(1 - \bar{R}_J) - 1;$$
$$\bar{R}_B = \frac{1 + \bar{R}_D}{k_J} - 1.$$

From an equivalent circuit to which the exciting winding resistance has been added, we have

$$U_1 = IR_c + I_J R_c + k_c \mathcal{E} + I\left(R_c + \frac{R_J}{1 + \bar{R}_B}\right) + \frac{\mathcal{E}}{1 + \bar{R}_B}. \tag{4.14}$$

where R_c is the resistance of the exciting winding.

To take R_c into consideration, we can use the dimensionless ratio

$$\bar{R}_c = \frac{R_c}{R_a}, \tag{4.15}$$

where

$$R_a = \frac{1}{\frac{1}{R_J} + \frac{1}{R_b} + \frac{1}{R_l}}.$$

Then the relationship for U becomes

$$U_1 = \frac{1}{1 + \bar{R}_B}\left[IR_J(1 + \bar{R}_c) + \mathcal{E}\right]. \tag{4.16}$$

The core of a conduction-type electromagnetic pump usually operates at below saturation flux densities. Hence, we can assume that the relationship between the current and the magnetic flux density is linear

$$B = nI. \tag{4.17}$$

where

$$n = \frac{w \mu_0}{\delta k_\delta k_\mu};$$

w is the number of turns of the exciting winding; $\mu_0 = 1.257 \cdot 10^{-6}$ henry/m is the magnetic permeability of vacuum; k_δ is the air gap coefficient; k_μ is the saturation factor.

Using Eq. (4.17) and expressing the emf in terms of the magnetic flux density and flowrate $\left(\mathcal{E} = \frac{QB}{\delta}\right)$, we obtain for p_a

$$p_a = \frac{U_1^2 n\left(1 - \bar{R}_D\right)\left(1 - \frac{Qn}{bR_J}\bar{R}_D\right)}{b\left[R_J(1 + \bar{R}_c) + \frac{Qn}{b}\right]^2}. \tag{4.18}$$

113

It is also possible to represent $p_a(Q)$ in relative units

$$\bar{p}_a = \left(1 - \frac{\bar{Q}_{nom}}{\bar{R}}\right)^2 \frac{1 - \bar{Q}}{\left(1 - \frac{\bar{Q}}{\bar{R}}\right)^2}, \tag{4.19}$$

where Q_{nom} is the nominal flowrate;

$$\bar{p}_a = p_{a0} \frac{(1 - \bar{R}_c)}{l B}; \quad \bar{Q} = Q \frac{B R_D}{b l R_d}; \quad \bar{R} = \bar{R}_0(1 + R_c).$$

The total efficiency of an electromagnetic pump is expressed as a product of the electromagnetic (η_a) and hydraulic (η_h) efficiencies

$$\eta = \eta_a \eta_h \tag{4.20}$$

where

$$\eta_a = \frac{p_a Q}{P_1} = \frac{p_a Q}{U_1 I}; \tag{4.21}$$

$$\eta_h = \frac{p Q}{r Q} = \frac{p_a}{p} = 1 - \frac{\Delta p}{p}. \tag{4.22}$$

Substituting U_1 from Eq. (4.16), the power used by the pump is given by

$$P_1 = U_1 I = \frac{1}{1 + R_B}[l^2 R_c(1 + R_c) + \delta I]. \tag{4.23}$$

Substituting Eqs. (4.18) and (4.23) into Eq. (4.21), we get an expression for the pump's electromagnetic efficiency

$$\eta_a = \frac{1 - \bar{Q}}{1 + \bar{R}\bar{Q}}. \tag{4.24}$$

When $\frac{\partial \eta_a}{\partial Q} = 0$, the efficiency is maximum. Here

$$\bar{Q}_0 = 1 + \bar{R}^2 - \bar{R}. \tag{4.25}$$

Figure 77 gives computed curves of $\bar{p}_a(\bar{Q})$ for different $\bar{R} = $ const. at $\bar{Q}_{nom} = \bar{Q}$.

Assuming the pressure losses in the duct to be proportional to the square of the mean velocity, we get an expression for the pump's overall efficiency

$$\eta = \frac{1 - \bar{Q}}{1 + \frac{\bar{R}}{\bar{Q}}} - \frac{k_1 \bar{Q}^2}{\bar{R}\left(1 - \frac{\bar{Q}_{nom}}{\bar{R}}\right)^2} - \frac{k_1 \bar{Q}^2}{\bar{R}\left(1 - \frac{\bar{Q}_{nom}}{\bar{R}}\right)^2} \tag{4.26}$$

114

where

$$\bar{k}_f = \frac{\Delta p_{nom}}{p_{nom}} \cdot \frac{1 - \bar{Q}_{nom}}{\bar{Q}_{nom}^2},$$

and p_{nom} is the nominal pressure in the duct.

Figure 78 shows curves of $\eta = f(\bar{Q})$ computed from Eq. (4.26) at $U_1 = $ const. and different values of $\bar{R}$ and the friction factor. We see that the pressure drop in the duct must be taken into account.
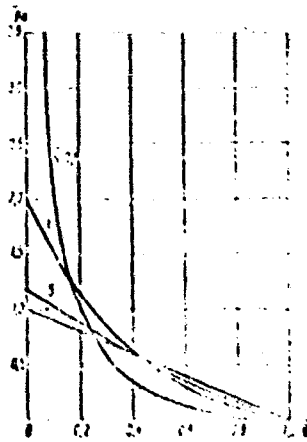
Fig. 77. Computed curves of $\bar{p}_a(\bar{Q})$.

Fig. 78. Computed curves of $\eta = f(\bar{Q})$.

The given data for design of electromagnetic pumps are usually the working pressure, output and physical properties of the conducting liquid (temperature, conductivity, viscosity and density). The engineering assignment may also list the maximum current, which is governed by the capacity of the supply source, and also other special requirements.

The main design task is to find the duct dimensions (a, b, $\mathcal{L}$) and the optimum ratio between the electromagnetic loads. This is done in a manner similar to electrical machine design, that is, by examining a number of versions using one of the generally-accepted methods [170, 180].

3. Homopolar Generators for Supplying Liquid-Metal DC Electromagnetic Pumps

Direct current electromagnetic pumps are supplied from low-voltage sources which must satisfy a number of specific requirements. It should be able to supply currents of the order of 10^3-10^5 A at 0.5-3 V. To reduce losses in the buses, the source must be near the pump and be able to operate at high ambient temperature and (possibly) in the presence of radioactivity.
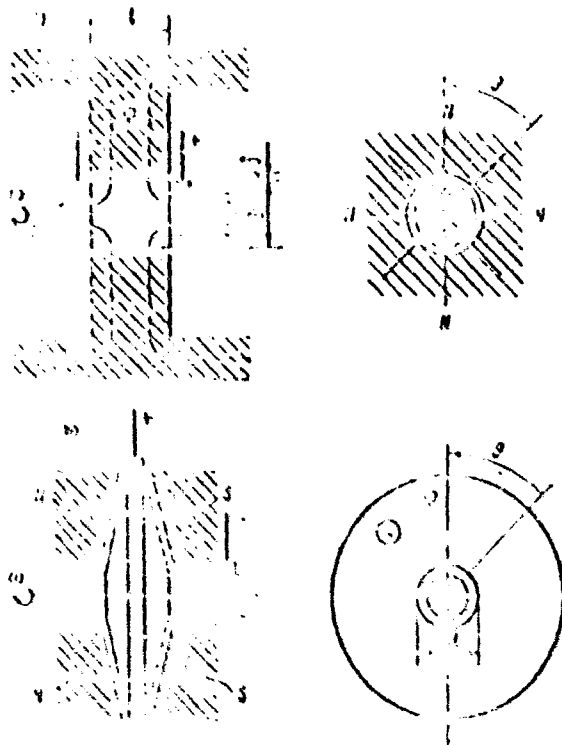
Fig. 79. The underlying principle of homopolar generators.

a) Annular generator; b) disk-type generator.

In theory, electromagnetic pumps may be supplied from rectifiers and (chemical) batteries. However, homopolar generators satisfy the above requirements much better.

According to published data, homopolar generators are 25% cheaper than rectifying devices, have a higher overload capacity and higher efficiencies [266]. They are cheaper and have a better weight size ratio than batteries.

Homopolar DC generators include brushless electrical machines, in which the direction of the induced emf remains constant. These generators were known for a long time; however, they have come under thorough experimental and theoretical scrutiny only recently [266, 267].

A homopolar generator operates as follows. The active generator element (cylinder or disk) rotates in a constant-polarity magnetic field (Fig. 79); the emf induced in this element, in accordance with the electromagnetic induction law, is

$$E = \omega \frac{\Phi}{2\pi},$$

where

$$\Phi = \pi \cdot B \cdot D^2$$

116

Within the limits of the magnet-assembly pole B = const. Here the following relationships [266] apply for annular and disk generators

$$S(\theta) = \int_0^{2\pi} \frac{D}{2} I \, d\theta; \quad \mathcal{E} = \frac{\omega}{2} B_\delta D l = \frac{\pi n}{60} B_\delta D l = \ldots; \tag{4.27}$$

$$S(\theta) = \int_0^{2\pi} \frac{D^2 - d^2}{8 \cos \alpha} \, d\theta; \quad \mathcal{E} = \frac{\omega}{8} B_\delta \frac{D^2 - d^2}{\cos \alpha} = \frac{\pi n}{240} B_\delta \frac{D^2 - d^2}{\cos \alpha} = \ldots \tag{4.28}$$

The current of a homopolar generator feeding power to a circuit is determined from the known expression

$$I = \frac{\mathcal{E}_I}{v_I + R_{arm}} = \frac{U}{R_I}. \tag{4.29}$$

The direction of current is the same as that of the emf and does not change with rotation of the active element (armature).

The ferromagnetic armature of homopolar annular generators may be smooth or massive and expanded. Sometimes the armature is made in the form of a hollow nonmagnetic cylinder. Disk-type homopolar generators have conically shaped nonmagnetic disks.

Annular homopolar generators with ferromagnetic armatures are preferred for supplying electromagnetic pumps, since their weight and power characteristics are better than those of disk-type generators. Design schematics of annular homopolar generators are shown in Fig. 80.
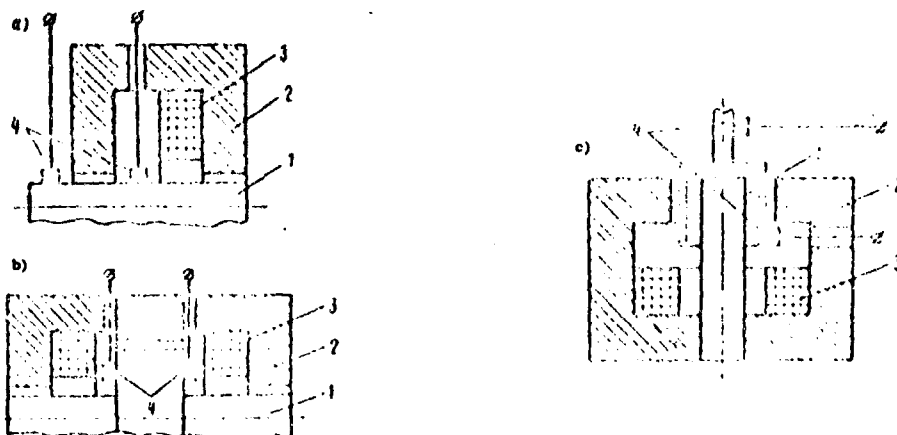
Fig. 80. Design schematics of annular homopolar generators.

a) Two-pole; b) multipole with expanded rotor; c) multipole with hollow rotor.
1) Armature; 2) stator; 3) excitation winding; 4) current contacts.

The operating current from homopolar generators is taken off by means of liquid-metal or ordinary brush-type contacts. Metal-graphite brushes can be used for current densities of up to 30 A/cm^2, and at currents of 10^3-10^5 A their size must be appreciable. This naturally also increases the friction losses. Hence high-current homopolar generators usually use liquid-metal contacts which can be used with current densities of 10^3 A/cm^2.

Modern homopolar generators with ring contact from an Na-K alloy have an efficiency of about 98% and a weight to power ratio about 2.5 kg/kW for powers of 10^3-10^4 kW.

Figure 81 shows curves of $G = f_1(n)$ and $I = f_2(n)$ for annular homopolar generators derived at different linear velocities. These characteristics may be varied within wide limits by changing the armature diameter D.
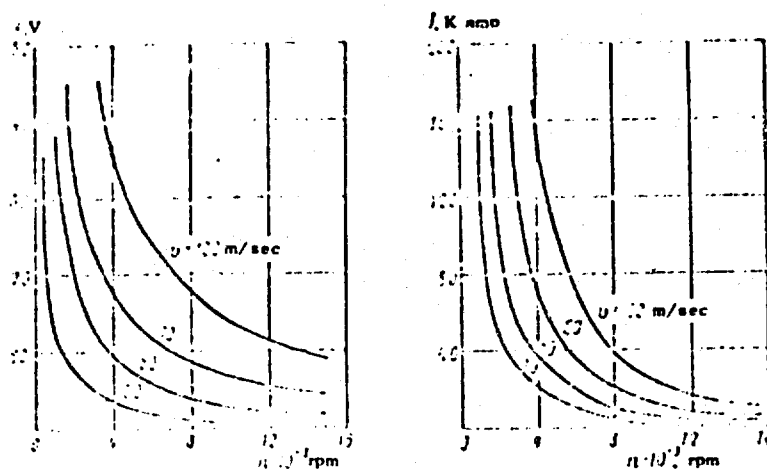
Fig. 81. Theoretical curves of $G = f_1(n)$ and $I = f_2(n)$ for homopolar generators.

As a rule, homopolar generators are separately excited, which makes it possible to use permanent magnets.

Table 13 presents the specifications of an annular homopolar generator with liquid-metal current contacts [267]. The weight of this experimental generator is 107 kg and the overall dimensions are 355 x 320 x 385 mm. The experimental output curves of this generator are presented in Fig. 82.

4. Theory of Flat Linear Induction Pumps

The main task of the theory of flat linear induction pumps [FLIP] is the study of the spatial distribution of the electric field intensity $E = f_1(x, y, z, t)$ and of the magnetic flux density $B = f_2(x, y, z, t)$; these factors must be known for determining currents and electromagnetic forces acting in the liquid metal.
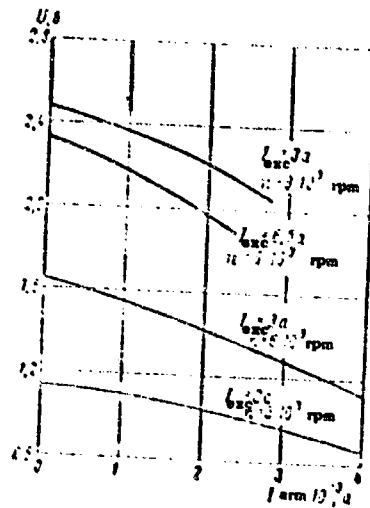
Fig. 82. Experimental output
characteristics of an annular
homopolar generator with
liquid-metal contacts.

Table 13. Specifications of
Homopolar Generator

Параметры A)	n, rpm		
	3600	6000	9000
в)Мощность, кэт	3,33	6,66	10,0
c)Ток якоря $I_{я}$, a	4000	4000	4000
D)Напряже-ние U, в	0,835	1,67	2,5
E)Ток возбу-ждения $I_{в}$, a	6,5	6,5	6,5
F) Мощность возбужде-ния, вт	170	170	170
G) К. п. д.	0,87	6,835	0,78

KEY: A) Parameters; B) rating,
kW; C) armature current, I_{arm},
A; D) voltage U, V; E) excitation
current I_{exc}, A; F) excitation
power, W; G) efficiency.

119
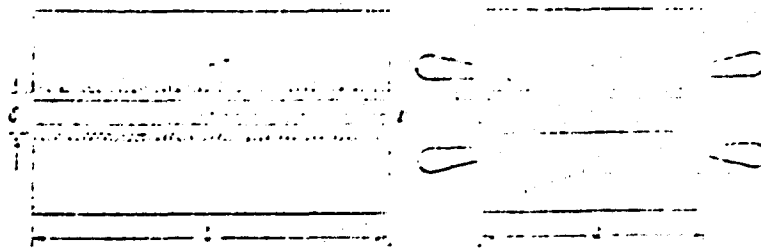
Fig. 83. Schematic of a flat linear induction pump.

The processes taking place in the ducts of flat electromagnetic pumps are much more complex than those in ducts of conduction-type pumps, due to the eddy behavior of electromagnetic forces, demagnetizing effect of currents in the liquid metal, edge effects (transverse and longitudinal), etc. Hence the modern theory of induction pumps is built on an idealization of the flow in the channel and on an idealized design. The basic work in the theory of induction pumps was done by A.I. Vol'dek [163, 165-167].

Figure 83 shows a schematic of a flat linear induction pump. The finite width a of the pump duct produces current density components j_z in the liquid metal. These components do not participate in production of the useful pump head, but reduce the magnitude of the useful component j_y by increasing the total length of the current lines. The distribution of the current lines is shown in Fig. 84.
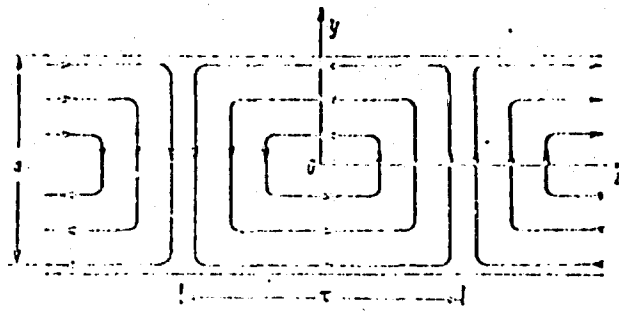
Fig. 84. Distribution of currents induced in the liquid metal flowing through an induction pump.

The problem of current and electromagnetic-force distributions in liquid metal flowing through a flat linear induction pump was solved by Vol'dek under the following assumptions [163]: the pump is infinitely long, the magnetic-field inductors have no gap and have an infinite magnetic permeability, the duct walls are isolators, and the magnetic field in the liquid metal is plane-parallel.

120

For the case of a plane-parallel magnetic field, one can write Eqs. (2.3) and (2.4), after substitution of Eq. (2.6)

$$
\left.
\begin{aligned}
\frac{1}{\mu}\frac{\partial B_z}{\partial y} &= \sigma E_z; \\
\frac{1}{\mu}\frac{\partial B_x}{\partial z} &= \sigma(E_y + E_\Delta); \\
\frac{\partial E_z}{\partial y} - \frac{\partial E_y}{\partial z} &= -\frac{\partial B_x}{\partial t},
\end{aligned}
\right\}
\tag{4.30}
$$

where E_Δ is the strength of the electric field induced in the liquid metal by the inductor.

The electric field and magnetic flux density are most conveniently represented in the complex form

$$
E = \dot{E}e^{i(\omega t - \alpha z)}; \quad B = \dot{B}e^{i(\omega t - \alpha z)},
$$

where $\alpha = \pi/\tau$; τ is the pole pitch (see Fig. 84) and ω is the angular velocity of the metal moving relative to the induced field. Here the complex amplitudes $\dot{B}$ and $\dot{E}$ are not functions of coordinate z, while $\dot{E}_\Delta$ is not a function of y.

Equations (4.30) in complex form will now be written in the form

$$
\left.
\begin{aligned}
-\frac{1}{\mu}\frac{d\dot{B}_x}{dy} &= \sigma \dot{E}_z; \\
-i\frac{\alpha}{\mu}\dot{B}_x &= \sigma(\dot{E}_y + \dot{E}_\Delta); \\
\frac{d\dot{E}_z}{dy} + i\alpha\dot{E}_y &= -i\omega\dot{B}_x.
\end{aligned}
\right\}
\tag{4.31}
$$

Eliminating from the above expression $\dot{E}_z$ and $\dot{E}_y$, we get the following second-order ordinary differential equation for $\dot{B}_x$

$$
\frac{d^2\dot{B}_x}{dy^2} - \lambda^2\dot{B}_x + i\alpha\omega\mu\dot{E}_\Delta = 0,
\tag{4.32}
$$

where

$$
\lambda^2 = \alpha^2(1 + i\varepsilon); \quad \varepsilon = \frac{\omega\mu\sigma}{\alpha^2}.
$$

The boundary conditions for Eq. (4.32) are

$$
\dot{B}_x = 0 \quad \text{for} \quad y = \pm\frac{a}{2}.
\tag{4.33}
$$

121

The solution of Eq. (4.32) is

$$H_z = C_1 \, ch \, \lambda y + C_2 \, ch \, \lambda y + \frac{j \omega \mu E_x}{\lambda^2} . \tag{4.34}$$

From the boundary conditions we get

$$C_1 = 0; \quad C_2 = - \frac{j \omega \mu E_x}{\lambda^2 \, ch \, \lambda \frac{a}{2}} , \tag{4.35}$$

and the solution takes the form

$$B_z = \frac{j \omega \mu E_x}{\lambda^2} \left(1 - \frac{ch \, \lambda y}{ch \, \lambda \frac{a}{2}} \right) . \tag{4.36}$$

In accordance with Eq. (2.3), we get the following expressions for the complex amplitudes of current densities

$$j_x = \frac{j \omega E_x}{\lambda} \cdot \frac{sh \, \lambda y}{ch \, \lambda \frac{a}{2}} ; \tag{4.37}$$

$$j_y = \frac{j \omega E_x}{\lambda^2} \left(1 - \frac{ch \, \lambda y}{ch \, \lambda \frac{a}{2}} \right) . \tag{4.38}$$

When $a \to \infty$, there is no transverse edge effect. Here

$$j_x = 0; \quad j_y = \frac{j E_x}{1 + j \varepsilon} . \tag{4.39}$$

In the above relationships

$$E_x = \cdots , \quad \lambda^2 = \cdots , \quad \varepsilon = j / \omega_0 . \tag{4.40}$$

where f is the current frequency in the liquid metal and B_Δ is the amplitude of the magnetic flux density of the traveling field of the inductor in the liquid metal.

In calculating the pressure developed by the pump, one need no integrate along the z axis. Here it suffices to take (in a manner similar to calculating the average effective power of sinusoidal alternating currents) the real part of the product of the effective complex of current density and the conjugate effective value of the magnetic flux density comples and multiply it by the inductor length ℓ

$$p = \frac{\ell}{\cdots} \int\limits_{-\frac{a}{2}}^{\frac{a}{2}} \int\limits_{0}^{b} Re \, [j_x B_z] \, dx \, dy . \tag{4.41}$$

JCIBLE

122

Upon substitution of Eqs. (4.38) and (4.40), we get

$$p' = \frac{\omega}{2a}\sigma B_\lambda^2 l k_{at} = \tau l f \sigma B_\lambda^2 k_{at}. \tag{4.42}$$

where k_{at} is the pressure attenuation factor due to the transverse edge effect

$$k_{at} = \mathrm{Re}\left[\frac{a^2}{\lambda^2}\left(1 - \frac{\mathrm{th}\,\lambda\frac{a}{2}}{\lambda\frac{a}{2}}\right)\right]. \tag{4.43}$$

A general expression for k_{at} was obtained by Vol'dek in the form

$$k_{at} = \frac{1}{1+\varepsilon^2}\left[1 - \frac{(1+\varepsilon^2)\,K + \varepsilon\,(2m^2+1)\,L}{2n\zeta\sqrt{1+\varepsilon^2}}\right], \tag{4.44}$$

where

$$K = \frac{\mathrm{sh}\,2m\zeta}{\mathrm{ch}\,2m\zeta + \cos 2n\zeta}; \quad L = \frac{\sin 2n\zeta}{\mathrm{ch}\,2n\zeta + \cos 2n\zeta};$$

$$m = \frac{1}{\sqrt{2}}\sqrt{1+\sqrt{1+\varepsilon^2}}; \quad n = \frac{\varepsilon}{\sqrt{2}\sqrt{1+\sqrt{1+\varepsilon^2}}}.$$

For low-conductivity liquid and small angular frequency ω, we have $\varepsilon \simeq 0$; then

$$k_{at} = 1 - \frac{\mathrm{th}\,\frac{\pi a}{2\tau}}{\frac{\pi a}{2\tau}}. \tag{4.45}$$

Figure 85 shows curves k_{at} vs. $a/2\tau$ at different ε = const.

The average power generated in a unit volume of liquid metal per unit time is

$$p'' = \mathrm{Re}\frac{l^2 j}{2} = \frac{\omega l^2}{2}\,\mathrm{Re}\left[\frac{a^2}{\lambda^2}\left(1 - \frac{\mathrm{th}\,\lambda\frac{a}{2}}{\lambda\frac{a}{2}}\right)\right]. \tag{4.46}$$

The power released in the entire volume of liquid metal is

$$P = l\int\limits_{-\frac{a}{2}}^{\frac{a}{2}}\int\limits_{-\frac{b}{2}}^{\frac{b}{2}} P''\,dx\,dy = k_a P_0. \tag{4.47}$$

where

$$P_0 = 2\omega l B_\lambda^2 \sigma l a b. \tag{4.48}$$

123

The power P_0 is released when there is no transverse edge effect, while factor k_{at} describes the decrease in the losses in the liquid metal when this effect is present.

Equations (4.42) and (4.47) were obtained for the case of stationary liquid metal, which corresponds to the case when the induction pump does not deliver any flow but is connected to the power supply.
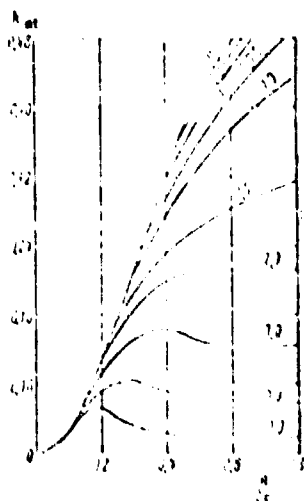
Fig. 85. Curves of k_{at}
$\varphi(a/2\tau)$ at different ε const.

As in asynchronous motors, the controlling operating parameter of induction pumps is the quantity s, which characterizes the slip of the liquid metal flow moving with average velocity v_0 relative to the traveling magnetic field

$$s \quad 1 \quad \frac{v_0}{v} \tag{4.49}$$

When the slip differs from 1, the formula for electromagnetic pressure developed by the pump must contain the factor s:

$$P_1 \quad P_0 \, s_{at} \tag{4.50}$$

where

$$P_0 \quad \varepsilon \tag{}$$

The slip is also included into the expression for ε

$$\varepsilon \tag{4.51}$$

where

$$\varepsilon \tag{}$$

Correction $b/\delta k_\delta$ in Eq. (4.51) takes into account the fact that $b < \delta$ and that the inductor is not smooth.

The use of high-conduction lateral channel walls is an effective means for reducing the transverse edge effect. Special short-circuiting bus bars are used for this purpose.

In our case (it is assumed that the busbars are ideal conductors)

$$k_{at} \tag{4.52}$$

124

The expression for the electromagnetic pressure takes the form [187]

$$p = \frac{18\mu_0 (k_w \omega l)^2}{k_\delta \pi \delta n b} N,$$ (4.53)

where

$$N = \frac{s}{1 + s^2};$$

n is the number of pole winding pairs and k_w is the winding factor.

The expression for B_Δ, used in deriving Eq. (4.53), was

$$B_\Delta = \frac{\mu_0 3 \sqrt{2} k_w \omega}{\pi \delta n k_\delta} l.$$ (4.54)

It follows from Eq. (4.53) that an induction pump with perfectly conducting side busbars and constant current supply to the inductor develops a maximum pressure when N is at maximum. Differentiating Eq. (4.53), we obtain that $N_m = 1$.

Similarly, we get an expression for the mechanical power

$$P_{mech} = 3I^2 x_\Delta N (1 - s),$$ (4.55)

where x_Δ is the inductive reactance of the liquid metal. This reactance is expressed in terms of the parameters of the inductor

$$x_\Delta = - \frac{2 |\mu_0 \omega l (k_w \omega)^2}{2 \pi k_\delta \delta n}.$$ (4.56)

The efficiency of a flat linear induction pump is written in the form [185]

$$\eta = \frac{1 - s}{1 + \frac{r}{x_\Delta} \cdot \frac{1}{N}},$$ (4.57)

where r is the active resistance of one phase of the inductor.

The efficiency is at maximum when the slip is

$$s_\eta = \cdots $$

where s_1 is the value of s at s = 1.

Figure 86 shows theoretical curves of the electromagnetic pressure and efficiency for a flat linear pump with ideally conducting side busbars as a function of the average velocity of the liquid metal.

125

Since p describes the electromagnetic pressure developed by the pump, the operating pressure is determined by subtracting from the electromagnetic pressure the pressure drop in the pump duct due to viscous friction and turbulent mixing

$$p = p_a - \Delta p.$$

While determination of Δp for DC electromagnetic pumps is quite easy and, in the case of flat channel, can be done by means of formulas of Chapter 2, in our case the problem is much more difficult.
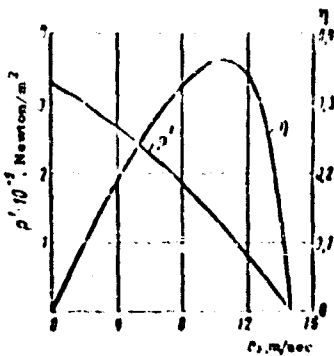
Fig. 86. Theoretical electromagnetic pressure and efficiency of a flat linear induction pump.

The MHD effects present in induction pumps may result in mixing of the liquid metal due to vortex-type electromagnetic forces [175].

From the equation of momentum (2.1), we find the condition for hydrostatic equilibrium of a liquid subjected to electromagnetic forces

$$\nabla p = [J \times B]. \qquad (4.58)$$

If the above equality is not satisfied, then $v > 0$, and there is no hydrostatic equilibrium. The condition for disturbance of hydrostatic equilibrium is satisfaction of the inequality

$$\text{curl } [\text{curl } [J \times B]] \neq 0. \qquad (4.59)$$

Consequently, if the electromagnetic forces determined under condition $v = 0$ satisfy inequality (4.59), i.e., they are not potential but vortex forces, then hydrostatic equilibrium is impossible.

In a flat induction pump with a two-sided inductor and highly conducting lateral busbars we find that in the general cast at $v = 0$ the magnetic flux density vector has two components in the liquid metal $B_z(z, x, t)$ and $B_x(z, x, t)$. In this case

$$\text{curl } [\text{curl }] = i_z\left(\frac{\partial^2}{\partial z^2} - \frac{\partial^2 B_z}{\partial x \partial z}\right) + i_x\left(\frac{\partial^2 B_z}{\partial x \partial z} - \frac{\partial^2}{\partial x^2}\right) \neq 0. \qquad (4.60)$$

In liquid metal there exists not only the useful force $f_z = i_y B_x$, but also the force $f_x = i_y B_z$. Since these forces are periodic, nonsynchronous and out of phase, conditions are created for mixing of the metal. This is a demonstration of the peculiarity of MHD effects appearing in liquid metals flowing in traveling magnetic fields.

Paper [175] presents a discussion pertaining to approximate computation of friction losses in ducts of induction pumps. However, there is now rigorous experimental confirmation of those conclusions.

5. Application and Characteristics of Experimental Electromagnetic Pumps

Direct-current conduction-type electromagnetic pumps are preferable for pumping low-conductivity liquid metals. In this case these pumps have an efficiency higher than induction pumps and have better weight to dimensions ratios.

In a number of cases such advantages of conduction pumps as design simplicity, moderate requirements as to electrical insulation (due to the low supply voltage and small number of windings on the excitation coils) make DC conduction pumps preferable even for pumping high-conductivity liquid metals at high temperatures. Pumping of low-conductivity liquids (electrolytes) is done only with conduction pumps.

There are many examples of successful operation of DC conduction-type electromagnetic pumps in pilot and regular production plants.

We now present the basic specifications of a pump developed by the Argonne National Laboratory (USA) for the EBR-I experimental breeding reactor [156]:

Working pressure p, Newtons/m² . . . . (1.5 – 3)·10^5
Output Q, m³/h 110
Efficiency (at p = 2.8·10^5 Newtons/m² and Q = 68 m³/hour), % . 43

The pump duct is made from Ni80Cr20 nichrome with wall thickness of about 0.6 mm. The duct cross section in the active zone is variable: duct height b varies from 46 to 36 mm, width a ranges from 74 to 86 mm. The pole shoe area is 100 x 380 mm. The excitation coil consists of two copper windings 150 x 150 mm in cross section and is connected in series with the electrodes. The power supply is a solid-state rectifier with U = 1 V and I = 20,000 A.

Figures 87 and 88 show experimental curves of p = f(Q) and $\eta = \varphi(Q)$ for this pump when pumping Na-K at T = 250°C. Each pressure curve in Fig. 87 was obtained at some constant supply power.
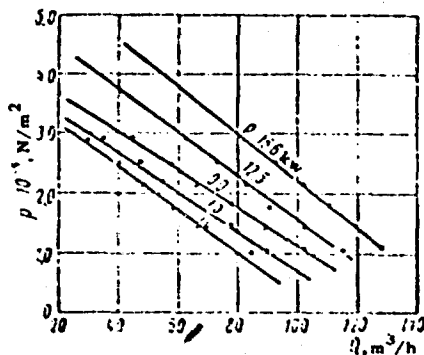
Fig. 87. Experimental curves of p = f(Q) for a DC conduction-type electromagnetic pump pumping Na-K alloy at T = 250°C.
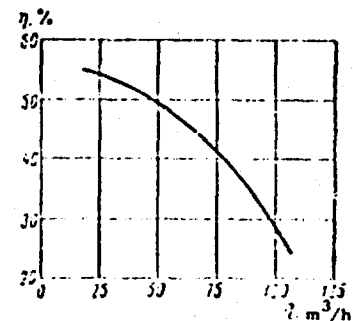
Fig. 88. Experimental curve of $\eta = \varphi(Q)$ of a DC conduction-type electromagnetic pump pumping Na-K alloy at T = 250°C.

127

Figure 89 shows a large DC conduction-type pump with a homopolar generator, used for the EBR-II breeder reactor [156]. The basic specifications of this pump are:

Working pressure p, Newtons/m³ . . . . $5.3 \cdot 10^5$
Throughput Q, m³/hour 2250
Duct dimensions a x b x l, mm . . . . 450 x 150 x 1070
Duct-wall thickness, mm 1.6

The pump has a novel current-supply arrangement consisting of steel shells welded to the side walls of the duct and of copper bars, which are inserted into these shells. Electrical contact is obtained by means of a thin layer of liquid Na. The liquid-metal reaction is compensated by a return current conductor arrangement. The power source is a homopolar generator ($I_l = 2.5 \cdot 10^5$ A, $U_l = 2.5$ V).

Direct current conduction electromagnetic pumps are successfully used outside of the USSR for pumping liquid metals at temperatures of ~800°C. They are cooled solely by natural convection of the surrounding air and by radiation.

Table 14. Specifications of DC Conduction-Type Electromagnetic Pumps

1) Тип насоса	2)	3)	4)	5)	6)	7)
a) КПД-1	Na	500	3	5	1.52	9) Обратный электропровод
a) КПД-2	Na	700	2	2	0.53	» »
a) КПД-3	10) Карналлит	730	0.5	15	20	11) Некомпенсация
a) КПД-4	Na-К	200	1.5	3.6	0.75	12) Суживающийся канал
a) КПД-5	In-Ga	30	1	0.011	0.52	13) Без компенсации
a) КПД-6	In-Ga	20	1.3	-	0.31	» »
a) КПД-7	In-Ga	100	1.5	0.03	-	» »

KEY: 1) Pump type; 2) liquid metal pumped; 3) liquid-metal temperature, °C; 4) pressure developed $p_a \cdot 10^{-5}$, Newtons/m²; 5) output Q, m³/hour; 6) pump supply contact voltage, V; 7) method of metal-reaction compensation; 8) KN; 9) return current conductors; 10) Carnallite; 11) uncompensated; 12) tapering duct.

Tables 14 and 15 present the basic specifications for similar pumps developed at the Physics Institute of the Latvian SSR Academy of Sciences [181]. Numerous cases of successful use of these pumps for pumping high-temperature liquid metals are known [170, 197, 201, 202, 205].
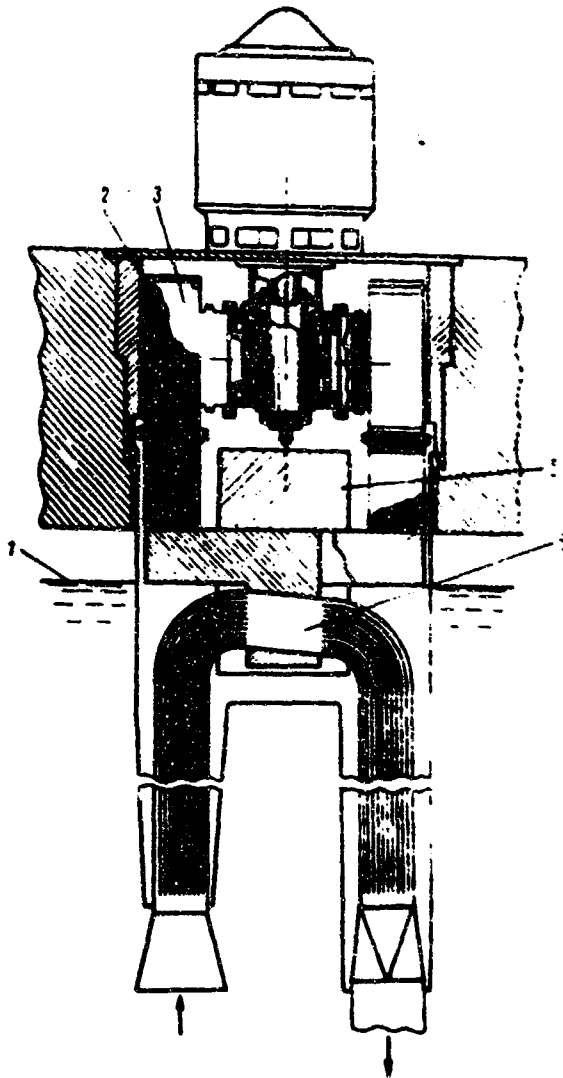
Fig. 89.   Large DC conduction pump with homo-
polar generator.

1) Liquid metal level; 2) copper bars; 3) liquid
metal filled cavity; 4) driving motor; 5) magnetic
core; 6) pump duct.

Table 15. Overall Dimensions of Type KN Conduction Electromagnetic Pumps.

Тип 1) насоса	2) Габаритные размеры, мм			Ориентировочный 3)вес, кг
	4) Длина	5) Ширина	6) Высота	
7) КН-1	530	440	410	150
7) КН-2	520	400	300	130
7) КН-3	1000	700	375	1800
7) КН-4	450	328	225	55
7) КН-5	378	212	205	35
7) КН-6	324	244	268	47
7) КН-7	520	275	262	77

KEY: 1) Pump type; 2) overall dimensions, mm; 3) approximate weight, kg; 4) length; 5) width; 6) height; 7) KN.

As an illustration we present test data for one of DC conduction-type electromagnetic pump [205], designed for pumping Na and Na-K alloy at T = 700°C:

Developed pressure (for I = 10,000 amps) p, Newtons/m^2 . . . $3 \cdot 10^5$
Output Q, m^3/hour 25.2
Supply voltage, U, V 0.6
Duct dimensions a x b x ℓ, mm . . . .   82 x 16 x 360
Duct-wall thickness, mm 0.7
Duct-wall material . . . .   Kh 18N9T steel
Number of turns on the excitation winding, w   2

The power for this pump is supplied by a homopolar generator. The test characteristics of this pump are presented in Figs. 90 and 91.

Fig. 90. Test p = f(Q) curves for a DC conduction-type electromagnetic pump for pumping Na-K.
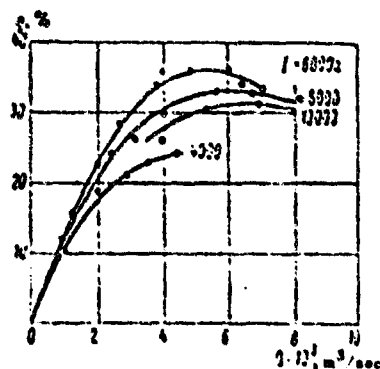
Fig. 91. Test $\eta = \varphi$(Q) curves for a DC conduction-type electromagnetic pump for pumping Na-K.

130

Experience with conduction-type electromagnetic pumps in the USSR shows them still functioning satisfactorily after more than 1000 hours of operation [205].

Due to their low efficiency, AC conduction-type electromagnetic pumps operating at 50 cps are used primarily in laboratory work. However, studies show [157] that in large pumps the efficiency can be brought close to that of DC pumps by reducing the supply-current frequency to 5-10 cps.

Following are the technical specifications for an AC conduction-type electromagnetic pump combined with a transformer and used for pumping mercury at $T = 100°C$ [127]:

Developed pressure, p, Newtons/m^2	$1.2 \cdot 10^5$
Output Q, m^3/hour	3.2
Efficiency, η, %	6.5
Duct cross section a x b, mm	24 x 8.6
Duct-wall thickness, mm	0.56
Input power P_1, kW	1.65
Power factor, cos φ	0.32
Overall dimensions of pump, mm	220 x 229 x 178
Pump weight, kg	39.5

The test characteristics of this pump are given in Fig. 92.

Alternating-current conduction-type electromagnetic pumps combined with a transformer are used in the Soviet Union for pumping the liquid Na at $T = 300°C$ [208]. The basic data for these pumps are

Developed pressure p, N/m^2	$2.5 \cdot 10^5$
Output Q, liter/sec	0.4
Efficiency η, %	7.7
Supply voltage U, V	150—200
Duct cross section a x b, mm	30 x 3.5
Duct-wall thickness, mm	0.5
Number of turns on primary transformer winding w_1	178
Number of turns on secondary transformer winding w_2	2

The test characteristics of this electromagnetic pump at different supply voltages are presented in Figs. 93 and 94. The pump was operated under test conditions for over 700 hours.

If a given liquid metal reacts strongly with all the electrically-conducting materials, then one uses an induction pump. Such pumps are also used when the DC supply source needed for a conduction pump is not available.

The most extensively used induction pumps are the flat and the annular linear induction pumps (FLIP and ALIP). A diagram of the efficient range of utilization of electromagnetic induction pumps is presented in Fig. 95 [196].

131
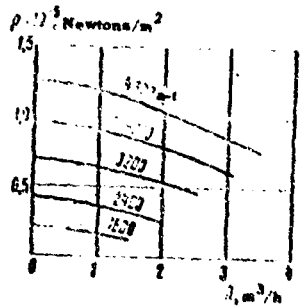
Fig. 92. Test p = f(Q) curves for an AC conduction-type electromagnetic pump for pumping mercury at different numbers of ampere turns.

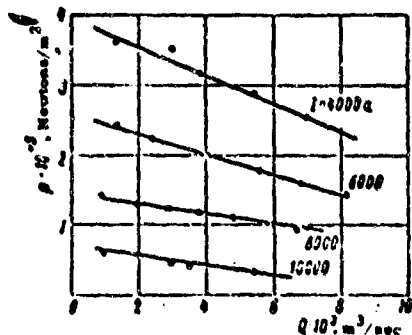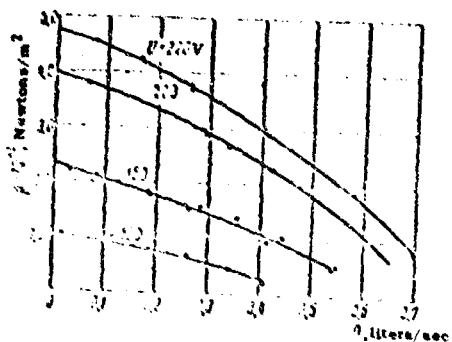Fig. 93. Test p = f(Q) curves for an AC conduction-type electromagnetic pump for pumping Na.
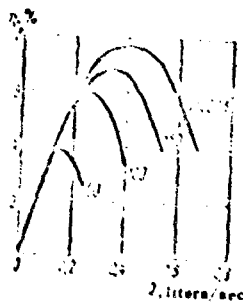
Fig. 94. Test $\eta = \varphi(Q)$ curves for an AC conduction-type electromagnetic pump for pumping Na.
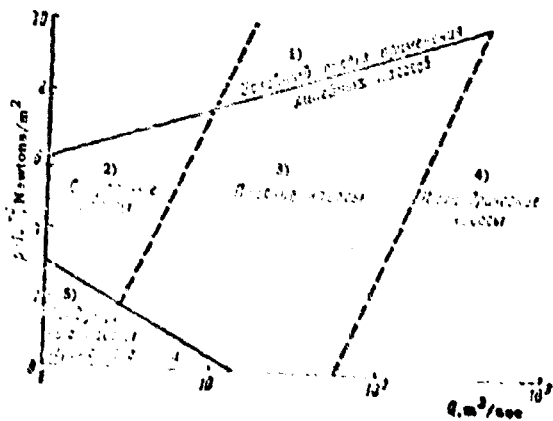
Fig. 95. Diagram of fields of efficient utilization of AC electromagnetic pumps.

KEY: 1) Conventional limit of utilization of linear pumps; 2) helical pumps; 3) flat pumps; 4) annular pumps; 5) AC conduction pumps.

132

Figure 96 shows schematically the flat linear induction pump for pumping Na used on the United States Navy submarine Seawolf [127]. The output of this pump is 115 m³/hour. The test characteristics of one of the FLIP of this series are shown in Figs. 97 and 98.
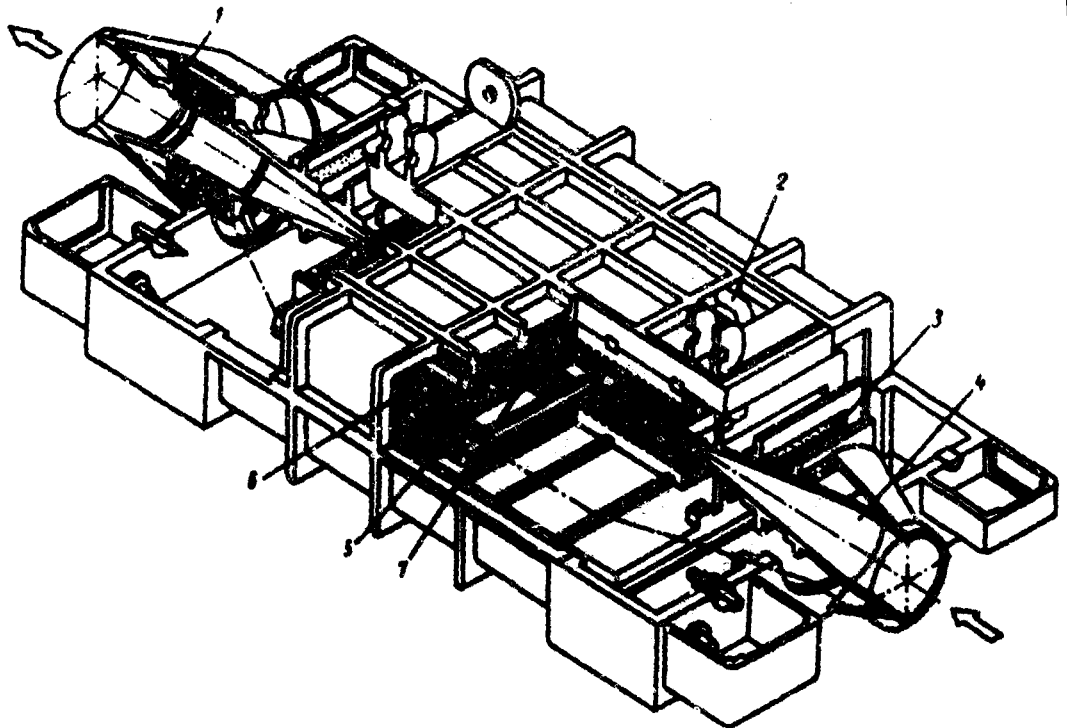
Fig. 96. Design of the flat linear induction pump for pumping Na used on the nuclear submarine Seawolf.

1) Expansion joint; 2) outlet coolant connection; 3) calrod heater element; 4) duct; 5) duct thermal insulation (outer strips turned up); 6) magnetic-field inductor winding; 7) inductor frame [core].

Flat linear induction pumps were developed in the USSR and other countries in several standard sizes, some of which have been in service for a long time. Table 16 presents some specifications of a FLIP developed by English Electric for pumping Na and Na-K alloys [170].

Table 17 presents the basic characteristics of FLIP and ALIP developed at the Physics Institute of the Latvian Academy of Sciences [196]. It is seen from the table that the efficiency of induction pumps depends on the conductivity of the pumped fluid.

Figure 99 shows the results of testing the IN-10 pump [200]. The duct of this pump is made from Kh18N10T steel, and is a flat slot 150 x 10 mm in cross section.

Fig. 97. Test p = f(Q) curves for a flat linear induction pump for pumping Na.
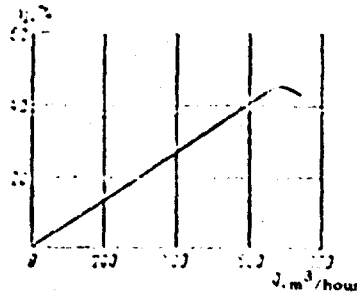
Fig. 98. Test $\eta = \varphi(Q)$ curve for a flat linear induction pump for pumping Na.
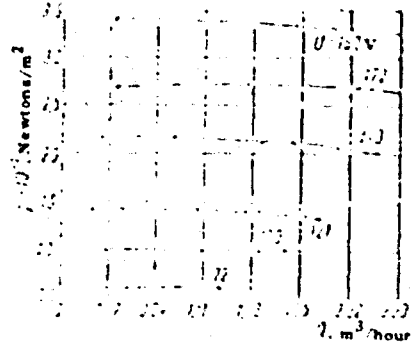
Fig. 99. Test p = f(Q) curves for the IN-10 flat linear induction pump.

Table 16. Specifications on the British Electric FLIP

1) Основные показатели	2) Тип насоса				
	1А	6	10	15	20
3) Производительность Q, м³/ч	7,2	40,7	103	270	635
4) Развиваемое давление p·10⁻³, н/м²	1,5	1,2	1,1	2,15	2,1
5) Габариты, мм:					
6) общая длина, включая диффузор	510	1020	1360	2000	2280
7) высота	150	205	510	610	610
8) ширина	150	305	760	1020	1250
9) Диаметр выходного отверстия диффузора, мм	25	51	102	152	213
10) Вес, кг	3,5	390	2000	12 800	16 000

KEY: 1) Basic characteristics; 2) pump type; 3) output Q, m³/hour; 4) developed pressure p· 10⁻⁵, Newtons/m²; 5) overall dimensions, mm; 6) total length, including diverging duct; 7) height; 8) width; 9) diverging duct outlet diameter, mm; 10) weight, kg.

134

Table 17. Specifications of FLIP and ALIP Developed by the
Physics Institute of the Latvian Academy of Sciences

1) Основные показатели	2) ИНIIН						3) СИНIIН	
	ИН-1 4)	ИН-7 4)	ИН-8 4)	ИН-9 4)	ИН-10 4)	ИН-11 4)	СИН-1 5)	СИН-3 5)
6) Перекачиваемый жидкий металл	Na—K	Na	Pb	Na	Hg	In—Ga	Na	Na
7) Температура, °C	200	400	550	650	100	80	400	400
8) Производительность Q, м³·ч	24	250	1,2	30	10	0,015	10	5
9) Развиваемое давление p·10⁻⁵, н/м²	7	5	2,5	5	3	0,5	6,5	5
10) К. п. д. η, %	21	38	1,5	23,6	11,55	0,1	19	29
11) Линейное напряжение, в	317	210	220	223	213	110	250	380
12) Линейный ток, а	144	500	91	133	115	2	70	270
13) Частота, гц	50	50	50	50	50	200	50	50
14) cos φ	0,81	0,37	6,1	0,32	0,32	0,51	0,1	0,14
15) Вес, кг	100	500	300	300	200	15	350	650
16) Полезная мощность, квт	4,53	34	0,03	1,03	1,63	0,2·10⁻³	1,75	7,2
17) Габариты, мм:								
18) длина	1700	1720	1518	1010	1270	265	1135	1915
19) ширина	300	600	390	400	450	115	300	750
20) высота	270	375	350	300	300	135	350	450

KEY: 1) Basic characteristics; 2) FLIP; 3) ALIP; 4) IN; 5)
SNI; 6) liquid metal pumped; 7) temperature, °C; 8) output Q,
m³/hour; 9) pressure developed p · 10⁻⁵ Newtons/m²; 10) effi-
ciency η, %; 11) line voltage, V; 12) line current, A; 13)
frequency, cps; 14) cos φ; 15) weight, kg; 16) net output
power, kW; 17) overall dimensions, mm; 18) length; 19) width;
20) height.

Further R x D work on electromagnetic induction pumps [177] has as a goal the in-
crease of their output to 2000 m³/hour, increasing the temperature of the pumped metals
in annular pumps to 600°C and in flat pumps to 1100-1500°C, increasing the average flow
velocity of light metals (for short-duration work) to 25-30 m/sec. Some requirements
call for operation with power supply frequency of 400-500 cps.

CHAPTER 5

MAGNETOHYDRODYNAMIC SHIP PROPULSION

The increase in sailing range and speeds of seagoing vessels which occurred during the past few years has necessitated the development of new propulsion systems primarily because of the reduction in the efficiency and poorer weight/power and size/power ratios of ship screw systems for higher speeds. Development of new types of engines is also made necessary by need for higher power.

One of the approaches to new-type propulsion system design is the use of magneto-hydrodynamic methods, based on the interaction of externally supplied currents or of currents induced in sea water with an applied magnetic field.

MHD propulsion systems usually employ the same principles as those governing the operation of conduction and induction pumps. MHD engines not directly analogous to electromagnetic pumps have also been designed.

The main advantages of MHD propulsion systems over ship's screws are; direct utilization of the ship's electric power for producing thrust, as well as reduced vibration and hydrodynamic noise levels. When using high-power nuclear generators and with MHD generators utilized for converting the reactor's thermal energy into electric power, in many cases one can also use MHD engines which exhibit much better weight and size ratios than bladed electric propulsion motors.

1. Induction-Type MHD Propulsion Systems

One of the first induction-type MHD propulsion systems suggested was designed for a submarine [241] and it is shown schematically in Fig. 100. In this arrangement field windings 3, placed between outer hull 1 and inner shell 2 of the submarine produce a magnetic field which travels from the bow to the stern of the ship.

According to Eq. (2.4) an emf will be induced in the sea water and currents will be generated, these directed along circles forming lobes parallel to the submarine's hull. The interaction of these currents with the traveling magnetic field results in induction of electromagnetic forces in sea water, the direction of these forces being the same as that of the magnetic field, with the result that the submarine is set into motion.

136

Since the submarine's length exceeds appreciably its width, in the mathematical statement the problem reduces to an infinite cylinder of radius a with a magnetic field traveling along its surface, with the normal component of this field on the cylinder's surface specified in the form

$$B_r = B_m e^{i(\omega_1 t - \alpha z)},$$ (5.1)

where B_m is the maximum magnetic induction, $\omega_1 = 2\alpha\tau f_1$ is the angular frequency

$$\alpha = \frac{\pi}{\tau};$$

τ is the pole pitch and f_1 is the frequency of the supply current. Here $2\tau f_1 = v_f$, where v_f is the linear velocity of the field.

Taking the curl of Eq. (2.3), and substituting Eqs. (2.4) and (2.6), we get

$$-\frac{1}{\mu\sigma} \, \text{curl curl } B - \text{curl } [v \times B] = -\frac{\partial B}{\partial t} .$$ (5.2)

Neglecting all the components of the fluid flow velocity and magnetic induction, with the exception of axial component v_z and radial component B_r, as well as assuming the flow to be inviscid, we get, using Eq. (2.5)

$$\text{curl } [v \times B] = 0,$$

after which Eq. (5.2) takes the form

$$-\frac{1}{\mu\sigma} \cdot \text{curl curl } B = -\frac{\partial B}{\partial t} .$$ (5.3)

Fig. 100. Schematic diagram of a free-field induction-type MHD propulsion system.

An examination shows that the ratio of the left-hand to the right-hand side of Eq. (5.3) is of the order of magnitude of $\mu \sigma \omega L^2$, where L is the submarine's length. For a submarine with $L \simeq 100$ m, with $\sigma \sim 1$ (ohm-m)$^{-1}$, $\omega \sim 10^{-1}$ sec^{-1} and $\mu \sim 10^{-6}$ henry/m, $\mu\sigma\omega L^2$ is of the order of 10^{-3}. This being so we may set

$$-\frac{1}{\mu\sigma} \cdot \text{curl curl } B = 0.$$ (5.4)

Using the assumptions made Eq. (5.4) reduces to the form [241]

$$\frac{\partial^2 B_r}{\partial r^2} + \frac{1}{r} \frac{\partial B_r}{\partial r} + \frac{\partial^2 B_r}{\partial z^2} - \frac{B_r}{r^2} .$$ (5.5)

We may set

$$B_r = F(r) e^{i(\omega_1 t - \alpha z)}.$$

Here function F(r) should satisfy the expression

$$\cdots \; \frac{1}{r} \cdots \; \left(\frac{1}{r^2} \cdots c \right) r \; \cdots \; 0, \tag{5.6}$$

whose boundary conditions are

$$F(\cdot) \quad \cdot \cdot_1 \tag{5.7}$$

$$F(\cdot) \quad 0. \tag{5.8}$$

Solving Eq. (5.6) with boundary conditions (5.7) and (5.8) we get [268]

$$F(r) \quad \cdots \cdot_n \; \frac{H_{(1)}(\cdots r)}{H_{(1)}(\cdots)}, \tag{5.9}$$

where $H_{(1)}$ are Hankel functions of the imaginary argument.

The real part of the radial component of the magnetic field in this case can be calculated from the expression

$$B_r \quad \cdots \; \frac{H_{(1)}(\cdots r)}{H_{(1)}(\cdots)} \cdots (\cdots \; \cdots \cdots_1 t). \tag{5.10}$$

Using Eq. (5.10) the electric field is given by

$$E_\varphi \quad \cdots \cdots \; \frac{H_{(1)}(\cdots r)}{H_{(1)}(\cdots)} \cos (\cdots - \cdots_1 t): \tag{5.11}$$

Here according to Ohm's law the longitudinal electromagnetic force is

$$f_z \quad \cdots j. B_r \; \cdots \; \sigma V_r B_r^2 \; \frac{H_{(1)}^2(\cdots r)}{H_{(1)}^2(\cdots)} \cos^2 (\cdots - \cdots_1 t). \tag{5.12}$$

The mean force exerted per unit submarine length is

$$\langle f_z \rangle \quad \cdots \; \frac{\cdots r B_m^2}{\cdots H_{(1)}^2(\cdots)} \int_{\cdots a}^{\sim} (\cdots r) \, H_{(1)}^2(\cdots r) \, d(\cdots r). \tag{5.13}$$

If $2a/L = 1/20$, then $\alpha a = 2a/L \simeq 0.15$. Under these conditions the integral in Eq. (5.13) has the value 0.58, whence

$$\langle f_z \rangle \quad \cdots \; \frac{\cdots \pi B_m^2 a^2}{\cdots H_{(1)}^2(\cdots)} \approx 0.14 \cdots \sigma_n B_m^2 a^2. \tag{5.14}$$

For a submarine of length L the thrust is

$$F_{th} \quad \cdots 0.14 \cdots \sigma_n B_m^2 a^2 L. \tag{5.15}$$

and the drag is

$$F_D = c_s \frac{\rho v_s^2}{2} A_{sub} \tag{5.16}$$

where $c_s \approx 0.05$ is the drag coefficient, v_{sub} is the submarine speed and A_s is the maximum cross sectional area.

For $L = 200$ m, $a = 5$ m, $A_s = 75$ m^2, $\sigma = 4$ ohm^{-1}m^{-1} and $\rho = 10^3$ kg-m^{-3}, equating Eqs. (5.15) and (5.16) we get

$$\frac{v_f B_m^2}{v_{sub}^2} = 2.1 \cdot 10^{-2}.$$

Since the power dissipated per unit volume due to Joule losses P_J is of the order of $\sigma B_m^2 v_f^2$, while the useful power is $P_2 \approx < f > v_{sub} \sim \sigma v_f v_{sub} B_m^2$, the efficiency of this engine is approximately

$$\eta \approx \frac{P_2}{P_2 + P_J} \approx \frac{v_{sub}}{v_f}. \tag{5.17}$$

Figure 101 shows the calculated η of this engine vs the magnetic induction, constructed for different v_{sub} = const.
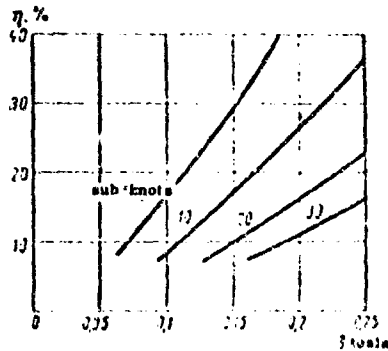
Fig. 101. Free-field propulsion efficiency as a function of magnetic induction.

It is seen from these curves that efficient use of this propulsion system with practically feasible magnetic fields is limited by very low submarine speeds. In addition, approximate calculations show that with the present state of art the coil dimensions will be excessively large.

139

Figure 102a shows a schematic of a duct-type induction engine, whose design is ilar to that of an annular linear induction type.
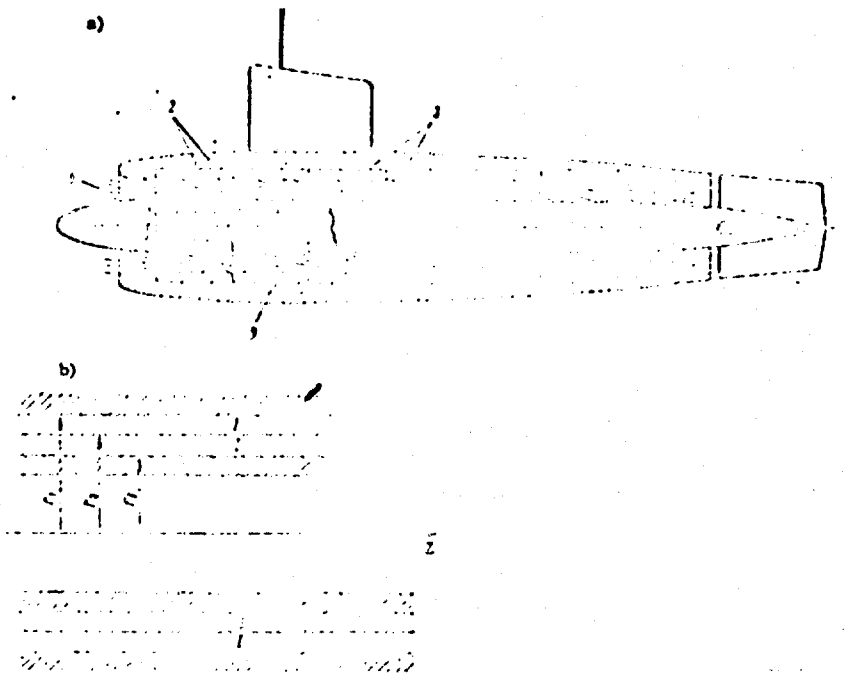
Fig. 102. Schematic diagram (a) and idealized scheme (b) of a duct-propulsion system.

In the case at hand the outer hull and inner shell 2 of the submarine serve as the tem's magnetic circuits, with annular duct 1 situated between them. Winding 3, ducing a magnetic field traveling from the bow to the stern is placed in slots of hull and shell. Living quarters 4 are situated in the inner shell. The duct system's antage over the free field system is the possibility of obtaining higher magnetic in-tion and efficiency in the former.

Due to the fact that this kind of propulsion system has a design identical to that of ular electromagnetic pumps, we can use the theory for ALIP [167]. In particular, magnetic field of currents in an inviscid conducting fluid should be described by a lar magnetic potential φ, satisfying the Laplace equation

$$\frac{1}{r}\frac{\partial}{\partial r}\left(r\frac{\partial \varphi}{\partial r}\right) + \frac{\partial^2 \varphi}{\partial z^2} = 0. \tag{5.18}$$

e φ should be expressed by

$$\varphi = F_m e^{i(\omega t - \alpha z)}. \tag{5.19}$$

Function F_m must satisfy the ordinary differential equation

$$\frac{d^2 F_m}{dr^2} + \frac{1}{r}\frac{dF_m}{dr} - \alpha^2 F_m = 0. \tag{5.20}$$

The solution of this equation for regions I and II (Fig. 102b) is written as

$$F_{m1} = A_1 I_0(\alpha r) + B_1 K_0(\alpha r); \\ F_{m2} = A_2 I_0(\alpha r) + B_2 K_0(\alpha r), \tag{5.21}$$

where I_0 and K_0 are modified zero-order Bessel functions of the first and second kind, respectively.

The boundary conditions may be written as

$$F_{m1}\big|_{r_1} = 0; \quad F_{m2}\big|_{r_2} = 0; \tag{5.22}$$

$$\frac{dF_{m1}}{dr}\bigg|_{r=r_0} = \frac{dF_{m2}}{dr}\bigg|_{r=r_0}. \tag{5.23}$$

Setting

$$j = j_m e^{i(\omega t - \alpha z)},$$

where j_m is the complex amplitude of the surface current density per unit length, we can write still another condition:

$$j_{m1} = i\alpha \left[F_{m2}\right]_{r=r_0} - i\alpha \left[F_{m1}\right]_{r=r_0}. \tag{5.24}$$

Conditions (5.22)–(5.24) yield the constants of integration

$$A_1 = -ir_0 j_m \frac{b}{c} K_0(\alpha r_1), \quad A_2 = -ir_0 j_m \frac{a}{c} K_0(\alpha r_2); \\ B_1 = ir_0 j_m \frac{b}{c} I_0(\alpha r_1), \quad B_2 = ir_0 j_m \frac{a}{c} I_0(\alpha r_2), \tag{5.25}$$

where

$$a = I_0(\alpha r_1) K_1(\alpha r_0) + K_0(\alpha r_1) I_1(\alpha r_0), \\ b = I_0(\alpha r_2) K_1(\alpha r_0) + K_0(\alpha r_2) I_1(\alpha r_0), \\ c = I_0(\alpha r_1) K_0(\alpha r_2) - K_0(\alpha r_1) I_0(\alpha r_2).$$

Here I_1 and K_1 are modified first-order Bessel functions of the first and second kind.

The electric field strength can be obtained from Eq. (3.4). Assuming

$$E_0 = E_{0m} e^{i(\omega t - \alpha z)},$$

and substituting Eq. (5.24), we find for $r = r_0$ that

$$E_{0m} = -i\mu_0 \omega r_0 D j_m. \tag{5.26}$$

141

where

$$D \quad \frac{\cdot}{c}; \quad j_{\omega} \quad \cdots(\dot{\omega}\cdots+\dot{\lambda}_{\cdots}); $$
$$\delta \quad r_1 \cdot r_2;$$

$E_{\Delta m}$ is the amplitude of the electric field strength, induced in the fluid by the coil's field.

The final expression for j_m has the form

$$j_{\omega} \quad \frac{\cdot \quad \Delta E_{\Delta \cdot}}{\frac{1}{\sigma} \cdots \vdots i_{\mu\omega\omega\delta r_0 D}} \cdot \tag{5.27}$$

The useful engine force is produced by interaction between the coil's magnetic field and the active component J_{ma} of current j_m:

$$\dot{\iota}_{\cdots a} \quad c\delta E_{\Delta \cdot} \cos^2 \dot{\varphi}, \tag{5.28}$$

where

$$\cos \dot{\varphi} \quad \frac{1}{\sqrt[4]{1+(\mu_{0}\omega\delta r_0 D)^2}} \cdot$$

Since $\delta \ll r_1, r_2$, then we may consider the equations of a flat channel instead of an annular one, which appreciably simplifies the relationships. In this case for a submarine with diameter 2a and length L the thrust is

$$F_{\mathrm{th}} \quad \pi \sigma_t \omega B_{\Delta}^2 a \delta L. \tag{5.29}$$

Substituting L = 100 m, a = 5 m, δ = 0.5 m, σ = 4 ohm^{-1}m, ρ = 10^3 kg/m^3, A_s = 75 m^2 and c_s into Eqs. (5.29) and (5.16), we get

$$\frac{\sigma_t B_{\Delta}^2}{v_{\mathrm{sub}}^2} \quad 0.5. \tag{5.30}$$

The efficiency of this kind of propulsion system may, as before, be expressed approximately as

$$\eta \approx \frac{v_s}{\cdots + v_s} \cdot \tag{5.31}$$

Figure 103 shows curves of efficiency vs. magnetic induction for different v_{sub} = const.

With acceptable dimensions of the magnetic circuit, the efficiency of this system at speeds of approximately 10 knots does not exceed 8%. In conjunction with this suggestions have been made abroad to combine the above system with a propeller.

142
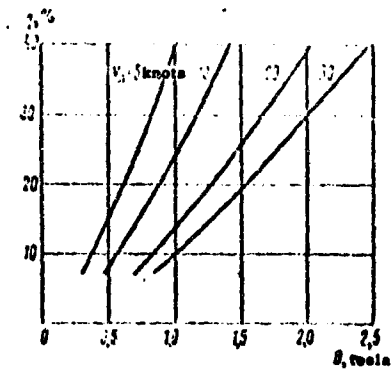
Fig. 103. Duct propulsion
efficiency.

2. Conduction-Type MHD Propulsion Systems

Free-field and duct propulsion system may also be designed for a constant mag-
netic field [242]. A schematic of such a free-field system is shown in Fig. 104. In
this case the surface of outer shell 1 is covered by lammellar magnet poles 2 and
electrodes 3 of alternating polarity. The sequence in which these are alternated in a
given direction determines the exponential decay of electromagnetic forces in the direc-
tion perpendicular to the shell of the propulsion system, with a characteristic decay
length, equal in order of magnitude to the pole alternation pitch [269]. When the force
is sufficiently strong, the longitudinal electromagnetic forces will determine the system's
thrust.
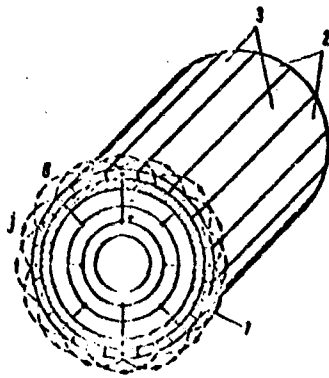
Fig. 104. Schematic dia-
gram of a free-field con-
duction-type MHD propul-
sion system.
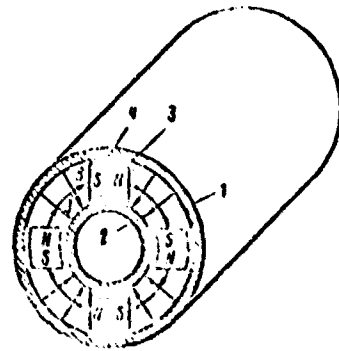
Fig. 105. Schematic dia-
gram of a duct conduction-
type MHD propulsion system.

A conduction-type duct propulsion system is shown schematically in Fig. 105. In
this case between outer hull 1 and inner shell 2 of the submarine are placed bar-shaped

143

permanent magnets 3 or electromagnets, which produce an azimuthal magnetic field in the annuli. The hull and shell, isolated by means of special liners 4, serve as electrodes to which is supplied a potential difference produced by passing current through sea water in the annuli. The interaction of externally supplied current and the applied magnetic field produces an electromagnetic force field which determines the system's thrust.

Due to low conductivity of sea water and to low magnetic induction which is produced by ordinary magnet systems, the efficiencies of these systems are low. However, it may be improved appreciably by using superconducting magnets which yield inductions of approximately 10 tesla.
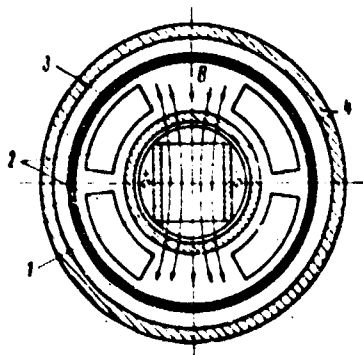
Fig. 106. Schematic view of an
MHD duct propulsion system with
superconducting magnets.

An MHD propulsion system with superconducting magnets was recently analyzed by R. A. Doragh [244] [the version considered being called MHD pump-jet]. It is depicted schematically in Fig. 106. Its principal elements are: 1 pump-jet channel 1 with electrodes to which a potential difference is supplied from a dc source contained in the submarine, superconducting field coils 2 held in inner Dewar 4 and producing magnetic induction of the order of 10 tesla in the channel; magnetic shield 4 for protecting the living quarters from magnetic field and for preventing the submarine's detection by the magnetic leakage flux. A diffuser section is provided at the inlet and a nozzle section at the outlet to provide for the necessary differences in cross section.

The system's operating principle is as follows: sea water at ambient pressure and at a velocity head is imparted a hydrostatic head by electromagnetic forces; this head is converted to an additional velocity head in the nozzle section. Thrust is provided by change in the momentum from inlet to outlet of the channel.

Table 18. MHD Submarine Propulsive Power

Скорость хода, узлы 1)	Эффективная мощность квт 2)	Упор. H 3)
5	63,8	$1,36 \cdot 10^4$
20	3 500	$1,82 \cdot 10^5$
30	3 800	$4,25 \cdot 10^5$
50	50 600	$1,06 \cdot 10^6$
100	374 000	$3,97 \cdot 10^6$

KEY: 1) Speed, knots; 2) effective power, kW; 3) thrust, H (in Newtons)

R. A. Doragh made calculations for a submarine with 2000 ton displacement and a length of 64.2 m. The length to diameter ratio was L/D = 7 and the prismatic coefficient was 0.6. His results are tabulated in Table 18. The calculations were made on the assumption that the system's thrust is equal to the submarine's drag.

The thrust was calculated from

$$T = \varrho Q \Delta v, \tag{5.32}$$

where Δv is the velocity change in jet.

The hydraulic efficiency was calculated from this thrust

$$\eta_k = \frac{T c_{sub}}{\gamma Q H_p}, \tag{5.33}$$

where γ is the fluid's density and H_p is the thrust developed in the channel [pumping head of pump section].

The electrical efficiency was calculated from this pumping head

$$\eta_{\boldsymbol{\omega}} = \frac{\gamma Q H_p}{U I}, \tag{5.34}$$

where U is the potential difference across the electrodes, while I is the current moving through them.

The overall efficiency was obtained by multiplying Eqs. (5.33) and (5.34)

$$\eta = \eta_\varepsilon \eta_b = \frac{T c_{sub}}{U I}. \tag{5.35}$$

The thrust of the pump-jet was approximately determined from Bernoulli's equation

$$H_p = \frac{c_{out}^2 - c_0^2}{2g} + \frac{p_{out} - p_0}{\gamma} + (z_{out} - z_0) + H_L. \tag{5.36}$$

145

where v_{out} and v_0 are the outlet and inlet sea water velocities, p_{out} and p_0 are the corresponding pressures; z_{out} and z_0 are the corresponding hydrostatic heads above datum, and H_L represents MHD losses in the channel and inlet and outlet losses.

All the terms of Eq. (5.36) were determined from a complete system of MHD equations, using an electronic computer. Values of electrode voltage, current density, hydraulic, electrical and overall efficiencies were obtained as a result.

Figure 107 gives the total efficiency of the MHD pump-jet as a function of submarine speed for various B_0 = const. The dashed lines in the figure are for η_e. The graphs were constructed from the following starting data: channel length 15.3 m, channel area 6.98 m^2, diffuser ratio 1.05, jet [nozzle] ratio 1.49.

It follows from the above data that the overall efficiency of an MHD pump-jet with superconducting magnets can be quite high.
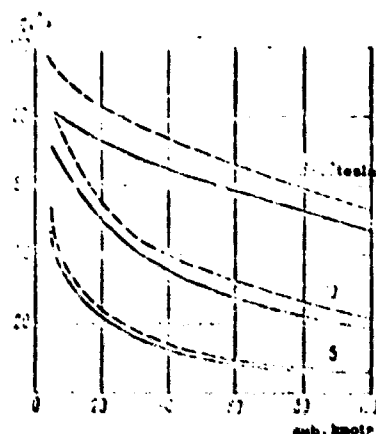
Fig. 107. Efficiency of MHD pump-jet with superconducting magnetic circuit.

A study was also made of the noise level of the MHD propulsion system, which showed that its noise level is 20 dB lower than that of a propeller.

At the same time it should be noted that realization of this system involves solving a number of scientific and technical problems, the major ones being

a) design of superconducting magnets capable of producing strong magnetic fields in large volumes;

b) developing a control system providing for effective protection of windings and for reliable control;

c) developing an effective system for removing gases produced at electrodes by electrolysis;

d) producing an optimal Dewar and cryogenic system for maintaining the necessary temperatures.

146

3. Peristaltic MHD Propulsion Systems

All the MHD propulsion systems examined above involve direct interaction of externally supplied currents or of currents induced in the sea water with an applied magnetic field. Efficient operation of these systems in the relatively low-conductivity sea water requires very large magnetic fields.

It is possible, in principle, to design an efficient propulsion system with ordinary magnets, using a special compressor which would act on sea water by means of an intermediate high-conductivity fluid [243]. The advantage of this system is the independence of its operation on the sea water conductivity.

A peristaltic MHD propulsion system is depicted schematically in Fig. 108. It consists of annulus 1 with a multiphase winding placed in its slots; annular sump 2 filled with high-conductivity fluid (liquid metal), and duct 3 filled with low-conductivity fluid (sea water). The high-and low-conductivity fluids are separated by an impermeable flexible membrane.

The field winding produces a magnetic field moving along the duct axis, and closed azimuthal currents are induced in the high-conductivity fluid, these interact with the traveling field thus generating axial and radial electromagnetic force components.

The axial velocity of the conducting fluid averaged across its annulus (per cycle), is zero, since it is constrained by end partitions. An axial pressure gradient is thus produced in the conducting fluid and it balances the axial force component, which is expressed by

$$\frac{\partial p}{\partial z} = \sigma v B_z^2.$$

This pressure gradient is transmitted to the pumped fluid via the mechanical coupling between the fluids. If the radial forces in the conducting fluid are sufficient to pinch and trap the pumped fluid, the ensuing motion of the latter will consist of trapped packets of fluid traveling at the speed of the flexible membrane against the pressure gradient induced in it by axial body forces induced in the conducting fluid, whence the name peristaltic is derived.
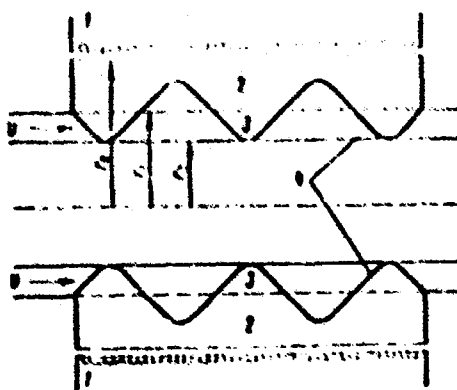
Fig. 108. Schematic diagram of a peristaltic MHD propulsion system.

The theoretical analysis of the operation of this type of propulsion system is quite complex [243]. Hence we restrict ourselves to consideration of only approximate relationships which describe its operation.

For a propulsion-system length $\mathcal{L}$, cross sectional area of water annulus A and conducting-fluid annulus thickness h, the total axial force produced by the system can be written as

$$F = \left(\frac{l}{r_0}\right)\frac{A}{\left(\frac{h}{r_0}\right)\left(1 - \frac{h}{r_0}\right)} \cdot G_1(\beta, \alpha h) \cdot \frac{B_0^2}{2\mu_0}, \tag{5.37}$$

where α is the wave number; αh is a dimensionless parameter; $\beta = R_{m\lambda}s$ is the product of magnetic Reynolds number and the slip: $s = (v_f - v)/v_f$: v_f is the traveling-wave velocity; v is the maximum velocity of the conducting fluid, and $R_{m\lambda} = \mu_0 \sigma \omega/\alpha^2$ is the fluid magnetic Reynolds number, based on wave speed and wavelength.
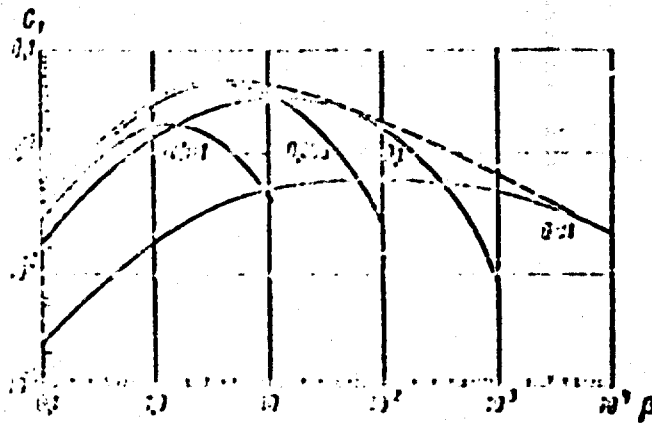
Fig. 109. Dimensionless function [axial body force] G_1 vs. β.

A plot of dimensionless function G_1 as a function of β for certain values of dimensionless parameter αh is given in Fig. 109. The dashed line gives the envelope of the given family of curves. Function G_1 has a maximum (0.0553) for $\beta_{opt} = 4.12$ and $(\alpha h)_{opt} = 0.309$.

The total power supplied to the conducting fluid is equal to the pumping power and the Joule heat losses.

Efficiency η_e of an electromechanical converter, which is the ratio of the pumping power to the total power, is approximately expressed in the form

$$\eta_e = \frac{1}{1 + \frac{s}{\gamma}}, \tag{5.38}$$

148

where

$$\gamma = \left[2 + 2(\beta^2 + 1)^{1/2}\right]^{\frac{1}{2}} a h.$$

If we denote the mass rate of flow through the system by $\dot{m}$, the exit velocity by v_1, and assume the exit pressure equal to the free-stream static pressure p_∞, then the propulsive force will be determined by the change in momentum

$$T = \dot{m}(v_1 - v_{sub}) \qquad (5.39)$$

where v_{sub} is the submarine speed.

Examining the ratio of the work performed during unit time Tv_{sub} to the sum of the performed work and the kinetic energy in cocurrent flow, i.e., $Tv_{sub} + 1/2\ m$ $(v_1 - v_{sub})$, and using Eq. (5.39) we get that the overall efficiency is

$$\eta = \frac{2}{1 + \dfrac{v_1}{v_{sub}}}. \qquad (5.40)$$

In order to impart constant translational velocity to the submarine, the propulsive thrust should be equal to the vessel's drag

$$F_D = c_x A_s \frac{\rho v_{sub}^2}{2}. \qquad (5.41)$$

If p_0 is the minimum permissible pump-inlet pressure, then the maximum permissible fluid velocity may be obtained from Bernoulli's equation, written for flow at infinity and in the pump

$$p_\infty + \frac{1}{2}\rho v_{sub}^2 = p + \frac{1}{2}\rho v^2. \qquad (5.42)$$

The free-stream static pressure may be written as

$$p_\infty = \rho g (d + d_a). \qquad (5.43)$$

where d is the water depth, while d_a is the depth of equivalent water corresponding to atmospheric pressure.

We have from Eqs. (5.42) and (5.43) that

$$v = v_{sub}\left[1 + \frac{2g(d + d_a)}{v_{sub}^2} - \frac{2p}{\rho v_{sub}^2}\right]^{\frac{1}{2}}. \qquad (5.44)$$

Equations (5.37), (5.39), (5.41) and (5.44) can be used for obtaining a number of approximate relationships describing the operation of a peristaltic propulsion system.

In particular, if ρ, v_{sub}, η, $c_s A_s$, r_0, ℓ, p_0, d and h are specified, we may obtain the following expressions:

a) for the traveling-wave frequency

$$v \simeq \frac{v_{sub}}{\ldots} \left(\frac{\ldots}{c_s A_s}\right)\left(1 - \ldots\right)\left(1 + \frac{\ldots(d+\ell)}{v_{sub}^2} - \frac{\ldots}{v_{sub}}\right); \tag{5.45}$$

b) for the magnetic-induction amplitude at the coil surface

$$B_0 = \left[\left(\frac{p_0}{a}\right)\left(\frac{\eta}{\ldots}\right)\left(\frac{c_s A_s}{\ldots}\right) \ldots \left(1 - \ldots(d+\ell)^2 - \frac{\frac{1}{2}\,c_{sub}^2}{v_{sub}^2} - \frac{\ldots}{v_{sub}}\right) \ldots \right]^{\frac{1}{2}}; \tag{5.46}$$

c) for the liquid-metal conductivity

$$\sigma = \frac{\ldots}{\ldots v_{sub}}\left(\frac{\ldots}{c_s A_s}\right)\left(1 - \ldots\right)\beta(\ldots); \tag{5.47}$$

d) for the water annulus thickness

$$h_1 = \eta h = \frac{r_0}{3}\left(\frac{c_s A_s}{\ldots}\right)\left(\frac{\ldots}{1-\eta}\right)\left[1 - \frac{2\,c\,(\ell+d_0)}{v_{sub}^2} - \frac{2\,r_0}{c^2 v_{sub}}\right]^{-\frac{1}{3}}. \tag{5.48}$$

Reference [243] presents results for a submarine and torpedo. It is assumed that the submarine length is L = 114.6 m, L/D = 10 and v = 30 knots. Here the length of the propulsion system was taken as 0.5L; the torpedo length was 5.33 m. In both cases the minimum inlet pressure p was taken as zero and it was assumed that the thickness of liquid-metal and sea water layers is the same.

The field's linear velocity as a function of submarine or torpedo speed are given for three submergence depths in Fig. 110. It is seen from these data that the maximum permissible wave velocity in the system (from the point of view of cavitation prevention) somewhat exceeds the free-stream pressure, but is of the same order of magnitude. As the submergence depth is decreased, the wave velocity approaches the vessel speed.

Figure 111 shows the required liquid-metal conductivity for $B_{0\,min}$ as a function of β. A curve of η_e as a function of dimensionless parameter γ [complex separation constant] is shown in Fig. 112.

It has been determined that the optimum value of γ is approximately 1. Then $\eta_e = 0.368$. It is possible to increase η_e for $0 < \gamma < 1$.
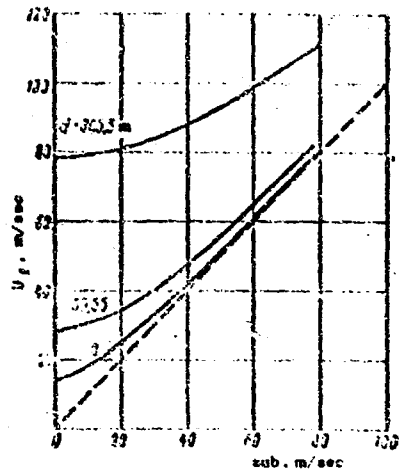
Fig. 110. Traveling wave veloc-
ity vs. submarine speed for dif-
ference submergence depths.
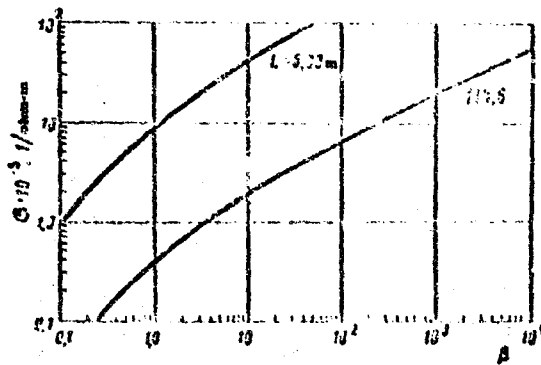
Fig. 111. The required liquid-metal conduc -
tivity as a function of β.

The optimum frequency of alternating magnetic field for the torpedo is 50 cps,
while for submarines it should be lower. Here the magnetic induction needed for pro-
pelling a submerged body at 30 knots should be approximately 0.1-1 tesla, irrespective
of the body's dimensions.

The above-described propulsion systems and their basic characteristics describe
primarily the theoretical possibilities of using MHD effects for propulsion of sea-going
vessels.

151
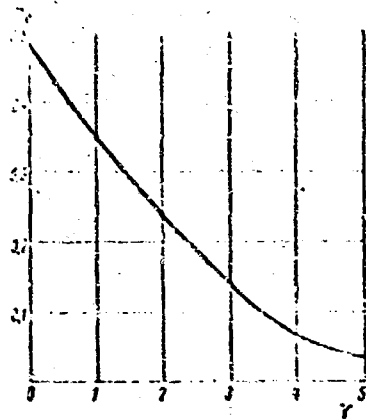
Fig. 112. Curve of $\eta_{\ominus} = \varphi(\gamma)$.

The need to solve many scientific and engineering problems for practical realization of these systems makes their development problematic. At the same time the information presented shows that extensive research is done in many countries in this direction. From this point of view the data presented here should be of some scientific and engineering interest.

CHAPTER 6

MAGNETOHYDRODYNAMIC POWER UNITS
FOR MOVING CRAFT USE

For several years now, development work has been done in the USSR and abroad not only on improvement of the already-developed MHD generators, but also on designs for the immediate future, among which we can cite water-moderated, water-cooled or gas-cooled nuclear propulsion systems for freight and passenger ships, as well as the use of direct conversion of energy of various fuels into electrical power for use on moving craft, primarily space craft and deep submersibles.

A large amount of complex scientific research and pilot-design work is done in these directions to solve the principal engineering and physical problems which would provide for efficient utilization of the above power converters, as well as for determining potentialities of improving the efficiencies and increasing the capacities of these new units.

Reliable and efficient operation of MHD facilities using an electrically conducting gas is possible only at high gas temperatures, which is limited by the available heat resistant materials. In plasma MHD generators, two kinds of energy conversions (conversion of thermal into kinetic energy and then of kinetic into electric power) are obtained using a single working fluid. However, each of these conversions may be attained by using a separate working fluid or by utilizing different aggregate states of the same fluid: gas (vapor) for converting the thermal into kinetic energy, and an electrically conducting liquid for converting the kinetic (or pressure) into electrical energy.

Liquid metals as working fluids are promising because their electrical conductivity is at least four orders of magnitude higher than that of ionized gas. However, the velocity of the working fluid in such an MHD generator can be by one-two orders of magnitude lower than when plasma is used. Since the energy density of an MHD generator is proportional to the product σU_0^2 (σ is the electrical conductivity and U_0 is the fluid velocity), then a liquid metal generator can provide the same power density as a plasma generator, or even a much higher one. This also solves the problem of materials.

To realize a power-generating MHD unit employing a liquid metal, one must impart to the metal a given kinetic energy during momentum transfer from the expanding vapor of this or some other metal; then one must remove, either completely or partially, the vapor from the mixture thus formed before the entry of this mixture into the MHD generator.

The vapor may be separated from the liquid by condensing it during transfer of heat to supercooled fluid injected into the chamber, or by mechanical separation. Depending on the method used, the MHD generator may operate on two principles: with condensation (Fig. 113) and with separation (Fig. 114). The working fluid in the first arrangement may be a single fluid which exists in different states at different points of the loop. In the second arrangement the working fluid may be either a single liquid, or two immiscible liquids.
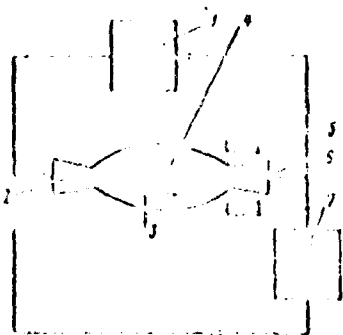
Fig. 113. Liquid-metal condensing MHD cycle.

1) Heat source; 2) nozzle; 3) liquid injection; 4) accelerating-condensing device [drift tube]; 5) MHD generator; 6) diffuser; 7) heat removal (radiator).

In these arrangements the MHD generator may be placed in any point of the liquid loop and operate with a vapor fraction or without it, using the pressure of the working fluid in the form of a velocity head or in the form of an ordinary pressure drop. As can be seen from Figs. 113 and 114, in both arrangements the metal flows continuously in a closed two-loop system.

In the condensing arrangement the heat source, i.e., the (nuclear) reactor, is placed in the vapor loop. The liquid metal is heated and partially vaporized in the reactor and then supplied to a two-phase nozzle, where it is expanded with attendant conversion of a part of the thermal into kinetic energy. Liquid metal, precooled in a radiator, is injected from the liquid loop into the expanding vapor. The injected metal is accelerated in the process of momentum transfer and the heat transfer attendant to mixing simultaneously condenses the vapor phase of the working fluid. As a result, the stream entering the MHD generator is predominantly in the liquid phase and has sufficient velocity and electrical conductivity. The liquid then decelerates through the production of electric power in the MHD generator and is fed to a diffuser where it is further decelerated and its pressure reconstituted. Part of the liquid is then vaporized in the heat resource and returned to the two-phase nozzle, while the other part is cooled in the radiator and returned to the injecting condenser. The loop may include a regenerator for preheating that part of the liquid which goes to the heat source.

In the separator cycle the heat source, i.e., the reactor, is placed in the liquid loop. The liquid is heated in the reactor and supplied to a mixer where the recycled condensate evaporates with attendant cooling. Then the liquid is accelerated in a two-phase nozzle while exchanging momentum with the expanding vapor, is separated from it in the separator, is decelerated in the MHD while performing useful work, and is then returned to the reactor through a diffuser.

The liquid circulating in the vapor loop flows from the separator into a cooler. From there it is recycled as a condensate (by an electromagnetic pump) to the mixer, where it is vaporized by heat supplied from the reactor. The vapor, together with the liquid, is expanded in the two-phase nozzle, and is then separated from the liquid phase in the separator.

154
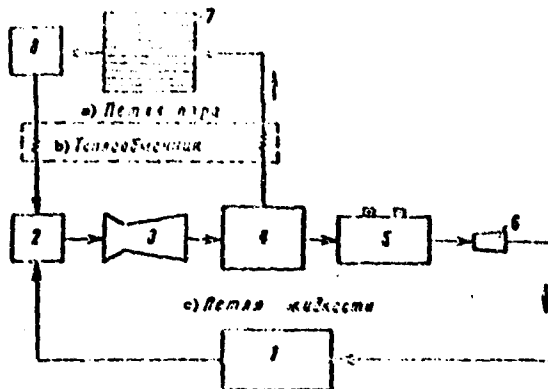
Fig. 114. Schematic diagram of a liquid-metal
MHD generator with separation.

1) Heat source; 2) mixer; 3) nozzle; 4) separator;
5) MHD generator; 6) diffuser; 7) radiator; 8)
pump.

KEY: a) Vapor loop; b) heat exchanger; c) liquid
loop.

To improve the cycle efficiency, the vapor leaving the separator may be passed
through a regenerator, where it cools by preheating the condensate leaving the radiator.

Below we consider problems of thermodynamic efficiency of an MHD generator
using the above cycles, the parts of the system as well as results of experimental and
design studies.

1. Liquid-Metal MHD Generators

It was noted previously that electromagnetic pumps for liquid metals are revers-
ible devices, i.e., they can operate in the generator mode. For this it suffices to set
the liquid metal in a magnetohydrodynamic channel into motion by means of an external
pressure drop and to short the electrodes (in the conduction type) through a load.

At present, development work is done on conduction as well as induction-type
liquid-metal MHD generators. The theory of DC conduction type generators is the most
developed at this time. These generators do not differ in design from DC conduction-
type electromagnetic pumps.

Conduction-type liquid-metal MHD generators, just as homopolar generators, are
high-current, low-voltage devices. When using ordinary magnet systems, efficient duct
design and liquid-metal velocities of several meters per second, the output voltage of
such generators does not exceed 10 V. Obtaining a higher output voltage requires in-
creasing appreciably the liquid metal velocity in the duct or using superconductive mag-
netic systems which yield high magnetic flux densities.

155

Extensive theoretical and experimental studies of conduction-type liquid-metal MHD generator with a divergent nozzle duct were performed recently by D. Elliot [222].

Theoretically a generator with a constant-cross section duct is a special case of an MHD generator with a diffuser. The theory of such an MHD generator is derived by Elliot on the assumption that the divergence angle of a constant-height diffuser is small, which makes it possible to neglect all the velocity components of the liquid metal, with the exception of the axial component. A schematic of the diffuser of such an MHD generator is shown in Fig. 115.
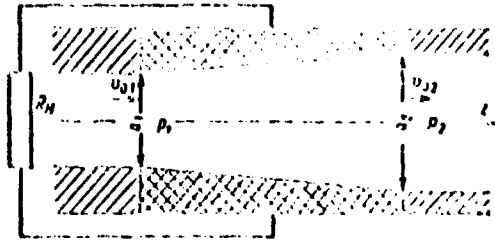
Fig. 115. Schematic of diffuser of a liquid-metal MHD generator.

To obtain the principal electrical relationships of such an MHD generator, we isolate in the moving liquid metal a fluid element with width a and cross section dxdx.

The resistance of this volume element and the emf induced at its ends are

$$r_i \quad \frac{a}{\sigma x \, dx} \quad \quad (6.1)$$

$$\varepsilon_i \quad \lambda_0 \int_0^a v_i \, dy. \quad \quad (6.2)$$

We shall assume that the diffuser is flat ($a \gg b$). In this case the electric fields strength in the liquid metal may be taken as constant (curl $E = 0$). Then, in accordance with Ohm's law (2.6) and Eqs. (6.1) and (6.2), the current passing through our fluid element is given by

$$J_i \quad \frac{\sigma}{a}(\varepsilon_i \quad \delta_0) \, dx \, dx, \quad \quad (6.3)$$

where $\lambda_0 \quad r_1 \quad r_2$.

Joule losses in our fluid element are

$$P_{j,i} \quad J_i^2 r_i \quad \frac{\sigma}{a}(r_i \quad \lambda_0)^2 \, dx \, dx. \quad \quad (6.4)$$

The current and the Joule losses in a liquid element with dimensions b x a x dz are given by

156

$$J(z) = \frac{\sigma}{a}\left[B_0\int_0^b\int_0^a v_z\,dx\,dy - \cdots\int_0^b\cdots dx\right]dz; \tag{6.5}$$

$$P_J(z) = \frac{\sigma}{a}\left[B_0^2\int_0^b\left(\int_0^a v_z\,dy\right)^2 dx - 2\Delta\varphi B_0\int_0^b\int_0^a v_z\,dx\,dy + \right.$$
$$\left. + (\Delta\varphi)^2\int_0^b dx\right]dz. \tag{6.6}$$

Since the liquid is incompressible (div v = 0), then its flow rate in each of the diffuser's cross sections will be constant

$$Q = v_1 a_1 b = v_{01} a_1 b = v_2 a_2 b = \int_0^b\int_0^a v_z\,dx\,dy = \text{const}, \tag{6.7}$$

where v_0 is the average metal velocity, while subscripts 1 and 2 refer to the inlet and outlet diffuser cross sections.

Upon substitution of Eq. (6.7), the expression for the current per unit length of the generator can be written as

$$J(z) = \sigma B_0 v_{01} a_1 b (1-k)\frac{dz}{a}. \tag{6.8}$$

where $k = \frac{\varphi_1 - \varphi_2}{v_{01}a_1 B_0}$ is the load factor.

When using ordinary magnet systems and high liquid metal velocities, parameter M^2/R is small. In this case we can neglect MHD effects of the first kind and specify the liquid metal velocity distribution in the form [252, 253]

$$\frac{v}{v_m} = \left(\frac{2x}{b}\right)^{\frac{1}{7}}. \tag{6.9}$$

Since the diffuser is flat, we can set $\int_0^a v_z\,dy = v_z a$. Making use of this, and also of the symmetry of the velocity distribution, we get the following as an estimate of the first term in the right-hand side of Eq. (6.6)

$$\int_0^b\left(\int_0^a v_z\,dy\right)^2 dx = 2\int_0^{\frac{b}{2}}\left(\int_0^a v_z\,dy\right)^2 dx = \frac{7}{9}v_m^2 a^2 b. \tag{6.10}$$

Similarly, it follows from Eq. (6.7) that

$$v_0 = \frac{7}{8}V_m. \tag{6.11}$$

157

Substituting Eqs. (6.7), (6.10) and (6.11) into Eq. (6.6), we find

$$\cdot j^{(1)}(z) \quad \cdots \quad \sigma^2 u_m^2 \left[1 \div \cdots + \frac{1}{M}\right] \frac{dz}{d} \qquad (6.12)$$

When using superconducting magnet systems and moderate liquid metal velocities, it may be assumed that the flow is laminar. It is easy to show that in this case, at large Hartmann numbers, the velocity distribution can be specified in the form

$$\frac{v}{v_0} \cdots 1 \quad e^{-\frac{Mz}{b}} . \qquad (6.13)$$

Since in this case the boundary-layer thickness is of the order of b/M, its thickness may be neglected as compared with the duct's height. Then, upon substitution of Eq. (6.13) we get

$$2 \int_0^b \left(\int_0^d v_z\, dy\right) dz \quad \cdots \quad \sigma^2 u_m^2 \left[\frac{b}{2} - \frac{25}{M}(1 \div e^{-0.5M}) + \frac{b}{2M}(1 - e^{-M})\right]. \qquad (6.14)$$

When using superconducting magnets the Hartmann numbers are of the order of 10^3–10^4, by virtue of which Eq. (6.14) takes the form

$$2 \int_0^b \left(\int_0^d \cdots \right)^2 dz \quad \cdots \quad \cdots b. \qquad (6.15)$$

And, similarly, we get from Eq. (6.7)

$$\cdots_0 \approx v_m. \qquad (6.16)$$

In this case the Joule losses per unit generator length are given by

$$P_J^{(1)}(z) \quad \sigma u_0^2 \sigma_1^2 u_1^2 b (1 - k)^2 \frac{dz}{d} . \qquad (6.17)$$

It is easily seen by comparing Eqs. (6.12) and (6.17) that the flattening of the velocity distribution brought about by the MHD effect of the first kind reduces the Joule losses.

Energy losses in the liquid metal element due to viscous dissipation can be represented as

$$P_\lambda(\cdot) \quad \cdots_2^A |(\cdots \div \cdots) d\cdots| \quad \cdots_2 \cdots \left(\cdots\right) dz. \qquad (6.18)$$

158

The surface friction factor λ at high liquid metal velocities and when using ordinary magnets can be obtained from Prandtl's universal friction law [252]. When using superconducting magnets and moderate liquid metal velocities, this factor should be derived from magnetohydrodynamic formulas.

Integrating Eqs. (6.8), (6.12), (6.17) and (6.18) from $z = 0$ to $z = L$, we get the following relationships for the total current and total power losses in the generator duct:

$$I = \frac{\sigma B_y v_{01} a_1 b l (1-k)}{a_{av}};$$ (6.19)

$$P_J^{(1)} = \frac{\sigma B_y^2 v_{01}^2 a_1^2 b l (1-k)^2}{a_{av}}\left[1 + \frac{1}{63(1-k)^2}\right];$$ (6.20)

$$P_J^{(2)} = \frac{\sigma B_y^2 v_{01}^2 a_1^2 b l (1-k)^2}{c_{av}};$$ (6.21)

$$P_\lambda = \frac{\rho \lambda a_1^3 v_{01}^3 l}{2 a_1} N.$$ (6.22)

where

$$a_{av} = a_1 \frac{\left(\dfrac{a_2}{a_1}\right)-1}{\ln\left(\dfrac{a_2}{a_1}\right)}; \quad N = 1 + \frac{3}{2}\left(\frac{1}{a_1} + \frac{1}{a_2}\right).$$

The output power of the generator is calculated from

$$P_{z0} = \Delta\varphi I = \frac{\sigma B_y^2 v_{01}^2 a_1^2 b l k (1-k)}{a_{av}}.$$ (6.23)

The total losses of liquid metal energy in an MHD generator duct are given by

$$P_{10} = P_{z0} + P_J + P_\lambda.$$

Here, for the two cases being discussed, power P_{10} can be expressed in the form

$$P_{10}^{(1)} = \frac{\sigma B_y^2 v_{01}^2 a_1^2 N (1-k)}{a_{av}}\left[k + \frac{1}{1-k}\left(\frac{1}{63} + (1-k)^2 + \frac{\rho\lambda a_{av}}{2\sigma B_y^2 a_1 b}N\right)\right];$$ (6.24)

$$P_{10}^{(2)} = \frac{\sigma B_y^2 v_{01}^2 a_1^2 l (1-k)}{a_{av}}\left[k + \frac{1}{(1-k)}\left((1-k)^2 + \frac{\rho\lambda a_{av}}{2\sigma B_y^2 a_1 b}N\right)\right].$$ (6.25)

The total losses are due to changes in the kinetic energy of the liquid (due to reduction of its velocity in the diffuser) and of the potential energy (due to the pressure reduction $\Delta p = p_1 - p_2$).

159

The kinetic energy in any duct cross section is

$$P_d = \int_0^b \int_0^a \frac{v^3}{2} \, dx \, dy. \tag{6.26}$$

Equation (6.26) for velocity distributions (6.9) and (6.13) becomes, respectively

$$P_d^{(1)} = 1.015 \frac{\dot{m} v_0^2}{2} ; \tag{6.27}$$

$$P_d^{(2)} = \frac{\dot{m} v_0^2}{2} , \tag{6.28}$$

where $\dot{m} = v_0 \rho \, ab$ is the mass rate of the liquid.

Using Eqs. (6.27) and (6.28), the power of the liquid entering the diffuser is given by

$$P_{13}^{(1)} = 0.522 \rho v_0^3 a_1 b \left[1 - \left(\frac{a_1}{a_2} \right)^2 \right] = v_{01} a_1 b \, \Delta p ; \tag{6.29}$$

$$P_{13}^{(2)} = 0.5 \rho v_0^3 a_1 b \left[1 - \left(\frac{a_1}{a_2} \right)^2 \right] = v_{01} a_1 b \, \Delta p . \tag{6.30}$$

From Eqs. (6.24), (6.25) and (6.29), (6.30) we get expressions for the required magnetic field flux density

$$B_0^{(1)} = \left\{ \frac{v_{01} \sigma_{av}}{\sigma I (1.015 - k)} \left[0.522 \frac{b}{a_1} \left(1 - \frac{a_1^2}{a_2^2} \right) + \frac{\Delta p}{\sigma_{av} a_1} - \frac{v}{2 a_1} N \right] \right\}^{1/2} ; \tag{6.31}$$

$$B_0^{(2)} = \left\{ \frac{v_{01} \sigma_{av}}{\sigma I (1 - k)} \left[0.5 \frac{b}{a_1} \left(1 - \frac{a_1^2}{a_2^2} \right) + \frac{b \Delta p}{\sigma_{av} a_1} - \frac{v}{2 a_1} N \right] \right\}^{1/2} . \tag{6.32}$$

Due to the fact that the electrodes and magnet poles are of finite length, as is the case in electromagnetic pumps, edge effects exist in MHD generators. Depending on the magnetic field distribution in the edge zones, these effects may increase or reduce the output power of the generator by the amount

$$\Delta P_2 = \frac{\sigma B_0^2 v_0^2}{2} \, v_0 b \, [1(\beta_1 + \beta_2) - (\sigma_1 + \sigma_2)] L \tag{6.33}$$

Here the required input power changes by the amount

$$\Delta P_1 = \frac{\sigma B_0^2 v_0^2 b}{2} \left[\frac{1(\beta_1 + \beta_2)}{2 k} - (\sigma_1 + \sigma_2) \right] . \tag{6.34}$$

173

Factors α_1 and α_2 are given by a gamma function and depend on the extension of magnetic field z_1 and z_2 past the electrode edges:

$$\alpha_1 = \frac{\pi z_1}{a_1}\left[1 - \frac{1}{\sqrt{\pi}} \cdot \frac{\Gamma\left(\frac{1}{2} + \frac{a_1}{2\pi z_1}\right)}{\Gamma\left(1 + \frac{a_1}{2\pi z_1}\right)}\right]; \tag{6.35}$$

$$\alpha_1 = \frac{\pi z_1}{a_1}\left[1 - \frac{1}{\sqrt{\pi}} \cdot \frac{\Gamma\left(\frac{1}{2} + \frac{a_2}{2\pi z_2}\right)}{\Gamma\left(1 + \frac{a_2}{2\pi z_2}\right)}\right]. \tag{6.36}$$

Factors β_1 and β_2 are functions of the attenuation factor γ of the magnetic field, which is defined as

$$\gamma_1 = \frac{2\pi z_1}{a_1}; \tag{6.37}$$

$$\gamma_2 = \frac{2\pi z_2}{a_2}. \tag{6.38}$$

For γ ranging from $0 \leq \gamma \leq 8$, β can be approximately expressed as a function of γ

$$\beta \approx 0.36 \operatorname{th}(0.28\gamma). \tag{6.39}$$

Using Eq. (6.33), the output power of a generator will be given by

$$P_1 = P_{20} - \Delta P_2 = \frac{\sigma \bar{v}_{av}^2 B_{av}^2 h l k (1-k)}{\sigma_{av}} \times$$
$$\times \left[1 - \frac{2h\sigma_{av}\ln 2}{\sigma l(1-k)} + \frac{c_{av}(\alpha_1 + \alpha_2)}{\sigma l(1-k)}\right]. \tag{6.40}$$

The total input power, according to Eqs. (6.34), (6.31) and (6.?) is given by

$$P_1 = P_{10} + \Delta P_1;$$

$$P_1^{(1)} = \frac{\sigma \bar{v}_{av}^2 B_{av}^2 h l (1-k)}{\sigma_{av}}\left\{k + \frac{1}{1-k}\left[\frac{1}{\sigma l} + \frac{\sigma_{av}}{l}\left(\beta_1 + \beta_2 - k(\alpha_1 + \alpha_2)\right) + \right.\right.$$

$$\left.\left. + (1-k)^2 + \frac{0.5h(1.013 - k)\sqrt{}}{0.33 l}\cdot\left(\frac{1}{a_1} + \frac{1}{a_2}\right)(\alpha_1 + \alpha_2) + \frac{\sqrt{}\gamma_1}{k\sigma_{av}a_1} + \frac{\gamma_1 \sqrt{}}{2}\right]\right\}; \tag{6.41}$$

$$P_1^{(2)} = \frac{\sigma \bar{v}_{av}^2 B_{av}^2 h l (1-k)}{\sigma_{av}}\left\{k + \frac{\sigma_{av}}{(1-k)l}\left[\frac{\beta_1 + \beta_2}{2} - k(\alpha_1 + \alpha_2)\right] + \right.$$

$$\left. + (1-k)^2 + \frac{0.5 \sqrt{}\gamma}{0.33 l}\cdot\left(\frac{1}{a_1} + \frac{1}{a_2}\right)(\alpha_1 + \alpha_2) + \frac{\sqrt{}\gamma_1}{k\sigma_{av}a_1} + \frac{\gamma_1 \sqrt{}}{2}\right\}. \tag{6.42}$$

161

The generator efficiency may be expressed as

$$\eta = \frac{P_s}{P_1},$$

which, for the two cases at hand, yields

$$\eta^{(1)} = k \quad \frac{1 - x(1 - \frac{\sigma_{av}}{\sigma})[2 \ln 2 - x_1 - z_1]}{8 \left[1 - \frac{1}{2}\left\{\frac{1}{b} + \frac{\sigma_{av}}{\sigma}\left[\frac{b_1 + b_2}{2} - 3(x_1 - z_1)\right]\right\}\right]}$$
$$+ (1 - k)^2 + \frac{0.5(1 - 15 - x)\lambda N}{2 \frac{l}{b}\left(\frac{1}{a_1} + \frac{1}{a_2}\right)(a_1 - a_2) + \frac{\lambda N}{2}} \quad (6.43)$$

$$\eta^{(2)} = k \quad \frac{1 - x(1 - \frac{\sigma_{av}}{\sigma})[2 \ln 2 - x_1 - z_1]}{8 \left[1 - \frac{1}{2} \frac{\sigma_{av}}{\sigma} \frac{l}{b}\left[\frac{b_1 + b_2}{2} - 3(x_1 - z_1)\right]\right]}$$
$$+ (1 - k)^2 + \frac{0.5 \lambda N}{0.5 \frac{l}{b}\left(\frac{1}{a_1} + \frac{1}{a_2}\right)(a_1 - a_2) + \frac{\Sigma a_2 \lambda N}{b_2 l_1 a_1} + \frac{\lambda N}{2}} \quad (6.44)$$

If the channel walls, which are perpendicular to the magnetic field, are conducting, then additional power losses must be taken into account. In the first approximation, this can be done by making an appropriate correction in the load factor:

$$k' = \frac{R_{in} - R_1}{R_{in} + R_1} \cdot \frac{1}{1 + \frac{R_{in}}{R_1} \cdot \frac{\sigma_w}{\sigma}\left(\frac{b_w}{b} - 1\right)} \quad (6.45)$$

where R_{in} and R_ℓ are the internal resistance of the generator and the load resistance; σ_w and σ are the wall and the liquid metal conductivities, and $\frac{b_w - b}{2}$ is the thickness of the wall perpendicular to the magnetic field.

All the above relationships are valid for liquid metal MHD generators with a constant cross section duct when

$$a_{av} = a_1 = a_2 = a.$$

The values of $\eta^{(1)}$ were calculated by D. Elliot [232] with the following initial data: $v_{\ell 1} = 91.8$ m/sec, $a_1 = 14.5$ mm, $a_2 = 24.2$ mm, $b = 6.05$ mm, $\ell = 148$ mm, $x_1 = z_1 = 22.5$ mm.

A curve of $\eta^{(1)}$ as a function of the load factor is shown in Fig. 116. Curve 2 is for inviscid flow without field extension, while curve 1 corresponds to data calculated from Eq. (6.43). Point A was obtained experimentally using a model of an MHD generator using a NaK alloy with parameters close to those used in calculations ($a_1 = 14.7$ mm, $b = 6.3$ mm, $a_2 = 24.3$ mm, $\ell = 148$ mm).
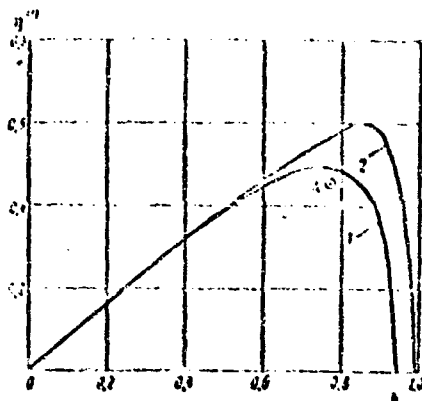
Fig. 116. Theoretical efficiency,
with and without a boundary layer
and field extension, of experimental
MHD generator with diverging duct,
as a function of load factor.

Figure 117 shows a theoretical curve of the output power of an MHD generator vs.
the average flow velocity of liquid metal at the diffuser inlet. The same figure shows
experimental data, which are found to be in good agreement with the theory.

Figure 118 depicts a theoretical curve of the pressure drop in an MHD generator
diffuser as a function of length. It also shows experimental data obtained for a given
magnetic induction ($B_0 = 0.6$ tesla). It is easy to see that in the range of $z/\ell \approx 0.4-0.8$,
the difference between theory and experiment is approximately 30%, which is attribu-
table to incomplete compensation of the liquid metal reaction.
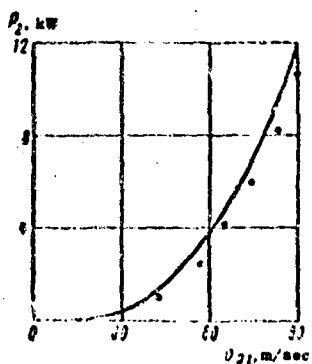
Fig. 117. Comparison of
experimental and theoreti-
cal output powers of an MHD
generator with diffuser vs.
liquid metal velocity at dif-
fuser inlet.
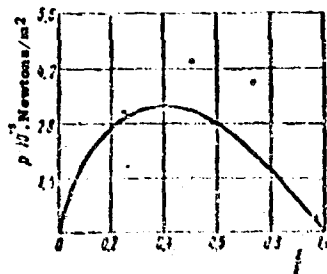
Fig. 118. Pressure distri-
bution in the diffuser of an
MHD generator.

163

Particular attention must be paid to compensation of liquid metal reaction in MHD generators. The detrimental effect of this reaction increases with increasing power of the MHD generator. Tables 19 and 20 present results of calculations for two MHD generators with constant-cross section ducts in the absence and presence of liquid metal reaction compensation [219]. It follows from these data that, all other conditions being equal, compensated MHD generators can be made smaller and are capable of handling higher pressure drops.

The liquid metal reaction in MHD generators is compensated in the same manner as is done with the corresponding electromagnetic pumps.

It should be noted, in conclusion, that a gas or a vapor-liquid mixture may be used in MHD generators as a working fluid instead of the liquid metal.

Paper [223] presents results of experimental studies of an MHD generator with a two-phase working medium (liquid metal and nitrogen). These studies show that the conductivity of this two-phase medium can be quite high and, depending on the gas phase fraction α, is defined empirically as

$$\sigma_{g \, av} = \frac{\sigma}{\epsilon^{1.5}} \cdot \tag{6.46}$$

Table 19. Characteristics of MHD Generators Without Compensation of the Liquid Metal Reaction

a) Характеристика	b) Значения характеристик для генератора с параметрами	
	$P_2 = 1$ kW $\Delta\varphi = 1$ v	$P_2 = 10$ kW $\Delta\varphi = 5$ v
η, %	90	85
$\rho\sigma v_0 l$	6	3
$\Delta p \cdot 10^{-5}$, Newtons/m²	2.86	4.125
$v_c l$, m²/sec	0.73	4.3
b, mm	4.7	8.1
Q, liters/sec	3.52	26.2
l/a	4	0.35

KEY: a) Quantity; b) for generator with parameters.

Under certain conditions, the presence of the gas phase in the liquid metal makes it possible to increase the generator efficiency.

It is obvious that, due to specifics of their operation, MHD generators for shipboard use should have a number of features distinguishing them from stationary MHD generators. In conjunction with this, studies of stationary MHD facilities cannot be extended without qualification to generators for vehicular use.

Table 20. Characteristics of MHD Generators with Compensation of the Liquid Metal Reaction

a) Характеристика	Значения характеристик для б) генератора с параметром	
	β > ... A ...	β > ... G ...
η, %	90	85
μ, g/l	6	3
Δp·10⁻⁵ newtons/m²	11.18	8.28
c·τ, m²/sec	0.09	3.7
δ, mm	1.3	2.9
Q, liters/sec	0.9	10.5
l/a	3.1	0.29

KEY: a) Quantity; b) for generator with parameters.

    An MHD generator for use as a marine power source should have a number of specific features which are determined basically by the conditions under which such power sources operate. Analysis of these conditions makes it possible to formulate, in the first approximation, the principal requirements on marine MHD generators.

    An MHD generator which is the principal marine power source must supply electric power to the main prime mover (or propulsion electric motor), the electrically-operated auxiliary mechanisms and devices which are a part of the main power unit, and to various independent groups of shipboard devices or users.

    Here, depending on the particular MHD scheme used, in addition to the MHD generator proper, the MHD unit may contain also other (auxiliary) electric power sources (for example, a conventionally-driven generator, a storage battery). The output of such an MHD generator is determined as the total power needed for providing the ship's propulsion and for supplying all the electric power needs, with consideration of their load balance and simultaneity of operation.

    The power actually delivered by a marine MHD generator must vary depending on the vessel speed, on the conditions under which mechanisms and devices servicing the main power unit operate, as well as on the mode of operation of the ship's electrically powered devices. For different modes of ship operation (sailing, loading, unloading, etc.) the relationships between the power used by its different subunits change, with the power used by one kind of unit changing independently of the power requirements of others and of the power used by the main propulsion system (or main propulsion electric motor).

    Individual power-using units (or their clusters) use electric power with different parameters with permissible deviations fully defined for each unit (with respect to voltage and frequency). It is most desirable that the MHD generator supply each independent cluster of electric-power users independently.

165

The marine MHD generator should have a given margin of life operability. Methods for achieving this have evolved from practice. The main method is provision for redundancy of all kinds: duplication of power equipment of the same type, so that when a given mechanism breaks down it is replaced by its back up unit; dividing the total capacity of a given power-unit element between several [smaller] elements of the same type; upon breakdown of one such element, the others supply sufficient power for below-capacity operation; and division of the total capacity into small units, simultaneously with replication of equipment, when one element of such a unit, supplying only a part of the total power, goes out of service, one can restore total power by actuating a backup mechanism (element).

Due to weight and space limitations it is impossible to install aboard a ship two independent MHD generators, each capable of supplying the total power and each equipped with its auxiliaries and associated systems. This is also useless since different major parts of MHD generators operate at far different conditions. The most drastic operating conditions are those prevailing in the MHD generator duct, in which flows a high-temperature, high-velocity working medium.

The requirement of flexible operation and adjustability of an MHD marine facility make it necessary to combine hydrodynamic and electromagnetic principles in varying the power of the MHD generator in response to power changes in the load circuit.

In developing layouts and designs of marine MHD generators consideration must also be given to obtaining the highest possible efficiencies at different operating modes.

The structural integrity and design of a marine MHD generator should make possible its operation with the ship rolling, and at different values of heeling and trim difference.

2. Liquid Metal Condensing MHD Generator [Condensing Ejector]

Thermal Efficiency of the MHD Unit

The MHD scheme with condensation depicted in Fig. 113 was suggested by Jackson and Brown [231]. A magnetohydrodynamic cycle using a two-phase nozzle and condensing acceleration chamber [henceforth called condensing ejector] was described in [227], [230] and [232]. Figure 119 depicts the enthalpy-entropy diagram for such a unit under steady-state conditions.

The stagnation state and the static state of the vapor are shown on this diagram by points 1' and 2', respectively. Analogous states of the fluid being accelerated are shown by points 1" and 2". Segments 1'-2' and 1"-2" describe the kinetic energies of the vapor and liquid streams. The static pressure in states 2' and 2" and after mixing remains constant. The total vapor and liquid pressures at the nozzle inlet (in states 1' and 1") are assumed to be same, i.e., the process is assumed to occur without additional losses (losses due to incompleteness of mixing, flow friction, etc.).

Vapor at state 1' enters the nozzle, is expanded, mixed in the condensing ejector [drift tube] with the fluid which is in state 1", and is partially or totally condensed. According to the law of conservation of energy, the enthalpy at termination of the vapor-liquid mixing will correspond to point a, located on line 1'-1" in such a manner that the distance from point a to points 1' and 1" is inversely proportional to the mass rates of flow of the vapor and liquid, respectively.

165

The kinetic energy of the mixed flow cannot be determined solely from thermodynamic laws, however; its maximum is limited by the available enthalpy difference, and is depicted by segment ab, where b is a point on line 2'-2". Here, points a and b do not describe the true state of the mixed flow. In fact, since the static pressure of this flow is p_2 (see Fig. 119), the stagnation and the static state should be depicted respectively by points c and e. Obviously, stagnation pressure p_c at point c is lower than p_a at point a. In addition, by virtue of the law of conservation of momentum, the kinetic energy of the mixed flow drops from magnitude ce to cd. Hence the static state of the mixed flow is displaced to point 2 on the constant pressure line p_2, while the stagnation pressure is displaced to point 1 on straight line 2'-1". Here, as was previously noted, additional losses are neglected.
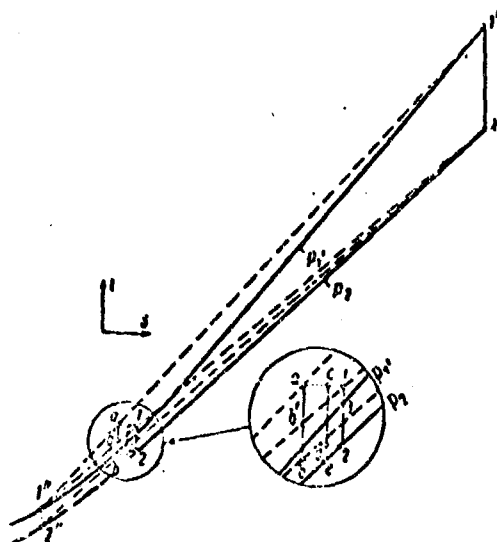
Fig. 119. The enthalpy-entropy diagram
of an MHD condensing ejector.

The mixed fluid flow passes through the MHD generator, where it performs useful work, and then is broken up into two parts, one recycled to the heat source and the other to the radiator (where it gives up its heat). If friction and diffusion losses are neglected, then the pressure p_3 at the generator outlet obviously should not be less than $p_{1'}$ and $p_{1''}$. Point 3 on constant-pressure line p_1, characterizes the general state of the flow at the generator outlet. Segment 1-3 corresponds to that fraction of the total enthalpy which is used for electric power generation.

The heat supplied to unit mass of working fluid is equal to the enthalpy difference $i_{1'} - i_3$. The thermal efficiency of the cycle is

$$\eta \cdots \frac{i_1 \cdots i_3}{x(i_{1'} \cdots i_3)} = \frac{i_{1'} \cdot i_{1'} \cdot i_1 \cdot i_3}{i_{1'} \cdot i_3 \cdot i_4 \cdot i_{b'}} , \qquad (6.47)$$

167

where i is the specific enthalpy at points marked on Fig. 119 (b' is a point on line 1"-2'), and x is the ratio of the vapor mass flow to the total mass flow of the working fluid.

On the right hand side of Eq. (6.47) x is expressed in terms of segments of the enthalpy-entropy diagram. The first factor on the right-hand side is the thermal efficiency of vapor expansion in the vapor nozzle, while the second denotes the efficiency of acceleration of the liquid flow during mixing with the vapor flow in the condensing ejector. This "bifurcation" of the efficiency is obviously arbitrary [to some extent]. In the numerator of the thermal efficiency of the Rankine cycle, the pump work (segment 2-3) is subtracted directly from the turbine work (segment 1'-2'). However, in the case at hand, this cannot be done, since both these types of work are performed simultaneously upon mixing in the drift tube.

It should be noted that the expression for η [Eq. (13)] in [230] is incorrect. In this expression the numerator has i_2, instead of i_3, while in the denominator i_3 has been replaced by i_1 (in the notation used here), which yields a somewhat higher than actual value of η.

In examining the flow of incompressible fluid, Eq. (6.47) can be transformed as follows. In this case

$$\Delta i = \frac{\Delta p}{\rho},$$

where Δi and Δp is the difference between the stagnation and static enthalpy and pressure and ρ is the liquid density.

Since $p_3 = p_{1''}$ and $p_2 = p_{2''}$ (see Fig. 119) then, neglecting density changes in the liquid phase, we have

$$i_1 - i_2 = i_{1'} - i_{2'} = \frac{v''^2}{2}, \qquad (6.48)$$

where v" is the velocity of the driven fluid.

By definition of the enthalpy

$$\left. \begin{array}{l} i_{1'} - i_{2'} = \frac{v'^2}{2}; \\[2mm] i_1 - i_2 = \frac{v^2}{2}, \end{array} \right\} \qquad (6.49)$$

where v' is the velocity of the driver flow, and v is the velocity of the mixed flow.

From the law of conservation of momentum

$$v = xv' + (1-x) v''$$

and

$$\frac{v^2}{2} = x \frac{v'^2}{2} + (1-x)\frac{v''^2}{2} - x(1-x) \frac{(v'-v'')^2}{2}.$$

168

The last term of the second expression characterizes kinetic energy losses in the process of mixing the liquid and vapor working-medium phases.

Using the above expressions and transforming, we have

$$i_1 - i_3 = \frac{v^2}{2} - \frac{v'^2}{2} - x\left[\frac{v'^2}{2} - \frac{v''^2}{2} - (1 - x)\frac{(v' - v'')^2}{2}\right] =$$

$$= x\,(i_{1'} - i_{3'})\left\{1 - \left(\frac{v'}{v'}\right)^2 - (1 - x)\left(1 - \frac{v''}{v'}\right)^2\right\}. \qquad (6.50)$$

Substituting the above value of $i_1 - i_3$ into Eq. (6.47), we find that the thermal efficiency of the cycle is

$$\eta = \frac{i_{1'} - i_{3'}}{i_{1'} - i_3}\left\{1 - \left(\frac{v'}{v'}\right)^2 - (1 - x)\left(1 - \frac{v''}{v'}\right)^2\right\}. \qquad (6.51)$$

The first factor in the right-hand side of this expression is the efficiency of the Rankine cycle (which is used in the heat-source loop in order to convert the thermal energy into kinetic energy of the vapor jet), while the second factor is the efficiency of acceleration of the mixed flow.

The thermal efficiency of a unit using the above scheme can be improved by using a regenerator. For this purpose, the heat of the fluid leaving the condensing ejector at a sufficiently high temperature is recirculated and used for preheating that part of the fluid which, upon leaving the MHD generator, is recycled to the heat source. An MHD generator with a regenerator is shown in Fig. 120 [230].
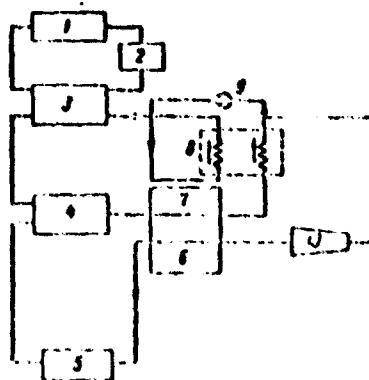

Fig. 120. Schematic of a condensing liquid-metal MHD generator with regeneration.

1) Reactor; 2) pump; 3) boiler; 4) condensing ejector (drift tube); 5) radiator/cooler; 6) and 7) MHD generators; 8) regenerator; 9) Joule-Thomson valve; 10) diffuser.

It should be noted that heat regeneration in the above cycle cannot be implemented in a manner similar to regenerative heating of feedwater in the Rankine cycle. This is due to the fact that the minimum temperature T_2 at which the liquid being preheated enters the regenerator must, in this arrangement, be appreciably below the minimum temperature $T_{2''}$ of the liquid in the cycle, with the result that the regenerating effect cannot be fully utilized. This limits the possibilities of increasing the efficiency of such a cycle by using a regenerator.

Returning to the analysis of the efficiency equation, we see that the efficiency of acceleration of the mixed flow in the condensing ejector depends on the ratio of the mass flows of the vapor and the total liquid mass flow x, and on the ratio of velocities of these flows v''/v'. The larger the x, the higher the efficiency of the acceleration process. However, the allowable value of x, due to the necessity of providing a fully specified liquid subcooling during mixing (in order to eliminate undesirable thermal losses), is limited by the requirement that the mixed flow should not boil.

Each value of x and each selected value of pressure p_2 has corresponding to it an optimal value of v''/v', for which the efficiency of the acceleration process is at maximum. It is defined by the expression

$$\left(\frac{v''}{v'}\right)_{opt} = \frac{1-x}{2-x}.$$

Here the efficiency of the acceleration process is

$$\eta_e = 1 - \frac{v''}{v'} = \frac{1}{2-x}.$$

Figure 121 shows curves of efficiency η_e as a function of ratio v''/v' for different values of x. The optimum values of η_e lie on the dashed line.

If we consider changes in the working fluid's density in the liquid phase, then, instead of Eq. (6.48), we have

$$i_1 - i_2 > i_{1'} - i_{2'}.$$

Here the thermal efficiency of the cycle will be somewhat below its value calculated from Eq. (6.51).

In [233] it is pointed out that analysis of cycles for a number of liquid metals and for a combination of two such metals shows that: 1) the optimum thermal cycle efficiencies are obtained when the weight of vapor fraction in the working fluid is not more than 10-15%; 2) the cycle efficiency is directly proportional to the working fluid specific heat, and is inversely proportional to its latent heat of vaporization.

Figure 122 compares cycles of a condensing MHD generator and of a steam-turbine unit by means of an s - T - v diagram. The T-s diagram is given in Fig. 123.

The working fluid leaves the MHD generator in state 1 and flows to the diffuser, where the pressure rises to a value corresponding to the reactor temperature T_R (segment 1-2). Between states 2 and 3 the liquid is heated, vaporized and converted into a [mist] two-phase mixture. The flow expands and is accelerated in the nozzle (3-4*), reaching the lowest cycle temperature at point 4*. Then the vapor phase of the working fluid is condensed at segment 4*-1*, where heat is removed from the cycle.

170
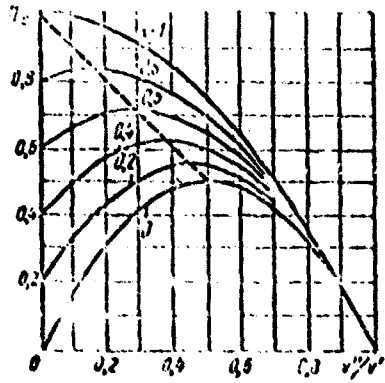
Fig. 121. Efficiency of acceleration in drift tube vs. the vapor/liquid velocity ratio (at various flows of the same)
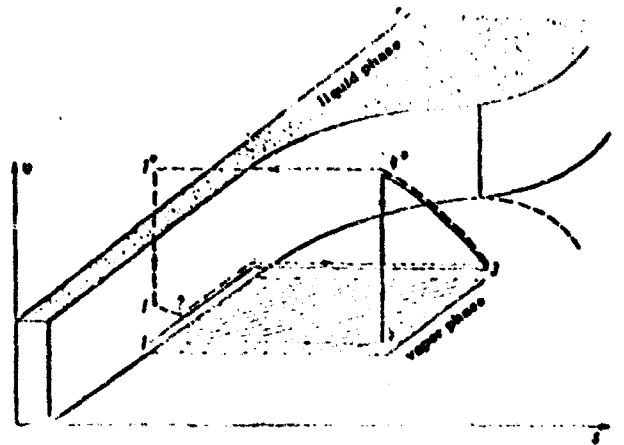
Fig. 122. $s - T - \overset{+}{v}$ diagrams of energy conversion in an MHD converter and in a steam turbine.

Then the liquid, which has a sufficiently high velocity, enters the MHD generator in state 1*. The solid line in Fig. 122 depicts the energy conversion in a steam turbine. The difference between these two processes of energy conversion is in the different sequences of condensation and energy extraction. In the turbine, the energy is extracted before condensation, i.e., when the working fluid is in the vapor phase. In the MHD generator, the useful energy of the cycle is extracted after condensation, when the working fluid is liquid.

The projections of the above energy conversion processes on a two-dimensional T-s diagram are depicted in Fig. 123 and consist of a Rankine cycle (the figure refers to MHD cycle using Hg, and a steam turbine cycle, where T_{cr} is the critical water temperature).

The highest temperatures T_R and the minimum temperatures T_{min} of both cycles are the same and, consequently, the Carnot efficiency of both processes is the same. However, the thermal efficiency of the steam cycle is lower than that of the MHD converter operating on Hg, due to the higher average temperature T_m of the metal as compared with T_w, the average temperature of the steam cycle.
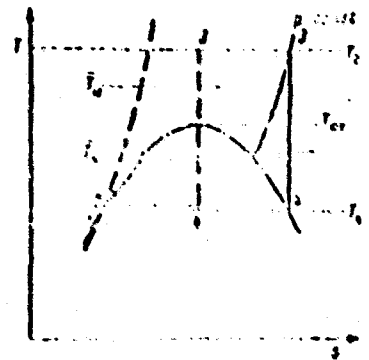
Fig. 123. Rankine cycles for Hg and H_2O at $T_R > T_{cr}$ (of H_2O).

- - - - Hg; ——————— H_2O.

---

* Translator's Note: v here denotes velocity and not volume. In the original wording of [232], Geschwindigkeit (velocity) v.

In the case of the Hg cycle, no superheating is needed, since all metals have sufficiently high critical temperatures. The left boundary curve for metals is very steep, which makes the thermodynamic efficiency of the metal cycle close to that of the Carnot cycle. In addition, the power density of the turbine, even in the case of high steam superheat, is several orders of magnitude lower than in the MHD generator.

Thermodynamic Acceleration of the Liquid in the Condensing Cycle

The most complex problem in the condensing cycle is thermodynamic acceleration of the liquid metal upon mixing with the vapor of the same metal, the vapor condensing during this heat transfer. Let us consider the mixing in the drift tube of the condensing ejector.

The high velocity of the "hot" stream as compared with that of the cold, and the consequent high impact losses, mean that the hydrodynamic efficiency of the acceleration will be low if a single constant-pressure injection of liquid into the vapor stream is used.

The efficiency of the thermo-kinetic process in the mixing section of the ejector can be improved by using the so-called thermodynamic $\dot{m}$-i transformation. The basic idea of this transformation is stepwise supply of the subcooled liquid to the expanding mixed stream in order to convert the available enthalpy drop into kinetic energy of the liquid stream, with an increasingly higher flowrate at each stage.

The condensing ejector was analyzed in extensive detail using computers [233]. The process was examined in the following sequence: the two-phase medium is expanded in a supersonic nozzle, a low-temperature liquid metal is continuously injected, momentum exchange takes place between the phases, and the vapor is condensed. This was done for different inlet variables, amounts of vapor along the nozzle and in the mixing part of the condensing ejector, injected-metal flowrates and temperatures, and different pressures.

The analysis showed that continuous injection of the liquid metal increases the cycle's thermal efficiency by about 10%, as compared with that of the cycle with single isobaric injection of the total amount of liquid metal.

To determine the losses in the mixing section, let us consider the idealized liquid acceleration with an infinite number of liquid-injection points [227].

A stream with mass rate $\dot{m}'$ upon passing through the reactor expands from initial state 1' (Fig. 119) using a certain portion of its available enthalpy. Here the velocity increases from v_2 to v_A (point A of Fig. 124). After this, the vapor flow mixes with some fraction of the subcooled liquid, the resulting flow assumes an equilibrium state B_1 with velocity v_{B_1} [etc.]. At the nth stage the available energy is fully utilized and the working fluid is in state D_1. The last stage terminates by injection of the remaining part of the liquid. The stream velocity at the ejector exit is v_e.

Figure 125 illustrates this process in an intermediate stage of the condensing ejector. The following notation is used: 1 is the mixed flow at the ejector outlet; 1' and 1" are the respective inlet vapor and liquid flows; $\dot{m}'$ and $\dot{m}''$ are the respective

172

vapor and liquid mass flows; x_0 is the relative vapor mass flow at the two-phase nozzle inlet [this quantity is identical to x in Eqs. (6.47) and (6.50)] and i' is the vapor enthalpy drop (segment 1'-2' in Fig. 119).
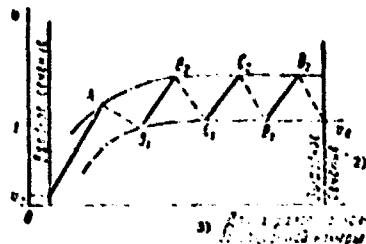
Fig. 124. Velocity diagram in condensing ejector mixing section [based on thermodynamic m-i transformation].

KEY: 1) Inlet section; 2) exit section; 3) mixing section length.

Fig. 125. Intermediate stage in the mixing section of a condensing ejector.

After a part of the available enthalpy has been utilized, the mixture velocity at the inlet to any intermediate stage is v (Fig. 125). During an infinitesimal time interval, the mixture expands by an amount corresponding to the pressure difference -dp. The corresponding enthalpy drop will then be di = -Vdp (V being the specific volume of the mixture in the given stage). The mixture velocity increases by d_1v and becomes v_1. With the mixture at this velocity, a quantity dx of the liquid is supplied to it, the mixture expands and thus acquires velocity v + dv. The flow velocity at the ejector exit with x = 1 (the flowrate being m' + m") reaches the value v_e.

We assume for our further discussion that the specific volume of the liquid is small as compared with that of the vapor. Then the energy equation which describes the work of expansion vd_1v = di and the momentum equation of the mixture

$$x (v + d_1 v) = (x + dx)(v + dv)$$

yield the differential equation

$$\int v\, dv = x\, dv + v\, dx \tag{6.52}$$

It will be assumed in solving this equation, that no additional condensation takes place at the time when liquid is injected. Then Eq. (6.52) for the corresponding mixture and expansion stage is written in the form

$$\left(\frac{v}{x}\right) v = x\, dv + v\, dx \tag{6.53}$$

173

Then we assume that ratio di'/dx = const; during the entire process the enthalpy drop i' will be utilized, with the mass flow ratio changing from x to 1. Then Eq. (6.53) becomes

$$\left(\frac{i'}{2} - v \right) dx = x\, dv_e \tag{6.54}$$

where

$$i = v_e^2 (1 - x_0). \tag{}$$

For an initial velocity $v_0 = 0$ and $x = x_0$ the velocity toward the end of mixing process (for $x = 1$) will be v_e and the corresponding kinetic energy

$$i_e = \frac{v_e^2}{2} = \frac{x_0 i'(1 + x_0)}{2}. \tag{6.55}$$

The kinetic energy of the flow leaving the condensing ejector thus comprises a $\dfrac{1 + x_0}{2}$ part of the initial kinetic energy $x_0 i'$. Its other part, $\dfrac{1 - x_0}{2}$ is lost in mixing.

In the case of single state mixing, then

$$i_e = x_0 i' \tag{6.56}$$

i.e., the energy loss according to Eq. (6.51) for $v'' = 0$ is twice as much, that is $(1 - x_0)$. Multistage injection thus can reduce mixing losses two-fold.

It is desirable to have at the inlet of a vehicle mounted MHD generator a two-phase mixture with a given vapor fraction. This is primarily due to the fact that the presence of the vapor (gas) phase in the liquid metal does not always result in reducing the generator efficiency. Conversely, in a given range of generator operation modes the efficiency increases with increasing the vapor content [223]. In addition, the efficiency and output power of a generator using a two-phase mixture is a function not only of the load, as in the case of a liquid-metal device, but also on the relative content of the gas phase [void fraction]. Thus the presence of the vapor (gas) phase in liquid metal provides for greater flexibility of generator operation. This may be used for controlling its output, which is particularly important for vehicular applications.

The maximum void fraction is determined by the limiting possible reduction in the mixture's thermal conductivity. Here it should be kept in mind that the mass vapor fraction is by several orders of magnitude lower than the volumetric vapor fraction, the allowable limit of which is approximately 0.75 [sic] [223]. Here MHD generator operation with practically pure (vapor-less) liquid metal may be of interest.

Let us consider the case when the flow leaving the condensing ejector is entirely liquid, i.e., when the vapor is fully condensed. The subcooling of the injected liquid in this case should be determined so as to obtain a saturated exit liquid flow, which eliminates excess thermal losses in the cycle.

174

We assume that vapor is condensed on expansion and mixing. The corresponding change in the energy drop is expressed as

$$x\,di = \frac{1-x}{1-x_0}\,x_0\,di'. \tag{6.57}$$

Here Eq. (6.53) for mixing and expansion takes the form

$$\frac{x_0}{v}\cdot\frac{1-x}{1-x_0}\,di' = x\,dv + v\,dx.$$

and instead of Eq. (6.54) we get

$$\left(A'\frac{1}{v}x - v\right)dx = x\,dv, \tag{6.58}$$

where

$$A' = x_0 i' (1-x_0)^2.$$

Solving this equation using integration factor xv for the same values of inlet and exit values of x ($x_2 = x_0$) and for $v_0 = 0$, we get

$$x^2 v^2 = A' v (2 - v) = A' v_0 (2 - v_0).$$

and when $x = 1$ we will get instead of Eq. (6.55) the expression

$$i_e = \frac{v_e}{2}\,i'. \tag{6.59}$$

Comparing this expression with Eq. (6.56) we can conclude that if a liquid flow is desired and the ejector exit, then stage-wise injection of liquid is expedient only when $x_0 < 1/2$.

Experiments on Acceleration of Liquid by a Gas Flow

The present section presents data on experimental study of the acceleration of liquid injected into a high-speed gas stream by the latter. The experiment was needed because known results on the drag, on which acceleration of the injected particles depends were obtained for aircraft, turbines and other airfoils and are not suitable for particles undergoing acceleration motion.

The most interesting experimental data on particle acceleration are presented in [253]. The two-phase vapor liquid metal mixture was modeled in the experimental setup by means of compressed air and spherical particles of sand of properly selected size. This is a conservative simulation, since air as the driver fluid is less dense than the two-phase liquid metal and the sand is denser than the injected liquid. The selection of air and sand permitted test operation at ambient temperatures and eliminated any problem due to change in particle size during acceleration.

175

The overall view of the setup is shown in Fig. 126. The sand was coated with contrasting black paint and a Fastax camera capable of taking 17,000 frames per second was used to photograph the travel of the sand particles. Separate test series were made with cylindrical and rectangular subsonic and supersonic nozzles. Sand injection occurred just downstream of the nozzle throat. The drift tube extending from the nozzle --modeling the condensing ejector -- was made of Pyrex glass and therefore photographic images of the sand could be obtained at various positions downstream of the nozzle. The test variables were: sand size - 177-500 μ diameter; sand mass flow - '45-12.5 g/sec; air pressure - 2.06-4.16 kg/cm², air mass flow - 40-90 g/sec.

The test data were used for constructing curves of drag coefficient c_d as a function of particle Reynolds number Re_p.
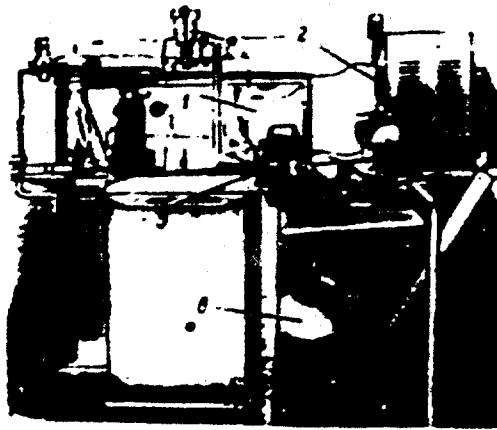
Fig. 126. Particle acceleration test apparatus.

1) Sand injector; 2) recording instruments;
3) glass drift tube; 4) camera; 5) nozzle;
6) air supply.

Figure 127 shows curves of $c_d = f(Re_p)$ for different values of parameter $v'_p d/v^2_p$ (v'_p is the particle acceleration, v^2_p is the particle velocity and d is the particle diameter). It is seen from Fig. 127 that the drag coefficient is proportional to the particle acceleration. The same effect was observed by other investigators with larger particles. It is seen from these graphs that c_d is dependent on the distance from the point of injection.

According to test data, a distance of only about 20 cm is needed for accelerating sand particles 500 μ in diameter from 0 to 120 m/sec. At a distance of 30-40 cm from the point of injection the particles acquire velocities equal to 60% of the air velocity. The experimentally determined acceleration exceeds theoretical values, found by extrapolating data on the drag of airfoils.
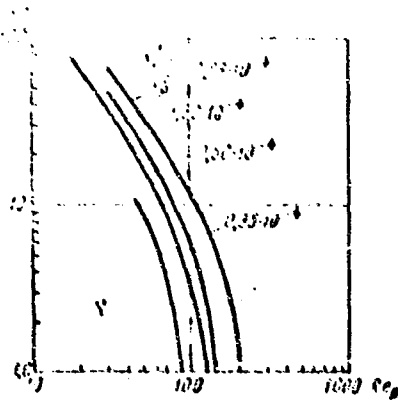
Fig. 127. Drag coefficient vs.
Reynolds number with accelera-
tion modulus as the parameter.

Experimental Heat-Transfer Studies
in a Condensing Ejector

The rate of heat transfer between the subcooled liquid and saturated vapor is studied by means of Heisler's diagrams for spherical particles [234]. However, these diagrams do not cover the entire range of parameters for which it is necessary to make calculations for liquid metal MHD units. In addition, the efficiency of condensation for small void fractions can be appreciably lower than that assumed in constructing these diagrams with the result that the heat transfer for alkali metals may not conform to theoretical data obtained from these diagrams. This made it necessary to set up the applicable experiment.

A stage of importance in preparing this experiment was developing a method for measuring the volume of the alkali metal vapor in the two-phase flow [233], which is needed for obtaining the condensation process characteristics. Prem and Parkins in their report to the International Symposium on MHD Electric Power Generation held in Paris in 1964 reported plans for study of heat transfer on a special test section which should be completed in 1964, with half a year of tests planned.

Figure 128 depicts schematically the heat transfer test section, which is a part of a potassium test loop developed for performing extensive tests of the MHD device. This section is used for study of heat transfer between potassium vapor and cooled liquid potassium. The program of tests includes study, within wide limits, of the effect on heat transfer of the flow velocity, temperature and pressure. The results of these tests are intended for determining the ratios of vapor and liquid phases ensuring optimal operating conditions for the two-phase nozzle which is a part of the condensing ejector and of the drift tube, as well as for design of these devices.

It should be noted that according to preliminary heat transfer calculations using Heisler's diagram, the condensation time in the ejector's mixing section should be of the same order as the acceleration time of the liquid phase [233]. Here the design

177

values of the heat transfer coefficients (for maximum difference in the temperatures of the vapor and liquid phases of the working fluid at the inlet and exit of the test section) were from $1.76 \cdot 10^2$ to $1.76 \cdot 10^5$ watt/m^2 -deg.
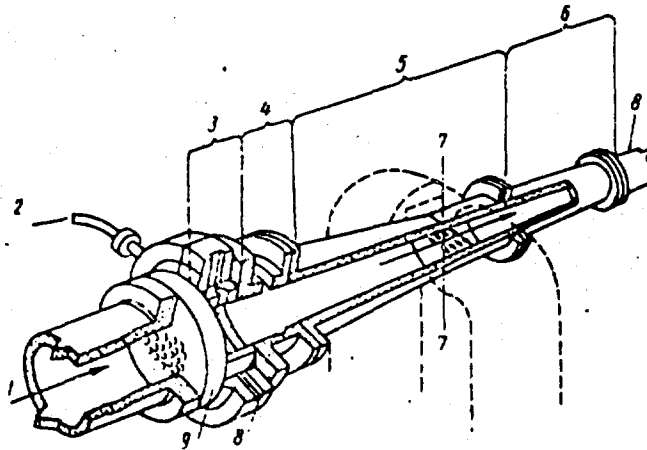
Fig. 128. Heat transfer test section in the condensing ejector.

1) Vapor or vapor-liquid inlet; 2) subcooled liquid injection; 3) injection chamber; 4) variable-length mixing chamber; 5) electromagnetic flowmeter; 6) variable-length and cross section transition section; 7) electrode location; 8) liquid injection nozzle or atomizer; 9) vapor flow straightener.

Figure 129 depicts schematically a potassium test loop facility, designed and constructed in the USA [233] for the study of necessary properties of liquid metals, testing individual unit elements and subsequent demonstration of the operation of the unit's prototype using this cycle. Its operating characteristics are:

Working fluid . . . . K
Maximum temperature, °C 870
Maximum metal vapor pressure, Newtons/m^2 . $2.7 \cdot 10^5$
Maximum liquid metal pressure, Newtons/m^2 . $11.75 \cdot 10^5$
Maximum vapor fraction (by weight), % . . . 5-20
Construction material . . . . type 316
                                              stainless steel

The major components of the loop, surrounded by an argon filled enclosure are: boiler 10, preheater 2, regenerative heat exchanger 12, reject heat exchanger 15, electromagnetic pump 13, various tanks, demountable test sections. Instrumentation is provided for measuring key parameters such as temperature, pressure and flowrate.

Potassium is supplied by a pump to the regenerative heat exchanger, then passes the boiler and test section, the other side of the regenerative heat exchanger to an argon

heat exchanger and back to the pump. The liquid metal from the pump flows to the argon heat exchanger, where it is cooled, and then flows to the test section.
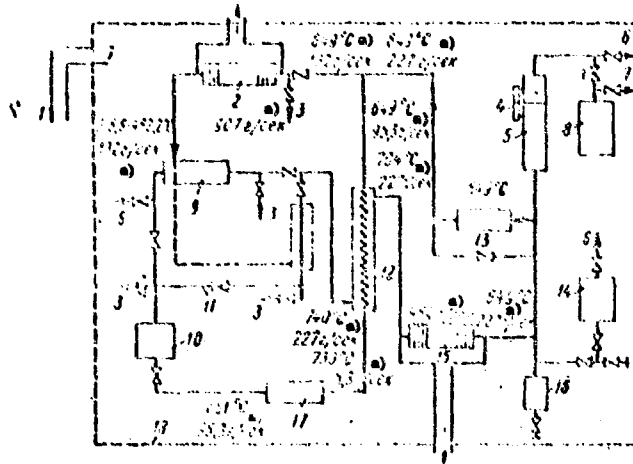
Fig. 129. Schematic of potassium test loop facility.

1) To argon cooler; 2) potassium-to-air heat exchanger No. 2; 3) to drain tank; 4) liquid level; 5) surge tank; 6) argon supply; 7) to vacuum pump; 8) vacuum tank; 9) test section; 10) boiler; 11) future line; 12) regenerative heat exchanger; 13) electromagnetic pump; 14) fill and drain tank; 15) potassium-air heat exchanger No. 1; 16) cold trap; 17) variable heater; 18) enclosure.

KEY: a) g/sec.

3. Liquid Metal MHD Generator Operating on a Separating Cycle

Thermal Efficiency of the MHD Generator

The cycle of an MHD unit with separation using one working fluid (single-component cycle) and with two immiscible liquids (two-component cycle) was analyzed in [218], [223], [235] and [236]. It was established that the efficiency of the two component cycle is higher than that of a single-component cycle (neglecting friction losses). The single-component cycle with separation is thermodynamically less efficient due to the need to heat the liquid to a temperature exceeding the average cycle temperature. The two-component separating cycle is examined in great detail on the following assumptions [218]:

1) the vapor is an ideal gas with constant specific heat;

2) the temperature in the two-phase nozzle decreases insignificantly as compared with the inlet temperature;

179

3) the liquid and the vapor condensate do not interact chemically;

4) the vapor is not soluble in the liquid;

5) the pressure of the saturated vapor of the liquid is zero;

6) the pressure along the MHD generator channel remains constant;

7) the liquid does not penetrate into the vapor loop and the vapor does not penetrate into the liquid loop.

Condition 1 results in a trivial error if use is made of the effective molecular weight, which yields the correct value for the nozzle exit density. Assumption 2 makes it possible to apply equations of isothermal flow in the nozzle, with the error for flow-rate ratios in mixtures of practical interest being quite insignificant. Conditions 3 and 4 are usually satisfied for liquids of interest here. The error due to assumption 5 is minor. Condition 6 makes it possible to examine separately the MHD generator and the diffuser, although partial or total pressure restoration may also take place in the MHD generator. Assumption 7 appreciably simplifies the problem, since then effects due to incompleteness of separation are not considered (below these effects are taken into account by the separation efficiency η_s).

The thermal efficiency of the cycle is given by

$$\eta = \frac{P_e}{P_0} \cdot \frac{P_d}{1 + \frac{P_e}{P_d}}, \tag{6.60}$$

where P_e is the electric power output of the cycle; P_0 is the thermal rating of the reactor; and P_{cl} is the cooling loss.

The electric power output of the cycle is equal to some fraction η_g of the kinetic energy converted in the MHD generator, less the electric power for driving the condensate pump, i.e.,

$$P_e = \frac{1}{2} \eta_g \dot{m}_{fl} \left(v_{g.\,in}^2 - v_{g.\,out}^2 \right) - \frac{\dot{m}_v (p_{p.out} - p_{p.in})}{\eta_p \rho_{con}}, \tag{6.61}$$

where η_g is the generator efficiency, $\dot{m}_{fl}$ is the mass flow of the liquid through the generator; $v_{g.\,in}$ and $v_{g.\,out}$ are the liquid velocities at the generator inlet and outlet; $\dot{m}_v$ is the mass flow of the vapor; $p_{p.\,in}$ and $p_{p.\,out}$ are the condensate pressures at the pump inlet and exit, η_p is the pump efficiency, and ρ_{con} is the condensate density.

The cooling loss P_{cl} will be calculated on the assumption that the process in the cooler takes place as follows: the vapor is first cooled from inlet temperature of the cooler $T_{in\ cl.}$ to critical condensation temperature T_w is condensed, and then cooled from T_w to the condensate temperature at the cooler exit $T_{out\ cl}$. Then

$$P_{cl} = \dot{m}_v [c_v (T_{d.\,in} - T_w) + L + c_{cond}(T_w - T_{c.\,out})]. \tag{6.62}$$

where c_p is the specific heat of the vapor, L is the latent heat of condensation and c_{con} is the specific heat of the condensate.

The kinetic energy at the separator exit (at the generator inlet) will be assumed to be some portion η_s of the kinetic energy of the liquid leaving the two-phase nozzle, i.e.,

$$v_{s.in}^2 = \eta_s v_{n.out}^2 \tag{6.63}$$

In the diffuser the pressure is raised by an amount $p_{in.\,r} - p_2$, where $p_{in.\,r}$ is the pressure of the fluid at the reactor inlet (at the diffuser exit) and p_2 is the pressure of the liquid leaving the two-phase nozzle. This pressure drop can be represented as a relationship for the velocity heat at the diffuser inlet:

$$p_{r.in} - p_2 = \frac{1}{2} \eta_d \rho_n v_{s.out}^2 \tag{6.64}$$

where η_d is the diffuser efficiency.

The velocity with which the liquid leaves the two-phase nozzle $v_{out.\,n}$ is assumed to be equal to some portion $(\eta_n)^{1/2}$ of the isentropic exit velocity v_i, i.e.,

$$v_{n.out}^2 = \eta_n v_i^2. \tag{6.65}$$

To derive an expression for v_i [237] we assume that vapor with molecular weight M, specific heat c_p and mass flow rate $\dot{m}_v$ enters the nozzle and is mixed with a liquid having density ρ_{fl}, specific heat c_{fl}, and mass flow rate $\dot{m}_{fl}$. Let p_1 be the pressure, T_1 the temperature and v_1 the mixture velocity at the nozzle inlet; s_v and s_{fl} the specific entropies and i_v and i_{fl} the specific enthalpies of the vapor and liquid, respectively.

The change in the specific entropy of the vapor flowing in the nozzle

$$\Delta s_v = s_{v2} - s_{v1} = c_p \ln \frac{T_2}{T_1} - \frac{R}{M} \ln \frac{p_2}{p_1}, \tag{6.66}$$

where R is the universal gas constant.

The corresponding change in the liquid's entropy

$$\Delta s_n = s_{n2} - s_{n1} = c_n \ln \frac{T_2}{T_1}. \tag{6.67}$$

The change in the mixture entropy

$$\Delta s = \dot{m}_v \Delta s_v + \dot{m}_n \Delta s_n = \dot{m}_v \left(c_v \ln \frac{T_2}{T_1} - \frac{R}{M} \ln \frac{p_2}{p_1} \right) + \dot{m}_n c_n \ln \frac{T_2}{T_1}. \tag{6.68}$$

181

In the flow of a homogeneous mixture heat transfer from the vapor to the liquid is reversible. Hence under adiabatic flow conditions and in the absence of friction the mixture flow is isentropic, i.e., $\Delta s = 0$. Then we get from Eq. (6.68)

$$\frac{p_2}{p_1} = \left(\frac{T_2}{T_1}\right)^{(c_v \dot{m}_v + c_{fl} \dot{m}_{fl})/(c_v \dot{m}_v / R_v + \dot{m}_{fl})}. \tag{6.69}$$

The change in specific vapor enthalpy for flow in a two-phase nozzle

$$\Delta i_v = i_{v2} - i_{v1} = c_p(T_2 - T_1), \tag{6.70}$$

the corresponding change in the liquid's enthalpy

$$\Delta i_{fl} = i_{fl2} - i_{fl1} = c_{fl}(T_2 - T_1) + \frac{p_2 - p_1}{\rho_{fl}}. \tag{6.71}$$

With the assumptions made, we get from the energy-balance equation for a steady-state process at the nozzle inlet and outlet

$$\frac{1}{2}(\dot{m}_v + \dot{m}_{fl})(v_2^2 - v_1^2) + \dot{m}_v \Delta i_v + \dot{m}_{fl} \Delta i_{fl} = 0. \tag{6.72}$$

Substituting Δi_v and Δi_{fl} from Eqs. (6.70) and (6.71) into Eq. (6.72), we get

$$\frac{1}{2}(\dot{m}_v + \dot{m}_{fl})(v_2^2 - v_1^2) + \dot{m}_v c_v(T_2 - T_1) +$$
$$+ \dot{m}_{fl}\left[c_{fl}(T_2 - T_1) + \frac{p_2 - p_1}{\rho_{fl}}\right]. \tag{6.73}$$

Substituting here T_2 from Eq. (6.69), we find v_1

$$v_1^2 = v_2^2 + 2 \frac{\rho_1}{\rho_{fl}\left(1 + \frac{\dot{m}_v}{\dot{m}_{fl}}\right)}\left\{\frac{\rho_{fl}T_1}{p_1}\left(c_v \frac{\dot{m}_v}{\dot{m}_{fl}} + c_{fl}\right) \times \right.$$
$$\left. \times \left[1 - \left(\frac{p_2}{p_1}\right)^{(c_v \dot{m}_v + c_{fl} \dot{m}_{fl})/(c_v \dot{m}_v / R_v + \dot{m}_{fl})}\right] + \frac{p_1 - p_2}{p_1}\right\}. \tag{6.74}$$

For low $\dot{m}_v/\dot{m}_{fl}$ which are of practical interest the exponential expression containing ratio p_2/p_1 can be approximated by two first terms of a series expansion of this expression

$$\left(\frac{p_2}{p_1}\right)^{(c_v \dot{m}_v + c_{fl} \dot{m}_{fl})/(c_v \dot{m}_v / R_v + \dot{m}_{fl})} \approx 1 + \frac{c_v \frac{\dot{m}_v}{\dot{m}_{fl}} + c_{fl}}{c_v \frac{\dot{m}_v}{R_v} + c_{fl}}\left(1 - \frac{p_2}{p_1}\right). \tag{6.75}$$

Substituting Eq. (6.75) into Eq. (6.74), we get

$$v_i^2 = v_i^2 + \frac{2\omega_1}{\rho_n\left(1 + \frac{\dot{m}_v}{\dot{m}_n}\right)} \left(\frac{\dot{m}_v}{\dot{m}_n}\cdot\frac{\rho_n RT_1}{Mp_1}\ln\frac{p_1}{p_2} + \frac{p_1}{\rho_1} - \frac{p_2}{\rho_2}\right). \qquad (6.76)$$

Upon simultaneous transformation of Eqs. (6.61)-(6.65) and (6.76) we get the ratio of the output electric power of the cycle to the cooling loss in the form

$$\frac{P_e}{P_{cl}} = \frac{1}{A}\left\{\frac{\eta_n \eta_i \eta_g^2 \rho_n RT_1}{\left(1 + \frac{\dot{m}_v}{\dot{m}_n}\right) 2Mp_1}\ln\frac{p_1}{p_2} - \frac{\eta_n \eta_i \eta_g \dot{m}_n (p_1 - p_2)}{\left(1 + \frac{\dot{m}_v}{\dot{m}_n}\right)\dot{m}_v p_1} \times \right.$$

$$\times \left[\left(\frac{1 + \frac{\dot{m}_v}{\dot{m}_n}}{\eta_n \eta_i \eta_d}\right)\left(\frac{p_{r.in} - p_1}{p_1 - p_2}\right) + \right.$$

$$\left.\left. + \left(\frac{1 + \frac{\dot{m}_v}{\dot{m}_n}}{\eta_n \eta_i \eta_g \eta_{pv}}\right)\left(\frac{\dot{m}_v \rho_n}{\dot{m}_n Q_{cod}}\right)\left(\frac{p_{p.out} - p_{p.in}}{p_1 - p_2}\right) - 1\right]\right\}, \qquad (6.77)$$

where

$$A = \left(\frac{\rho_n}{\rho_1}\right)[L + c_n(T_3 - T_{d.out}) - c_p(T_1 - T_{d.out})].$$

Substituting this value of P_e/P_{cl} into Eq. (6.60) we get the thermal efficiency of the cycle, which is not presented here due to cumbersomeness of the expression.

Acceleration of Liquid in a Two-Phase Nozzle with a Separator

As was mentioned previously, an MHD cycle with separation is thermodynamically more efficient when two working fluids are used (two-component cycle). One of the basic problems in operating a facility with this cycle is efficient acceleration of the liquid phase of the working medium in the two-phase nozzle by means of the kinetic energy of expanding vapor of the second working fluid. These working fluids should be mutually immiscible, or little soluble over the entire range of cycle temperatures.

One-dimensional flow of a two-phase nozzle on assumption of absence of friction and heat transfer to the nozzle wall was examined in great detail by Elliot in the Jet Propulsion Laboratory of California Institute of Technology, with the results reported, among others, in [225] and [238]. It was assumed in his analysis that the liquid forms spherical droplets all of the same initial diameter, and that the droplets break up whenever the Weber, based on the slip velocity was

$$We = \frac{\rho_v d(v_a - v_n)^2}{2\sigma} > 6. \qquad (6.78)$$

183

if the slip velocity $(v_v - v_{fl})$ is maintained during a time longer than the natural oscillation period of the droplet $\tau_j \tfrac{j'}{} \tau_n \tfrac{j'}{}$, as is generally the case in a two-phase nozzle.

In the above expressions ρ_v is the vapor density, ρ_{fl} is the liquid density, d is the droplet diameter, v_v is the vapor velocity, v_{fl} is the liquid velocity and σ is the liquid's surface tension.

It was also assumed that the dimensions of the newly formed droplets are such that for them $We = 6$. Here the maximum or critical droplet diameter was determined from

$$D_{cr} \approx \frac{12}{\rho_v s^2 \bar{v}^2} \sigma$$ (6.79)

where $s = v_v v_{fl}/\bar{v}$ is the slip and $\bar{v}$ is the steady state equilibrium velocity.

Let us consider the two-phase flow in a nozzle section at distance x from the inlet. The pressure in this section is denoted by p and the cross sectional area by F. It is obvious that

$$F = \dot{m}_v \left(\frac{1}{\rho_v v_v} + \frac{r}{\rho_n v_n} \right),$$

where

$$r = \frac{\dot{m}_n}{\dot{m}_v}.$$

The momentum of the mixture at steady state equilibrium velocity $\bar{v}$ and constant pressure is

$$M = \dot{m}_v v_v + \dot{m}_n v_n = (\dot{m}_v + \dot{m}_n) \bar{v}.$$

Whence

$$\bar{v} = \frac{v_v + r v_n}{1 + r}.$$

Since $\dot{m}_v + \dot{m}_{fl} = \text{const}$, then the gradient of the momentum is

$$\frac{dM}{dx} = (\dot{m}_v + \dot{m}_n) \frac{d\bar{v}}{dx} = \dot{m}_v (1 + r) \frac{d\bar{v}}{dx}.$$

When there is no friction at the nozzle walls dM/dx is equal to the negative of the pressure gradient over the entire flow area, i.e.,

$$\dot{m}(1 + r) \frac{d\bar{v}}{dx} = - F \frac{dp}{dx}.$$

184

Substituting here the previously obtained value of F, we have

$$\text{(6. 80)}$$

We now express the gas (vapor) velocity in terms of s and $\bar{v}$

$$v_v \quad \text{(6. 81)}$$

$$\text{(6. 82)}$$

Substituting the above values of v_v and v_{fl} into Eq. (6. 80) and making use of the fact that $2\bar{v}d\bar{v} = d\bar{v}^2$, we get an expression for the momentum in the form

$$\frac{d\bar{v}^2}{dt} \quad \text{(6. 83)}$$

In the limit of isentropic flow the slip is zero and then the sought isentropic velocity gradient is given by

$$\frac{d\bar{v}^2}{dt} \quad \text{(6. 84)}$$

A second important feature of the flow, i.e., the gradient of the slip, can be found as follows. Each drop is acted upon by drag pressure F_v and force F_p produced by pressure difference

$$F_v \quad \text{(6. 85)}$$

$$F_p \quad \text{(6. 86)}$$

where c_d is the drag coefficient.

It may be assumed approximately for small Reynolds numbers (Re $\leq$ 0.1)

$$c_d \quad \frac{24}{Re}$$

and for high Reynolds numbers (Re $\geq 2 \cdot 10^4$)

$$c_d \quad 0.157.$$

The sum of forces F_v and F_p is equal to the product of droplet mass and its acceleration

$$\text{(6. 87)}$$

185

From the last three equations we get the value of the velocity gradient

$$\text{(6.88)}$$

From Eq. (6.82) dv_{fl}/dx is written in the form

$$\text{(6.89)}$$

Solving the above expression for ds/dx and expressing in the process dv_{fl}/dx by means of Eq. (6.88), we get the slip gradient

$$\text{(6.90)}$$

The total enthalpy of the two-phase flow in the case of no heat transfer to the nozzle walls and neglecting vapor formation during expansion of the mixture remains constant and can be expressed as

$$\text{(6.91)}$$

The transfer of heat between the liquid and vapor phases during nozzle flow is characterized by equations presented below. The rate of convective transfer of heat from the liquid droplets to the vapor is

$$\text{(6.92)}$$

where k is the heat transfer coefficient and $N \sim 6\dot{m}_{fl}/\pi d^3 v_{fl}$ is the number of droplets.

The heat transfer coefficients can be obtained from the relationships [239]:
for Re < 1.0

for 1.0 ≤ Re ≤ 25.0

for Re > 25.0

186

Due to circulation of the fluid inside the droplets, their inside temperature is uniform, so that

$$\frac{dQ}{dt} = \ldots \alpha \ldots \frac{dT_n}{t} \ldots \tag{6.93}$$

From Eqs. (6.92) and (6.93) we get the gradient of the liquid's temperature along the flow

$$-\frac{dT_n}{dx} = \ldots \frac{\alpha(T_n - T_c)}{dc_n^{\prime}\rho^{\prime}v_n} . \tag{6.94}$$

This equation does not take into account the effect due to formation of additional vapor during nozzle expansion of the mixture. However, as is noted in [238], this effect is insignificant.

Experimental Studies of the Two-Phase Nozzle

The previously presented system of equations was used for computer calculation of the theoretical characteristics of a two-phase nozzle for the flow of nitrogen-water and Freon 1301 (CBrF$_3$) - water mixtures [238]. The calculations were made for droplet diameters of 0.05-0.127 cm. It was established that due to breakup of large drops according to Eq. (6.79) the exit velocity does not depend on the initial droplet diameter, if it is below a certain value (in the case at hand 0.0254 cm). This conclusion points to the theoretical feasibility of efficient nozzle operation without preatomization of the liquid.

Calculations showed that the exit velocity for the nitrogen-water mixture is 85% of the isentropic exit velocity corresponding to zero droplet diameter, while for the Freon-water mixture it is 91%. This is attributable to the higher Freon density, which requires less slip for the same drag on the water droplets.

Figure 130 presents theoretical and experimental values of the exit velocities of the nitrogen-water mixture for a nozzle inlet pressure of 10.5 atm abs, exit pressure 1.05 atm abs and temperature 21.6°. Theoretical curve 1 was obtained for above-critical droplet sizes. The same figure shows by a dashed line the isentropic velocity curve for $d = 0$. Figure 131 presents these curves for the Freon-water mixture for the same inlet and exit conditions and temperatures from 4.7 to 12.2°C.

It should be noted that the experimental characteristics of the two-phase nozzle were obtained with rough initial (at the nozzle inlet) atomization of the liquid and with total absence of droplets with critical and below-critical diameters. This derives the theoretical conclusion that it is possible to obtain efficient acceleration of the liquid without fine pre-atomization.

Figure 132 depicts a test section for experiments with the two-phase nozzle [238]. The nozzle contour was selected so that the slip velocity varies along the nozzle approximately as $(v/p)^{1/3}$, where v and p are the local mean velocity and pressure, respectively. The nozzle was 127 cm long, with a 35.6 cm entrance diameter and 13.2 exit diameter, the throat diameter being 8.07 cm. The size corresponds roughly to a conversion system of 125 kv electric output.
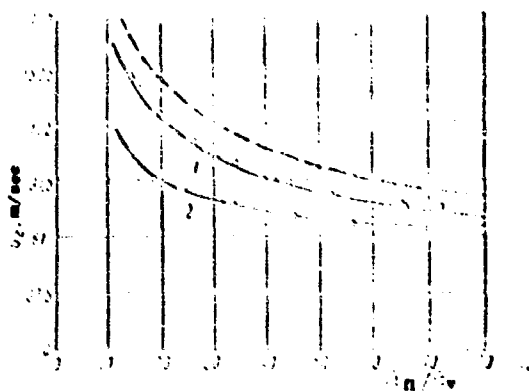
Fig. 130. Comparison of predicted and measured nozzle and separator exit velocities for the nitrogen-water mixture.

1) Nozzle; 2) separator.

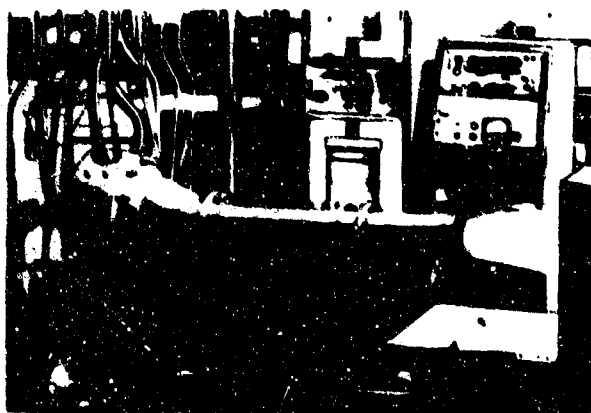Fig. 131. Comparison of predicted and measured nozzle exit velocity of the Freon 1301-water mixture.

Fig. 132. Overall view of experimental two-phase nozzle in operation.

The semivertex angle of the convergent part of the nozzle is 20°, while the semi-vertex angle of the divergent part is 2.5°. The nozzle cross section near the throat changes quite smoothly, so that the slip would be limited to 0.5. The mixer (injector) has 1656 pairs of impinging jets of nitrogen and water, uniformly distributed across the entrance diameter of the nozzle. This provided uniform mixture-ratio distribution by making the water jets converge at a right angle. The holes were rectangular with sides of 0.0127 x 0.33 cm for nitrogen and 0.1015 x 0.33 cm for water. The nozzle was tested for a range of water/nitrogen mixture ratios from 15 ($\dot{m}_v$ = 2.76 kg/sec, $\dot{m}_{fl}$ = 4.17 kg/sec) to 70 ($\dot{m}_v$ = 1.18 kg/sec, $\dot{m}_{fl}$ = 82.5 kg/sec). The pressure drop along the injection jets was 11.95-2.11 atm abs for nitrogen and 0.98-2.67 atm abs for water. The mean veloc-ity $\bar{v}$ was calculated by dividing the total flow by the nozzle throat cross section. The measured velocities at the nozzle exit ranged from 144 to 89 m/sec for a flow-rate ratio range from 15 to 70. The experimental and theoretical data are compared in Fig. 130.

In the Freon experiment the latter was supplied to the mixer (injector) at t = -56.7°C was evaporated after injection, reaching a superheat from -18 to -9.5°C, changing in the process the water temperature from -15 to -7°C. Figure 131 compares the experimental data with calculated results obtained on assumption of total evaporation of the Freon. It is seen from this figure that total liquid vaporization will yield full agreement between the theoretical and experimental nozzle characteristics.

It was concluded in [238] on the basis of analysis of experimental data for a two-phase nozzle operating on a Freon-water mixture that Li in such a nozzle will efficiently vaporize Cs (or K, or Pb), since the heat-transfer properties of liquid metals are better than those of the Freon-water mixture.

Figure 133 shows a theoretical curve of a two-phase nozzle for Li-Cs for an inlet mixture pressure of 14.15 abs atm, exit pressure of 1.41 atm abs and temperature 1100°C [238]. The vapor pressure of Li in the calculations was assumed to be constant and approximately equal to 0.14 atm abs, while its surface tension was taken as 23 Newtons/m². The concentration of Cs dissolved in Li was assumed to be 6% by weight. The initial diameter of droplets was taken as 0.127 cm, and it was assumed that the exit velocities do not change up to droplet diameters of 0.0507 cm.

The dashed curve in Fig. 133 is that for isentropic velocity. It is seen from the figure that the predicted exit velocities of the Li-Cs mixture comprise 88% of the isen-tropic velocity. The theoretical and experimental studies thus show that it is possible in two-phase nozzles of acceptable length exit velocities amounting to from 85 to 90% of the isentropic leaving velocity.

Separator Experiments

A conical separator placed at the inlet of the two-phase nozzle was tested first in conjunction with the development of jet pumps for rocket engines [237]. These experi-ments showed that it is possible to develop such a pump with a two-phase nozzle and a separator as its main elements.

Figure 134 shows one such separator operating together with a two-phase nozzle being tested on an air-water mixture. The separator was conical with semivertex angle of 15°, passing into a toroid of 32 mm radius curvature. The conical part deflects the gas from rectilinear motion upon leaving the nozzle and collects the atomized liquid into
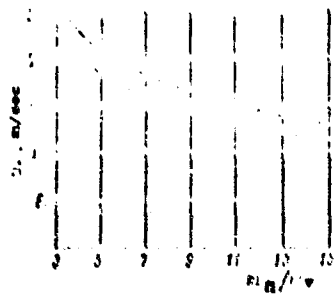
Fig. 133. Predicted nozzle-
exit velocities of cesium-
lithium mixture.
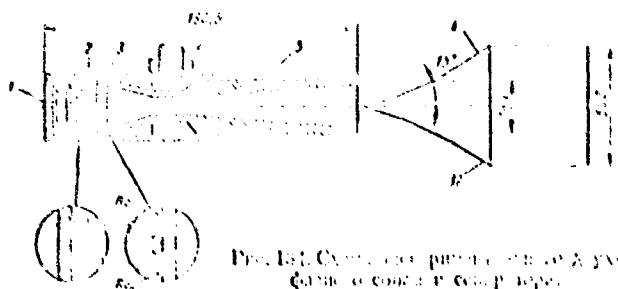
Fig. 134. Experimental two-phase drive nozzle and
experimental conical separator.

1) Liquid inlet; 2) liquid-injection tubes; 3) aperture
plate; 4) gas vapor inlet; 5) nozzle; 6) separator.

a film; the bulk of the remaining gas is removed by centrifugal forces produced in the
flow in the toroid. These experiments determined η_s, the ratio of the kinetic energy

of the liquid at the separator exit to the kinetic energy of the liquid at the two-phase
nozzle outlet, which when recalculated for a separator for a 500 kW unit amounted to
$\eta_s = 0.85$ [222].

A relationship was also obtained between the liquid loss in the separator and the
width of the annulus which taps the liquid film at the separator exit, for different values
of gas, liquid ratios at the separator inlet. It was established that with an increase in
the width of this annulus the liquid flow through it first increases quite rapidly, then
slower and for a given annulus width (0.51 mm) it reaches a maximum. It was found
that about 20% of the total liquid leaving the nozzle is atomized to such an extent that it
does not impinge on the separator body, and that part which does impinge forms of
foam-like mixture with a gas, liquid volume ratio of about 4. Losses of liquid in the
separator (by being carried away by the vapor) depends on the gas to liquid ratio and
according to the tests made comprised not less than 6% of the total mass flow of the
mixture. It is obvious that these characteristics had to be substantially improved before
the separator can be used as a part of an MHD facility.

190

Subsequently this type of separator was tested as a part of an MHD facility [222]. The purpose here was to evolve structural elements of the separator which would provide for minimum hydraulic losses, reduce losses (bypass) of the liquid as well as obtaining a liquid film with a specified vapor content.

Figure 135 shows the arrangement of a two-phase nozzle, separator and MHD generator for a 500 kw facility using an Li-Cs mixture. The separator of this facility together with a two-phase nozzle was tested on the nitrogen-water mixture [225]. The initially tested separator had an annulus at the end of its conical part, for liquid removal (Fig. 136).

The measured velocities at the separator exit are shown in Fig. 130, which also depicts a theoretical curve calculated on assumption of liquid flowing along a flat plate with boundary-layer thickness equal to the thickness of the liquid film at the separator surface. As is seen from Fig. 130, the experimental points are in quite satisfactory agreement with the predicted velocity distribution.

The measured separator exit velocity was 70% of the nozzle exit velocity for a mixture ratio $\dot{m}_{fl}/\dot{m}_v = 14$ and 83% of the nozzle exit velocity for $\dot{m}_{fl}/\dot{m}_v = 70$.
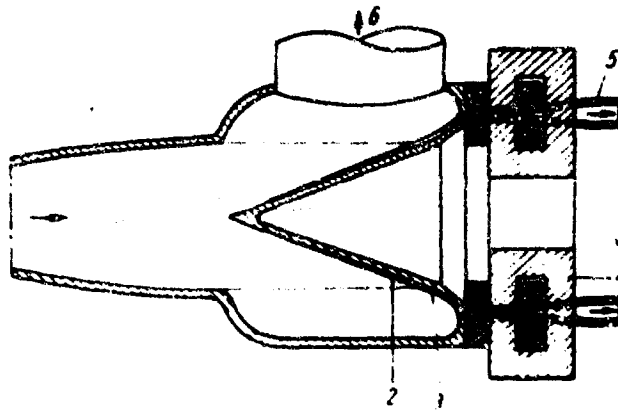
Fig. 135. Schematic layout of two-phase nozzle, separator and MHD generator of a 500 kW vacility.

1) Two-phase nozzle; 2) separator; 3) lithium film; 4) MHD generator; 5) diffuser; 6) to radiator.

Due to the relatively high liquid losses in this separator, its design was modified (Fig. 137). In addition to the primary liquid-capture slot at the MHD generator inlet a secondary capture slot was provided for removing liquid carried by the gas past the first slot. A set of extension rings was used to determine the effect of primary capture slot position relative to the geometric impingement point of the jet. In addition, a second separator with a straight cone, shown by the dotted line, was used for comparison with the curved cone. The experimentally determined efficiency of capture by the primary slot as a function of the gas and liquid volume ratio V_v/V_{fl} at the primary slot inlet for different slot widths b is shown in Fig. 138.

191
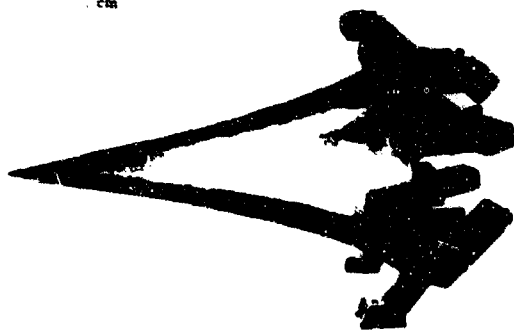
Fig. 136. Conical part of experimental separator.

Fig. 137. Experimental conical separator.

1) Flow in; 2) curved cone; 3) point of return of secondary flow; 4) straight cone; 5) geometric impingement point; 6) extension ring; 7) secondary capture slot; 8) gas outlet; 9) secondary liquid outlet; 10) liquid outlet; 11) primary capture slot.

By reducing the slot width it was possible to reduce the amount of gas entering the primary slot together with the liquid; this increased the flow bypassing the primary slot. This effect made it possible to obtain a liquid film with volumetric gas/liquid ratios from 0.5 to 2.0. For ratios from 1.0 and above less than 5% of the liquid bypasses the primary slot.

The effectiveness of the secondary slot is illustrated by Fig. 139. As is seen, the secondary slot collects from 60 to 80% of the liquid bypassing the primary slot. Here the total liquid losses (by weight) in the separator amount to 0.5-1.5% of the separator flow.

192
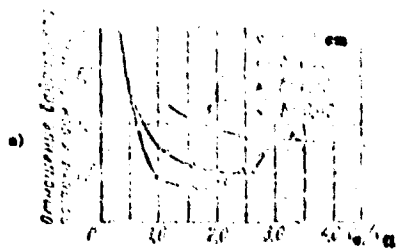
Fig. 138. Capture effect-
iveness of primary slot.

1) $m_{fl}/m_v = 20$; 2) $m_{fl}/m_v =$
$= 40$; 3) $m_{fl}/m_v = 65$.

KEY: a) Percent liquid flow
bypassing primary slot.
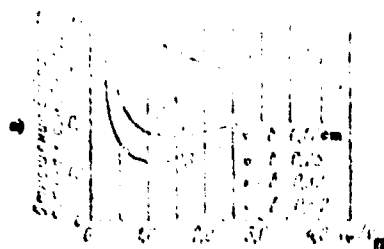
Fig. 139. Capture effect-
iveness of primary and sec-
ondary slots combined.

1) $m_{fl}/m_v = 20$; 2) $m_{fl}/m_v =$
$= 40$; 3) $m_{fl}/m_v = 65$.

KEY: a) Percent liquid flow
bypassing primary slot.

Experiments with replaceable extension rings measured the bypass of liquid past
the primary slot in order to determine the effect of primary slot location. Figure 140
shows the bypass of liquid past the primary slot as a function of the ratio of the cone
cross sectional area where the extension ring is installed (primary slot) to the area of
the exit cross section of the two-phase nozzle b^2/a^2 (for volume ratio $\dot{m}_{fl}/\dot{m}_v = 40$). This
experiment shows that reducing b^2/a^2 to 2.0 does not appreciably reduce the separation
effectiveness. When b^2/a^2 is reduced to 1.5 the liquid loss amounts to 9% with the curved
and to 18% with the straight cone. The amounts of liquid bypassing the secondary capture
slot were 0.7 and 1.6% respectively, i.e., approximately equal to the bypass observed
with higher b^2/a^2. The separator exit velocity was found to be the same for both the
curved and straight separators.

The separator with the curved cone was used to study the effect of returning to
the cycle, through a slot in the cone's surface (point 3 in Fig. 137) of the liquid cap-
tured by the secondary slot. The curves of flow velocity reduction in the separator due
to injection of the secondary liquid flow through this slot as a function of the liquid flow
through this slot to the liquid flow through a two-phase nozzle are shown in Fig. 141,
which also depicts the theoretical curve for $\dot{m}_{fl}/\dot{m}_v = 62$ (top curve), which is in satis-
factory agreement with test data. The velocity losses in this case are 50-70% of the
secondary flow velocity. The amount of fluid removed from the separator does not
change due to secondary injection.

The experiments thus proved the feasibility of designing a separator the liquid
loss (bypass) in which does not exceed 1%, with liquid-velocity losses below 20%. The
liquid removed from the separator may be returned to the cycle by secondary injection.
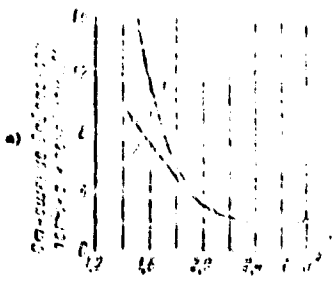
Fig. 140. Bypass of
liquid past primary slot
as a function of the area
of cone cross section with
the extension ring of the
primary slot to the nozzle
outlet cross sectional area.

1) Straight cone; 2) curved
cone.

KEY: a) Percent liquid
flow bypassing primary
slot.
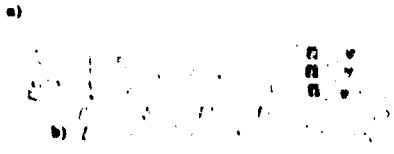
Fig. 141. Experimental and
theoretical reduction of sepa-
rator exit velocity due to sec-
ondary mixture injection
through separator cone sur-
face.

KEY: a) Separator velocity
reduction, %; b) secondry
injected flow, %.

Experiments with the Two-Phase Diffuser

To find a suitable diffuser geometry a series of rectangular and annular diffusers
with various contraction ratios and divergence angles were tested [225]. The best
geometries for volume ratios in the neighborhood of 2.0 were found to incorporate a
contraction area ratio of about 0.75, a throat-length/gap ratio (for the rectangular
diffuser) of about 15, and a divergence half-angle of 3.75°. Figure 142 presents the
efficiency of the annular diffuser and the best rectangular diffusers as a function of
inlet gas/liquid volume ratio at inlet velocities between 42.5 and 91.5 m/sec. The
efficiency is the ratio of diffuser discharge pressure to inlet isentropic stagnation
pressure. It is seen from the figure that the efficiencies of the best diffusers lie on
a straight line and range from $\eta_d = 0.86$ at a volume ratio of 0 to $\eta_d = 0.50$ at
$V_v/V_{fl} = 4.0$.
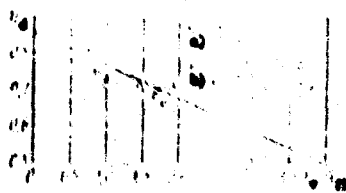
Fig. 142. Experimental
two-phase diffuser effici-
ency.

KEY: a) Annular diffuser;
b) rectangular diffusers.

194

Simulated Tests of the Unit, Testing of Working Fluids and Materials

The schematic of the section for simulated facility tests is shown in Fig. 143 [225]. This facility simulated the basic elements of a missile power plant developed in the USA for use with the SNAR-50 reactor. The tests were performed at the Jet Propulsion Laboratory of the California Institute of Technology [225] to clarify the conditions and the operating features of various closed-cycle operating modes, with the loop including an injector, two-phase nozzle, separator, liquid return line for the liquid removed from the separator and auxiliaries. The facility was tested with a nitrogen-water mixture. Six return lines were connected from the diffuser outlet to the injector inlet through check valves to prevent reverse flow after starting. The main pump provided starting flow through the start line, the nitrogen flow was adjusted in keeping with the set-up's operation.

Makeup water flow to compensate for the water lost with the nitrogen exhaust was provided from an auxiliary pump through a pressure regulator.

Smooth startup of the facility on closed-loop operation was provided by a throttle valve located at the diffuser exit. The throttle valve was closed gradually on start up until the diffuser discharge pressure exceeded the injector inlet pressure, causing the return check valves to open. Further closing of the throttle valve, accompanied by reduction of the main pump flow, caused an increasing proportion of the injector flow to be supplied from the return lines. Finally the throttle valve was fully closed, the main pump was turned off, and closed-loop operation was established at partial flow.
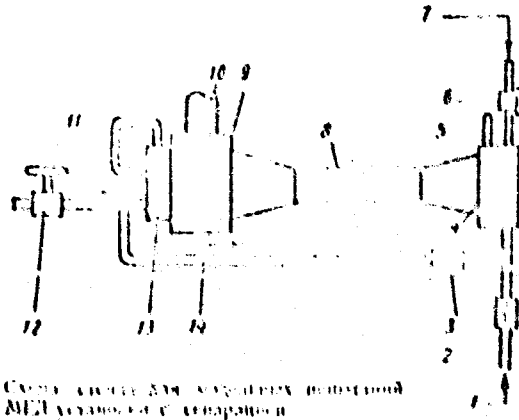
Fig. 143. Piping arrangement for closed-loop tests.

1) From main pump [water]; 2) start line; 3) check valves; 4) injector; 5) nitrogen line; 6) pressure regulator; 7) makeup line [water]; 8) nozzle; 9) separator; 10) nitrogen exhaust; 11) secondary flow return line; 12) throttle valve; 13) diffuser; 14) return line (for closed-loop operation).

195

Operation under closed-loop conditions was found to be smooth and stable, and any operating point within the closed-loop range could readily be reached by varying the nitrogen flow rate and the makeup feed pressure.

A survey was made of possible working fluids for use in space. For operation at 1000-1100°C nozzle inlet temperature there are four fluids with vapor pressures suitable for the vapor loop: cadmium, cesium, potassium and rubidium. For the liquid loop there are eight liquids with low enough vapor pressures to prevent excessive carry-over to the vapor loop, and low enough melting points to avoid plugging of the radiators: aluminum, bismuth, gallium, indium, lead, lithium, magnesium, and tin. Of the resulting 32 possible working-flu'd pairs, adequate solubility data for cycle analysis exists only for the potassium-lithium and cesium-lithium combinations.

Studies of solubility of potassium in lithium showed that at 815°C approximately 10% and at 980°C as much as 15% of the potassium is dissolved in the lithium. These values are excessive and hence the K-Li combination was discarded in favor of Cs-Li. The solubility of cesium in lithium at 1100°C is about 7.5%.

To determine the nozzle inlet pressure for performance analysis, the vapor pressure of a saturated solution of lithium in cesium over the temperature range 925-1100°C was measured [225, 240].

To determine the conditions which would ensure the required lifetime of the facility a number of tests was set up on the erosion of the metal by a high-velocity flow of liquid and of the effect of lithium on the insulation of MHD generators [225]. These tests showed that a service life of 1000 hours is possible even with the presently available materials.

4. Evaluation of Liquid Metal MHD Units for Moving Craft

Condensing MHD Conversion Systems

Condensing conversion systems (see Fig. 113) are examined in prospective designs for producing power in the 10 kW to 100 MW range and more. Application of such cycles is being investigated for the supply of power at locations where access is limited (space, underwater and remote terrestrial locations) [233]. The outstanding features of the liquid metal MHD in such an application are high reliability, since there are no moving mechanical components, and high-temperature heat rejection which permits obtaining a high power density.

Below are presented certain characteristics of such a unit for a low-output space power system. Its use at central stationary generating plants where it would be used as the topping portion of a binary cycle will be discussed further on.

As an example of the expected performance in a space application, work was done for a cycle based on the use of a mixture containing four parts of lithium and one part of potassium [233]. The theoretical efficiency of an unoptimized cycle with cycle inlet and radiator inlet temperatures of 1090 and 760, respectively, was determined to 16%. Assuming 70% for the electrical generator efficiency and 70% for the mechanical efficiency (losses due to all other factors such as nozzle performance and pumping requirements), the actual conversion efficiency from heat to electricity is 8%. Due to the better sink conditions for a remote terrestrial or underwater power supply, a still higher efficiency can be realized.
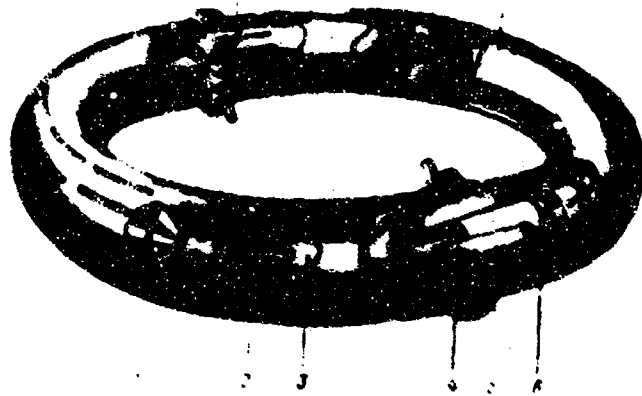
Fig. 144. Phantom view of 500 kW nuclear-powered spacecraft MHD conversion system USA project.

1) MHD generator; 2) inner coaxial tube with shell; 3) diffuser; 4) reactor control system; 5) manifold ahead of radiator; 6) main-flow injection-fluid bypass; 7) condensing ejectors; 8) radial injector; 9) last stage of condensing ejector; 10) manifold downstream of radiator; 11) condensation zone.

Figure 144 depicts in phantom view a 500 kW nuclear-powered MHD converter rated at 500 kW and using Na as the working fluid [232]. The converter uses regenerative preheating of the working fluid in the vapor loop. The probable working dimensions of the individual components made it advisable to adopt an annular form in which the diffusor is made up of two concentric components, of which the outer (annular) diffuser decelerates the working mixture thus extracting its kinetic energy. At the exit from this diffuser the flow breaks up into two streams. One stream passes through the radiator heat exchanger for subcooling, while the other passes through the regenerative heat exchanger to a two-phase nozzle. The inner diffuser delays some 5% of the total flow and raises it to the reactor pressure level.

The reactor is composed of two coaxial and expanding tubes of which the inner movable tube serves for reactor control and scram. The requisite controls and instruments are built into the inner tube.

The transformation zone consists of several nozzle and mixing sections [condensing ejectors] having approximately equal cross section. Injection is effected via radially located nozzle tubes fed from the inner tube.

Below are enumerated the principal data for the above 500 kW, AC MHD conversion system using Na as the working fluid:

Temperature, °C:
      at the reactor inlet   550
      at the reactor exit   950
Reactor diameter, cm:
      inside   8
      outside   40
Number of transformation stages   6
Maximum working-fluid velocity in the loop, m/sec   140
Average diameter of MHD generator duct, cm   4
Working fluid parameters in the MHD duct:
      velocity, m/sec   50
      electrical conductivity (ohms-m)$^{-1}$ . . . . $2 \cdot 10^{6}$
      temperature, °C   550
Ratio of compression work to useful (output) power 0.08

It is stated in [232] that such a system was designed for 50 Megawatts 20 kV,
50 cps. Overall efficiency is estimated at 32 % when using mercury at temperatures
from 600 to 160°C.
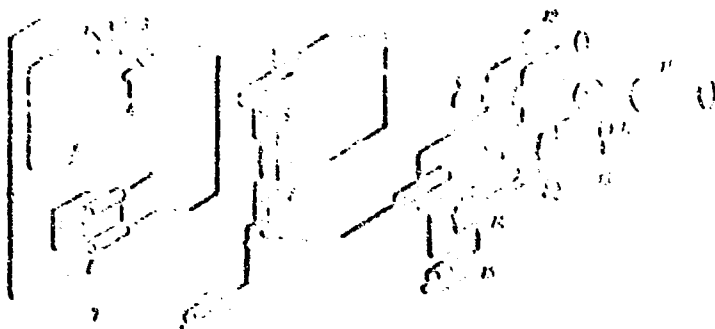
Fig. 145. MHD-steam binary cycle.

1) Nozzle; 2) MHD generator; 3) drift tube; 4) converter; 5)
liquid-vapor mixture line (10% vapor, 90% liquid); 6) liquid
metal boiler; 7) liquid metal line; 8) steam generator; 9)
superheater; 10) reheater; 11) steam-turbine generator; 12)
condenser; 13) condensate pump; 14) regenerative heaters;
15) feed pump.

Figure 145 shows schematically a binary cycle, in which the liquid-metal con-
verter serves as a topping unit of a conventional steam cycle. The heat is supplied to
the liquid-metal working fluid by combustion of a fossil fuel or in a reactor. The liquid
metal leaving the MHD generator enters the steam superheater and then the steam gen-
erator, where the sensible heat of the liquid metal is transferred to the conventional
steam cycle.

For a binary cycle of 1000 Megawatts consisting of MHD and conventional steam
cycle operating at maximum temperature of 870°C, the MHD topping unit generates
about 125 Megawatts. This results in an overall efficiency 14% higher than the achiev-
able steam cycle efficiency. The annual fuel savings for a 30 ¢ per 10^6 BTU fuel
amounts to $2.8 \cdot 10^6$ The structural material used was type 316 stainless steel [233].

Some outstanding features of the liquid metal MHD topping cycle are: 1) higher plant efficiency; 2) required temperatures are in a range where available materials can be used for components; 3) multiple steam reheat can be conveniently engineered in the plant design and further improves the steam-cycle performance; 4) only low vapor quality metal is required from the heat raising unit, which reduces the possibility of tube burnout; 5) with an alkali metal furnace the highest cycle temperature is associated with low steam pressure, resulting in better tube material utilization.

Separating MHD Conversion Systems

The project of MHD converters with separation studied in greatest detail and most extensively researched is that of a nuclear MHD system rated at 300-500 kW and using Cs-Li [225]. The experimental data obtained with this facility were presented above. The assumptions employed in the analysis were as follows: 1) 0.5% of the lithium entering the separator flows to the vapor loop; 2) the facility uses a separator with primary and secondary liquid capture slots, 9% of the liquid bypasses the primary slot and is returned to the separator with a 3% velocity reduction; 3) the generator efficiency (considering friction losses between the separator and generator, as well as between the generator and diffuser) is 70%; 4) the diffuser efficiency is 85%; 5) the efficiency of the vapor-loop electromagnetic pump is 50%; 6) the pressure drops across the reactor, radiator and mixer is 0.7 atm abs; 7) a DC converter is used (from 20 V at the MHD generator output to 5000 V).

Results of analysis of cycle efficiency (ratio of output electric power less the power for driving the vapor-loop pump, to the thermal output of the reactor) are presented in Fig. 146. It is seen from the figure that the maximum cycle efficiency on the above assumptions is 5.7%. The thermal power of the reactor for the above efficiency is 6100 kW. Such a reactor using Li with a high burnup is about 700 kg. A more conventional design would weigh about 1600 kg.
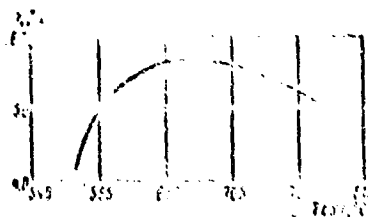
Fig. 146. Estimated efficiency of cesium-lithium cycle.

1) Nozzle inlet temperature is 1100°C.

The weight of the conversion system (nozzle, separator, diffusers, cesium pump, piping and generators, including magnets and busbars) for a Nb-Zr magnet system is about 900-1600 kg.

199

Table 21. Weight of Basic Components of a 300 kW Liquid-Metal MHD Power Plant with Separation

a)	b) вес, кг	c) уд. вес, кг/квт
d) Реактор	700 1000	2.25 3.3
e) Система преобразования		3.7
d) ...	...	3.7
e) ...	11.. 1..	....
h) ...	... (..)	....

KEY: a) Component; b) weight, kg; c) specific weight, kg/kw; d) reactor; e) conversion system; f) voltage converter; g) radiator; h) total.

The 20 to 5000 V converter would have an efficiency of about 86.5% and a specific weight of 3.76 kg/kw. For an output of 300 kw the converter input power should be 347 kw and weigh 1100 kg.

According to design studies the specific weight of the radiator should be 6.83 kg/m^2, a radiator for a 800 kw facility thus weighing 1100 kg. It is more realistic to assume a specific radiator weight of 13.7 kg/m^2, giving a total radiator weight for a 300 kw plant of 1800 kg.

Table 21 presents the weights of the system's basic components.

The shield weight of the nuclear reactor depends strongly on the spacecraft configuration and on the system's location. Approximately the shield weight is estimated at 900-1800 kg for a total dose of neutron and gamma radiation of 10^{13} neutrons/cm^2 and 10^9 erg/gm, respectively.

As was previously noted, available data make it possible to construct such a conversion system even at present and have it operate continuously for not less than 1000 hours.

REFERENCES

Theoretical Magnetohydrodynamics

1. Hartmann, J.   Theory of the Laminar Flow of an Electrically Conductive Liquid in a Homogeneous Magnetic Field, Hg.-Dynamics, Kgl. Danske Videnskab. Selskab. mat.-fys. Medd., 15, No. 6, 1937.

2. Landau, L. D. and Ye. M. Lifshits. Elektrodinamika sploshnykh sred [Electrodynamics of Continuous Media]. Gostekhizdat Press, 1957.

3. Cowling, T.   Magnetohydrodynamics. Interscience Publishers, Inc. New York, 1957.

4. Kulikovskiy, A. G. and G. A. Lyubimov.   Magnitnaya gidrodinamika [Magnetohydrodynamics]. Fizmatgiz Press, 1962.

5. Pai-Shih-I.   Magnetogasdynamics and Plasma Dynamics. Prentice Hall, 1962.

6. Globe, S.   Laminar Steady State Magnetohydrodynamic Flow in an Annular Channel, Phys. Fluids, 2, 404, 1959.

7. Zimin, E. P.   Techeniye elektroprovodyashchey zhidkosti v ploskom MGD-kanale [Flow of an Electrically Conducting Fluid in a Flat MHD Channel]. IFZh, 6, No. 4, 92, 1963.

8. Chang, C. and J. Yen.   Magnetohydrodynamic Channel Flow as Influenced by Wall Conductance, Z. angew. Math. Phys., 13, No. 3, 266, 1962.

9. Yakubenko, A. Ye.   Nekotoryye zadachy dvizheniya provodyashchey zhidkosti v ploskom kanale [Certain Aspects of the Flow of Conducting Fluid in a Flat Channel]. PMTF, No. 6, 7, 1963.

10. Regirer, S. A.   Techeniye vyazkoy provodyashchey zhidkosti v trubakh pri nalichii magnitnogo polya [Pipe Flow of Viscous Conducting Fluid in the Presence of a Magnetic Field]. Voprosy magnitnoy gidrodinamiki i dinamiki plazmy [Problems of Magnetohydrodynamics and of Plasma Dynamics], Vol. 2, Latvian Acad. Sci. Press, 1962.

11. Braginskiy, S. I.   K magnitnoy gidrodinamika slaboprovodyashchkih zhidkostey [Concerning the Magnetohydrodynamics of Weakly Conducting Fluids]. ZhETF, 37, No. 5, 1417, 1959.

12. Grinberg, G. A.   Ob ustanovivshemsya dvizhenii provodyashchey zhidkosti po trubam, nakhodyashchimsya v poperechnom magnitnom pole [Concerning the Steady Flow of a Conducting Fluid in Pipes Placed in a Transverse Magnetic Field]. ZhTF, 31, No. 1, 18, 1961.

13. Shercliff, J.A.   Steady Motion of Conducting Fluids in Pipes under Transverse Magnetic Fields, Proc. of the Cambridge Phil. Soc., 49, No. 1, 136, 1953.

14. Uflyand, Ya.S.   Ustanovivsheyesya techeniye elektroprovodyashchey zhidkosti v pryamougol'nom kanale pri nalichii poperechnogo magnitnogo polya [Steady Flow of Electrically Conducting Fluid in a Rectangular Channel in the Presence of a Transverse Magnetic Field], ZhTF, 30, No. 10, 1258, 1960.

15. Grinberg, G.A.   Ob ustanovivshemsya techenii provodyashchey zhidkosti po nakho-dyashcheysya vo vneshnem magnitnom pole pryamougol'noy trube s dvumya provo-dyashchimi i dvumya neprovodyashchimi stenkami [Concerning the Steady Flow of a Conducting Fluid in a Rectangular Tube with Two Conducting and Two Nonconduct-ing Walls, Placed in an External Magnetic Field], DAN SSSR, 141, No. 2, 330, 1961.

16. Grinberg, G.A.   O nekotorykh sluchayakh techeniya provodyashchey zhidkosti po trubakh pryamougol'nogo secheniya, nakhodyashchikhsya v magnitnom pole [Con-cerning Certain Cases of Flow of Fluids in Rectangular Tubes under a Magnetic Field], PMM, 25, No. 6, 1024, 1961 and 26, No. 1, 80, 1962.

17. Chang, C. and T. Lundgren.   Duct Flow in Magnetohydrodynamics, Zeitschrift für angewandte Math. Phys., 12, No. 2, 100, 1961.

18. Hunt, J.   Magnetohydrodynamic Flow in Rectangular Ducts, J. Fluid. Mech., 21, No. 4, 577, 1965.

19. Williams, W.   Magnetohydrodynamic Flow in a Rectangular Tube at High Hartmann Number, J. Fluid. Mech., 16, No. 2, 266, 1963.

20. Grinberg, G.A.   Ob ustanovivshemsya techenii vyazkoy provodyashchey zhidkosti po pryamolineynym trubam, nakhodyashchimsya v poperechnom vneshnem magni-tnom pole [Concerning the Steady Flow of Viscous Conducting Fluid in Straight Pipes under a Transverse External Magnetic Field], ZhTF 34, No. 10, 1721, 1964.

21. Berezin, O.A.   Ob ustanovivshemsya dvizhenii elektroprovodnoy zhidkosti v pryamo-ugol'nom kanale pri nalichii poperechenogo magnitnogo polya [Concerning the Steady Motion of an Electrically Conducting Fluid in a Rectangular Channel under a Transverse Magnetic Field], PMTF, No. 3, 155, 1963.

22. Tani, J.   Steady Flow of Conducting Fluids in Channels under Transverse Magnetic Fields, with Consideration of Hall Effect, J. Aero Space Sci., 29, No. 3, 297, 1962.

23. Ryabinin, A.G. and A.I. Khozhainov.   Ustanovivsheyesya laminarnoye techeniye elektroprovodyashchey zhidkosti v pryamougol'noy trube pod deystviyem pondero-motornykh sil [Steady State Laminar Flow of an Electrically Conducting Fluid in a Rectangular Tube under the Action of Ponderomotive Forces], ZhTF, 32, No. 1, 15, 1962. [Translated in Soviet Physics - Technical Physics, Vol. 7, No. 1 (1962)].

24. Khozhainov, A.I.   Koeffitsiyent soprotivleniya magnitogidrodinamicheskikh potokov v kanalakh pryamougol'nogo secheniya s proizvol'nym otnosheniyem storon [Fric-tion Factor for Magnetohydrodynamic Flows in Rectangular Channels with Arbitrary Aspect Ratio]. Trudy nauchno-tekhnicheskoy konferentsii VVMIOLU im. F.E. Dzerzhinskiy [Proceedings of the F.E. Dzerzhinskiy], Vol. 2, 1965.

25. Uflyand, Ya.S.   Zadacha Gartmana dlya krugloy truby [The Hartmann Problem for a Circular Pipe], ZhTF, 30, No. 10, 1258, 1960.

26. Yakubenko, A.Ye.   Statsionarnoye dvizheniye vyazkoy neszhimayemoy zhidkosti po trubam v odnorodnom i neodnorodnom magnitnykh polyakh [Steady State Motion of Viscous Incompressible Fluid in Pipes in Homogeneous and Inhomogeneous Mag-netic Fields], Izvestiya AN SSSR, Mekhanika mashin, No. 1, 90, 1961.

27. Gold, R.   Magnetohydrodynamic Pipe Flow, p. 1, J. Fluid. Mech., 13, No. 4, 505, 1962.

28. Ihara, S., A. Matsushima, K. Tadzima and I. Osima.   Va seda daygaku rikogaku kenkyuse hokoku. Bull. Sci. and Eng. Res. Lab., Waseda University, 22, No. 1, 1963.

29. Fishman, F. Steady Magnetohydrodynamic Flow through a Channel of Circular Section, Advanced Energy Convers., 4, No. 1, 1, 1964.
30. Shercliff, J. The Flow of Conducting Fluids in Circular Pipes under Transverse Magnetic Fields, J. Fluid. Mech., No. 1, 644, 1956.
31. Shercliff, J. Magnetohydrodynamic Pipe Flow, p.r., High Hartmann Number, J. Fluid. Mech., 13, No. 4, 513, 1962.
32. Yakubenko, A. Ye. Nekotoryye resheniya uravneniy ustanovivshegosya techeniya neszhimayemoy, vyazkoy i elektroprovodyashchey zhidkosti [Certain Solutions of Equations of Steady Flow of Incompressible, Viscous and Electrically Conducting Fluid]. PMTF, No. 2, 73, 1963.
33. Vatazhin, A. B. O techenii v diffuzore v prisustvii magnitnogo polya [Diffuser Flow in the Presence of a Magnetic Field]. PMM, 24, No. 3, 524, 1960.
34. Kukin, I. K. and G. G. Smolin. Nekotoryye zadachi dvumernogo techeniya neszhimayemoy zhidkosti v kanale pri nalichii elektricheskogo i magnitnogo poley [Certain Problems of Two-Dimensional Channel Flow of an Incompressible Fluid in the Presence of an Electrical and a Magnetic Field]. Magnitnaya gidrodinamika, No. 1, 43, 1965.
35. Shercliff, J. Entry of Conducting and Nonconducting Fluids in Pipes, Proc. of the Cambridge Phil. Soc., 52, No. 3, 573, 1956.
36. Yakubenko, A. Ye. Zadacha o vkhode provodyashchey zhidkosti v ploskiy kanal [Entry of Conducting Fluids into Rectangular Channels]. Izvestiya AN SSSR, mekhanika mashin, No. 6, 12, 1963.
37. Roidt, M. and R. D. Cess. An Approximate Analysis of Laminar Magnetohydrodynamic Flow in the Entrance Region of a Flat Duct. Transactions of ASME - Journal of Applied Mechanics, No. 1, 1962.
38. Ching-Lai, H. and F. Liang Tseng. A Finite Difference Analysis of Laminar Magnetohydrodynamic Flow in the Entrance Region of a Flat Rectangular Duct, Applied Sci. Res., B 10, No. 3-4, 329, 1963.
39. Rossow, V. On Flow of Electrically Conducting Fluids over a Flat in the Presence of a Transverse Magnetic Field, NACA, TN 3971, 1957.
40. Yen, K. Incompressible Wedge Flows of an Electrically Conducting Viscous Fluid in the Presence of a Magnetic Field, J. Aero Space Sci., 27, No. 1, 74, 1960.
41. Gershuni, G. Z. and Ye. M. Zhukhovitskiy. Obtekaniye shara provodyashchey zhidkost'yu pri nalichii sil'nogo magnitnogo polya [Flow of a Conducting Fluid around a Sphere in a Strong Magnetic Field]. ZhTF, 30, No. 8, 925, 1960.
42. Kalis, Kh. E., A. B. Tsinober, A. G. Shtern and E. V. Shcherbinin. Obtekaniye kruglogo tsylindra elektroprovodyashchey zhidkost'yu v poperechenom magnitnom pole [Flow of an Electrically Conducting Fluid around a Circular Cylinder in a Transverse Magnetic Field]. Magnitnaya gidrodinamika, No. 1, 18, 1965.
43. Stuart, J. On the Stability of Viscous Flow between Parallel Planes in the Presence of a Coplanar Magnetic Field, Proc. Roy. Soc., A 221, 189, 1954.
44. Lock, R. The Stability of the Flow of an Electrically Conducting Fluid between Parallel Planes under a Transverse Magnetic Field, Proc. Roy. Soc., A 233, 105, 1955.
45. Velikhov, Ye. P. Ustoychivost' ploskogo puazeyleva techeniya ideal'noprovodyashchey zhidkosti v prodol'nom magnitnom pole [Stability of Two-Dimensional Poiseulle Flow of an Ideally Conducting Fluid in a Longitudinal Magnetic Field]. ZhETF, 36, No. 4, 1192, 1959.
46. Pavlov, K. V. and Yu. A. Tarasov. Ob ustoychivosti techeniya vyazkoy provodyashchey zhidkosti mezhdu parallelnymi ploskostyami v poperechnom magnitnom pole [Concerning the Flow Stability of a Viscous Conducting Fluid between Parallel Planes in a Transverse Magnetic Field]. PMM, 24, No. 4, 723, 1960.

47. Arkhipov, V. N.   Vliyaniye magnitnogo polya na ustoychivost' techeniya v pogranichnom sloye [Effect of a Magnetic Field on the Flow Stability in a Magnetic Field].   DAN SSSR, 129, No. 4, 751, 1959.

48. Pavlov, K. V.   Ob ustoychivosti ploskogo techeniya Kuetta v prisustvii magnitnogo polya [On the Stability of Two-Dimensional Couette Flow in the Presence of a Magnetic Field].   Voprosy magnitnoy gidrodinamiki i dinamiki plazmy (see [10]), Vol. 2, Latvian SSR Acad. Sci. Press, 1962.

49. Dyer, R. and D. Edmunds.   On the Stability of Magnetohydrodynamic Flow in a Curved Channel, Quart. J. Mech. and Appl. Math., 15, No. 3, 377, 1962.

50. Batchelor, G.   On the Spontaneous Magnetic Field in a Conducting Liquid in Turbulent Motion, Proc. Roy. Soc., A 201, 405, 1950.

51. Chandrasekhar, S.   The Invariant Theory of Isotropic Turbulence in Magnetohydrodynamics, Proc. Roy. Soc., p. 1, A 204, 435, 1950; p. 2, A 207, 301, 1951.

52. Harris, L. P.   Hydromagnetic Channel Flows.   John Wiley & Sons and the MIT Press, 1960.

53. Ryabinin, A. G. and A. I. Khozhainov.   Turbulentnoye techeniye elektroprovodyashchey zhidkosti v trubakh pryamougol'noye secheniya pod deystviyem elektrodinamicheskikh ponderomotornykh sil [Turbulent Flow of an Electrically Conducting Fluid in the Rectangular Pipes under the Action of Electrodynamic Ponderomotive Forces]. ZhTF, 33, No. 1, 80, 1963.

54. Branover, G. G.   Poluempiricheskaya teoriya turbulentnogo potoka zhidkogo metalla v poperechnom magnitnom pole [A Semiempirical Theory of Turbulent Flow of Liquid Metal in a Transverse Magnetic Field].   Prikladnaya magnitogidrodinamika [Applied Magnetohydrodynamics].   Trudy instituta fiziki AN Latv. SSR [Proceedings of the Physics Institute of the Latvian SSR Acad. Sci.], No. 12, 167, 1961.

55. Vulis, L. A. and B. A. Fomenko.   O perekhodnykh rezhimakh techeniya v magnitnoy gidrodinamike [Concerning Transient Magnetohydrodynamics Flows].   Magnitnaya gidrodinamika, No. 1, 74, 1966.

56. Kapur, D. and R. Dzhayn.   Magnitnogidrodinamicheskoye turbulentnoye techeniye mezhdu parallelnymi plastinkami [Turbulent Magnetohydrodynamic Flow between Parallel Plates].   In the book: L. Harris.   Magnitogidrodinamicheskoye techeniye v kanalakh [Collection of Translated Short Monographs and Articles with [52] as the Leading Item].   Foreign Literature Publishing House, Moscow, 1963.

57. Levin, V. B.   O stabiliziruyushchem vliyanii prodol'nogo magnitnogo polya na neodnorodnyye turbulentnyye techeniya [Stabilization of Inhomogeneous Turbulent Flows by a Longitudinal Magnetic Field].   Magnitnaya gidrodinamika, No. 2, 3, 1965.

58. Kovner, D. S.   Ispol'zovaniye gipotezy lokal'nosti v turbulentnom techenii elektroprovodyashchey zhidkosti v magnitnom pole [Using the Theory of Local Similarity (Theory of Universal Equilibrium) in Turbulent Flow of Electrically Conducting Fluids in a Magnetic Field].   Magnitnaya gidrodinamika, No. 2, 11, 1965.

59. Kovner, D. S. and V. B. Levin.   O turbulentnom techenii elektroprovodnoy zhidkosti v trube v prodol'nom magnitnom pole [Concerning the Turbulent Pipe Flow of an Electrically Conducting Fluid in a Longitudinal Magnetic Field].   TVT, 2, No. 5, 742, 1964.

60. Kruger, C. H. and O. K. Sonju.   On the Turbulent Magnetohydrodynamic Boundary Layer, Proc. 1964.   Heat Transfer and Fluid Mech. Inst. Berkeley, Calif., Standord Univ. Press, 1964.

61. Napolitano, L.   On Turbulent Magneto-Fluid Dynamic Boundary Layers, Revs. Mod. Phys., 32, No. 4, 785, 1960.

62. Sharikadze, D. V.   Ustanovivshiyesya techeniya vyazkoy provodyashchey zhidkosti po poristym trubam postoyannogo secheniya [Steady-State Flows of Viscous Conducting Fluids in Porous Constant Cross Section Pipes].   Trudy Tbiliskogo gos. un-ta [Proceedings of the Tbilisi State University], Vol. 102, 1964.

63. Nigam, S. and S. Singh. Heat Transfer by Laminar Flow between Parallel Plates under the Action of Transverse Magnetic Field, J. Mech. Appl. Math., 13, No. 1, 85, 1960.

64. Yen, J. Effect of Wall Electrical Conductance on Magnetohydrodynamic Heat Transfer in a Channel, Paper, Amer. Soc. Mech. Eng., WA-171, 7, 1962.

65. Gramer, K. Joule Heating in Magnetohydrodynamic Free Convection Flows, J. Aero Space Sci., 29, No. 6, 746, 1962.

66. Regirer, S. A. Neustanovivsheyesya techeniye elektroprovodnoy zhidkosti v prisustvii magnitnogo polya [Unsteady Flow of Electrically Conducting Fluids in a Magnetic Field]. IFZh., 2, No. 8, 43, 1959.

67. Caratoiu, M. Sur le mouvement lent d'un fluide visqueux conducteur entre deux plans paralleles. C. R. Acad. Sci., Paris, 249, No. 14, 1192, 1959.

68. Chekmarev, L. B. Nestatsionarnoye techeniye provodyashchev zhidkosti v ploskom kanale pri nalichii poperechnego magnitnogo polya [Unsteady Flow of Conducting Fluids in a Flat Channel in a Transverse Magnetic Field]. ZhTF, 30, 3, 338, 1960.

69. Uflyand, Ya. S. and L. B. Chekmarev. Issledovaniye neustanovivshegosya techeniya provodyashchey zhidkosti v ploskom kanale s dvizhushchimisya granitsami [A Study of Unsteady Flow of Conducting Fluids in a Flat Channel with Moving Boundaries]. ZhTF, 30, No. 5, 465, 1960.

70. Chekmarev, I. B. Nekotoryye osobennosti perekhodnykh rezhimov v magnitnoy gidrodinamike [Certain Features of Transient Magnetohydrodynamic Flows]. Trudy LPI im M. I. Kalinina, [Proceedings of the M. I. Kalinin Leningrad Polytechnic Institute], 217, 102, 1961.

71. Ogawa, B. A. and J. Sone. On the Commencement of the Hartmann Flow of Conducting Fluid, J. Phys. Soc. of Japan, 16, No. 7, 1423, 1961.

72. Lungren, T. S., B. H. Atabek and C. Chang. Transient Magnetohydrodynamic Duct Flow, Phys. of Fluids, 4, No. 7, 1006, 1961.

73. Grausse, E., R. Causse and J. Poirier. Mise en vitesse entre plans paralleles indefinis d'un liquide électroconducteur soumis à un champ magnétique transversal, C. R. Acad. Sci., Paris, 254, No. 2, 216, 1962.

74. Tao, L. N. On Transient Magnetohydrodynamic Flow in Channels, J. AIAA, 1, No. 2, 461, 1963.

75. Grausse, E., J. Poirier and C. Vives. Étude théorique du mouvement oscillatoir, libre entre deux plans verticaux paralleles et indefinis d'une colonne de liquide pesant, visqueux et électroconducteur en presence d'un champ magnétique, C. R. Acad. Sci., Paris, 256, No. 4, 886, 1963.

76. Ryabinin, A. G. and A. I. Khozhainov. Issledovaniye nestatsionarnogo techeniya provodyashchey zhidkosti v magnitogidrodinamicheskikh kanalakh [A Study of Unsteady Flow of Conducting Fluids in Magnetohydrodynamic Channels]. ZhTF, 37, No. 2, 1967.

77. Patrashev, A. N., A. G. Ryabinin and A. I. Khozhainov. Nestatsionarnyye techeniya provodyashchey zhidkosti v magnitogidrodinamicheskikh kanalakh pri malykh magnitnykh chislakh Reynoldsa [Unsteady Flows of Conducting Fluids in Magnetohydrodynamic Channels with Low Reynolds Numbers]. Trudy 5-go Rizhskogo soveshchaniya po magnitnoy gidrodinamike, MGD-generatory [Proceedings of the 5th Riga Conference on Magnetohydrodynamics, MHD Generators]. Latvian USSR Acad. Sci. Press, 1966.

78. Regirer, S. A. Laminarnyye techeniya provodyashchey zhidkosti v trubakh i kanalakh pri nalichii magnitnogo polya [Laminar Flows of Conducting Fluids in Pipes and Channels in the Presence of a Magnetic Field]. Magnitnaya gidrodinamika, No. 1, 5, 1965.

79. Kirko, I. M.   Issledovaniye elektromagnitnykh yavleniy v metallakh metodom razmernosti i podobiya [A Study of Electromagnetic Phenomena in Metals by Dimensional Analysis and Similitude].   Latvian SSR Acad. Sci. Press, 1959.

80. Povkh, I. L.   Tekhnicheskaya gidromekhanika [Engineering Hydromechanics].   Mashinostroyeniye Press, 1964.

Experimental Magnetohydrodynamics

81. Hartmann, J. and F. Lazarus.   Experimental Investigations on the Flow of Mercury in a Homogeneous Magnetic Field.   Hg.-Dynamics, Kgl. Danske Videnskab. Selskab. Mat.-fys. Medd. 15, No. 7, 1937.

82. Khvol'son, O. D.   Kurs fiziki [A Course in Physics], Vol. 4, Petrograd, 1915.

83. Murgatroyd, W.   Experiments on Magnetohydrodynamic Channel Flow, The Philosophical Magazine, 44, No. 359, 1346, 1953.

84. Lehnert, B.   Eksperimental'noye issledovaniye nelaminarnogo techeniya rtuti v magnitnom pole [An Experimental Study of Nonlaminar Flow of Mercury in a Magnetic Field].   In the book: L. Harris, Magnitogidrodinamicheskiye techeniya v kanalakh (see [56]).

85. Shercliff, J.   The Flow of Conducting Fluids in Circular Pipes under Transverse Magnetic Fields, J. Fluid Mech., No. 1, 644, 1956.

86. Grausse, E. and J. Poirier.   On Laminar Flow of an Electrically Conducting Liquid Subjected to a Transverse Magnetic Field, C.R. Acad. Sci., Paris, 244, 2694, 1957.

87. Globe, S.   The Suppression of Turbulence in Pipe Flow of Mercury by an Axial Magnetic Flow, Heat Transfer and Fluid Mechanics Inst., Los Angeles, 1959.

88. Prikladnaya magnitnaya gidrodinamika [Applied Magnetohydrodynamics], Trudy in-ta fiziki AN Latv. SSR [Proceedings of the Physics Institute of the Latvian SSR Academy of Sciences], No. 12, 1961.

89. Voprosy magnitnoy gidrodinamiki i dinamiki plazmy [Problems of Magnetohydrodynamics and of Plasma Dynamics], Vol. 2, Latvian SSR Acad. Sci. Press, 1962.

90. Voprosy magnitnoy gidrodinamiki [Problems of Magnetohydrodynamics], Vol. 3, Latvian SSR Acad. Sci. Press, 1963.

91. Liyelausis, O.A.   Vliyaniye elektromagnitnykh sil na techeniye zhidkikh metallov i elektrolitov [Effect of Magnetic Forces on the Flow of Liquid Metals and Electrolytes].   Author's abstract of Candidate Dissertation, MIFI [Moscow Engineering and Physics Institute], 1961.

92. Branover, G.G.   O gidravlike turbulentnykh potokov zhidkogo metalla v prisutstvii poperechnogo magnitnogo polya [The Hydraulics of Turbulent Liquid Metal Flows in the Presence of a Transverse Magnetic Field].   Author's abstract of Candidate Dissertation MAI [Moscow Order of Lenin Sergo Ordzhonikidze Aviation Institute], 1961.

93. Tsinober, A.B.   Obtekaniye tel zhidkikh metallov v poperechnom magnitnom pole [Flow of Liquid Metals around Bodies in a Transverse Magnetic Field].   Author's abstract of Candidate Dissertation.   Latvian SSR Acad. Sci. Press, 1964.

94. Kirko, I.M.   Zhidkiy metal v magnitnom pole [Liquid Metals in a Magnetic Field].   Energiya Press, 1964.

95. Branover, G.G. and O.A. Liyelausis.   Osobennosti vliyaniya poperechnogo magnitnogo polya na turbulentnyye techeniya zhidkogo metalla pri razlichnykh chislakh Reynol'dsa [Peculiarities of the Effect of a Transverse Magnetic Field on Turbulent Flow of Liquid Metal with Different Reynolds Numbers].   ZhTF, 35, No. 2, 235, 1965.

96. Dukure, R.K.   Vliyaniye otnositel'noy sherokhovatosti na techeniye elektroprovodyashchey zhidkosti v prisutstvii magnitnogo polya [Effect of Relative Roughness on the Flow of an Electrically Conducting Fluid in a Magnetic Field].   Magnitnaya gidrodinamika, No. 1, 29, 1965.

97. Branover, G.G., I.M. Kirko and O.A. Liyelausis. Eksperimenta'noye
izucheniye vliyaniya poperechenogo magnitnogo polya na raspredeleniye
skorostey v potoke rtuti [An Experimental Study of the Effect of a Magnetic
Field on the Velocity Distribution in a Flow of Mercury]. Prikladnaya mag-
nitogidrodinamika [Applied Magnetohydrodynamics], Trudy in-ta fiziki AN
Latv. SSR [Proceedings of the Physics Institute of Latvian SSR Acad. Sci.],
No. 2, 167, 1962.

98. Branover, G.G. and O.A. Liyelausis. Nekotoryye rezul'taty eksperimental'nogo
issledovaniya turbulentnogo potoka zhidkogo metalla v poperechnom magnitnom
pole [Certain Results of an Experimental Study of Turbulent Liquid Metal Flow
in a Transverse Magnetic Field]. Voprosy magnitnoy gidrodinamiki i dinamiki
plazmy, (see [89]), Vol. 2, Latvian SSR Acad. Sci. Press, 1963.

99. Tsinober, A.B. Voprosy vliyaniya magnitnogo polya na obtekaniye tel [Problems
of the Effect of the Magnetic Field on Flow about Bodies]. Voprosy magnitnoy
gidrodinamiki (see [90]), Vol. 3, Latvian SSR Acad. Sci. Press, 1963.

100. Dukure, R.K. and O.A. Liyelausis. Eksperimental'noye izucheniye vliyaniya
elektromagnitnykh sil na obtekaniye tel elektrolitom [Experimental Study of the
Effect of Electromagnetic Forces on the Flow of Electrolytes about Bodies].
Voprosy magnitnoy gidrodinamiki i dinamiki plazmy (see [89]), Vol. 2, Latvian
SSR Acad. Sci. Press, 1962.

101. Bronillette, E.C. and P.S. Lykoudis. Measurements of Skin Friction for Tur-
bulent Magneto Fluid Mechanics Channel Flow, Purdue Univ. Lafayette, Ind.
August, 1962.

102. Grausse, E. and P. Cachon. Actions électromagnétiques sur les liquides en
mouvement, notamment dans la couche limite d'obstacles immerges. C.R.
Acad. Sci., Paris, 238, No. 26, 2488, 1954.

103. Kuznetsov, I.L. Eksperimental'noye izucheniye vliyaniya elektromagnitnogo
polya na obtekaniye tsilindra [An Experimental Study of the Effect of an Electro-
magnetic Field on the Flow about a Cylinder]. ZhTF, 30, No. 9, 1041, 1960.

104. Poirier, J. Contribution à l'étude expérimentale de la magnetodynamique des
liquides, Publs. Sci. Univ. Algar, B 6, No. 1, 1960.

105. Kalis, Kh.E., A.B. Tsinober, A.G. Shtern and E.V. Shcherbinin. Obtekaniye
kruglogo tsilindra elektroprovodyashchey zhidkost'yu v poperechnom magnitnom
pole [Flow of Electrically Conducting Fluids about a Circular Cylinder in a
Transverse Magnetic Field]. Magnitnaya gidrodinamika, No. 1, 18, 1965.

106. Turchin, N.M. Vliyaniye provodimosti stenki na soprotivleniye zhidkogo metalla
v krugloy trube v magnitnom pole [Effect of Wall Conductivity on the Resistance
of Liquid Metal in a Circular Pipe in a Magnetic Field]. TVT, 1, No. 1, 118,
1963.

107. Jackson, W. and J. Ellis. Friction Factor Measurements in Liquid MHD Chan-
nel Flows. Proceedings of Fifth Symposium on the Engineering Aspects of Mag-
netohydrodynamics, Sponsored by Massachusetts Inst. of Technology, April 1-2,
1964.

108. Kovner, D.S. and Ye. Yu. Krasil'nikov. Eksperimental'noye issledovaniye tur-
bulentnogo techeniya elektroprovodnoy zhidkosti v trube v prodol'nom magnitnom
pole [An Experimental Study of Turbulent Flow of Electrically Conducting Fluids
in a Pipe in a Longitudinal Magnetic Field]. DAN SSSR, 163, No. 5, 1096, 1965.

109. Genin, L.G. and V.G. Zhilin. Vliyaniye prodol'nogo magnitnogo polya na koef-
fitsiyent soprotivleniya pri techenii rtuti v krugloy trube [Effect of a Longitudinal
Magnetic Field on the Friction Factor in the Flow of Mercury in a Magnetic
Field]. TVT, 4, No. 2, 233, 1966.

110. Khozhainov, A.I. Statsionarnoye techeniye zhidkogo metalla v magnitogidrodina-
micheskom kanale pryamougol'nogo secheniya [Steady State Flow of Liquid Metal
in a Rectangular Magnetohydrodynamic Channel]. Izvestiya AN SSSR, mekhanika
zhidkostey i gazov, No. 4, 114, 1966.

111. Khozhainov, A.I. Turbulentnoye techeniye zhidkogo metalla v magnitogidrodinami-cheskikh kanalakh kruglogo secheniya [Turbulent Flow of Liquid Metals in Circular Magnetohydrodynamic Channels]. ZhTF, 36, No. 1, 147, 1966.

112. Lykoudis, P.S. Experimental Studies for the Determination of Transport Properties in the Presence of a Magnetic Field for a Conducting Medium Flowing Turbulently. Report to the Moscow International Symposium on Properties and Use of Low Temperature Plasma. VINITI Press, 1965.

113. Bolonov, N.I., B.A. Kolovandin, I.L. Povkh and Ye. F. Skrinnik. Issledovaniye struktury magnitogidrodinamicheskikh potokov induktsionnym anemometrom [A Study of the Structure of Magnetohydrodynamic Flows Using an Induction Anemometer]. Izvestiya vuzov, Energetika, No. 1, 65, 1966.

114. Grausse, E., R. Causse and J. Poirier. Étude expérimentale de la mise en régime turbulent, dans un tube de section rectangulaire, d'un liquide électroconducteur en présence d'un champ magnétique, C.R. Acad. Sci., Paris, 255, 10, 1962.

115. Grausse, E., R. Causse and J. Poirier. Étude expérimentale de la mise en vitesse laminaire ou turbulente dans un tube de section circulaire d'un liquide électroconducteur, en présence d'un champ magnétique transversal, C.R. Acad. Sci., Paris, 256, No. 24, 5055, 1963.

Magnetohydrodynamic Devices and Sy   .ns

116. Faraday, M. Experimental Researches in Electricity. London, Quaritch, 1839-55.

117. Smith, C.G. and J. Slepian. Electromagnetic Ship's Log, U.S. Patent 1?49530, Dec. 1917.

118. Chubb, L. Vacuum Pump, U.S. Patent 1928664, Dec. 1919.

119. Tryapitsyn, P. Ye. Elektricheskiy nasos dlya pod"yema metallov, makhodyash-chikhsya v zhidkom sostoyanii, i elektrolitov [An Electric Pump for Raising Liquid Metals and Electrolytes]. Patent 6574, 1927.

120. Einstein, A. and L. Szillard. Pump Especially for Refrigerating Machines, U.S. Patent 344881. March 1931.

121. Williams, E.J. The Induction of E.M.Fs. sin a Moving Liquid by a Magnetic Field and Its Application to an Investigation of the Flow of Liquids, Proc. Phys. Soc., 42, 466, 1930.

122. Kolbasko, Ye. I. Nasos dlya tokoprovodyashchikh zhidkostey [A Pump for Current-Conducting Fluids]. Author's certificate 42798, 1934.

123. Shkolin, I.D. Induktsionnyy nasos dlya rtuti [An Induction Pump for Mercury]. Author's certificate 45351, 1935.

124. Cage, J.F. and E.H. Schoch. Description and Test Results of a 400-GPM Liquid Metal Induction Pump. KAPL, AECD-3459, Technical Information Service, Oak Ridge, Tennessee, 1951.

125. Collins, G.D. Operation and Analysis of a 100-PSI Electromagnetic Pump KAPL-668 Technical Information Service, Oak Ridge, Tennessee, 1952.

126. Cage, J. Electromagnetic Pumps for High Temperature Liquid Metals, Mech. Eng., 75, No. 6, 467, 1953.

127. Woollen, W. Electromagnetic Pumps for Reactors, Nuclear Power, 2, No. 15, 267, 1957.

128. United States Atomic Energy Commission. Reactor Handbook. Vol. 2. Engineering. Washington, D.C. 1955.

129. Ageykin, D.I., B. Ye. Galkin and A.A. Desova. Printsip deystviya i ekvivalent-naya skhema elektromagnitnogo raskhodomera [The Operating Principle and Equivalent Circuit of an Electromagnetic Flowmeter]. VINITI [All-Union Institute of Scientific and Technical Information], 1967.

130. Ageykin, D. I., Ye. N. Kostina and P. N. Kuznetsova. Datchiki sistem avtomati-
cheskogo kontrolya i regulirovaniya [Sensors of Automatic Control and Monitor-
ing Systems]. Mashgiz Press, 1959.

131. Nikitin, B. I., I. D. Vel't and V. K. Rukovishnikova. Induktsionnyye raskhodo-
mery tipa RI [RI-Type Induction Flowmeters]. Teploenergeticheskiye i
khimiko-tekhnologicheskiye pribory i regulyatory [Heat-Power and Chemical-
Process Instruments and Control Devices], Mashgiz, 1961.

132. Nikitin, B. I. Razrabotka normal'nogo ryada induktsionnykh raskhodomerov
[Development of a Standard Series of Induction Flowmeters]. Pribory i
sredstva avtomatizatsii, No. 7, 429, 1962.

133. Bogdanenko, A. L., E. G. Zvenigorodskiy and B. I. Nikitin. Ispol'zovaniya
nekotorykh MGD-vzaimodeystviy dlya kontrolya raskhoda zhidkikh metallov v
truboprovodakh [Utilization of Certain MHD Effects for Monitoring the Flow of
Liquid Metals in Pipelines]. Tekhnicheskaya elektromagnitnaya gidrodinamika
[Engineering Magnetohydrodynamics]. Vol. 3, Metallurgiya Press, 1967.

134. Kirillov, P. L., V. D. Kolesnikov, V. A. Kuznetsov and N. M. Turchin.
Atomnaya energiya, 9, No. 3, 173, 1960.

135. Leypunskiy, A. I. Proceedings of the 2nd International Conference on the Peace-
ful Use of Atomic Energy, Geneva 1958. Reports of Soviet Scientists, Vol. 2
Nuclear Reactors and Nuclear Energetics. Atomizdat Press, 1959.

136. Elektromagnitnyy izmeritel' techeniy GM-15 [The GM-15 Electromagnetic Sea
Current Meter]. Gidrometeoizdat Press, 1963.

137. Sysoyev, I. N. Apparatura i metody izmereniya techeniy v okeanakh i moryakh
[Apparatus and Methods of Measuring Ocean and Sea Currents]. Byulleten'
okeanograficheskoy komissii, No. 2, 47, 1958.

138. Mikhaylov, Yu. M. Primeneniye elektromagnitnogo metoda k izmereniyu skorosti
morskikh techeniy na raznykh glubinakh [The Use of the Electromagnetic Method
for Measuring Sea Current Velocities at Different Depths]. Trudy Gos. okeano-
graficheskogo in-ta, No. 40, 47, 1957.

139. Kolin, A. Principle of Electromagnetic Flowmeter without External Magnet,
J. Appl. Phys., 27, No. 8, 965, 1956.

140. Kolin, A. Alternating Field Induction Flowmeter of High Sensitivity, Rev. Sci.,
Instr., No. 16, 5, 1945.

141. Kolin, A. A Method for Adjustment of the Zero Setting of an Electromagnetic
Flowmeter without Interruption of the Flow, Rev. Sci. Instr., No. 24, 178,
1953.

142. Shercliff, J. The theory of the D. C. Electromagnetic Flowmeter for Liquid
Metals, A. E. R. E., X/R, 1052, 1953.

143. Shercliff, J. Relation between the Velocity Profile and the Sensitivity of Electro-
magnetic Flowmeters, J. Appl. Physics, 25, 6, 817, 1954.

144. Shercliff, J. Edge Effects in Electromagnetic Flowmeters, J. Nuclear Energy,
1, No. 3, 305, 1956.

145. Vatazhin, A. B. Magnitogidrodinamicheskoye techeniye v ploskom kanale s konech-
nymi elektrodami [Magnetohydrodynamic Flow in a Flat Channel with Finite Elec-
trodes]. Izvestiya AN SSSR. Seriya mashinostroyeniye, No. 1, 52, 1962.

146. Shercliff, J. A. Theory of Electromagnetic Flow Measurement. Cambridge Uni-
versity Press, New York, 1962.

147. Korsunskiy, L. M. Elektromagnitnyye gidrometricheskiye pribory [Electromag-
netic Hydrometric Instruments]. Published by the State Committee on Standards,
Measures and Measuring Devices. Moscow, 1964.

148. Turchin, I. M. Magnitnyye raskhodomery [Magnetic Flowmeters]. Magnitnaya
gidrodinamika, No. 1, 147, 1965.

149. Holdaway, H. W. A Note on Electromagnetic Flowmeters of Rectangular Cross
Section, Helv. Phys. Acta, 30, No. 1, 85, 1957.

209

150. Gold, R. Magnetohydrodynamic Pipe Flow, p. 1, J. Fluid. Mech., 13, No. 4, 505, 1962.

151. Gushchin, G. I. and N. I. Loginov. Elektromagnitnyye raskhodomery s osesimmetricheskoy formoy kanala dlya zhidkometallicheskikh teplonositeley [Electromagnetic Flowmeters with Axisymmetric Channels for Liquid Metal Coolants]. Voprosy magnitnoy gidrodinamiki (see [90]), Vol. 3, Latvian SSR Acad. Sci. Press, 1963.

152. Nikitin, B. I., I. D. Vel't and V. I. Petrushaytis. Induktsionnyye raskhodomery znrubezhnykh firm [Induction Flowmeters of Foreign Manufacture]. Pribory i sredstva avtomatizatsii, No. 7, 441, 1962.

153. Kremlevskiy, P. P. Raskhodomery [Flowmeters]. Mashgiz Press, 1963.

154. Regirer, S. A. O vliyanii pogranichnogo sloya na raspredeleniye toka pri techenii provodyashchey zhidkosti po kanalu [Concerning the Effect of the Boundary Layer on the Current Distribution in Channel Flow of Conducting Fluids]. Voprosy magnitnoy gidrodinamiki (see [90]), Vol. 3, Latvian SSR Acad. Sci. Press, 1963.

155. Barnes, A. H. Direct Current Electromagnetic Pumps, Nucleonics, No. 11, 16, 1953.

156. Barnes, A. H. Pumping of Liquid Metals, Proc. of the International Conference on the Peaceful Use of Atomic Energy, Geneva, August, P 121, No. 9, 319, 1955.

157. Blake, L. R. Conduction and Induction Pump for Liquid Metals. Proc. of the Inst. Elec. Eng., 104A, No. 13, 49, 1957.

158. Blake, L. R. Electromagnetic Pump for Liquid Metals, Reactor Technol., No. 1, 65, 1959.

159. Blake, L. R. A Theoretical Survey of the Electromagnetic Pumps for Liquid Metals, A. E. R. E., X/PR, 2115, 1951, 1959.

160. Watt, D. A. A Study in Design of Traveling Field Electromagnetic Pumps for Liquid Metals, A. E. R. E., ED/R, 1696, 1955.

161. Watt, D. A. Electromagnetic Pumps for Liquid Metals, Engineering, 181, 4703, 264, 1956.

162. Vol'dek, A. I. O nekotorykh voprosakh proyektirovaniya lineynykh induktsionnykh nasosov [Certain Problems in Designing Linear Induction Pumps]. Voprosy magnitnoy gidrodinamiki i dinamiki plazmy (see [89]), Vol. 1, Latvian SSR Acad. Sci. Press, 1959.

163. Vol'dek, A. I. Toki i usiliya v sloye zhidkogo metalla ploskikh induktsionnykh nasosov [Currents and Forces in a Liquid Metal Sheet of Flat Induction Pumps]. Izvestiya VUZ, Elektromekhanika, No. 1, 3, 1959 (see also No. 5, 3, 1960, No. 6, 587, 1962 and No. 8, 839, 1962).

164. Vol'dek, A. I. Elektromagnitnyye nasosy dlya zhidkikh metallov [Electromagnetic Pumps for Liquid Metals]. Elektrichestvo, No. 5, 22, 1960.

165. Vol'dek, A. I. Sostoyaniye i zadachi po razrabotke induktsionnykh nasosov [The State and Problems in Development of Induction Pumps]. In the collection: Issledovaniye i proyektirovaniye induktsionnykh nasosov dlya transporta zhidkikh metallov [Study and Design of Induction Pumps for Transporting Liquid Metals]. Seriya A, 197, Tallin Polytechnic Institute Press, 1962.

166. Vol'dek, A. I. and Kh. I. Yanes. Poperechnyy krayevoy effekt v ploskikh induktsionnykh nasosakh pri kanale zhidkogo metalla s provodyashchimi stenkami [Transverse Fringing in Flat Induction Pumps Having a Liquid Metal Duct with Conducting Walls]. Voprosy magnitnoy gidrodinamiki i dinamiki plazmy (see [89], Vol. 2, Latvian SSR Acad. Sci. Press, 1962.

167. Vol'dek, A. I. Toki i usiliya v sloye zhidkogo metalla tsylindricheskikh induktsionnykh nasosov [Currents and Forces in a Liquid Metal Sheet of Annular Induction Pumps]. Izvestiya VUZ, Elektromekhanika, No. 6, 687, 1962.

168. Kirko, I. M. Issledovaniye elektromagnitnykh yavleniy v metallakh metodom razmernosti i podobiya [Study of Electromagnetic Phenomena in Metals by Dimensional Analysis and Similarity Methods]. Latvian SSR Acad. Sci. Press, 1959.

169. Kirko, I. M. Zhidkiy metal v magnitnom pole [Liquid Metal in a Magnetic Field]. Energiya Press, 1964.

170. Tyutin, I. A. Elektromagnitnyye nasosy dlya zhidkikh metallov [Electromagnetic Pumps for Liquid Metals]. Latvian SSR Acad. Sci. Press, 1959.

171. Tyutin, I. A. Mekhanicheskiye sily v begushchem elektromagnitnom pole [Mechanical Forces in Traveling Magnetic Fields]. Voprosy energetiki [Problems of Energetics], No. 3. Latvian SSR Acad. Sci. Press, 1955.

172. Tyutin, I. A. and E. K. Yankop. Elektromagnitnyye protsessy v induktsionnykh nasosakh dlya zhidkogo metalla [Electromagnetic Processes in Induction Pumps for Liquid Metals]. Prikladnaya magnitogidrodinamika [Applied Magnetohydrodynamics]. Trudy in-ta fiziki AN Latv. SSR, No. 8, 65, 1956.

173. Okhremenko, N. M. Elektromagnitnyye yavleniya v ploskikh induktsionnykh nasosakh dlya zhidkikh metallov [Electromagnetic Phenomena in Flat Induction Pumps for Liquid Metals]. Elektrichestvo, No. 3, 48, 1960.

174. Okhremenko, N. M. Magnitogidrodinamicheskiye yavleniya v kanale ploskogo induktsionnogo nasosa s uchetom zatukhaniya elektromagnitnogo polya [Magnetohydrodynamic Phenomena in the Duct of a Flat Induction Pump, with Consideration of Electromagnetic Field Damping]. Voprosy magnitnoy gidrodinamiki i dinamiki plazmy (see [89]), Vol. 2, Latvian SSR Acad. Sci. Press, 1962.

175. Okhremenko, N. M. Vliyaniye begushchego magnitnogo polya na gidravlicheskoye soprotivleniye turbulentnomu techeniyu provodyashchey zhidkosti v kanalakh [Effect of Traveling Magnetic Field on the Friction Factor of Turbulent Flow of Conducting Fluids in Channels]. Voprosy magnitnoy gidrodinamiki (see [89]), Vol. 3, Latvian SSR Acad. Sci. Press, 1963.

176. Okhremenko, N. M. Issledovaniye prostranstvennogo raspredeleniya magnitnykh poley i elektromagnitnykh yavleniy v induktsionnykh nasosakh [A Study of the Spatial Distribution of Magnetic Field and Electromagnetic Phenomena in Induction Pumps]. Magnitnaya gidrodinamika, No. 1, 97, 1965.

177. Okhremenko, N. M. Induktsionnyye nasosy s begushchim magnitnym polem [Induction Pumps with Travelling Magnetic Field]. Magnitnya gidrodinamika, No. 4, 3, 1965.

178. Birzvalk, Yu. A. Analiticheskiy raschet raspredeleniya potentsiala v krayevoy zone nasosa postoyannogo toka [Analytical Calculation of Potential Distribution in the Edge Zone of a DC Pump]. Izvestiya AN Latv. SSR, No. 12, 49, 1959.

179. Birzvalk, Yu. A. Analiz optimal'nykh kriteriyev, primenyayemykh v raschetakh nasosov postoyannogo toka [Analysis of Optimality Criteria Used in DC Pump Design]. Izvestiya AN Latv. SSR, No. 11, 91, 1960.

180. Birzvalk, Yu. A. Ekvivalentnaya skhema kanala nasosa postoyannogo toka i raschet nasosa na maksimum k. p. d. [Equivalent Circuit of a DC Pump and Designing a Pump for Maximum Efficiency]. Prikladnaya magnitogidrodinamika [Applied Magnetohydredynamics]. Trudy in-ta fiziki AN Latv. SSR, No. 12, 25, 1961.

181. Birzvalk, Yu. A. Elektromagnitnyye protsessy v nasosakh postoyannogo toka dlya zhidkikh metallov [Electromagnetic Processes in DC Pumps for Liquid Metals]. Author's abstract of Candidate Dissertation. G. M. Krzhizhanovskiy Energetics Institute, 1961.

182. Liyelpeter, Ya. Ya. O teplovykh protsessakh v elektromagnitnom induksionnom nasose [The Thermal Processes in an Electromagnetic Induction Pump]. Izvestiya AN Latv. SSR, No. 9, 91, 1959.

211

183. Llyelpeter. Ya. Ya. and I. A. Tyutin. Metodika rascheta induktsionnykh nasosov [Methods of Induction Pump Design]. Prikladnaya magnitogidrodinamika [Applied Magnetohydrodynamics], Trudy in-ta fiziki AN Latv. SSR, No. 8, 95, 1956.

184. Llyelpeter Ya. Ya. Elektromagnitnyye i gidrodinamicheskiye protsessy v kanale induktsionnogo nasosa [The Electromagnetic and Hydrodynamic Processes in an Induction Pump Duct]. Author's abstract of Candidate Dissertation, MEI [Moscow Order of Lenin Energetics Institute], 1960.

185. Yanes, Kh. I. Uchet vliyaniya vtorichnoy sistemy v lineynoy ploskoy magnito-gidrodinamicheskoy sisteme [Consideration of the Effect of a Secondary System in a Linear Planar Magnetohydrodynamic System]. Trudy Tallinskogo poli-tekhnicheskogo in-ta. Seriya A, 197, 37, 1962 (see also 197, 63, 1962, 197, 215, 1962 and 214, 11, 1964).

186. Yanes, Kh. I. O parametrakh elementov skhemy zameshcheniya magnitogidrodi-namicheskoy induktsionnoy mashiny [Concerning Parameters of Elements of an Equivalent System of a Magnetohydrodynamic Induction Machine]. Tekhniches-kaya elektromagnitnaya gidrodinamika [Engineering Magnetohydrodynamics], Vol. 2, Metallurgiya Press, 1965.

187. Liyn, Kh. A. and Kh. I. Yanes. O rezhimakh raboty ploskogo lineynogo indukt-sionnogo nasosa so sverkhprovodyashchimi bokovymi shinami [Concerning the Operating Modes of a Flat Linear Induction Pump with Superconducting Side Bus Bars]. Voprosy magnitnoy gidrodinamiki (see [90]), Vol. 3, Latvian SSR Acad. Sci. Press, 1963.

188. Polishchuk, V. P. Odnofaznyy induktsionnyy nasos-dozator dlya zalivki zhidkogo metalla [Single Phase Induction Metering Pump for Pouring Liquid Metals]. Elektrichestvo, No. 5, 1963.

189. Yankop, E. K. Odnofaznyye nasosy peremennogo toka [Single Phase AC Pumps]. Prikladnaya magnitogidrodinamika [Applied Magnetohydrodynamics]. Trudy in-ta fiziki AN Latv. SSR, No. 8, 107, 1956.

190. Ulmanis, L. Ya. K voprosu o poperechnom krayevom effekte v induktsionnykh nasosakh [Concerning Transverse Fringing in Induction Pumps]. Voprosy magnitnoy gidrodinamiki i dinamiki plazmy (see [89]), Vol. 2, Latvian SSR Acad. Sci. Press, 1962.

191. Mezhburd, V. I., R. R. Parts, L. Kh. Rannu, M. M. Saar and V. A. Teearu. K proyektirovaniyu kanalov maloshumnykh nasosov postoyannogo toka vysokogo davleniya [On the Design of Ducts of Low-Noise, High-Pressure DC Pumps]. Voprosy magnitnoy gidrodinamiki (see 90]), Vol. 3, Latvian SSR Acad. Sci. Press, 1963.

192. Veske, T. A. Resheniye uravneniy elektromagnitnogo polya ploskoy lineynoy in-duktsionnoy mashiny s uchetom vtorichnykh poperechenogo i tolshchinnogo krayevykh effektov [Solving Equations of the Electromagnetic Field of a Flat Linear Induction Machine with Consideration of Transverse and Depth Fringing]. Magnitnaya gidrodinamika, No. 1, 87, 1965.

193. Andreyev, A. M., V. A. Glukhikh and V. G. Karasev. Printsipy ratsional'nogo proyektirovaniya elektromagnitnykh nasosov postoyannogo toka [Principles of Efficient Design of DC Electromagnetic Pumps]. Magnitnaya gidrodinamika, No. 2, 114, 1965.

194. Yakovlev, V. S. Opredeleniye optimal'nogo k. p. d. magnitogidrodinamicheskogo nasosa [Determining the Optimum Efficiency of a Magnetohydrodynamic Pump]. Tekhnicheskaya elektromagnitnaya gidrodinamika [Engineering Magnetohydro-dynamics], Vol. 2, Metallurgiya Press, 1965.

195. Kirillov, P.G., Ya. Ya. Liyelpeter, A. E. Mikel'son and G. A. Okunev. Opyt razrabotki elektromagnitnykh nasosov v in-te fiziki AN Latv. SSR [Experiment in Development of Electromagnetic Pumps in the Physics Institute of the Latvian SSR Academy of Sciences]. Voprosy magnitnoy gidrodinamiki i dinamiki plazmy (see [89]), Vol. 1, Latvian SSR Acad. Sci. Press, 1959.

196. Bushman, A.K., I.A. Veklenko, Ya. Ya. Klyavin' and Ya. Ya. Liyelpeter Opyt konstruktorskoy razrabotki elektromagnitnykh induktsionnykh nasosov v institute fiziki AN Latv. SSR [Experience in Design Development of Electromagnetic In-duction Pumps in the Latvian SSR Academy of Sciences Physics Institute]. Voprosy magnitnoy gidrodinamiki (see [90]), Vol. 3, Latvian SSR Acad. Sci. Press, 1963.

197. Kirillov, P.L., V.A. Kuznetsov, N.M. Turchin and Yu.M. Fedoseyev. Nekotoryye konstruktsii i ekspluatatsiya nasosov dlya natriya i splavov natriya s kaliyem [Certain Designs and the Performance of Pumps for Sodium and for Sodium-Potassium Alloys]. Atomnaya energiya, 7, No. 1, 11, 1959.

198. Vol'dek, A.I. and Kh.I. Yanes. Eksperimental'noye issledovaniye ploskikh induktsionnykh nasosov [Experimental Study of Flat Induction Pumps]. Voprosy magnitnoy gidrodinamiki i dinamiki plazmy (see [89]), Vol. 2, Latvian SSR Acad. Sci. Press, 1962.

199. Veze, A.K., I.M. Kirko and O.A. Liyelausis. Tsentrobezhnyy induktsionnyy nasos [The Centrifugal Induction Pump]. Voprosy magnitnoy gidrodinamiki i dinamiki plazmy (see [89]), Vol. 2, Latvian SSR Acad. Sci. Press, 1962.

200. Ivashchenko, N.I., I.S. Kudryavtsev and Ye. D. Fedorovich. Rezul'taty ispytaniy induktsionnykh elektromagnitnykh nasosov dlya perekachivaniya natriya i rtuti [Results of Testing Induction Electromagnetic Pumps for Sodium and Mer-cury]. Voprosy magnitnoy gidrodinamiki (see [90]), Vol. 3, Latvian SSR Acad. Sci. Press, 1963.

201. Grinberg, D.A., Ya. Ya. Zandart, Yu.K. Zander and I. Ya. Laumanis. Issle-dovaniye eksperimental'nogo konduktsionnogo nasosa postoyannogo toka [A Study of an Experimental DC Conduction Pump]. Voprosy magnitnoy gidrodinamiki (see [90]), Vol. 3, Latvian Acad. Sci. Press, 1963.

202. Avstreykh, G.A., M.V. Levin, M.B. Lyandres and V.V. Timofeyev. Elektro-magnitnyy nasos postoyannogo toka dlya perekachki metalla v sisteme okhlazh-deniya elementov elektrolizera [An Electromagnetic DC Pump for Circulating Metal in the Cooling System of Electrolyzer Elements]. Voprosy magnitnoy gidrodinamiki (see [90]), Vol. 3, Latvian Acad. Sci. Press, 1963.

203. Avilova, Ye. M., T. V. Doktorova, N.I. Marin, V.A. Povsten' and N.M. Turchin. Razrabotka i ekspluatatsiya vintovykh induktsionnykh nasosov [Development and Operation of Spiral Induction Pumps]. Magnitnaya gidrodinamika, No. 1, 110, 1965.

204. Mikel'son, A.E., U.A. Saulite and A. Ya. Shkerstena. Issledovaniye tsylindri-cheskikh besserdechnikovykh nasosov [A Study of Annular Coreless Pumps]. Magnitnaya gidrodinamika, No. 2, 92, 1965.

205. Avilova, Ye. M., T.V. Doktorova, V.K. Lutikov, N.I. Marin, V.A. Povsten' and N.M. Turchin. Osobennosti konstruktsii i rezul'taty ispytanii konduktsionnykh nasosov [Design Details and Results of Testing of Conduction Pumps]. Magnit-naya gidrodinamika, No. 3, 121, 1965.

206. Tiysmus, Kh.A., Kh.I. Yanes, E. M. Ristkheyn and Kh.A. Tammemyagi. Opyt transportirovaniya zhidkogo magniya po metallicheskim trubam pri pomoshchi elektromagnitnogo nasosa [Experiment in Using an Electromagnetic Pump for Transporting Liquid Magnesium over Metal Pipelines]. Tekhnicheskaya elektro-magnitnaya gidrodinamika [Engineering Magnetohydrodynamics], Vol. 2, Metal-lurgiya Press, 1965.

207. Parts, R. R. and V. A. Teearu. Asinkhronnyy nasos s vintorym kanalom dlya perekachki zhidkogo metalla [Asynchronous Volute Pump for Liquid Metals]. Tekhnicheskaya elektromagnitnaya gidrodinamika, Vol. 2, Metallurgiya Press, 1965.

208. Grishin, V. K. and A. G. Kuznetsov. Kharakteristiki elektromagnitnogo induktsionnogo nasosa na zhidkom natrii pri $T = 500°C$ [Characteristics of an Electromagnetic Induction Pump for Liquid Sodium at $T = 500°C$]. Magnitnaya gidrodinamika, No. 1, 127, 1966.

209. Barinberg, A. D. Elektricheskiye rtutnyye apparaty s elektromagnitnymi nasosami [Electrical Mercury Devices with Electromagnetic Pumps]. Tekhnicheskya elektromagnitnaya gidrodinamika, Vol. 2, Metallurgiya Press, 1965.

210. Barinberg, A. D. Razrabotka i issledovaniye gidromagnitoelektricheskikh kommutiruyushchikh apparatov [Development and Study of Hydromagnetoelectrical Switching Devices]. Author's abstract of Candidate Dissertation, MEI [Moscow Order of Lenin Energetics Institute], 1966.

211. William, S. The Magnetohydrodynamic Slider Bearing. Trans. ASME, D 84, No. 1, 197, 1962.

212. Hughes, W. Magnetohydrodynamic Lubrication and Application to Liquid Metals. Sci. Lubricat, 15, No. 3, 125, 1963.

213. Khozhainov, A. I. Vliyaniye kontaktnogo soprotivleniya na pokazaniya magnitnykh raskhodomerov [Effect of Contact Resistance on the Readings of Magnetic Flowmeters]. Izmeritel'naya tekhnika, 11, 1965.

214. Voprosy magnitnoy gidrodinamiki i dinamiki plazmy [Problems of Magnetic Hydrodynamics and Plasma Dynamics]. Vol. 1, 1959, Vol. 2, 1962. Latv. SSR Acad. Sci. Press.

215. Voprosy magnitnoy gidrodinamiki [Problems of Magnetohydrodynamics], Vol. 3, Latv. Acad. Sci. Press, 1963.

216. Tekhnichskaya elektromagnitnaya gidrodinamika [Engineering Magnetohydrodynamics]. Vol. 2, 1965, Vol. 3, 1967. Metallurgiya Press.

217. Elektromagnitnyye nasosy dlya transporta zhidkikh metallov [Electromagnetic Pumps for Liquid Metals]. Collection of Scientific and Engineering Articles. Issue 2, Energiya Press, 1965.

218. Elliott, D. A two-Fluid Magnetohydrodynamic Cycle for Nuclear Electric Power Conversion, ARS Space Flight Report to the Nation, 1961. [Also ARS J. 32, 924-928 (1962)].

219. Jackson, W. Liquid Metal Faraday-type MHD Generators, IEEE Trans. Power Apparatus and Systems, No. 69, 904, 1963.

220. Brown, G., W. Jackson, K. Lee and M. Reid. MHD Power Generation with Liquid Metals, MIT, Cambridge Massachusetts, Proc. of Fifth Symposium on the Engineering Aspects of Magnetohydrodynamics Sponsored by Massachusetts Inst. of Technology, April 1-2, 1964.

221. Marston, C. Separated Liquid Driven Vortex MHD Generator, Proc. of Fifth Symposium on the Eng. Aspects of Magnetohydrodynamics, Sponsored by Massachusetts Inst. of Technology, April 1-2, 1961.

222. Elliott. D. G. DC Liquid Metal Magnetohydrodynamic Power Generator. Sixth Symposium on the Engineering Aspects of Magnetohydrodynamics, University of Pittsburg, Pittsburg, Pa (April 21-23, 1965). [Also AIAA Journal, No. 1, 1966].

223. Petrick, M. and K. Y. Lee. Performance Characteristics of a Liquid Metal MHD Generator. Paper 62. Proceedings of International Symposium on Magnetohydrodynamic Electrical Power Generation, Vol. 2, Paris, 1964.

224. Keith, P. MHD Magnetos, Michigan Technic., No. 7, 82, 1964.

225. Elliot, D., D. Cerini and E. Weinberg. Investigation of Liquid MHD Power Conversion. AIAA, 64-760, Third Biennial Aerospace Power Systems Conference, Phila., Pa., September 1-4, 1964.

226. Petrick, M.   Liquid Metal Magnetohydrodynamic, IEEE, Spectrum 2, No. 3, 137, 1965.

227. Dzung, L.   Beschleunigungeines Flüssig-keitsstroms durch einen Dampfstrahl als Antrieb enies MHD-G, Brennstoff Wärme-Kraft, 17, No. 1, 13, 1965.

228. Proceedings of Fifth Symposium on the Engineering Aspects of Magnetohydrodynamics, Sponsored by Massachusetts Inst. of Technology, April 1-2, 1964.

229. International Symposium on Magnetohydrodynamic Electrical Power Generation, Paris, July 1964. O.E.C.D., Europ. Nucl. Energy Agency and French Inst. Nat. Sci. and Nucl. Techn,. S.I., 19.

230. Brown, G.A. and K.S. Lee.   A Liquid Metal MHD Power Generation Cycle Using a Condensing Ejector. Paper 60, [223].

231. Jackson, W.D. and C.A. Brown.   Liquid Metal Magnetohydrodynamic Power Generation Utilizing the Condensing Ejector, Patent Disclosure, M.I.T., Cambridge, Mass., October 15, 1962.

232. Radebold, R.D., H. Lang, W. Westphal and W. Lochte-Holtgreven.   Energy Conversion with Liquid Metal Working Fluids in MHD "Staustrahlrohr." Paper 64, [223].

233. Prem, L.L. and W.E. Parkins.   A New Method of MHD Power Conversion Employing a Fluid Metal. Paper 63, [223].

234. Jakob, M.   Heat Transfer, New York, John Wiley & Sons, 1949.

235. Larson, J.W.   Study of Two Phase MHD Report N APR-1020, Pratt and Whitney Aircraft, East Hartford, Conn., June, 1962.

236. Craig, R.T. and W.F. Wade.   Proposed Investigation of a Two Phase Magnetofluidmechanical Energy Conversion System. Report N ER-5402. Thompson Ramo Wooldridge, Inc., Cleveland, Ohio, June, 1963.

237. Elliott, D.G.   Progress in Astronautics and Rocketry, Liquid Rockets and Propellants, Vol. 2, 1960.

238. Elliott, D.G.   Analysis of the Acceleration of Lithium in a Two Phase Nozzle, Proceedings of the Third Annual High Temperature Liquid Metal Heat Transfer Technology Conference, Oak Ridge, Tenn., Sept., 1963.

239. Krieth, F.   Principles of Heat Transfer, International Textbook Co., 1960.

240. Tepper, F., A. Murchioson and J. Zelenak.   Thermophysical Properties of Rubidium and Cesium, Fifth Quarterly Progress Report, April-May-June, 1963, Report No. Ms AR 63-102, MSA Research Corp., Callery, Penn.

241. Phillips, O.   The Prospects for Magnetohydrodynamic Ship Propulsion, I. Ship. Res., 5, No. 4, 43, 1962.

242. Rice, W.A.   Propulsion System, U.S. Patent 799547, 1958.

243. Joseph, B., L. Neuringer, E. Migotsky, J.H. Turner and R.M. Haag. J. of Ship Res., 9, No. 4, 56, 1965.

244. Darach, R.A.   Magnetohydrodynamic Ship Propulsion Using Superconducting Magnets. The Soc. of Naval Architects and Marine Eng. Transactions, 71, 1963.

General References and Handbooks

245. Bergmann, L. [Engineering] Ultrasonics. John Wiley & Sons. Translated from the German.

246. Shuleykin, V.V.   Ocherki po fizike morya [Essays on the Physics of the Sea]. USSR Acad. Sci. Press, 1962.

247. Anderson, N.S. J. Acoustical Soc. America, 25, No. 3, 539, 1953.

248. Bonetti, A.   Velocita degli ultrasuoni in campo elettrico e influenza della temperatura Ric. Sci., No. 18, 777, 1948.

249. Nolle, A.W.   Electric-Field Modulation of Ultrasonic Signals in Liquids, J. Appl. Phys., No. 20, 589, 1949.

250. Spravochnik khimika [The Chemist's Handbook], Vol. 3, Khimiya Press, 1964.
251. Ewing, M. and J. L. Worzel. Long-Range Sound Transmission. In the collection: Propagation of Sound in the Ocean. Contribution 415 from Woods Hole Oceanographic Institution. October 1948.
252. Schlichting, H. Boundary Layer Theory. McGraw-Hill, 1960.
253. Patrashev, A. N. Gidromekhanika [Hydromechanics]. Voyenmorizdat Press, 1953.
254. Schiller, L. Dvizheniye zhidkosti v trubakh [Motion of Fluids in Pipes]. [Translated from German and published by] ONTI Press, 1936.
255. Schiller, L. Über den Strömungswiederstand von Rohren, ZAMM, No. 3, 11, 1923.
256. Nikuradze, J. Turbulente Strömung in nicht kreisförmigen Rohren, Ing.-Arch., No. 1, 306, 1930.
257. Kamke, E. Spravochnik po obyknovennym differentsial'nym uravneniyam [Handbook on Ordinary Differential Equations]. Fizmatgiz, 1961.
258. Slezkin, N. A. Dinamika vyazkoy neszhimayemoy zhidkosti [Dynamics of Viscous Incompressible Fluids]. GITTL Press, 1955.
259. Grinberg, G. A. Izbrannyye voprosy matematicheskoy teorii elektricheskikh i magnitnykh yavleniy [Selected Problems of the Mathematical Theory of Electrical and Magnetic Phenomena]. USSR Acad. Sci. Press, 1948.
260. Boussinesq, T. V. Laminare Kanaleinlaufströmung, J. Math. pur et appl., No. 13, 377, 1868.
261. Andreyev, P. A., A. A. Kanayev and Ye. D. Fedorovich. Zhidkometallicheskiye teplonositeli yadernykh reaktorov [Liquid Metal Coolants for Nuclear Reactors]. Sudpromgiz Press, 1959.
262. Dukure, R. K. and G. P. Upit. Nekotoryye voprosy kontaktnykh svoystv metallicheskikh poverkhnostey [Certain Problems of Contact Properties of Metal Surfaces]. Prikladnaya magnitogidrodinamika [Applied Magnetohydrodynamics]. Trudy in-ta fiziki AN Latv. SSR, No. 12, 237, 1961.
263. Kalantarov, P. L. and L. R. Neyman. Teoreticheskiye osnovy elektrotekhniki [Theoretical Fundamentals of Electrical Engineering]. Gosenergoizdat Press, 1951.
264. Ukhov, K. S. Navigatsiya [Navigation]. Morskoy Transport Press, 1952.
265. Leykis, D. I. and B. N. Kabanov. Nepolyarizuvushchiyesya elektrody dlya izmereniya malykh raznostey potentsialov v more [Nonpolarizing Electrodes for Measuring Small Potential Differences in the Seas]. Trudy instituta okeanologii, No. 29, 112, 1956.
266. Aliyevskiy, B. L., A. I. Bertinov, V. N. Kalugin and V. Kh. Khan. Unipolyarnyye generatory postoyannogo toka dlya pitaniya konduktsionnykh nasosov [Homopolar DC Generators for Supplying Conduction Pumps]. Voprosy magnitnoy gidrodinamiki (see [90]), Vol. 3, Latv. SSR Acad. Sci. Press, 1963.
267. Aliyevskiy, B. L. and A. I. Bertinov. Rezul'taty eksperimental'nogo issledovaniya unipolyarnogo generatora nizkogo napryazheniya dlya pitaniya konduktsionnykh nasosov postoyannogo toka [Results of an Experimental Study of a Low Voltage Homopolar Generator for Supplying DC Conduction Pumps]. Magnitnaya gidrodinamika, No. 4, 125, 1965.
268. Gradshteyn, I. S. and I. M. Ryzhik. Tablitsy integralov, summ, ryadov i proizvedeniy [Tables of Integrals, Sums, Series and Products]. Fizmatgiz Press, 1962.
269. Grinberg, E. Ya. K opredeleniyu svoystv nekotorykh potentsialnykh poley [Concerning the Determination of Certain Potential Fields]. Prikladnaya magnitogidrodinamika [Applied Magnetohydrodynamics]. Trudy instituta fiziki AN Latv. SSR, No. 12, 147, 1961.

APPENDIX 1: Physical Properties of Certain Liquid Metals and Alloys

1) Жидкая среда	2) Температура плавления, °C	3) Теплота плавления, 10⁻³	4) Температура °C ρ	5)	6) Плотность		7) Теплоёмкость		8) Динамическая вязкость		9) Теплопроводность	
					10) T, °C	кг/м³	11) T, °C	дж/кг·°С	12) T, °C	н·сек/м²	13) T, °C	вт/м·°С
14) Висмут Bi (Ат. вес 209,0)	271,0	50,4	1477	853	300 400 600 800	10 030 9 910 9 020 9 400 1 250	271 400 800 1000	0,148 0,155 0,159 0,167 0,176	300 700	13,92		
15) Галлий Ga (Ат. вес 69,72)	29,92	82,4	1983	4260			125 245	0,344	32,0	13,04	77	
16) Калий K (Ат. вес 39,096)	—	61,4	760	2084			75 245	0,822 0,782 0,747 0,726	50,6	5,15		
17) Литий Li (Ат. вес 6,94)	179	664	1317	19 600			500					87,0
18) Натрий Na (Ат. вес 22,997)	97,8	114.	853	4220	100 200 300 400 700 820	927 904 882 859 824 743 757		1,35 1,31	100 300 500 700	7,35 4,5 3,45 2,84	100 300 500	85,8 81,6 76,0 71,4 67,5
19) Сплав Na22K78 (Ат. вес 33,0)	—11	—	784	—	100 200 300 500 600 700	847 823 799 751 727 703	100 200 300 400 500 600 700	0,95 0,91 0,90 0,89 0,88 0,88 0,89	100,7 250 400 700	4,00 3,36 2,79 2,05	100 400	21,5
20) Сплав Na56K44 (Ат. вес 28,1)	19	—	825	—	100 200 300 400 500 600 700	887 862 838 814 789 765 740	100 200 300 400 500 600 700 800	1,13 1,1 1,07 1,05 1,04 1,04 1,05 1,06	100 250	5,40 0,76	100	23,9

APPENDIX 2. Specific Heats of Some Electrolytes

1) Жидкая среда	2) Температура плавления, °C	3) Теплота плавления, 10^{-3} J/кг	4) Температура кипения при $p = 10^5$ н/м², °C	5) Теплота испарения, 10^{-3} J/кг	6) Плотность		7) Теплоемкость		8) Динамическая вязкость		9) Теплопроводность	
					10) T, °C	$\frac{кг}{м^3}$	T, °C	11) $\frac{Дж}{кг\cdot град}\cdot 10^{-3}$	T, °C	12) $\frac{н\cdot сек}{м^2}\cdot 10$	T, °C	13) $\frac{вт}{м\cdot град}$
21) Олово Sn (Ат. вес 118,7)	213,9	61	2270	2410	400 523 574 648 704	6904 6761 6720 6671 6640	250 1100	0,244 0,319	240 300 450 500 600	19,1 17,7 13,5	240	33,6 32,0 32,7
22) Ртуть Hg (Ат. вес 200,61)	−38,87	11,73	357	293	−20 +20 100 200 300	13.645 13.546 13.352 13.115 12.881	0 100 200 300 450	0,140 0,138 0,136 0,135 0,136	−20 0 20,8 100 200	18,5 16,8 15,5 12,4 10,1	0 20 100 200	8,21 8,71 10,75 12,75
23) Рубидий Rb (Ат. вес 85,48)	39,0	25,6	688	891	39	1475	39—126	0,333	38 50 59,7 140,5 220,1	6,724 6,208 4,944 4,133 3,234	$T_{пл}$ 50	29,4 31,5
24) Сурьма Sb (Ат. вес 121,76)	630,5	161	1440	1610	640 700 800 970	6490 6450 6390 6290	650—950	0,276	702 801 930 1002	12,96 11,12 9,94 9,05	720— 930	21,8— 21,0
25) Свинец Pb (Ат. вес 207,21)	327,4	24,7	1737	860	400 500 600 800 1000	10 510 10 390 10 270 10 040 9 810	327 400 500	0,164 0,155 0,155	441 436 551 703 844	21,16 20,59 17,03 13,40 11,85	330 400 500 600 700	16,4 16,0 15,3 15,0 13,1
26) Сплав Pb—Bi (Ат. вес 208)	125	—	1670	—	200 400 600 800 1000	10 470 10 100 9 910 9 640 9 360	144—358	0,147	330 430 500 730 860	17,0	200 400 600	10,0
27) Цезий Cs (Ат. вес 132,91)	28,5	15,8	705	613	28	1840	28,5	0,252	43,4 90,0 140,5 168,0 210,0	6,230 4,753 4,035 3,735 3,480	$T_{пл}$	18,5

KEY: 1) Liquid; 2) melting temperature, °C; 3) Heat of fusion, 10^{-3} J/kg; 4) boiling temperature at $p = 10^5$ Newtons/m², °C; 5) heat of vaporization, 10^{-3} J/kg; 6) density; 7) specific heat; 8) dynamic viscosity; 9) thermal conductivity; 10) kg/m³; 11) J/kg-deg.; 12) Newtons-sec/m²; 13) watt/m-deg.; 14) bismuth, Bi (atomic weight 209.0); 15) gallium, Ga (atomic weight 69.72); 16) potassium, K (atomic weight 39.096); 17) lithium, Li (atomic weight 6.94); 18) sodium, Na (atomic weight 22.997); 19) alloy Na22K78 (atomic weight 33.9); 20) alloy Na56K44 (atomic weight 28.1); 21) tin, Sn (atomic weight 118.7); 22) mercury, Hg (atomic weight 200.61); 23) rubidium, Rb (atomic weight 85.48); 24) antimony, Sb (atomic weight 121.76); 25) lead, Pb (atomic weight 207.21); 26) alloy of Pb-Bi (atomic weight 208); 27) cesium, Cs (atomic weight 132.91).

APPENDIX 2. Specific Heats of Some Electrolytes

1) Электролит	T, °C	2) Уделн. теплоемкость $\left(\frac{\partial}{\partial}\right)\cdot$			
		n · 10	· 25	n · 50	n · 100
HNO₃	18	3,2?	?,??	3,80	4,03
H₂SO₄	21	2,93	?,57	3,?3	4,?0
KOH	15	--	?,?	3,83	3,??
NaOH	1?	-	?,?	3,91	4,05
NH₄Cl	18	3,2?	?,??	3,?2	4,0?
NaCl	18	3,31	?,??	3,90	4,0?
CuSO₄	18—?3	--	--	3,?2	3,?0

KEY: 1) Electrolyte; 2) specific heat * (J/kg-deg) · 10^3.

A) Note: Values of specific heat are presented for electrolytes dissolved in the proportion of one mole of electrolyte per n moles of water. All the data are for a pressure of 10^5 Newtons/m² (760 mm of Hg).

APPENDIX 3. Thermal Conductivity of Certain Electrolytes

1) Электролит	2) Коэфф. теплопроводности, вт/м·град, при T · 20°С и концентрации, %						
	0	::	20	25	30	40	50
HNO₃	0,5??	--	—	0,5?6	--	--	0,?50
H₂SO₄	0,5??	--	--	0,531	--	--	0,16??
KOH	0,5??	?,??	?,?0?	--	0,585	0,5??	0,5??
NaOH	0,5??	?,???	?,6?0	--	0,616	0,616	--
NH₄Cl	0,5??	?,???	?,?1	--	--	--	--
NaCl	0,5??	?,??	?,??	--	--	--	--
CuSO₄	6,5??	?,??	—	--	--	--	--

KEY: Electrolyte; 2) thermal conductivity coefficient, watt/m--degree, at T = 20°C and concentration, %.

APPENDIX 4. Viscosity of Sea Water [236]

1)	2)								
	0	1	2	3	4	5	1	2	3
0									
0.5									
1.0									
1.5									
2.0									
2.5									
3.0									
3.5									
4.0									

KEY: 1) Concentration of salts; 2) ratio of viscosity of sea water to the viscosity of potable* water at temperature, °C.

* The viscosity of potable water is taken at 0°C.

APPENDIX 5. Composition of Salts in Sea Water* [232]

1)	2) per 1 kg H₂O	3)	1)	2) per 1 kg H₂O	3)
Cl⁻	18.980	54.05	H₃O₂	0.003	0.01
Br⁻	0.065	0.19	Mg⁺⁺	1.272	3.69
SO₄	2.649	7.68	Ca⁺⁺	0.400	1.16
CO₃	0.071	0.21	Sr⁺⁺	0.013	0.01
HCO₃	0.11	0.11	K⁺	0.380	1.10
F⁻	0.001	0.01	Na⁺	10.556	30.61

KEY: 1) Ions; 2) number of grams of ions per 1 kg of H₂0; 3) in % of the total weight of all the ions.

* For a total salinity of s = 34.482°/₀

DATA HANDLING PAGE

01-ACCESSION NO.	98-DOCUMENT LOC	39-TOPIC TAGS
TM0000344		magnetohydrodynamics, marine engineering, electromagnetic pump, MHD generator

09-TITLE MAGNETOHYDRODYNAMICS IN MARINE ENGINEERING -U-

47-SUBJECT AREA

13, 20

42-AUTHOR CO-AUTHORS	10-DATE OF INFO
VASIL'YEV, L. L. ;16-KHOZHAINOV, A. I.	------67

43-SOURCE	
MAGNITNAYA GIDRODINAMIKA V SUDOVOY TEKHNIKE. LENINGRAD. SUDOSTROYENIYE (RUSSIAN)	68-DOCUMENT NO. FTD-HT-23-237-69
	69-PROJECT NO. 72301-78

63-SECURITY AND DOWNGRADING INFORMATION	64-CONTROL MARKINGS	97-HEADER CLASN
UNCL. O	NONE	UNCL

76-REEL/FRAME NO.	77-SUPERSEDES	78-CHANGES	40-GEOGRAPHICAL AREA	NO. OF PAGES
			UR	220

CONTRACT NO. F33657-68-D-0866 PC02	X REF ACC. NO. 65-AM8011437	PUBLISHING DATE 94-	TYPE PRODUCT TRANSLATION	REVISION FREQ NONE

STEP NO. 02-UR/0000/67/000/000/0001/0247

ABSTRACT (UNCL, O) ABSTRACT OF REPORT. This book is intended for scientific personnel and engineers in the shipbuilding industry and related fields. It can also be useful to graduate students and students of corresponding specialties. The book is concerned with the new, rapidly developing branch of science called magneto hydrodynamics and its practical application in marine engineering. The present state and development of magnetohydrodynamics and devices operating on the magnetohydrodynamic principle are discussed. The magnetohydrodynamic effects produced by the interaction of an incompressible conducting fluid with a transverse magnetic field are discussed. Elements of the theory, design, and operating char acteristics of magnetic flow meters, electromagnetic pumps, MHD generators, marine MHD power plants, and MHD power plants for trans port vehicles are discussed. A significant part of the book is devoted to original experimental research, and it is based primarily on materials published by domestic and foreign scientists, as well as on research by the authors themselves. The authors express special appreciation to I. L. Povkh, Corresponding Member of the AN UkrSSR, for his review and advice. (The parent document contains a bibliography of two hundred sixty nine titles, which is available on microfiche.)